

TOPICS IN
ORGANOMETALLIC CHEMISTRY

26

Volume Editor Zhibin Guan

Metal Catalysts in Olefin Polymerization

 Springer

26

Topics in Organometallic Chemistry

Editorial Board:

**M. Beller · J. M. Brown · P. H. Dixneuf · A. Fürstner
L. S. Hegedus · P. Hofmann · P. Knochel · G. van Koten
S. Murai · M. Reetz**

Topics in Organometallic Chemistry

Recently Published and Forthcoming Volumes

Metal Catalysts in Olefin Polymerization

Volume Editor: Z. Guan
Vol. 26, 2009

Bio-inspired Catalyst

Volume Editor: T. R. Ward
Vol. 25, 2009

Directed Metallation

Volume Editor: N. Chatani
Vol. 24, 2007

Regulated Systems for Multiphase Catalysis

Volume Editors: W. Leitner, M. Hölscher
Vol. 23, 2008

Organometallic Oxidation Catalysis

Volume Editors: F. Meyer, C. Limberg
Vol. 22, 2007

N-Heterocyclic Carbenes in Transition Metal Catalysis

Volume Editor: F. Glorius
Vol. 21, 2006

Dendrimer Catalysis

Volume Editor: L.H. Gade
Vol. 20, 2006

Metal Catalyzed Cascade Reactions

Volume Editor: T. J. J. Müller
Vol. 19, 2006

Catalytic Carbonylation Reactions

Volume Editor: M. Beller
Vol. 18, 2006

Bioorganometallic Chemistry

Volume Editor: G. Simonneaux
Vol. 17, 2006

Surface and Interfacial Organometallic Chemistry and Catalysis

Volume Editors: C. Copéret, B. Chaudret
Vol. 16, 2005

Chiral Diazaligands for Asymmetric Synthesis

Volume Editors: M. Lemaire, P. Mangeney
Vol. 15, 2005

Palladium in Organic Synthesis

Volume Editor: J. Tsuji
Vol. 14, 2005

Metal Carbenes in Organic Synthesis

Volume Editor: K.H. Dötz
Vol. 13, 2004

Theoretical Aspects of Transition Metal Catalysis

Volume Editor: G. Frenking
Vol. 12, 2005

Ruthenium Catalysts and Fine Chemistry

Volume Editors: C. Bruneau, P. H. Dixneuf
Vol. 11, 2004

New Aspects of Zirconium Containing Organic Compounds

Volume Editor: I. Marek
Vol. 10, 2004

Precursor Chemistry of Advanced Materials

CVD, ALD and Nanoparticles
Volume Editor: R. Fischer
Vol. 9, 2005

Metallocenes in Stereoselective Synthesis

Volume Editor: T. Takahashi
Vol. 8, 2004

Transition Metal Arene π -Complexes in Organic Synthesis and Catalysis

Volume Editor: E. P. Kündig
Vol. 7, 2004

Metal Catalysts in Olefin Polymerization

Volume Editor: Zhibin Guan

With Contributions by

Edmund M. Carnahan · T. Diesner
Terunori Fujita · Vernon C. Gibson · Brian L. Goodall
Zhibin Guan · Phillip D. Hustad · Koji Kawai
Roger L. Kuhlman · Krzysztof Matyjaszewski
Tomislav Pintauer · Chris S. Popeney · B. Rieger
Gregory A. Solan · C. Troll

 Springer

The series *Topics in Organometallic Chemistry* presents critical overviews of research results in organometallic chemistry. As our understanding of organometallic structure, properties and mechanisms increases, new ways are opened for the design of organometallic compounds and reactions tailored to the needs of such diverse areas as organic synthesis, medical research, biology and materials science. Thus the scope of coverage includes a broad range of topics of pure and applied organometallic chemistry, where new breakthroughs are being achieved that are of significance to a larger scientific audience.

The individual volumes of *Topics in Organometallic Chemistry* are thematic. Review articles are generally invited by the volume editors.

In references *Topics in Organometallic Chemistry* is abbreviated *Top Organomet Chem* and is cited as a journal.

Springer WWW home page: springer.com

Visit the TOMC content at springerlink.com

ISBN 978-3-540-87750-9

e-ISBN 978-3-540-87751-6

DOI 10.1007/978-3-540-87751-6

Topics in Organometallic Chemistry ISSN 1436-6002

Library of Congress Control Number: 2008944102

© 2009 Springer-Verlag Berlin Heidelberg

This work is subject to copyright. All rights are reserved, whether the whole or part of the material is concerned, specifically the rights of translation, reprinting, reuse of illustrations, recitation, broadcasting, reproduction on microfilm or in any other way, and storage in data banks. Duplication of this publication or parts thereof is permitted only under the provisions of the German Copyright Law of September 9, 1965, in its current version, and permission for use must always be obtained from Springer. Violations are liable to prosecution under the German Copyright Law.

The use of general descriptive names, registered names, trademarks, etc. in this publication does not imply, even in the absence of a specific statement, that such names are exempt from the relevant protective laws and regulations and therefore free for general use.

Cover design: SPi Publisher Services

Printed on acid-free paper

springer.com

Volume Editor

Prof. Zhibin Guan

University of California, Irvine
5042 D, Frederick Reines Hall
Irvine CA 92697-2025
USA
zguan@uci.edu

Editorial Board

Prof. Dr. Matthias Beller

Leibniz-Institut für Katalyse e.V.
an der Universität Rostock
Albert-Einstein-Str. 29a
18059 Rostock
matthias.beller@catalysis.de

Dr. John M. Brown

Dyson Perrins Laboratory
South Parks Road
Oxford OX13QY
john.brown@chem.ox.ac.uk

Prof. Alois Fürstner

Max-Planck-Institut für Kohlenforschung
Kaiser-Wilhelm-Platz 1
45470 Mülheim an der Ruhr, Germany
fuerstner@mpi-muelheim.mpg.de

Prof. Peter Hofmann

Organisch-Chemisches Institut
Universität Heidelberg
Im Neuenheimer Feld 270
69120 Heidelberg, Germany
ph@phindigo.oci.uni-heidelberg.de

Prof. Gerard van Koten

Department of Metal-Mediated Synthesis
Debye Research Institute
Utrecht University
Padualaan 8
3584 CA Utrecht, The Netherlands
vankoten@xray.chem.ruu.nl

Prof. Manfred Reetz

Max-Planck-Institut für Kohlenforschung
Kaiser-Wilhelm-Platz 1
45470 Mülheim an der Ruhr, Germany
reetz@mpi-muelheim.mpg.de

Prof. Pierre H. Dixneuf

Campus de Beaulieu
Université de Rennes 1
Av. du Gl Leclerc
35042 Rennes Cedex, France
Pierre.Dixneuf@univ-rennes1.fr

Prof. Louis S. Hegedus

Department of Chemistry
Colorado State University
Fort Collins, Colorado 80523-1872
USA
hegedus@lamar.colostate.edu

Prof. Paul Knochel

Fachbereich Chemie
Ludwig-Maximilians-Universität
Butenandstr. 5–13, Gebäude F
81377 München, Germany
knoch@cup.uni-muenchen.de

Prof. Shinji Murai

Faculty of Engineering
Department of Applied Chemistry
Osaka University
Yamadaoka 2-1, Suita-shi, Osaka 565
Japan
murai@chem.eng.osaka-u.ac.jp

Topics in Organometallic Chemistry

Also Available Electronically

For all customers who have a standing order to Topics in Organometallic Chemistry, we offer the electronic version via SpringerLink free of charge. Please contact your librarian who can receive a password or free access to the full articles by registering at:

springerlink.com

If you do not have a subscription, you can still view the tables of contents of the volumes and the abstract of each article by going to the SpringerLink Homepage, clicking on “Browse by Online Libraries”, then “Chemical Sciences”, and finally choose Topics in Organometallic Chemistry.

You will find information about the

- Editorial Board
- Aims and Scope
- Instructions for Authors
- Sample Contribution

at springer.com using the search function.

Color figures are published in full color within the electronic version on SpringerLink.

Preface

Billions of pounds of polyolefins are produced annually. Through a simple insertion reaction, inexpensive and abundant olefins are transformed into polymeric materials for a wide range of applications, including plastics, fibers, and elastomers. Despite its long history, the polyolefin industry is continuing to grow steadily and remains technologically driven because of continuous discoveries of new catalysts, processes, and applications. The key technology that continues to drive the polyolefin industry is transition metal catalyzed polymerization. The discovery of the Ziegler–Natta catalysts in the 1950s not only revolutionized polyolefin production, but also catalyzed the development of the entire organometallic chemistry field. The next milestone in olefin polymerization catalysis was the development of metallocene catalysts in the 1980s. Whereas the Ziegler–Natta and metallocene catalysts remain as the workhorse in the polyolefin industry, the last decade has witnessed a number of major breakthroughs in the development of non-metallocene catalysts, including late transition metal catalysts for olefin polymerizations. These new systems show many exciting features, including high catalytic efficiency, excellent control of polyolefin stereoregularity and branching topology, and most excitingly the tolerance and incorporation of functional olefins.

This volume highlights some of the most important discoveries that have occurred recently in both early and late transition metal olefin polymerization catalysis. In Part A, a number of important developments in early transition metal catalysts for olefin polymerization are presented. Examples include the design of new metallocene catalysts for improved stereospecific polymerization, non-metallocene early transition metal catalysts, and the combination of different catalysts for efficient design of new polymer architectures. Part B highlights some important advancements in the development of late transition metal catalysts for olefin polymerization. Late transition metal catalysts offer important and unique features that early transition metal catalyst systems do not possess, such as the ability to control polymer branching topology and tolerance and incorporation of polar functional olefins. In addition to metal-coordinated insertion polymerizations, the recent development of late transition metal complexes for living/controlled radical polymerizations is also highlighted in the end.

This volume is not intended to provide a comprehensive review of all the important developments in olefin polymerization catalysis in recent years; instead, it highlights a representative series of important examples in this area. I am extremely grateful to the experts who have contributed by writing a chapter and hope this volume will be helpful to researchers, teachers, and students interested in organometallic and polymerization chemistry.

Irvine, California
December 2008

Zhibin Guan

Contents

Part A Early Transition Metal Catalysis

Discovery and Development of FI Catalysts for Olefin Polymerization: Unique Catalysis and Distinctive Polymer Formation	3
Koji Kawai and Terunori Fujita	

Hafnocene-Based Olefin Polymerizations.....	47
T. Diesner, C. Troll, and B. Rieger	

Chain Shuttling Catalysis and Olefin Block Copolymers (OBCs)	65
Timothy T. Wenzel, Daniel J. Arriola, Edmund M. Carnahan, Phillip D. Hustad, and Roger L. Kuhlman	

Part B Late Transition Metal Catalysis

Iron-Based and Cobalt-Based Olefin Polymerisation Catalysts	107
Vernon C. Gibson and Gregory A. Solan	

Late Transition Metal Catalysts for the Copolymerization of Olefins and Polar Monomers	159
Brian L. Goodall	

Recent Progress in Late Transition Metal α-Diimine Catalysts for Olefin Polymerization	179
Zhibin Guan and Chris S. Popeney	

Structural and Mechanistic Aspects of Copper Catalyzed Atom Transfer Radical Polymerization	221
Tomislav Pintauer and Krzysztof Matyjaszewski	
Index	253

Discovery and Development of FI Catalysts for Olefin Polymerization: Unique Catalysis and Distinctive Polymer Formation

Koji Kawai and Terunori Fujita

Abstract This review describes the discovery and development of phenoxyimine-based catalysts (FI catalysts) for olefin polymerization. High-activity catalysts have been discovered on the basis of the “ligand oriented catalyst design concept,” a new catalyst design concept for olefin polymerization. The concept has created a series of highly active FI catalysts, many of which display high activities comparable to those of group 4 metallocene catalysts. In addition, FI catalysts can produce a wide variety of polymers that possess unique and unprecedented molecular architectures that are either difficult or impossible to achieve using conventional catalysts.

Keywords Block copolymer, FI catalysts, Living polymerization, Olefin polymerization, Phenoxy-imine

Contents

1	Introduction.....	4
2	Catalyst Design Concept for Acquiring High-Activity Catalysts.....	7
3	Discovery of Highly Active Molecular Catalysts for Ethylene Polymerization.....	9
3.1	Ethylene Polymerization Activity of FI Catalysts.....	10
3.2	Structures of FI Catalysts.....	11
3.3	Origin of the High Activity Displayed by FI Catalysts.....	13
3.4	Ethylene Polymerization Activity of Zr- and Ti-FI Catalysts.....	14
4	Ethylene Polymerization Behavior of FI Catalysts with Cocatalysts Other than MAO ...	17
4.1	$i\text{-Bu}_3\text{Al/Ph}_3\text{CB}(\text{C}_6\text{F}_5)_4$ Cocatalyst.....	17
4.2	MgCl_2 -Based Cocatalyst.....	18

K. Kawai and T. Fujita(✉)
Catalysis Science Laboratory, Research Center, Mitsui Chemicals Inc., 580-32 Nagaura,
Sodegaura-City, Chiba 299-0265, Japan
e-mail: terunori.fujita@mitsui-chem.co.jp

5	Synthesis of Unique Olefin-Based Materials with FI Catalysts.....	19
5.1	Vinyl- and Al-Terminated PEs.....	19
5.2	Well-Defined Multimodal PEs.....	22
5.3	Ultra-High Molecular Weight (Co)polymers.....	22
5.4	Highly Syndiotactic PPs.....	24
5.5	Highly Isotactic PPs.....	25
5.6	Stereo- and Regioirregular High Molecular Weight Poly(Higher α -Olefin)s.....	26
6	Living Olefin Polymerization.....	27
6.1	Living Ethylene Polymerization.....	28
6.2	The Origin of Living Polymerization.....	32
6.3	Stereospecific Living Propylene Polymerization.....	36
6.4	Syntheses of Well-Defined Polyolefinic Block Copolymers.....	39
6.5	Catalytic Production of Living Polymers.....	41
7	Summary.....	43
	References.....	43

1 Introduction

Polyolefinic materials, as represented by polyethylenes (PEs), polypropylenes (PPs), ethylene/ α -olefin amorphous copolymers, and ethylene/propylene/diene elastomers (EPDMs) are not only huge molecules, but they are also manufactured and consumed in huge amounts. Their worldwide consumption exceeded 100 million tons in the year 2006, and this is predicted to increase at an average annual growth rate of more than 5%. These materials display many useful properties, including low density, high mechanical strength, flexibility, and good processability. Moreover, these materials are cost-effective and, furthermore, possess good chemical inertness and recyclability. The applications include plastic shopping bags, food packages, shampoo and detergent bottles, containers, storage boxes, toys, disposable diapers, sneakers, bullet-proof vests, and automotive interior and exterior parts (e.g., instrument panels, glass run channels, door trim, fuel tanks, bumpers) (Fig. 1). Thus, they have become indispensable materials for modern living and directly impact our daily lives in countless beneficial ways.

As is well-known, most polyolefinic materials are produced using transition-metal-catalyzed olefin polymerization technology. While the multisited heterogeneous Ziegler–Natta catalysts represented by $MgCl_2$ -supported $TiCl_4$ catalysts currently dominate the market, molecular catalysts (single-site catalysts) represented by group 4 metallocene catalysts and constrained geometry catalysts (CGCs) are gaining an increasing presence in the market (Fig. 2).

Benefits of the single-site catalysts include the ability to produce polymers with controlled molecular weight, specific tacticity, improved molecular weight distribution, and better comonomer distribution and content. With these advantages, the single-site catalysts have allowed the preparation of a wide variety of new or differentiated polyolefinic materials, which include high-performance linear low-density PEs, polyolefinic elastomers, cyclic olefin copolymers, ethylene/styrene copolymers, highly isotactic and syndiotactic PPs (iPPs and sPPs), and highly syndiotactic polystyrenes (sPPS)



Fig. 1 Examples of polyolefin applications

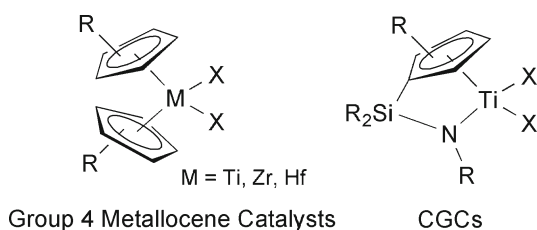


Fig. 2 General structures of group 4 metallocene catalysts and CGCs

[1–3]. Additionally, recently emerging non-metallocene single-site catalysts (Fig. 3) have enabled us to synthesize distinctive polymers such as hyperbranched PEs, ethylene/polar monomer copolymers, monodisperse poly(higher α -olefin)s, and higher α -olefin-based block copolymers, which are difficult or virtually impossible to produce using group 4 metallocene catalysts and CGCs [4–10].

Moreover, the molecular catalysts have provided systematic opportunities to study the mechanisms of the initiation, propagation, and termination steps of coordination polymerization and the mechanisms of stereospecific polymerization. This has significantly contributed to advances in the rational design of catalysts for the controlled (co)polymerization of olefinic monomers. Altogether, the development of high performance molecular catalysts has made a dramatic impact on polymer synthesis and catalysis chemistry. There is thus great interest in the development of new molecular catalysts for olefin polymerization with a view to achieving unique catalysis and distinctive polymer synthesis.

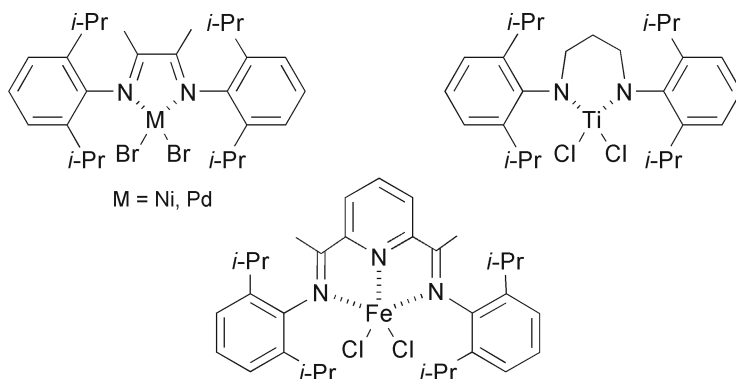


Fig. 3 Examples of non-metallocene single-site catalysts

In our own effort to develop new molecular catalysts for olefin polymerization, we have carried out research based on a “ligand oriented catalyst design concept,” a concept that is founded on the belief that, from among the catalyst components, ligands play the predominant role in polymerization and should have a flexible electronic nature as a necessary requirement for achieving high activity [11]. In our studies, we have deliberately focused on non-symmetric ligands since transition metal complexes incorporating such ligands have been investigated less than olefin polymerization catalysts.

Such approaches have resulted in the discovery of a number of highly active catalysts, including bis(phenoxo-imine) early transition metal complexes (FI catalysts) [12–15], bis(pyrrolide-imine) group 4 transition metal complexes (PI catalysts) [16–18], bis(indolide-imine) Ti complexes (II catalysts) [19], bis(phenoxo-ether) Ti complexes (FE catalysts) [20], and bis(imine-phenoxo) Ti and Zr complexes (IF catalysts) [21] (Fig. 4). Among these high-activity catalysts, FI catalysts exhibit the highest ethylene polymerization activities, exceeding those for group 4 metallocene catalysts and CGCs [12, 14].

FI catalysts combined with appropriate activators afforded a wide variety of polyolefinic materials with unique architectures [14]. The polymers include selective vinyl- and Al-terminated PEs [22, 23], well-defined and controlled multimodal PEs [24, 25], ultra-high molecular weight ethylene/propylene copolymers [26], and stereo- and regioirregular high molecular weight poly(higher α -olefins) [27]. In addition, these catalysts can produce highly isotactic and syndiotactic PPs [28–32] and polyolefinic block copolymers from ethylene, propylene, and higher α -olefins [33–35]. Moreover, and importantly, research on these catalysts for olefin polymerization has provided a lot of information on polymerization catalysis and mechanisms, including stereochemical and electronic requirements for accomplishing high activity, highly syndiospecific propylene polymerization with a C_2 -symmetric catalyst, high-incorporation ability for higher α -olefins, and highly controlled living olefin polymerization. Therefore, FI catalysts have offered extraordinary opportunities to synthesize polyolefinic materials possessing distinctive architectural

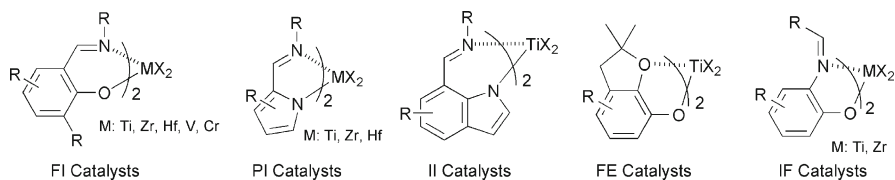


Fig. 4 Examples of highly active catalysts developed at Mitsui Chemicals

characteristics and at the same time offered a chance to study catalysis and mechanisms for olefin polymerization [11, 14]. Subsequent studies performed on FI catalysts by Busico, Cavallo, Coates, Mühlaupt, Pellecchia, Repo, Talsi and others have made significant contributions to the further development of this important class of new olefin polymerization catalysts [36–49].

In this contribution, we describe the discovery and application of phenoxy-imine ligated early transition metal complexes (FI catalysts) for olefin polymerization, including the concept behind our catalyst design, the discovery and the polymerization behavior of FI catalysts, and their applications to new polyolefinic materials.

2 Catalyst Design Concept for Acquiring High-Activity Catalysts

Historically, the discovery of highly active catalysts for ethylene polymerization has been the key to creating novel polymers with differentiated macromolecular structures, as is clearly demonstrated by the discovery of $\text{TiCl}_4/\text{R}_3\text{Al}$ catalysts, MgCl_2 -supported TiCl_4 catalysts, group 4 metallocene catalysts and CGCs. Learning from this history, we decided to pursue high activity since it would be the most fundamental prerequisite for polymerization catalysis. We believe that a high-activity catalyst that can bear modification enough to enhance a specific selectivity would in turn result in a desired product with satisfactory efficiency. Hence, the purpose of this research has been the discovery of high-activity ethylene polymerization catalysts and their applications to value-added polyolefinic materials with new or improved material properties.

A transition-metal-based olefin polymerization catalyst is generally comprised of a metal, ligand(s), a growing polymer chain, a coordinated olefin, and a cocatalyst (activator), as depicted in Fig. 5.

During the course of research into ethylene and propylene polymerization with group 4 metallocene catalysts, we noticed that catalysts with Cp-based ligands (Cp: cyclopentadienyl) possessing wider π -conjugation systems such as indenyl, fluorenyl, and phenyl Cp normally show higher activities; namely, the high-activity catalysts usually have a small energy gap between HOMO (the highest occupied molecular orbital) and LUMO (the lowest unoccupied molecular orbital) of the ligand. These results unambiguously indicate that the electronic properties of a ligand play a pivotal role in managing catalytic activity.

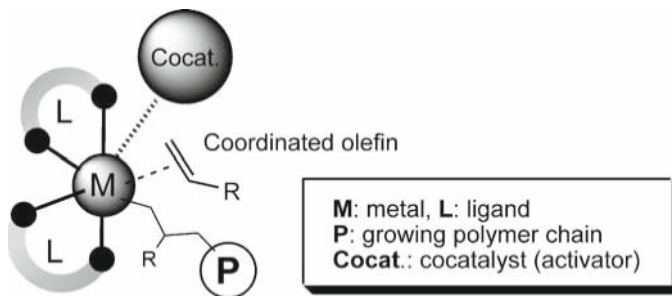


Fig. 5 Schematic structure of a molecular catalyst for olefin polymerization

To gain further insight into the effect of the electronic nature of a ligand, DFT calculations were performed on a model metallocene catalyst ($\text{H}_2\text{SiCp}_2\text{ZrMe}^+$) for ethylene polymerization. The results suggest that ethylene polymerization is a process that involves intense electron exchange between a ligand and a metal, probably to reduce the energy increase during the course of the polymerization. This fact suggests that, in an attempt to achieve high activity, ligands must be electronically flexible enough to receive electrons from the coordinated olefin through a metal and to release electrons whenever required to facilitate the olefin insertion process. We believe that this is potentially achieved by a ligand that possesses a small energy gap between HOMO and LUMO.

Because all transition metals (even Mn and Fe) inherently have olefin insertion ability, we have reasoned that the combination of a transition metal and electronically flexible ligand(s) can yield a highly active catalyst when activated, as long as any cationic species derived from the resulting complex has an appropriate electron deficiency (10- to 16-electron species) as well as a pair of *cis*-located sites for efficient polymerization. In short, we have postulated that ligands play the predominant role in controlling polymerization activity among the typical catalyst components of the catalyst and that the electronically flexible properties of ligands are a requirement for achieving high activity. We have given the name “ligand oriented catalyst design concept” to the concept that attaches great importance to the electronically flexible properties of the ligand [11, 18].

Since transition metal complexes bearing non-symmetric ligands had been less extensively investigated than olefin polymerization catalysts when we initiated this research, we deliberately focused on non-symmetric ligands that have an electronically flexible nature. We anticipated that such ligands might form non-symmetric polymerization sites depending on the coordination modes of the ligands, leading to the generation of unique microstructure polymers. Altogether, transition metal complexes featuring non-symmetric ligands that have electronically flexible properties were considered to be new and viable catalysts for olefin polymerization. Figure 6 summarizes our catalyst design procedures for developing highly active catalysts on the basis of the ligand oriented catalyst design concept.

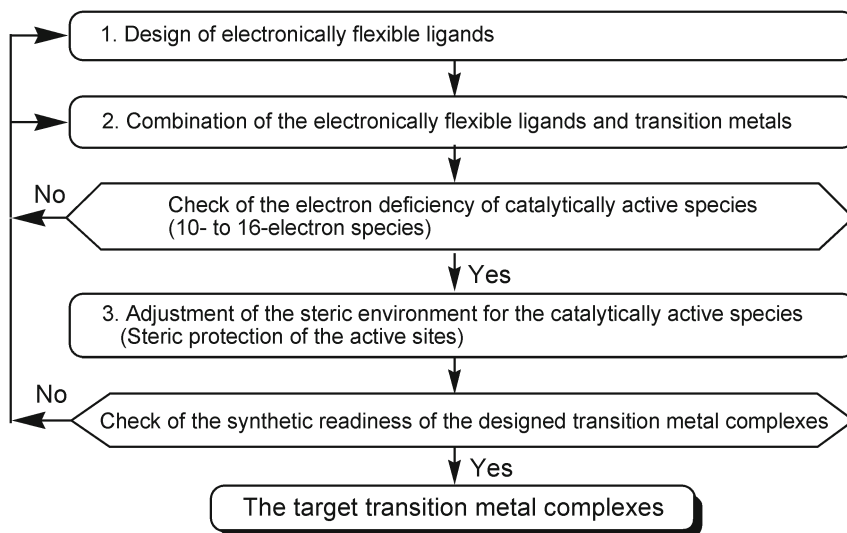


Fig. 6 Catalyst design procedures for the development of highly active catalysts

3 Discovery of Highly Active Molecular Catalysts for Ethylene Polymerization

Examples of non-symmetric and electronically flexible ligands are shown in Fig. 7, including neutral monoanionic as well as dianionic ligands. The ligands possess HOMO/LUMO energy gap values of <8.5 eV for neutral ligands and <7.0 eV for anionic ligands, at the MNDO-PM3 level calculations.

A large number of transition metal complexes whose cationic complexes are 10- to 16-electron species (including those with the ligands summarized in Fig. 7) were investigated to determine their potential as ethylene polymerization catalysts with methylaluminumoxane (MAO) activation at 25 °C under atmospheric pressure. As a result, we discovered a number of high-activity catalysts for ethylene polymerization that contain electronically flexible ligands [11].

Figure 8 displays examples of newly discovered catalysts, which include phenoxy-imine ligated early transition metal complexes (FI catalysts) [12–15], pyrrolide-imine ligated group 4 transition metal complexes (PI catalysts) [16–18], indolide-imine ligated Ti complexes (II catalysts) [19], phenoxy-ether ligated Ti complexes (FE catalysts) [20], imine-phenoxy ligated Ti and Zr complexes (IF catalysts) [21], and phenoxy-pyridine ligated Ti complexes (FP catalysts) [50]. The names of these catalysts are derived from the Japanese pronunciation of the ligands since these catalysts were discovered on the basis of the ligand oriented catalyst design concept. Many of the above high-activity catalysts display ethylene polymerization activities comparable to those obtained with group 4 metallocene catalysts and CGCs.

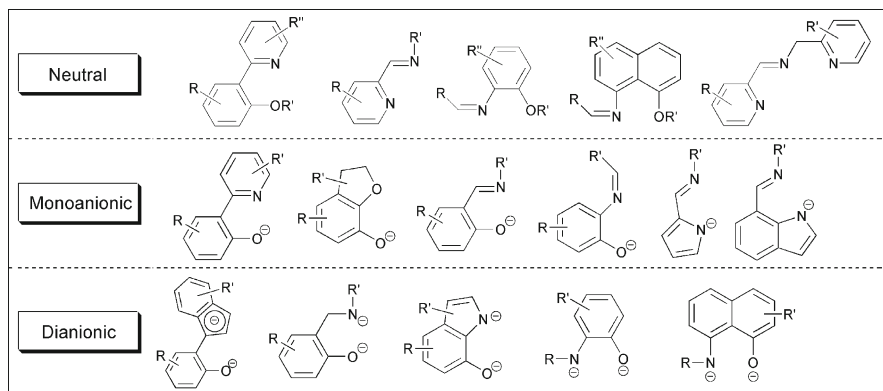


Fig. 7

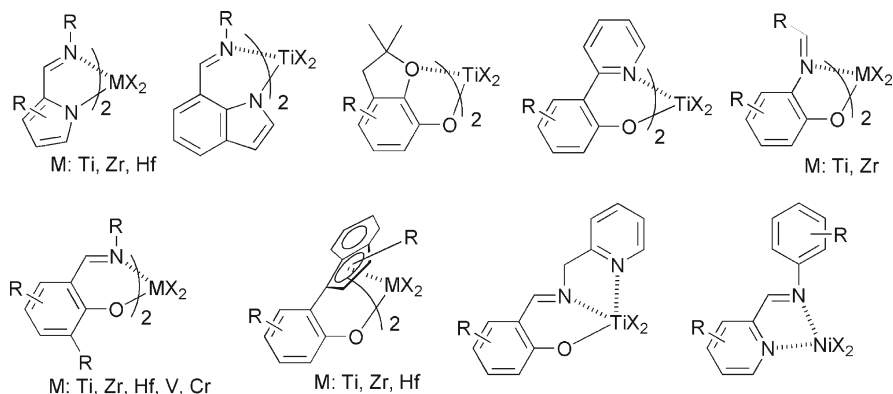
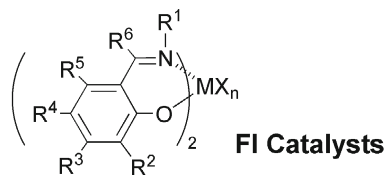


Fig. 8 Highly active catalysts discovered on the basis of the “ligand oriented catalyst design concept”

3.1 Ethylene Polymerization Activity of FI Catalysts

Among the highly active catalysts introduced above, bis(phenoxy-imine) early transition metal complexes (Fig. 9) in particular show strikingly high activities for the polymerization of ethylene [14, 51–54].

For example, a bis(phenoxy-imine) Zr complex, bis[*N*-(3-*tert*-butylsalicylidene)anilinato]zirconium(IV) dichloride (FI catalyst **1**), in combination with MAO at 25 °C under ethylene at atmospheric pressure displayed an extremely high activity of 519 kg mmol⁻¹ h⁻¹ (kg PE per mmol catalyst per h), which is an order of magnitude larger than that obtained with Cp₂ZrCl₂/MAO (20 kg mmol⁻¹ h⁻¹) under the same conditions. In addition, we revealed that Ti, Hf, V, and Cr congeners (FI catalysts **2–5**) with MAO activation also converted ethylene to PEs with very high



catalyst	MX_n	R^1	R^2	R^3	R^4	R^5	R^6
1	ZrCl_2	Ph	<i>t</i> -Bu	H	H	H	H
2	TiCl_2	Ph	<i>t</i> -Bu	H	H	H	H
3	HfCl_2	Ph	<i>t</i> -Bu	H	H	H	H
4	VCl_2	Ph	<i>t</i> -Bu	H	H	H	H
5	CrCl	Ph	<i>t</i> -Bu	H	H	H	H

Fig. 9 General structure of FI catalysts and structures of FI catalysts **1–5**

activities [2 3; 3 26; 4 4 (with EtAlCl_2); and 5 1 $\text{kg mmol}^{-1} \text{h}^{-1}$]. These results indicate that phenoxy-imine ligands can produce highly active catalysts when attached to a variety of transition metals, which supports the idea that ligands play the predominant role in controlling polymerization activity and electronically flexible ligands can engender highly active catalysts. An important feature of phenoxy-imine ligated early transition metal complexes is that they possess ligands that can be readily tailored synthetically from both an electronic and steric point of view, and hence possess a wide range of possibilities in terms of catalyst design.

Because phenoxy-imine ligated early transition metal complexes were discovered based on the ligand oriented catalyst design concept, we named the newly discovered complexes “FI catalysts”, following the Japanese pronunciation of the ligand *Fenokishi-Imin Haiishi* (*Haiishi* means a ligand). FI catalysts also stands for “Fujita group invented” catalysts. Since the discovery of FI catalysts, extensive research efforts have been devoted, in particular, to developing high-performance group 4 metal FI catalysts in both academic and industrial research groups [36–49]. Therefore, the following section deals with the structures, olefin polymerization catalysis, and unique polymer synthesis regarding group 4 metal FI catalysts, i.e., Ti-, Zr-, and Hf-FI catalysts.

3.2 Structures of FI Catalysts

Because an FI catalyst has a pair of non-symmetric phenoxy-imine ligands, it potentially possesses five isomers stemming from the coordination modes of ligands. Zr-, Ti-, and Hf-FI catalysts **1–3** display three sets of signals in ^1H NMR, attributed to the imine proton, suggesting that these FI catalysts exist as isomeric mixtures in solution, which is probably an intrinsic feature of FI catalysts. On the basis of the symmetry of the possible isomers **A–E** (Fig. 10), as well as the relative formation

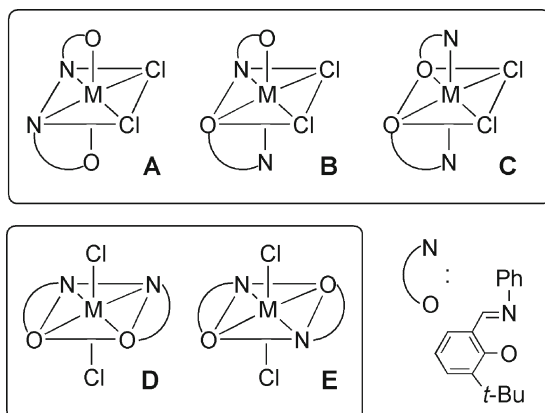


Fig. 10 Possible isomers of an FI catalyst

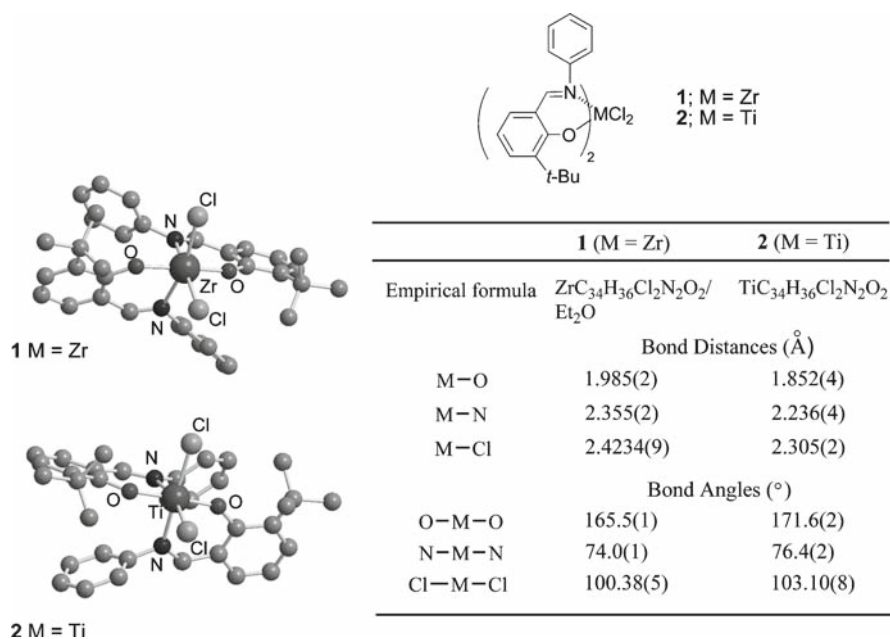


Fig. 11 Molecular structures of Zr- and Ti-FI catalysts **1** and **2**

energies of the isomers estimated by DFT calculations, we have concluded that FI catalysts predominantly exist as isomer **A** (*trans*-O, *cis*-N, and *cis*-Cl arrangement: C_2 symmetry) but some molecules exist as isomer **B** (*cis*-O, *cis*-N, and *cis*-Cl arrangement: C_1 symmetry) in solution [14, 24].

X-ray crystallographic analyses demonstrate that, in the solid state, Zr- and Ti-FI catalysts **1** and **2** possess approximately octahedrally coordinated metal centers and C_2 symmetry, with a *trans*-O, *cis*-N, and *cis*-Cl disposition (isomer **A**) (Fig. 11).

These results indicate that FI catalysts favor the isomer **A** structure, and that they can be present as a mixture of isomers **A** and **B** in solution. It is important to note that an FI catalyst generally exhibits fluxional character in solution, which can result in unique polymerization catalysis.

3.3 Origin of the High Activity Displayed by FI Catalysts

We postulated that the electronically flexible properties of the phenoxy-imine ligand are, in principle, responsible for the high activities of FI catalysts. However, the ethylene polymerization activities obtained with FI catalysts, in particular with Zr-FI catalyst **1**, were beyond our expectations. Therefore, DFT calculations were performed in order to gain information about the cause of the very high activity observed. The calculations for an ethylene-coordinated cationic methyl complex, generated from FI catalyst **1** and MAO indicate that the cationic complex possesses a distorted octahedral geometry with a *trans*-O, *cis*-N, and *cis*-Me/coordinated-ethylene (angle 74.6°) disposition (Fig. 12). This is potentially significant for achieving high activity because a crucial requirement for a high efficiency catalyst is to have a pair of *cis* located sites for polymerization [54].

Additionally, and interestingly, the DFT calculations suggest that the Zr–N bonds that lie on the same plane as the polymerization sites expand and contract according to the reaction coordinate of the ethylene insertion (2.23–2.34 Å), while the Zr–O bond length remains virtually unchanged (Fig. 13). From studying these results, we

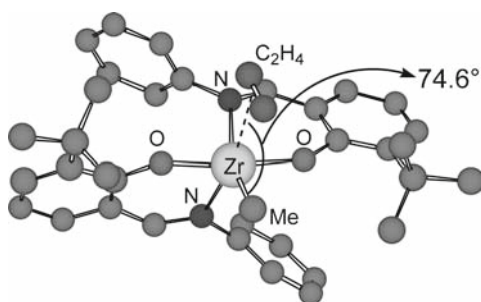


Fig. 12 Calculated structure of an ethylene-coordinated cationic methyl species derived from FI catalyst **1**

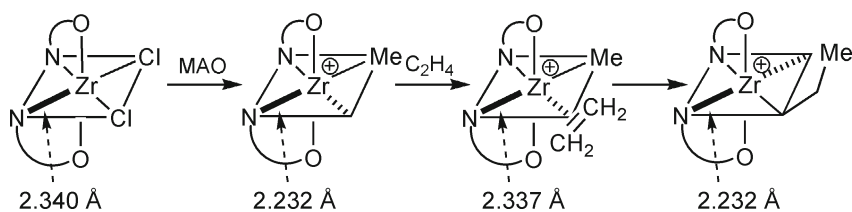


Fig. 13 DFT calculation results for ethylene polymerization with FI catalyst **1**/MAO

believe that this variable Zr–N bond length (which facilitates a smooth and flexible electron exchange between the metal and the ligands) and the *cis* located active sites, as well as the electronically flexible nature of the phenoxy-imine ligands, are responsible for the high polymerization activities of FI catalysts.

3.4 Ethylene Polymerization Activity of Zr- and Ti-FI Catalysts

The FI ligand structure has a significant influence on the ethylene polymerization activity; in particular, modification of the R² substituent has a dramatic effect on the activity (Table 1) [12, 54, 55]. Namely, R² substituents that are sterically smaller than a *t*-Bu group [i.e., *i*-Pr (**6**), Me (**7**)] significantly reduce the activity (activity < 1 kg mmol⁻¹ h⁻¹). By contrast, R² substituents that are sterically larger than the *t*-Bu group markedly enhance the activity. The activity is thus directly correlated to the steric bulk of the R² substituent. For example, in the sequence *t*-Bu (**1**, **8**) < adamantyl (**9**) < cumyl (**10**) < 1,1-diphenylethyl (**11**), the activity increases from 519 (**1**: R¹ = phenyl, R² = *t*-Bu) to 2383 kg mmol⁻¹ h⁻¹ (**11**: R¹ = phenyl, R² = 1,1-diphenylethyl).

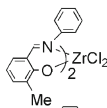
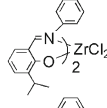
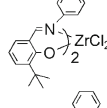
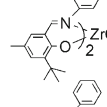
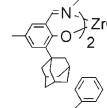
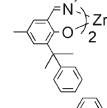
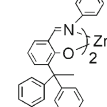
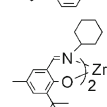
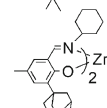
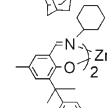
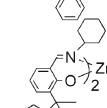
With a cyclohexyl group in the R¹ position, the R² effect is more pronounced. Zr-FI catalyst **12**, which has cyclohexyl as R¹, *t*-Bu as R², and methyl as R³, exhibits only 82 kg mmol⁻¹ h⁻¹ of activity, while the insertion of the 1,1-diphenylethyl group as R² (Zr-FI catalyst **15**) enhances the activity to 6552 kg mmol⁻¹ h⁻¹. This strikingly high activity corresponds to a catalyst turnover frequency (TOF) of 64,900 s⁻¹ atm⁻¹, which is two orders of magnitude greater than that seen with Cp₂ZrCl₂/MAO under identical conditions. This TOF is probably the largest recorded, not only for olefin polymerization, but for any catalytic reaction under atmospheric pressure conditions. Thus, the FI catalyst **15** displays the highest catalytic activity.

Our rationalization of the significant effect of R² with regard to the activity enhancement is as follows:

1. The sterically encumbered R² substituents give steric protection to the oxygen-donors that are attached to the metal centers from coordination with Lewis acids such as MAO, or from another molecule of the catalytically active cationic species, which are supposed to be highly electrophilic. The coordination increases steric congestion near the polymerization center, which at least hampers ethylene coordination to the metal. Even worse, it may cause catalyst decay by, for instance, loss of the ligand.
2. Large R² substituents induce effective ion-separation between the cationic active species and an anionic cocatalyst, which allows more space for ethylene coordination to the metal and for its insertion into the carbon–metal bond. In addition, electronically, the ion separation increases the electrophilicity of the catalytically active species and hence enhances the reactivity toward ethylene.

Conversely, Ti-FI catalysts with MAO normally show lower (but still high) ethylene polymerization activities and form higher molecular weight PEs relative to the Zr congeners. The ethylene polymerization activities of Ti-FI catalysts were also

Table 1 Ethylene polymerization with Zr-FI catalysts

Entry	FI Catalyst	Activity ^a (kg mmol ⁻¹ h ⁻¹)
1	7 ; 	0.4
2	6 ; 	0.9
3	1 ; 	519
4	8 ; 	331
5	9 ; 	714
6	10 ; 	2096
7	11 ; 	2383
8	12 ; 	82
9	13 ; 	434
10	14 ; 	4315
11	15 ; 	6552

Polymerization conditions: in toluene (250 mL); atmospheric ethylene (0.1 MPa); 25 °C; 5 or 10 min; MAO (1.25 mmol); Al/Zr = 250 (Entries 1 and 2), 62,500 – 125,000 (Entries 3 - 7)

^akg PE per mmol Zr per h

Table 2 Ethylene polymerization with fluorinated Ti-FI catalysts

Entry	FI Catalyst	R ¹	$M_v/10^{-3}$	Activity ^a (kg mmol ⁻¹ h ⁻¹)
1	2		326	3.58
2	16		419	3.96
3	17		623	34.8
4	18		378	43.3
5	19		542	3.6
6	20		1,365	40.3

Polymerization conditions: toluene 250 mL, catalyst 0.5–5.0 μmol , MAO 1.25 mmol, 5 min 25 °C, ethylene gas feed 100 Lh⁻¹

^akg PE per mmol catalyst per h

enhanced by ligand modification. Unlike Zr-FI catalysts, the introduction of two or more electron-withdrawing substituents (i.e., F, CF₃) to the phenyl group on the imine-N has a significant effect on the polymerization activity. A summary of ethylene polymerization results with Ti-FI catalysts/MAO is shown in Table 2 [56, 57].

As can be seen from Table 2, Ti-FI catalysts **18** and **20** exhibit very high ethylene polymerization activities (**18** 43.3 kg mmol⁻¹ h⁻¹; **20** 40.3 kg mmol⁻¹ h⁻¹), exceeding those seen with early group 4 metallocene catalysts, Cp₂MCl₂ (M = Ti and Zr) with MAO, under the given conditions. To our knowledge, the activity displayed by **18** is the highest for a Ti-based ethylene polymerization catalyst.

The activity enhancement is probably ascribed to the increased electrophilicity of the active Ti species, demonstrating that the electrophilicity of the Ti center plays a dominant

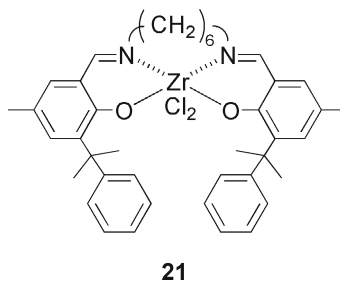


Fig. 14 Structure of Zr-FI catalyst **21**

role in determining the catalytic activity of the Ti-FI catalysts. This observation is in sharp contrast to the behavior of group 4 metallocene catalysts, whose activity is decreased by introducing electron-withdrawing substituent(s) to cyclopentadienyl ligands.

From an industrial point of view, catalysts that exhibit higher activities at higher temperatures are urgently required. The quest for such catalysts is economically driven, since higher temperature activity relates to faster polymerization kinetics and higher throughput of product. Although early FI catalysts displayed noticeably reduced activities at elevated temperatures, elaborate catalyst design work has given rise to the development of a number of FI catalysts that have outstanding performance at higher temperatures with excellent efficiency. For example, Zr-FI catalyst **21** (Fig. 14) with MAO demonstrates a very high activity of $142.9 \text{ kg mmol}^{-1} \text{ h}^{-1}$ under commercially relevant solution polymerization conditions ($150 \text{ }^\circ\text{C}$, 3.0 MPa ethylene pressure) [58]. This remarkably high activity at the high temperature of $150 \text{ }^\circ\text{C}$ is viewed as promising from a commercial point of view.

4 Ethylene Polymerization Behavior of FI Catalysts with Cocatalysts Other than MAO

The ethylene polymerization behavior of FI catalysts has been described in previous sections. It is often observed that the cocatalyst that is employed has an influence on the catalytic behavior of a transition metal-based olefin polymerization catalyst. FI catalysts can exhibit unique catalytic behavior depending on the cocatalyst that is used for polymerization.

4.1 *i*-Bu₃Al/Ph₃CB(C₆F₅)₄ Cocatalyst

Ti-, Zr- and Hf-FI catalysts show totally different catalytic behavior when activated with *i*-Bu₃Al/Ph₃CB(C₆F₅)₄. Ethylene polymerizations using these FI catalysts in combination with *i*-Bu₃Al/Ph₃CB(C₆F₅)₄ provide markedly enhanced molecular weight PEs with lower activities (but still appreciable) compared to those using MAO activation [54, 59]. For example, Zr-FI catalyst **1** (Fig. 9) combined with *i*-Bu₃Al/Ph₃CB(C₆F₅)₄ at $50 \text{ }^\circ\text{C}$ under atmospheric pressure produces a PE with the

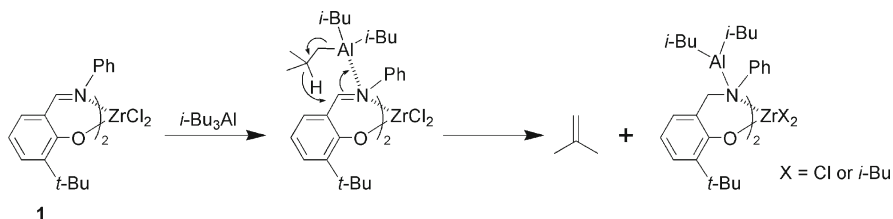


Fig. 15 Reaction scheme for the formation of a phenoxy-amine complex

exceptionally high viscosity-average molecular weight (M_v) of 5,050,000 and with a high activity of $11 \text{ kg mmol}^{-1} \text{ h}^{-1}$ (MAO activation, M_v 10,000, activity $519 \text{ kg mmol}^{-1} \text{ h}^{-1}$). This is one of the highest molecular weight PEs ever prepared. Likewise, many of the FI catalysts in combination with $i\text{-Bu}_3\text{Al}/\text{Ph}_3\text{CB}(\text{C}_6\text{F}_5)_4$ afford ultra-high molecular weight PEs ($M_v > 3,000,000$) with notably high activities.

^1H NMR studies of a mixture of Zr-FI catalyst **1** and $i\text{-Bu}_3\text{Al}$ at 25°C suggested that the phenoxy-imine ligand is reduced by $i\text{-Bu}_3\text{Al}$ (and its contaminant $i\text{-Bu}_2\text{AlH}$) to a phenoxy-amine ligand with the concomitant production of isobutene. The addition of $\text{Ph}_3\text{CB}(\text{C}_6\text{F}_5)_4$ and then ethylene gas to the resulting mixture in the NMR tube gave PE. These results indicate that Zr-FI catalyst **1** with $i\text{-Bu}_3\text{Al}/\text{Ph}_3\text{CB}(\text{C}_6\text{F}_5)_4$ forms a bis(phenoxy-amine) complex with a $i\text{-Bu}_2\text{Al}$ group attached to the amine-donor as a catalytically active species (Fig. 15). Similar observations (i.e., imine reduction with $i\text{-Bu}_3\text{Al}$ to form amine-functionality) were made for the corresponding Ti- and Hf-FI catalysts. The sterically encumbered amine moiety $\text{PhNAl}(i\text{-Bu})_2$ is probably responsible for the formation of ultra-high molecular weight polymers.

4.2 MgCl_2 -Based Cocatalyst

We found that $\text{MgCl}_2/\text{R}_m\text{Al}(\text{OR}')_n$ works as a good cocatalyst for FI catalysts [15, 60–63]. The electronic interaction between the O/N heteroatoms in the ligands and the MgCl_2 is presumably responsible for the cocatalytic performance. The combinations of FI catalysts and $\text{MgCl}_2/\text{R}_m\text{Al}(\text{OR}')_n$ can form highly active single-site catalysts (Ti-FI catalysts), exceptionally active catalysts (Zr-FI catalysts), or highly active, thermally robust, single-site catalysts (V-FI catalysts) for ethylene polymerization. For example, Ti-FI catalyst **22** (Fig. 16) combined with $\text{MgCl}_2/i\text{-Bu}_m\text{Al}(\text{OR}')_n$ displays high ethylene polymerization activity ($36.3 \text{ kg mmol}^{-1} \text{ h}^{-1}$, 0.9 MPa ethylene pressure, 50°C) and provides PE with a narrow molecular weight distribution (M_w/M_n) of 2.40 [60]. This represents the first example of an MAO- and borate-free, highly active, single-site Ti catalyst system.

Additionally, Zr-FI catalyst **23** (Fig. 16) with $\text{MgCl}_2/i\text{-Bu}_m\text{Al}(\text{OR}')_n$ polymerizes ethylene with strikingly high activity ($1819 \text{ kg mmol}^{-1} \text{ h}^{-1}$, 0.9 MPa ethylene pressure, 50°C) [62, 63]. Moreover, V-FI catalyst **24** (Fig. 16) with $\text{MgCl}_2/\text{Et}_n\text{Al}(\text{OR}')_m$ exhibits high activity at elevated temperatures ($65 \text{ kg mmol}^{-1} \text{ h}^{-1}$, atmospheric

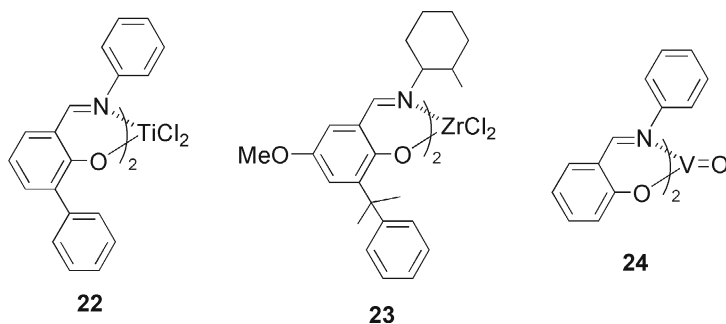


Fig. 16 Structures of FI catalysts 22–24

ethylene pressure, 75 °C) and is the first reported example of a highly active, thermally robust, single-site V olefin polymerization catalyst [61]. A reasonable hypothesis for these high performance catalyst combinations is that the $R_nAl(OR)_m$ species function as in-situ alkylating reagents for FI catalysts as well as scavengers in a polymerization system, and that the $MgCl_2$ that is used acts as a Lewis acid to generate a cationic active species from an alkylated FI catalyst.

It turns out that FI catalyst/ $MgCl_2/R_nAl(OR)_m$ combinations are in fact supported and, therefore, possess a technological advantage vis-à-vis control over polymer morphology, which is essential for commercial applications. The development of $MgCl_2$ -supported Zr-FI catalysts (e.g., **25**, Fig. 17) allows the preparation of extremely high molecular weight PEs ($M_v > 3,000,000$) with an exceptionally high bulk density value of 0.50 g mL^{-1} , which is probably the highest bulk density ever achieved for PEs. Additionally, $MgCl_2$ -supported Zr-FI catalysts allow access to ultra-high molecular weight ($M_v > 3,000,000$) non-coherent spherical PE particles of $10 \mu\text{m}$ in size (Fig. 17) [15]. It should be emphasized that $MgCl_2/R_nAl(OR)_m$ can function as cocatalyst and support for the early-to-late transition metal complexes that possess heteroatom-based ligands.

5 Synthesis of Unique Olefin-Based Materials with FI Catalysts

5.1 Vinyl- and Al-Terminated PEs

Upon activation with MAO, a series of Zr-FI catalysts incorporating phenoxy-cycloalkylidene ligands are capable of producing vinyl-terminated low molecular weight PEs, with high productivity [23]. For example, at 25 °C FI catalysts **26–30** (Fig. 18) with MAO polymerize ethylene to afford vinyl-terminated low molecular weight PEs (M_w 2000–14,000, vinyl selectivity 90–96%) while maintaining higher catalytic activities than Cp_2ZrCl_2/MAO ($28 \text{ kg mmol}^{-1} \text{ h}^{-1}$) under the same conditions (Table 3). Product analyses have revealed that the vinyl-terminated PEs have linear structures with practically no branching.

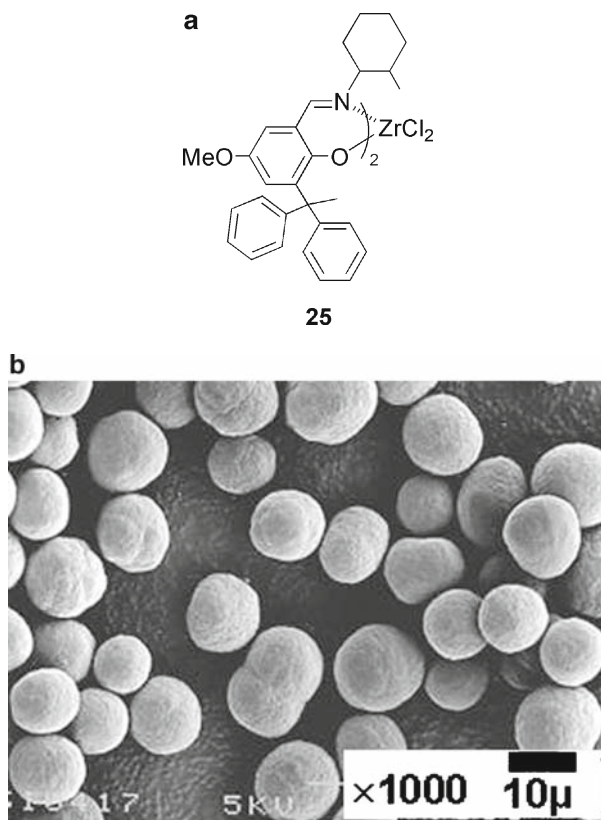


Fig. 17 Ultra-high molecular weight non-coherent spherical PE particles formed with **25**/ MgCl_2

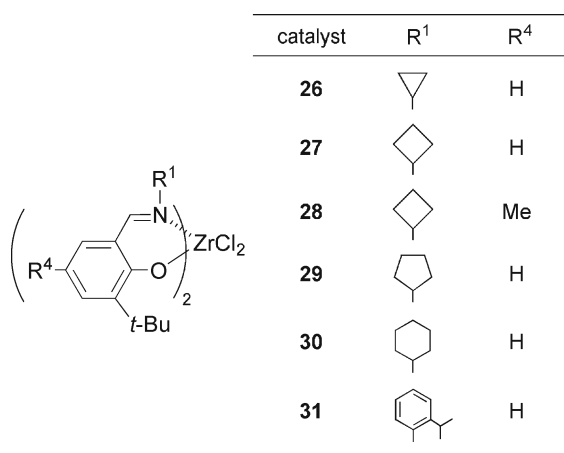


Table 3 Ethylene polymerization results with Zr-FI catalysts **26–30**

Entry	FI catalyst	Activity ^a (kg mmol ⁻¹ h ⁻¹)	M_w^b ($\times 10^{-3}$)	M_w/M_n^b	Vinyl end ^c (%)
1	26	50.4	4.4	2.0	91
2	27	31.6	2.0	1.7	95
3	28	22.0	2.0	1.7	94
4	29	67.2	3.6	2.1	96
5	30	87.7	14	1.7	90

Conditions: 25 °C, atmospheric pressure, 5 min, ethylene gas feed 100 L h⁻¹, catalyst 0.5 μ mol, MAO 0.625 mmol as Al, toluene 250 mL

^akg polymer per mmol catalyst per h

^bDetermined by GPC

^cDegree of vinyl unsaturation at one of the two polymer chain ends, determined by ¹H NMR

These are the first examples of group 4 metal-based catalysts that yield vinyl-terminated low molecular weight PEs with high efficiency at ambient temperatures. The vinyl-terminated low molecular weight PEs can be transformed by chain-end functionalization to form end-functionalized PEs. For example, the vinyl-terminated PEs are readily transformed to the corresponding epoxy-terminated PEs by H₂O₂ oxidation, and to diol-terminated PEs by subsequent hydrolysis, allowing the creation of PE/polyethylene glycol block copolymers and polyesters with PE branches. In addition, these PEs may serve as macromonomers in copolymerization with ethylene or α -olefins to give long-chain branched polymers, which are anticipated to have a good combination of material properties and processability.

Ethylene pressure studies have revealed a first-order dependence on ethylene for both the rate of chain propagation and the rate of chain transfer. This polymerization behavior together with X-ray analyses and DFT calculations has provided strong support for β -H transfer to an incoming monomer, which is responsible for the production of vinyl-terminated PEs. The calculations thus suggest that the catalysts disfavor β -H transfer to the Zr metal because of the extreme instability of the Zr hydride species that is produced in such a chain transfer process.

Conversely, we have also demonstrated that Zr-FI catalyst **31** (Fig. 18) having a 2-*i*-Pr group on the imine-N in combination with MAO or MAO plus trimethylaluminum exhibits a marked preference for chain transfer to aluminum, and quantitatively generates Al-terminated PEs (Al-PEs) possessing low-to-very-high molecular weights and narrow-to-broad molecular weight distributions with high productivity (Table 4) [22].

The isopropyl group discourages β -H transfer, leading to the exclusive formation of Al-PEs. The Al-PEs can be readily transformed to a variety of functionalized PEs and to PE-based and polar polymer-based block and graft copolymers, using established methods. The selective synthesis of vinyl- and Al-terminated PEs with Zr-FI catalysts shows the critical importance of the substituent on the imine-N for polymerization catalysis.

Table 4 Ethylene polymerization results for Zr-FI catalysts **1** and **31** with MAO or MAO/tri-methylaluminum (TMA)

Entry	FI catalyst	MAO (mmol)	TMA (mmol)	Al/Zr	Activity ^a (kg mmol ⁻¹ h ⁻¹)	M_w^b ($\times 10^{-3}$)	M_w/M_n^b	V/M ^c
1	1	1.250	0	2500	116	9	2.4	47/53
2	31	1.250	0	2500	66	90	2.0	0/100
3	31	0.625	0	1250	66	159	2.3	0/100
4	31	0.250	0	500	58	716	2.6	0/100
5	31	0.250	3.5	7500	34	12	2.0	0/100
6 ^d	31	0.250	0.2	900	41	201	5.9	0/100

Conditions: 25 °C, atmospheric pressure, 5 min, ethylene gas feed 100 L h⁻¹, catalyst 0.5 μ mol

^akg polymer per mmol catalyst per h

^bDetermined by GPC

^cChain-end group: vinyl/methyl (molar ratio)

^d30 min instead of 5 min

5.2 Well-Defined Multimodal PEs

As described, an FI catalyst potentially possesses five isomers arising from the coordination modes of ligands in an octahedral geometry, suggesting that an FI catalyst has the ability to form well-defined multimodal polymers that are expected to possess an excellent combination of material properties and processability. In fact, on activation with MAO, Zr-FI catalyst **32** furnishes uni-, bi- and tri-modal PEs in a controlled manner, simply by varying the polymerization temperatures (Fig. 19) [24, 25].

¹H, ¹³C and ¹⁵N NMR studies have suggested that **32** exists as a mixture of isomers. In addition, the multimodal PEs formed with **32**/MAO possess highly linear structures, and polymerization time and Al/Zr ratio have little influence on catalytic activities and multimodal behavior. Altogether, we can conclude that the multimodal behavior originates from isomers of the catalytically active species. These are the first examples of well-defined bi- and tri-modal PEs originating from structural isomers that arise from different modes of the ligand coordination. These results, therefore, provide a unique strategy for producing well-defined multimodal polyolefins by a single homogeneous catalyst in a single-stage polymerization process.

5.3 Ultra-High Molecular Weight (Co)polymers

One goal for olefin-based polymers has been to develop catalysts that provide high molecular weight polymers, since olefin-based polymers with high molecular weights display better mechanical properties relative to those with low molecular weights. As described, an FI catalyst combined with *i*-Bu₃Al/Ph₃CB(C₆F₅)₄, which forms a phenoxy-amine complex as a catalytically active species, can produce ultra-high molecular weight olefin-based polymers. For example, Zr-FI catalyst **33** with

$i\text{-Bu}_3\text{Al}/\text{Ph}_3\text{CB}(\text{C}_6\text{F}_5)_4$ at 70 °C under 0.9 MPa ethylene/propylene total pressure provides an exceptional molecular weight amorphous ethylene/propylene copolymer with a uniform microstructure (propylene content 20 mol%) and a M_w of 10,200,000 (vs. PS standards) (M_w/M_n 2.52) (Fig. 20), displaying a very high activity of 36 kg $\text{mmol}^{-1} \text{h}^{-1}$ (kg polymer per mmol catalyst per h) [26].

The molecular weight (M_w 10,200,000) represents the highest molecular weight known to date for a linear, synthetic copolymer. DFT calculations suggest that steric congestion, derived from the triethylsilyl group and the amine moiety, near the polymerization reaction center diminishes the rates of chain termination or transfer processes yet permits the monomer access to the active site and the monomer's insertion into the metal–carbon bond (Fig. 21).

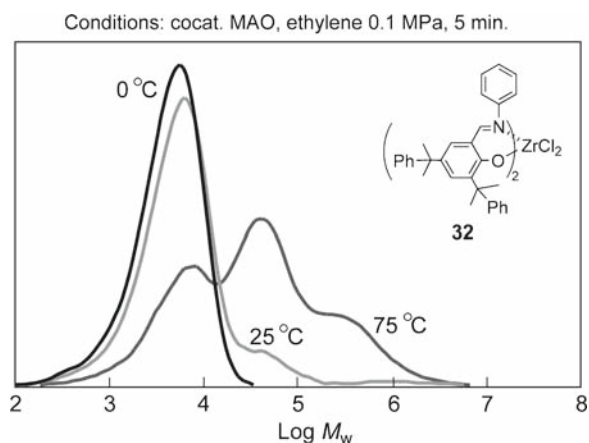


Fig. 19 GPC profiles of PEs formed with Zr-FI catalyst **32**/MAO at different temperatures

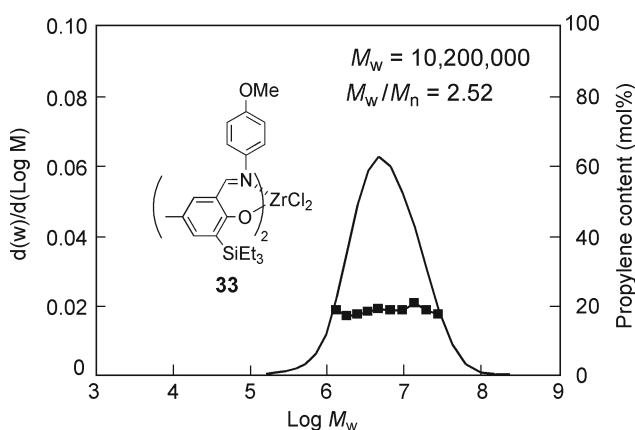


Fig. 20 GPC-IR chart for the ethylene/propylene copolymer formed with Zr-FI catalyst **33**/ $i\text{-Bu}_3\text{Al}/\text{Ph}_3\text{CB}(\text{C}_6\text{F}_5)_4$

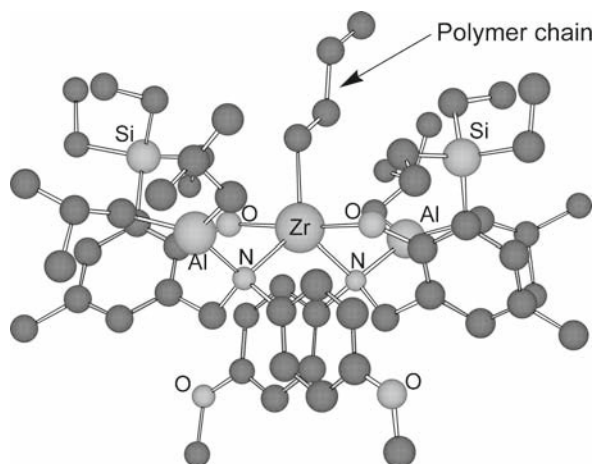


Fig. 21 Calculated structure of an active species derived from Zr-FI catalyst **33** with *i*-Bu₃Al/Ph₃CB(C₆F₅)₄ cocatalyst system (polymer chain model: *n*-butyl group). Reproduced with permission from Ishii et al. [26]. Copyright 2002, Wiley-VCH.

Additionally, Ti-FI catalyst **2** forms an ultra-high molecular weight atactic PP (aPP) (M_w 8,286,000, no T_m) with a somewhat broad molecular weight distribution (M_w/M_n 4.15) [32]. The molecular weight makes it one of the highest molecular weight aPPs ever synthesized. The ultra-high molecular weight (co)polymers described above may find applications as additives, compatibilizers, and adhesives.

5.4 Highly Syndiotactic PPs

An FI catalyst normally assumes a C_2 -symmetric *trans*-O, *cis*-N, and *cis*-Cl configuration as the predominant isomer. In addition, DFT calculations suggest that a catalytically active species derived from an FI catalyst favors a C_2 -symmetric configuration with a *trans*-O, *cis*-N, and *cis*-polymer chain/coordinated olefin arrangement. Thus, FI catalysts have been targeted as catalysts capable of producing iPP via a site-control mechanism.

With MAO activation, Zr- and Hf-FI catalysts **1** and **3** exhibit fairly high reactivity toward propylene and produce propylene oligomers [64, 65]. Conversely, the corresponding Ti-FI catalyst/MAO **2** forms semicrystalline PP (1 °C polymerization), which displays a peak melting temperature of 97 °C, indicative of the formation of a stereoregular polymer. To our surprise, microstructural analysis by ¹³C NMR indicates that the resultant polymer is syndiotactic (*rr* 79%), and that a chain-end control mechanism is responsible for the observed stereocontrol, regardless of the C_2 symmetric catalyst ([28]; for the first report on syndiospecific propylene

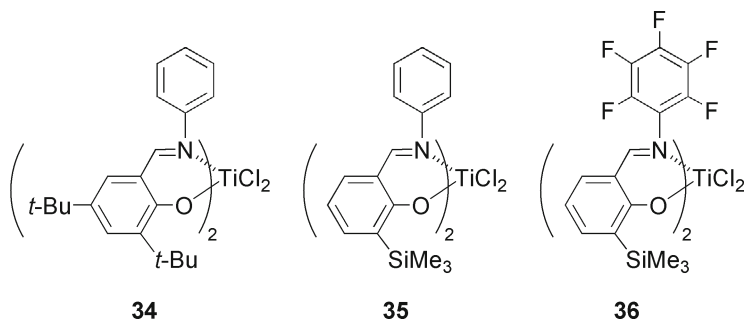


Fig. 22 Structures of Ti-FI catalysts **34–36**

polymerization, living ethylene and propylene polymerization, and block copolymer synthesis with Ti-FI catalysts, see [29]). Based on combinatorial methods, Coates and coworkers obtained Ti-FI catalyst **34** (Fig. 22), which is a modified version of **2** and has an additional *t*-Bu group in the phenoxy-benzene ring [66]. **34**/MAO displays propylene polymerization behavior similar to **2** and forms moderately syndiotactic PPs. These results show that a combinatorial approach can be used for the screening of catalysts for stereoselective propylene polymerization.

Further research has resulted in the discovery of Ti-FI catalyst **35** (Fig. 22), which possesses a trimethylsilyl group *ortho* to the phenoxy-O and which generates a highly syndiotactic PP (*rr* 91%, 1 °C polymerization) with a very high melting temperature (T_m) of 140 °C [28]. Moreover, the corresponding fluorinated Ti-FI catalyst **36** (Fig. 22) with MAO at 0 °C affords enhanced tacticity PP (*rr* 94%) with an extremely high T_m of 156 °C, representing one of the highest T_m s for sPPs ever synthesized [30]. A detailed propylene polymerization mechanism with Ti-FI catalysts/MAO will be discussed later.

5.5 Highly Isotactic PPs

Although, on activation with $i\text{-Bu}_3\text{Al}/\text{Ph}_3\text{CB}(\text{C}_6\text{F}_5)_4$, a Ti-FI catalyst provides ultra-high molecular weight aPPs, as introduced, Zr- and Hf-FI catalysts with the same cocatalysts can mediate isoselective propylene polymerization. For example, Zr- and Hf-FI catalysts **1** and **3** combined with $i\text{-Bu}_3\text{Al}/\text{Ph}_3\text{CB}(\text{C}_6\text{F}_5)_4$ at 25 °C to produce iPPs with high molecular weights (**1** M_w 209,000, M_w/M_n 2.42, *mm* 46%, T_m 104 °C; **3** M_w 412,000, M_w/M_n 2.15, *mm* 69%, T_m 124 °C) [32]. The active species for the isoselective polymerization is a phenoxy-amine ligated Zr or Hf complex. Elaborate catalyst design work focusing on the substituents *ortho* to the phenoxy-O and on the imine-N has led to the discovery of FI catalysts that yield highly isotactic PPs that are comparable to those made by the best heterogeneous Ziegler–Natta catalysts. Namely, Zr- and Hf-FI catalysts **13** and **37** (Fig. 23) form highly isotactic PPs (25 °C polymerization; **13** *mmmm* 97%, **37** *mmmm* 97%) with exceptionally high peak melting temperatures (**13** 164 °C, **37** 165 °C) [31].

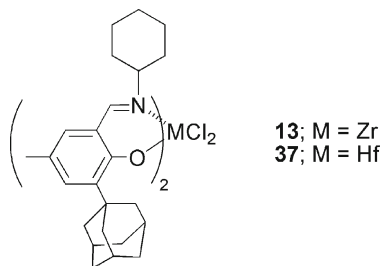


Fig. 23 Structures of Zr- and Hf-FI catalysts **13** and **37**

The T_m s and the isotacticity obtained with these FI catalysts represent some of the highest values for iPPs ever synthesized. The isotactic propylene polymerization proceeds via a 1,2-insertion with a site-control mechanism.

The production of highly isotactic PPs with Zr- and Hf-FI catalysts/*i*-Bu₃Al/Ph₃CB(C₆F₅)₄ (phenoxy-amine complexes; site-controlled polymerization with 1,2-insertion) is in sharp contrast to that of highly syndiotactic PPs with Ti-FI catalysts/MAO (phenoxy-imine complexes; chain-end controlled polymerization with 2,1-insertion), which will be described later [64].

5.6 Stereo- and Regioirregular High Molecular Weight Poly(Higher α -Olefin)s

While Ti-FI catalysts in combination with MAO are poor catalysts for higher α -olefin polymerization, on activation with *i*-Bu₃Al/Ph₃CB(C₆F₅)₄ Ti-FI catalysts display unique polymerization behavior toward these olefins [27, 67]. The active species generated from Ti-FI catalysts with *i*-Bu₃Al/Ph₃CB(C₆F₅)₄ are phenoxy-amine ligated Ti complexes, as already discussed. For example, at 25 °C Ti-FI catalyst **2** (Fig. 9) favors the 2,1-insertion of 1-hexene and forms high molecular weight (M_w 846,000, M_w/M_n 1.65) atactic poly(1-hexene)s having ca. 50 mol% of regioirregular units with high efficiency (Table 5)

Likewise, the same catalyst system produces high molecular weight atactic poly(1-octene)s (M_w 906,000, M_w/M_n 1.68), poly(1-decene)s (M_w 850,000, M_w/M_n 1.75), and poly(4-methyl-1-pentene)s (M_w 1,450,000, M_w/M_n 1.71), all of which include frequent regio-errors (Table 5). To the best of our knowledge, the molecular weight of the poly(4-methyl-1-pentene) is the highest encountered for homogeneous olefin polymerization catalysts. Ethylene/higher α -olefin copolymers having a wide variety of higher α -olefin contents were prepared with Ti-FI catalyst **2**/*i*-Bu₃Al/Ph₃CB(C₆F₅)₄.

Considering that 2,1-insertion normally encourages chain termination (which causes low molecular weights), the production of high molecular weight regioirregular poly(higher α -olefin)s is highly significant. These represent the first examples of stereo- and regioirregular high molecular weight poly(higher α -olefin)s (“ultra-random polymers”).

Table 5 Higher α -olefin polymerization results for Ti-FI catalyst **2** with i -Bu₃Al/Ph₃CB(C₆F₅)₄

Entry	Monomer	Activity ^a	M_w^b	M_w/M_n^b
		(kg mmol ⁻¹ h ⁻¹)	($\times 10^{-3}$)	
1	1-Hexene	1.30	846	1.65
2	1-Octene	1.94	906	1.68
3	1-Decene	2.59	850	1.75
4	4-Methyl-1-pentene	3.00	1450	1.71

Conditions: 25 °C, atmospheric pressure, 20 min, monomer 0.211 mol, *n*-heptane 90 mL, pretreated solution of FI catalyst **2** (5 μ mol)/*i*-Bu₃Al (0.15 mmol), Ph₃CB(C₆F₅)₄ 6 μ mol, *i*-Bu₃Al 50 μ mol

^akg polymer per mmol catalyst per h

^bDetermined by GPC

To our surprise, the Ti-FI catalyst **2**/*i*-Bu₃Al/Ph₃CB(C₆F₅)₄ system displays higher activities toward higher α -olefins with sterically bulkier substituents (activity order: 4-methyl-1-pentene > 1-decene > 1-octene > 1-hexene) (Table 5). This is remarkable, because an olefin polymerization catalyst generally exhibits lower reactivity toward sterically larger olefins due to steric hindrance. This highly unusual behavior can be explained as follows: a sterically bulkier side chain derived from the last inserted higher α -olefin of the growing polymer chain opens the phenoxy–amine ligands wider, which facilitates the higher α -olefin's coordination to the metal and its insertion into the metal–carbon bond. DFT calculations suggest that one of the amine-donors of the phenoxy-amine ligands is detached during the course of the polymerization (Fig. 24), providing a wider space for polymerization [27].

Surprisingly, the polymerization rate has practically a zeroth-order dependence on the concentration of the monomer, which is a rare example for a group 4 metal-based catalyst. Although the reason for the zeroth-order dependence is unclear at the current time, one possible explanation is that, under the conditions examined, the cationic complex virtually exists as a (higher α -olefin)-coordinated form, presumably due to the highly electrophilic and sterically open nature of the cationic active species.

6 Living Olefin Polymerization

The production of polymers with perfect control over the molecular weight, the composition, and the architecture of the polymer has been a long-standing challenge for synthetic polymer chemists. Living olefin polymerization is a powerful tool for controlling the molecular weight as well as the composition and architecture of olefin-based polymers, and thus it can be used for the preparation of precisely controlled polyolefinic materials (living polymers). Despite significant advances in living radical, anionic, and cationic polymerizations, the development of living olefin polymerization catalysts has been notably slower. We recently

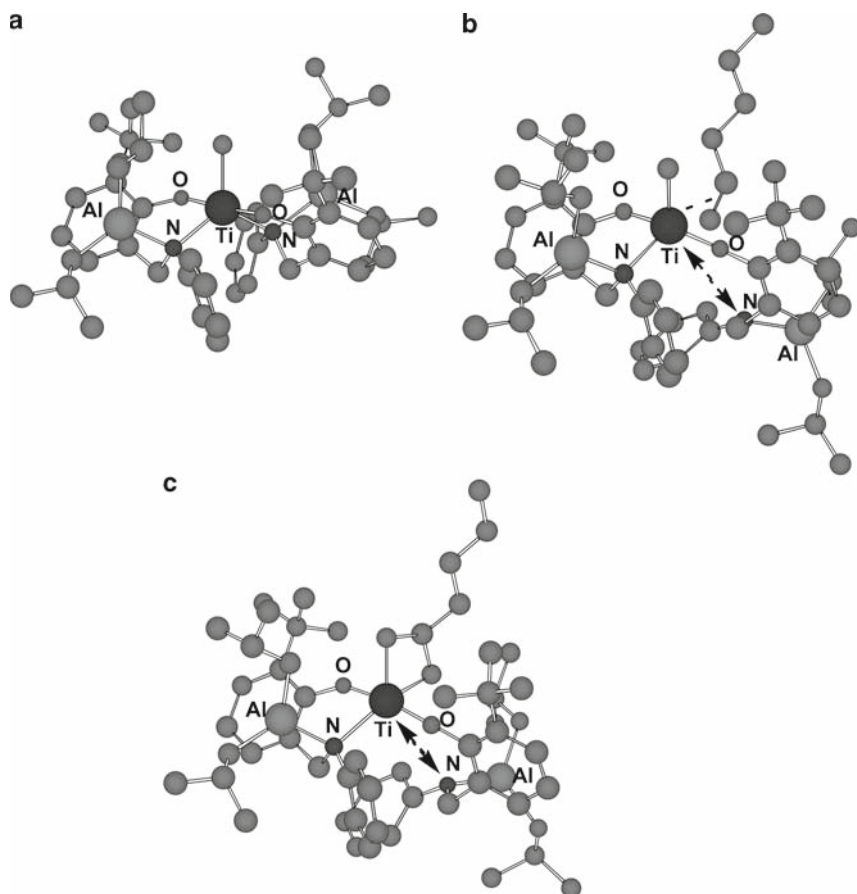


Fig. 24 Calculated structures of cationic phenoxy-amine complexes in the absence of 1-hexene (a), in the presence of 1-hexene (1-hexene-coordinated state) (b), and for transition state (c) (polymer chain model: methyl group). Reproduced with permission from Saito et al. [27]. Copyright 2006, American Chemical Society

discovered unprecedented living olefin polymerization catalysts (fluorinated Ti-FI catalysts), which allow for the preparation of a variety of precisely controlled polyolefinic materials including monodisperse polymers, end-functionalized polymers, and block copolymers from ethylene, propylene, and higher α -olefins.

6.1 Living Ethylene Polymerization

As reported, a common Ti-FI catalyst combined with MAO possesses some characteristics of living ethylene polymerization under limited conditions (e.g., short polymerization time and/or controlled ethylene concentration in a polymerization medium).

For example, we have described that nearly monodisperse PEs can be formed by **2**/MAO (1 min polymerization, atmospheric pressure; 25 °C M_n 52,000, M_w/M_n 1.12; 50 °C M_n 65,000, M_w/M_n 1.17) and **38** (Fig. 25)/MAO (1 min polymerization, atmospheric pressure; 25 °C M_n 8000, M_w/M_n 1.05; 50 °C M_n 9000, M_w/M_n 1.08) [28, 68, 69]. Additionally, Coates and coworkers subsequently reported that Ti-FI catalysts **34** (Fig. 22) and **39** (Fig. 25) can form nearly monodisperse PEs under controlled conditions [70]. With these Ti-FI catalysts, however, synthesizing high molecular weight and narrow molecular weight distribution PEs is generally difficult (e.g., 5 min polymerization, atmospheric pressure, 50 °C; **2** M_n 132,000, M_w/M_n 1.83; **38** M_n 24,000, M_w/M_n 1.46) [28, 68]. Moreover, normally, these catalysts cannot be applied to block copolymer formation.

We discovered that Ti-FI catalyst **40** (Fig. 25) with MAO activation carries out living ethylene polymerization at a high temperature of 50 °C and affords a very high molecular weight PE with an extremely narrow molecular weight distribution (M_n 424,000, M_w/M_n 1.13) [71]. ^{13}C NMR and IR analysis indicated that the PE possesses a linear structure with virtually no branching (branching less than 1 per 1000 carbon atoms, T_m 135 °C). The living nature was confirmed by the linear relationship between M_n and polymerization time as well as by the narrow molecular weight distributions observed. Significantly, there is virtually no chain termination or transfer operation in the Ti-FI catalyst **40**/MAO system for at least 60 min at 25 °C, even in the absence of ethylene. The M_n value of 424,000 represents one of the highest molecular weights among PEs produced in a living manner. In addition, the TOF of 21,500 $\text{min}^{-1}\text{atm}^{-1}$ is the highest activity reported to date with respect to living ethylene polymerization, and is comparable to that seen in $\text{Cp}_2\text{ZrCl}_2/\text{MAO}$, under identical conditions. Considering that the MAO used as the activator is a potential chain transfer agent and that normally living olefin polymerization can only be achieved using a borate instead of MAO, living ethylene polymerization with Ti-FI catalyst **40**/MAO is highly significant.

Surprisingly, at higher temperatures such as 75 °C and even at 90 °C, this catalyst provides very narrow molecular weight distribution PEs ($M_w/M_n < 1.3$). These results show that Ti-FI catalyst **40** initiates highly controlled, thermally robust living ethylene polymerization [35]. Interestingly, Ti-FI catalyst **40**/MAO mediates the room-temperature living copolymerizations of ethylene/propylene and ethylene/higher α -olefins and provides high molecular weight monodisperse ethylene/

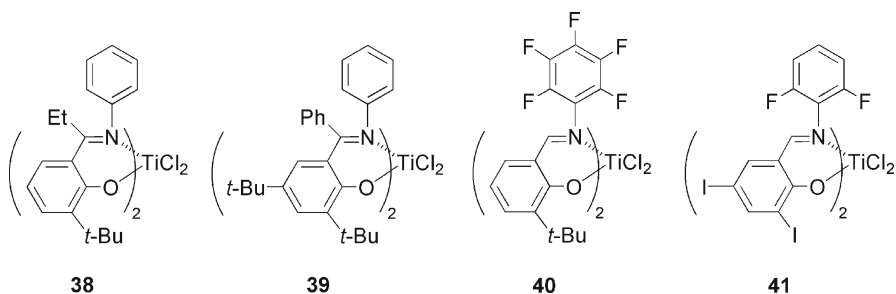


Fig. 25 Structures of Ti-FI catalysts **38–41**

propylene and ethylene/higher α -olefin copolymers (e.g., ethylene/propylene copolymers: $M_n > 80,000$, M_w/M_n 1.07–1.13, propylene content up to 48%) [33, 34]. Using Ti-FI catalyst **41** (Fig. 25) bearing iodines in the ligand, Weiser and Müllhaupt prepared ultra-high molecular weight PE with a fairly narrow molecular weight distribution (M_w 5,500,000, M_w/M_n 1.57) [49].

In a study on the solution structure of the active species in fluorinated Ti-FI catalysts by ^1H NMR spectroscopy, we observed, for the first time, the formation of cationic species $\text{L}_2\text{Ti}^+\text{Me}$ (L: phenoxy-imine ligand) derived from **40**/MAO and its living propagating species [72]. Additionally, Bryliakov and Talsi characterized cationic species formed from Ti-FI catalyst **40** with MAO or $\text{AlMe}_3/[\text{CPh}_3]^+[\text{B}(\text{C}_6\text{F}_5)_4]^-$ by ^1H , ^{19}F , and ^{13}C NMR and electron paramagnetic resonance (EPR) spectroscopy. They observed the generation of outer-sphere ion pairs and the formation of the polymeryl species after reaction with ethylene.

We successfully synthesized dimethyl complexes of the fluorinated Ti-FI catalysts **42** and **43** (Fig. 26), which possess an essentially octahedrally coordinated Ti center and C_2 symmetry, with a *cis*-O, *cis*-N, *cis*-methyl arrangement (Fig. 27) [73].

The Ti-FI dimethyl complexes **42** and **43** can readily be activated with $\text{B}(\text{C}_6\text{F}_5)_3$ or $[\text{CPh}_3]^+[\text{B}(\text{C}_6\text{F}_5)_4]^-$ to form a methyl cationic species. The addition of ethylene to the cationic species derived from **42** allows room temperature observation of the living propagating species, which displays ^1H NMR peaks centered at 1.45 and 2.88 ppm that are attributed to the diastereotopic α -methylene protons connected

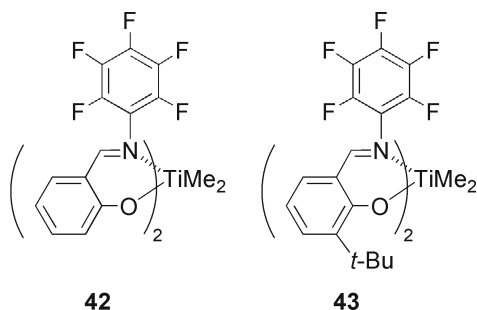


Fig. 26 Structures of Ti-FI catalysts **42** and **43**

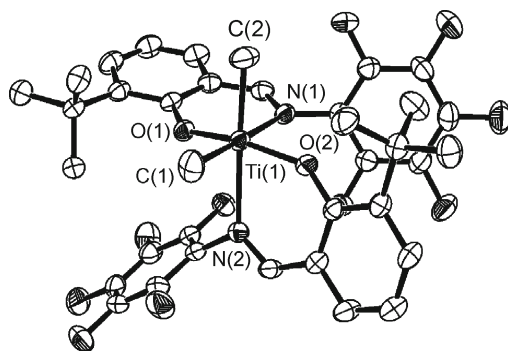


Fig. 27 Molecular structure of Ti-FI catalyst **43**. Reproduced with permission from Makio et al. [73]. Copyright 2005, The Chemical Society of Japan

to the Ti metal (Fig. 28). These results further confirm the highly controlled, thermally robust living nature of the fluorinated Ti-FI catalysts [73].

We demonstrated that a series of Ti-FI catalysts **40** (Fig. 25) and **44–47** (Fig. 29) possessing a *t*-Bu, cyclohexyl, *i*-Pr, Me, and H *ortho* to the phenoxy-O (thus having various steric environments in close proximity to the active site) all initiate room temperature living ethylene polymerization, though, for the non-fluorinated congeners, the steric bulk of the substituent *ortho* to the phenoxy-O significantly influences product molecular weight (Table 6) [28, 33].

These facts suggest that, for the fluorinated Ti-FI catalysts that we discovered, the steric hindrance provided by the substituent *ortho* to the phenoxy-O exercises no significant influence on the living nature, implying that steric factors do not play a pivotal role in achievement of the living polymerization [68, 74].

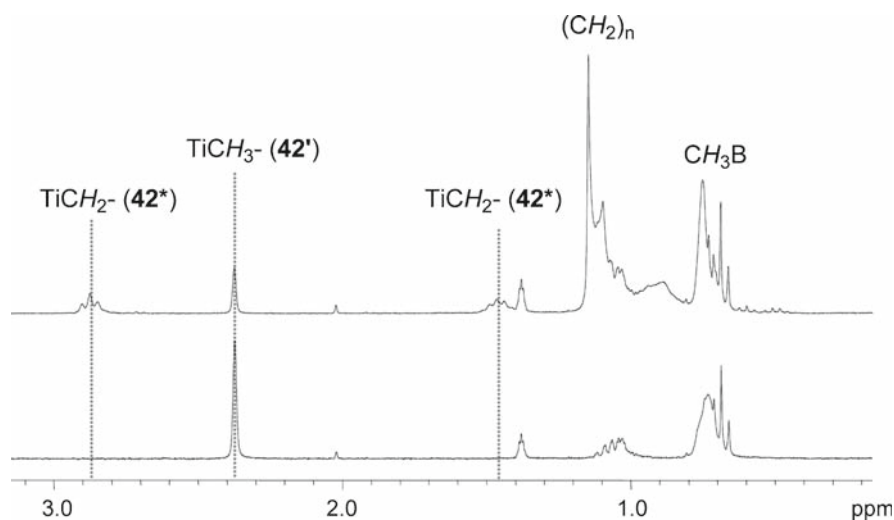
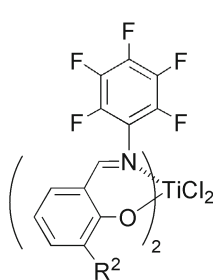


Fig. 28 ^1H NMR spectra (270 MHz; BrC_6D_5) of $[\text{C}_6\text{F}_5\text{N}=\text{CH}(2\text{-O-C}_6\text{H}_4)]\text{TiMe}^+[\text{MeB}(\text{C}_6\text{F}_5)_3]^-$ (**42'**, bottom) and $[\text{C}_6\text{F}_5\text{N}=\text{CH}(2\text{-O-C}_6\text{H}_4)]\text{Ti}(\text{CH}_2\text{CH}_2)_n\text{Me}^+[\text{MeB}(\text{C}_6\text{F}_5)_3]^-$ (**42***, top). Reproduced with permission from Makio et al. [73]. Copyright 2005, The Chemical Society of Japan

Fig. 29 Structures of Ti-FI catalysts **44–47**



catalyst	R^2
44	cyclohexyl
45	<i>i</i> -Pr
46	Me
47	H

Table 6 Ethylene polymerization results with Ti-FI catalysts **40** and **44–47**

Entry	FI catalyst	Activity ^a (kg mmol ⁻¹ h ⁻¹)	M_w^b ($\times 10^{-3}$)	M_w/M_n^b	T_m^c (°C)
1	40	34.0	412	1.13	136
2	44	3.5	49	1.05	134
3	45	3.9	51	1.10	135
4	46	5.7	75	1.16	136
5	47	2.5	44	1.08	134

Conditions: 25 °C, atmospheric pressure, 1 min, ethylene gas feed 100 L h⁻¹, catalyst **40** 0.5 μmol, catalyst **44–47** 5 μmol

^akg polymer per mmol catalyst per h

^bDetermined by GPC

^cMeasured by DSC

6.2 The Origin of Living Polymerization

To gain information on the origin of this unprecedented living polymerization, we investigated the ethylene polymerization behavior of various fluorinated Ti-FI catalysts **16–18**, **40**, and **48–51** (Fig. 30).

As summarized in Table 7, Ti-FI catalysts with *ortho*-F(s) form PEs with an extremely narrow molecular weight distribution (M_w/M_n 1.05–1.13) whereas FI catalysts possessing no *ortho*-F furnish PEs with M_w/M_n values of approximately 2 under the conditions examined. These results show that the *ortho*-F is a requirement for living polymerization. In addition, end-group analyses of the PEs arising from non-living type FI catalysts (¹³C NMR, IR) show the presence of almost equal amounts of vinyl and methyl chain-end groups, indicating that the predominant mechanism for chain termination with non-living type FI catalysts is by β-H transfer. Accordingly, the *ortho*-F suppresses the β-H transfer [35, 75].

It should be emphasized that, though the *ortho*-fluorinated Ti-FI catalyst **50** mediates the living polymerization, the corresponding non-fluorinated and *ortho*-methylated Ti-FI catalysts **2** and **51** (Fig. 30) do not initiate the living polymerization under identical conditions. The experimental evidence described above indicates that steric hindrance provided by the *ortho*-F does not play a key role in the achievement of living ethylene polymerization, suggesting that the *ortho*-F is involved electronically in the achievement of highly controlled living polymerization [68, 74]. DFT calculations were performed on an active species derived from Ti-FI catalyst **40** to elucidate the role of the *ortho*-F on living polymerization (Fig. 31).

At first we believed that the living nature originated from the stabilization of the Ti center by the *ortho*-F. However, the calculations show that the distance between the Ti and the *ortho*-F (the nearest F) is about 4 Å, which is too long for an effective interaction. Alternatively, the *ortho*-F is revealed to interact with a β-H on a polymer chain (bond distance 2.275 Å). The electrostatic energy between the negatively charged F and the positively charged β-H is estimated to be a relatively large value,

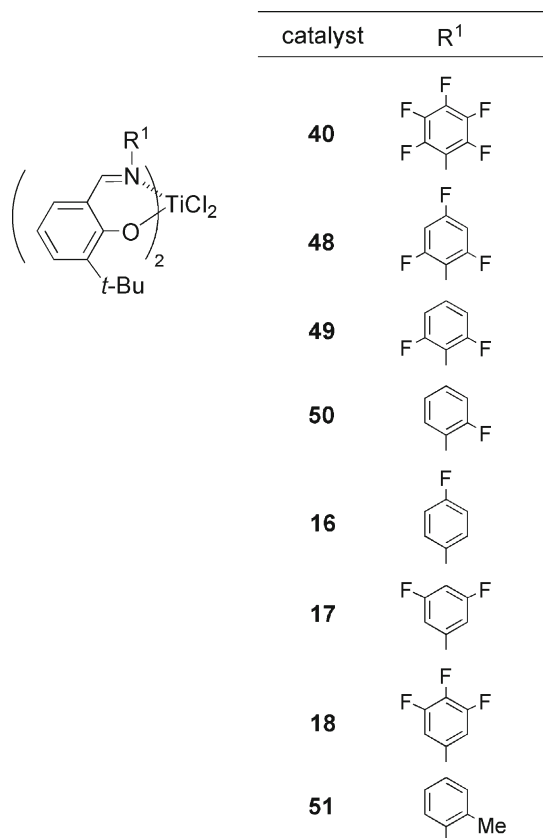


Fig. 30 Structures of Ti-FI catalysts **16–18**, **40**, and **48–51**

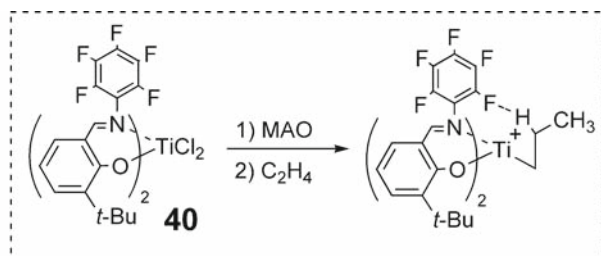
Table 7 Ethylene polymerization results with Ti-FI catalysts **16–18**, **40**, and **48–51**

Entry	FI catalyst	Time (min)	Activity ^a (kg mmol ⁻¹ h ⁻¹)	M_n^b ($\times 10^{-3}$)	M_w/M_n^b
1	40	1	36	424	1.13
2	48	5	2	145	1.25
3	49	5	1	64	1.05
4	50	5	0.1	13	1.06
5	16	5	5	128	2.18
6	17	1	32	129	1.78
7	18	1	45	98	1.99
8	51	30	0.3	355	2.14

Conditions: 50 °C, atmospheric pressure, ethylene gas feed 100 L h⁻¹, MAO 1.25 mmol

^akg polymer per mmol catalyst per h

^bDetermined by GPC



Calcd F–H interaction

$$q(\text{F})^{\text{a}} \quad -0.466$$

$$q(\text{H}_{\beta})^{\text{b}} \quad 0.095$$

$$\text{ES}(\text{H}_{\beta}-\text{F})^{\text{c}} \quad -27.1 \text{ kJ/mol}$$

^a Mulliken charge of the nearest *ortho*-F to H_{β}

^b Mulliken charge of H_{β}

^c Electrostatic energy for F– H_{β} interaction

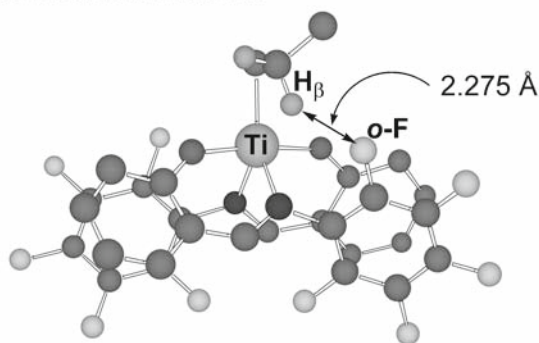


Fig. 31 Calculated structure of an active species derived from Ti-FI catalyst **40**/MAO. Reproduced with permission from Nakayama et al. [76]. Copyright 2003, The Society of Synthetic Organic Chemistry, Japan

27 kJ mol⁻¹. Additionally, a degree of C–H_β bond elongation (1.113 Å) was suggested by the calculations, which is probably the result of the interaction between the *ortho*-F with the β-H. This attractive interaction reduces the reactivity of the β-H toward the Ti metal and/or a reacting monomer, which prevents β-H transfer. This remarkable *ortho*-F effect represents a novel strategy for the design of a new transition metal complex for living olefin polymerization [75].

The *ortho*-F effect has been further confirmed by the polymerization behavior of the corresponding fluorinated Zr- and Hf-FI catalysts. Namely, we found that the introduction of the C₆F₅ group on the imine-N in place of the C₆H₅ group for Zr- and Hf-FI catalysts **52** and **53** (Fig. 32) resulted in the formation of enormously enhanced (more than 20 times greater) molecular weight PEs (5 min polymerization, 25 °C; M_w **1** 7000; **52** 157,000; **3** 17,000; **53** 410,000), even though the increase in catalytic activity is merely 40–50% [57].

Kui and Chan reported the first NMR and X-ray structural evidence for an attractive interaction between an F in the ligand and an H of a benzyl group attached to group 4 metal catalysts. Moreover, by a neutron diffraction study, Chan, Cole and their co-workers elucidated the structural parameters of the F/H interaction. The F/H distances were 2.572(6) and 2.607(5) Å, and F/H angles 103.3(4) and 108.2(3), suggesting the presence of the attractive interaction between the F in the ligand and the H of the alkyl group attached to the group 4 metal. These results demonstrate that the F/H interaction suggested by DFT calculations is experimentally feasible [77, 78].

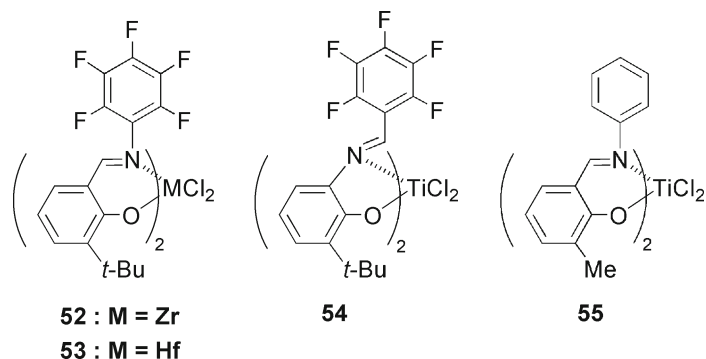


Fig. 32 Structures of Ti-FI catalysts **52–55**

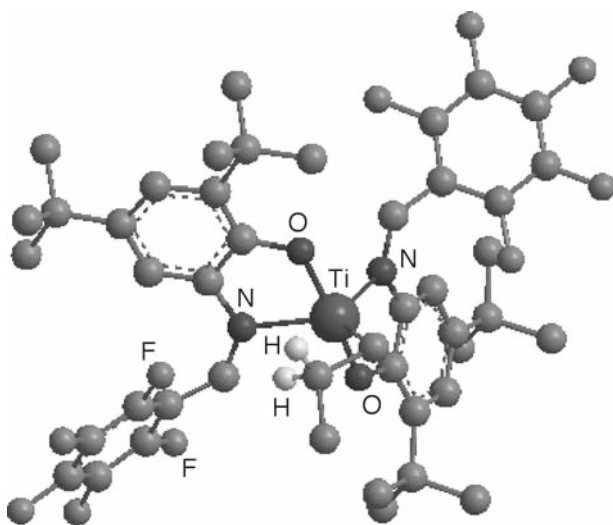


Fig. 33 Calculated structure of a catalytically active species (polymer chain model: *n*-propyl group). Reproduced with permission from Suzuki et al. [21]. Copyright 2006, Wiley-VCH

It should be pointed out that a structurally related bis(imine-phenoxy)Ti complex **54** (Fig. 32) having a C₆F₅ on the imine-N with MAO activation does not initiate living ethylene polymerization. Interestingly, DFT calculations suggested that there is virtually no interaction between the *ortho*-F and the β-H (*ortho*-F/β-H distance 3.66 Å) (Fig. 33) [21].

Based on the results and discussions described so far, we concluded that the steric bulk provided by the *ortho*-F does not play an important role and that the attractive non-bonding interaction of the *ortho*-F with the β-H of the growing polymer chain is responsible for the unprecedented living polymerization, representing the first example of an attractive interaction between the ligand and other components in a catalyst system, which dramatically enhances catalyst performance [35, 68, 74, 75].

6.3 Stereospecific Living Propylene Polymerization

Ti-FI catalysts with no *ortho*-Fs in the ligands can also display some living propylene polymerization characteristics. We have revealed that Ti-FI catalyst **55** (Fig. 32) having a Me group *ortho* to the phenoxy-O can form a high molecular weight PP (M_w 101,000) with a fairly narrow molecular weight distribution of 1.47 at 1 °C, though the PP produced has an atactic nature. Additionally, as described, the fluorinated Ti-FI catalyst **40** (Fig. 25)/MAO mediates the room temperature living copolymerization of ethylene and propylene [34]. It is interesting to note that, for propylene polymerization with the fluorinated Ti-FI catalyst **40**, the attractive interaction between the *ortho*-F and the β -H is illuminated by DFT calculations (30.7 kJ mol⁻¹, 2,1-insertion). These experimental and DFT calculations suggest that fluorinated Ti-FI catalysts might promote living propylene polymerization.

As anticipated, Ti-FI catalyst **40** with MAO enabled room temperature living propylene polymerization to form highly syndiotactic PP with extremely narrow molecular weight distribution (M_w/M_n 1.11, M_n 28,500, *rr* 87%, T_m 137 °C) via a chain-end control mechanism [29, 30, 79]. The living nature of the polymerization was confirmed by the linear increase in M_n with polymer yield. These results could indicate that the attractive interaction capable of suppressing chain transfers sets a standard for controlled living polymerization of simple olefins via insertion chemistry. Another research group, however, has reported that the effect of the *ortho*-F for living propylene polymerization with fluorinated Ti-FI catalysts is primarily steric, based on QM/MM calculation results [80]. As described so far, the well-established experimental results show that only a single *ortho*-F is a requirement for the living polymerization of propylene as well as ethylene [35, 81]. This fact probably suggests that steric factors do not play a key role in the achievement of living propylene polymerization, since, for the single *ortho*-F Ti-FI catalyst, the 2-fluorophenyl group on the imine-N can rotate to evade steric hindrance that may suppress chain transfer reactions. The discrepancy between the calculations and the experimental data probably stems from the fact that the calculations do not take into consideration the solvent, activator influence though the solvent, and the activator employed, which are known to have a significant influence on the polymerization behavior of Ti-FI catalysts (activity, molecular weight, molecular weight distribution).

FI catalyst **40** is the first example of a simultaneous living and highly stereoselective catalyst for the polymerization of propylene. In addition, **40** is the first example of a catalyst that mediates the living polymerization of both ethylene and propylene. Coates and coworkers subsequently reported on Ti-FI catalyst **56** ($R^1 = C_6F_5$, $R^2 = R^4 = t\text{-Bu}$, $R^3 = R^5 = R^6 = H$), a pentafluorinated version of **34** (Fig. 22), which exhibits practically the same catalytic performance for living propylene polymerization as Ti-FI catalyst **40** (**56rr** 86%, T_m 135 °C; **40rr** 87%, T_m 137 °C, 25 °C polymerization) (for a patent on modified Ti-FI catalysts relating to the basic patent of 2001, see [82]).

We have demonstrated that despite a chain-end control mechanism, the steric bulk of the substituent *ortho* to the phenoxy-O controls the syndioselectivity of the

polymerization, and that the sterically encumbered substituent results in highly syndiospecific propylene polymerization (Fig. 34) [30].

We have given the name “ligand-directed chain-end controlled polymerizations” to these unprecedented propylene polymerizations (i.e., chain-end controlled polymerizations that are evidently governed by the ligand structures). Of note is that we have found an exceptional catalyst, Ti-FI catalyst **36** (Fig. 22), which incorporates a sterically encumbered trimethylsilyl group *ortho* to the phenoxy-O. This FI-catalyst with MAO furnishes highly syndiotactic monodisperse PP (25 °C, rr 93%, M_n 47,000, M_w/M_n 1.08) with an extremely high T_m (152 °C). To our surprise, at 50 °C, **36** initiated living propylene polymerization and yielded monodisperse sPP with a very high T_m of 150 °C, which represents the first example of living propylene polymerization at a temperature as high as 50 °C [30].

A site-inversion mechanism (the key feature of which is that isomerization between diastereomeric and Λ configurations is rapid on the propylene-insertion time scale) based on theoretical calculations was proposed by Cavallo and coworkers in order to explain the ligand-directed chain-end controlled polymerizations (Fig. 35) [42]. The site-inversion mechanism allows chain-end control to work in concert with the site control effects. Our experimental results and the expected catalytic behavior resulting from the site-inversion mechanism concur with each other very well.

We and others have revealed that syndiospecific propylene polymerization is exclusively initiated by 1,2-insertion followed by 2,1-insertion as the principal mode of polymerization [64]. This is the first example of a predominant 2,1-insertion mechanism for chain propagation exhibited by a group 4 metal-based catalyst. The unusual preference for 2,1-regiochemistry displayed by the Ti-FI catalysts compared with the Zr- and Hf-FI catalysts is apparently inconsistent with the crystallographically characterized structures, which indicate that the Ti is shielded more by the phenoxy-imine ligands and thus possesses higher steric compression. The reason for the unusual preference in the regiochemistry of Ti-FI catalysts is unclear at the present time.

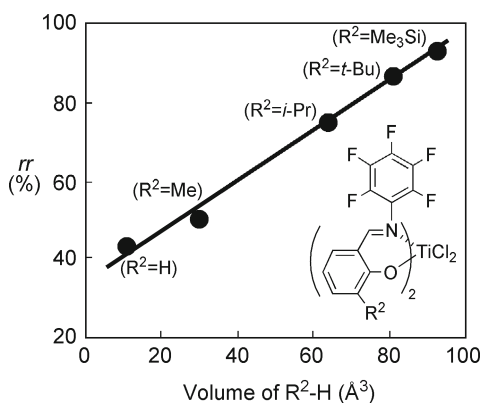


Fig. 34 Plots of rr triad values as a function of calculated R²-H volume for propylene polymerization

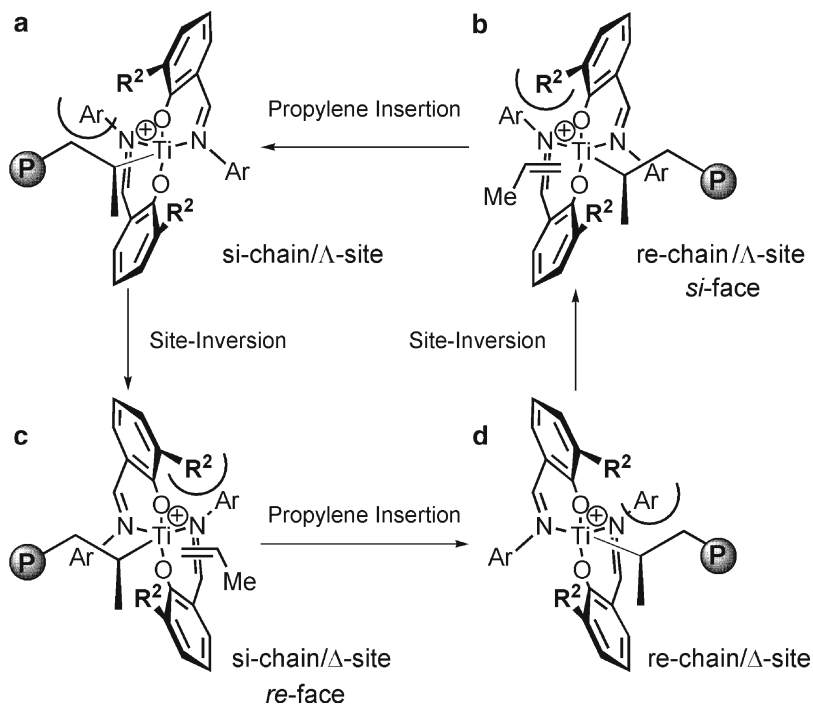


Fig. 35 Site-inversion mechanism for propylene polymerization promoted by FI catalysts. Reproduced with permission from Furuyama et al. [68]. Copyright 2005, Elsevier

Interestingly, **36** (Fig. 22) combined with $\text{MgCl}_2/i\text{-Bu}_n\text{Al(OR)}_{3-n}$ (MAO-free, MgCl_2 -supported catalyst system) forms higher tacticity PP with higher T_m (rr 97%, T_m 155 °C) than that of the MAO-activated homogeneous system described above [83]. This result probably suggests that the immobilization of the Ti-FI catalyst onto $\text{MgCl}_2/i\text{-Bu}_n\text{Al(OR)}_{3-n}$ does not suppress the site inversion process. The T_m of 155 °C represents one of the highest known values for sPPs synthesized at room temperature. The formation of high T_m sPPs is remarkable in view of the tremendous technological significance of such sPPs.

^{13}C NMR spectroscopy has revealed that the highly syndiotactic PPs, formed with Ti-FI catalysts **36** (Fig. 22) and **40** (Fig. 25), contain a significant amount of regioirregular units, and possess a block-like structure involving long regioirregular and short consecutive regioirregular units [30, 74].

Recently, in combination with MAO, Ti-FI catalyst **57** ($\text{R}^1 = \text{C}_6\text{F}_5$, $\text{R}^2 = \text{Me}$, $\text{R}^3 = \text{R}^5 = \text{H}$, $\text{R}^4 = \text{Me}$, $\text{R}^6 = \text{Ph}$) having a phenyl group on the imine-C was described by Coates and coworkers to form moderately isotactic and nearly monodisperse PP (0 °C polymerization, mm 53%, T_m 69.5 °C, M_n 27,900, M_w/M_n 1.11), probably due to the suppression of a site-inversion process by the phenyl group on the imine-C [84]. The corresponding Ti-FI catalysts possessing a sterically bulkier *ortho*-substituent (which is expected to form higher tacticity PPs) exhibit virtually no reactivity

toward propylene. Therefore, highly isospecific and living propylene polymerization with FI catalysts has not yet been achieved, which seems improbable when one considers the catalyst structure and performance relationships elucidated by us [30, 74].

6.4 Syntheses of Well-Defined Polyolefinic Block Copolymers

One of the most attractive features of a living olefin polymerization catalyst system lies in its capability to create well-defined polyolefinic block copolymers. As described, fluorinated Ti-FI catalysts activation with MAO can efficiently synthesize PEs, ethylene/propylene copolymers, ethylene/higher α -olefin copolymers, aPPs, and sPPs in a living manner, allowing the creation of block copolymers with various architectures from ethylene, propylene, and higher α -olefins, which has been a long-standing scientific challenge [68, 74]. We have thus demonstrated the utility of the fluorinated Ti-FI catalysts through the syntheses of ethylene, propylene, and higher α -olefin-based block copolymers consisting of crystalline and amorphous segments and/or two different kinds of crystalline segments (Table 8), most of which were inaccessible prior to our work.

For example, a PE-*b*-poly(ethylene-*co*-propylene) diblock composed of crystalline PE and amorphous ethylene/propylene copolymer segments was synthesized from ethylene and ethylene/propylene. The addition of MAO and Ti-FI catalyst **40** (Fig. 25) to an ethylene-saturated toluene at 25 °C resulted in the rapid formation of a living PE (M_n 115,000, M_w/M_n 1.10). The addition of ethylene/propylene (1:3 volume ratio) to this living PE formed a PE-*b*-poly(ethylene-*co*-propylene) block copolymer (M_n 211,000, M_w/M_n 1.16, propylene content 6.4 mol%) [30]. As expected, the polymer exhibits a high T_m of 123 °C, indicating that this block copolymer shows good elastic properties at much higher temperatures than the conventional random copolymers of similar densities.

Similarly, sPP-*b*-poly(ethylene-*co*-propylene), PE-*b*-sPP, PE-*b*-poly(ethylene-*co*-propylene)-*b*-PE, and PE-*b*-poly(ethylene-*co*-propylene)-*b*-sPP block copolymers were also prepared with the **40**/MAO by the sequential addition of the corresponding monomers. Additionally, **46** (Fig. 29) combined with MAO forms ethylene/higher α -olefin block copolymers such as PE-*b*-poly(ethylene-*co*-1-hexene) and PE-*b*-poly(ethylene-*co*-1-octene) [33]. Thus, the usefulness of FI catalysts/MAO systems for the syntheses of a wide array of block copolymers has been demonstrated. The PE-*b*-poly(ethylene-*co*-propylene) and sPP-*b*-poly(ethylene-*co*-propylene) were analyzed by atomic force microscopy (AFM) and transmission electron microscopy (TEM) to demonstrate their high potential as novel materials [34, 85]. The unique block copolymers formed with the FI catalysts have potential uses in a broad spectrum of applications including compatibilizers, elastomers, and composite materials. Using Ti-FI catalysts **41** and **56**, Mülhaupt, Coates and associated coworkers have prepared block copolymers, including sPP-*b*-poly(ethylene-*co*-propylene), similar to that synthesized by us, PE-*b*-poly(ethylene-*co*-cyclopentene), and PE-*b*-polystyrene [49, 86–88].

Table 8 Unique block copolymers created by fluorinated Ti-FI catalysts

Entry	First			Second			Third							
	Segment	M_n^a ($\times 10^{-3}$)	M_w/M_n^a	T_m^b ($^{\circ}\text{C}$)	Segment	M_n^a ($\times 10^{-3}$)	M_w/M_n^a	P or H content ^c (mol%)	T_m^b ($^{\circ}\text{C}$)	Segment	M_n^a ($\times 10^{-3}$)	M_w/M_n^a	P or H content ^c (mol%)	T_m^b ($^{\circ}\text{C}$)
1	PE	115	1.10	133	sPP	136	1.15	16.1	131	-	-	-	-	-
2	PE	115	1.10	133	E/P ^d	211	1.16	6.4	123	-	-	-	-	-
3	PE	115	1.10	133	E/P ^d	211	1.16	6.4	123	sPP	235	1.15	14.1	123
4	PE	115	1.10	133	E/P ^d	211	1.16	6.4	123	PE	272	1.14	6.6	120
5	sPP	27	1.13	137	E/P ^d	161	1.51	40.3	127	-	-	-	-	-
6	PE	38	1.11	135	E/H ^e	80	1.21	15.0	130	-	-	-	-	-

^aDetermined by GPC^bMeasured by DSC^cOverall propylene(P) or 1-hexene(H) content, determined by ¹H NMR^dPoly(ethylene-co-propylene)^ePoly(ethylene-co-1-hexene)

6.5 Catalytic Production of Living Polymers

Fluorinated Ti-FI catalysts have achieved some of the important goals concerning the synthesis of polyolefinic materials using their highly controlled living nature (i.e., syntheses of high molecular weight monodisperse PEs, PPs, and ethylene/ α -olefin copolymers, highly syndiotactic monodisperse PPs, and a wide variety of block copolymers from ethylene, propylene, and higher α -olefins). While these living polymers possess many potential applications in various fields as new materials, living-type FI catalysts suffer from extremely low catalyst productivity. This is because such FI catalysts can only produce one polymer chain during the polymerization, rendering the living polymers arising from the FI catalysts economically unattractive.

Consequently, a crucial goal that still remains to be realized is the catalytic production of living polymers that increase the polymer/catalyst ratio and thus enhance catalyst productivity. The catalytic production of living polymers is feasible if we develop FI catalysts that incorporate monomers without termination, even in the presence of a chain transfer agent, and which only undergo chain transfer in the absence of a reacting monomer.

To our delight, elaborate catalyst design work focusing on the substitution pattern of fluorines as well as the selection of the substituent *ortho* to the phenoxy-oxygen, has resulted in the discovery of FI catalysts that are capable of catalytically producing living polymers in combination with chain transfer agents (e.g., H₂, Et₂Zn) [68, 75, 89]. For example, the catalytic production of Zn-terminated PEs was achieved by Ti-FI catalyst **58**. The polymerization procedures are summarized in Fig. 36.

The first step was saturation of the reaction medium with ethylene, followed by living ethylene polymerization (step A in Fig. 36). Et₂Zn (80 equiv. to **58**) was then added to the reaction medium (step B), followed by ethylene polymerization once again (step C). Quenching the reaction after step B yielded monodisperse PE (M_n 36,700, M_w/M_n 1.20) whereas quenching following the complete sequence provided an approximately double yield of PE with virtually the same molecular weight and molecular weight distribution (M_n 37,100, M_w/M_n 1.31) (Fig. 37).

In this system, a living PE chain-end reacts with Et₂Zn only after all ethylene has been consumed, leading to a Zn-terminated PE chain and a Ti species capable of growing another living chain upon addition of monomer. This is the first example of the production of multiple living polymer chains per catalyst.

Likewise, with Ti-FI catalyst **48** (Fig. 30), catalytic production of monodisperse PEs and PE-*b*-poly(ethylene-*co*-propylene) were accomplished for the first time using H₂ as a chain transfer agent. The combination of specifically designed FI catalysts with appropriate chain transfer agents will provide a new strategy for the catalytic production of living polymers. The strategy is expected to render the displacement of some of the existing polyolefin-based materials by high-performance living polymers economically viable.

In addition to the above achievements, researchers at Dow reported on the catalytic production of multiblock copolymers comprised of PE and amorphous poly(ethylene-*co*-1-octene) segments, by a catalyst system comprised of Zr-FI catalyst **59**, Hf complex **60** (Fig. 38), and Et₂Zn [11, 90].

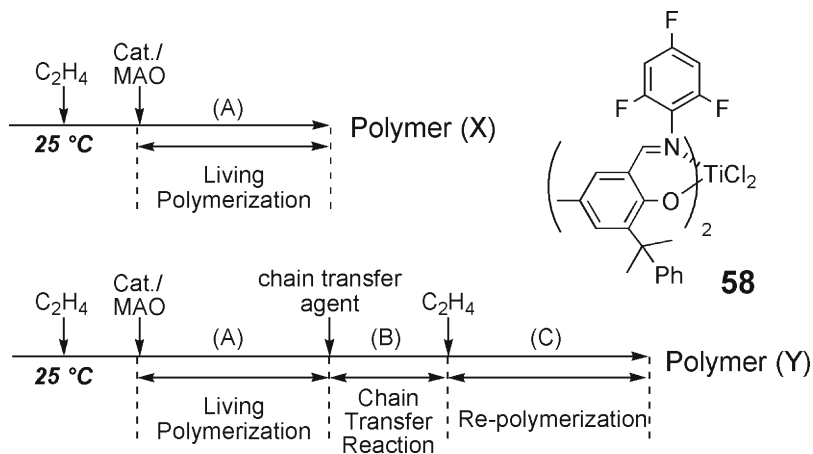


Fig. 36 Procedures for catalytic production of Zn-terminated PEs. Reproduced with permission from Nakayama et al. [76]. Copyright 2003, The Society of Synthetic Organic Chemistry, Japan

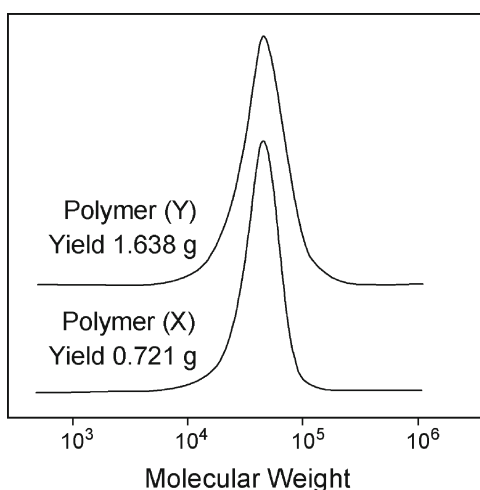


Fig. 37 GPC profile of PEs obtained by **58**. Polymer X: M_n 36,700, M_w/M_n 1.20. Polymer Y: M_n 37,100, M_w/M_n 1.31. Reproduced with permission from Nakayama et al. [76]. Copyright 2003, The Society of Synthetic Organic Chemistry, Japan

The Zr-FI catalyst selectively forms PE even in the presence of ethylene and 1-octene, while the Hf complex affords amorphous copolymers, resulting in the catalytic generation of PE- and poly(ethylene-*co*-1-octene)-based multiblock copolymers through a reversible chain transfer reaction mediated by R₂Zn. The development of an FI catalyst with extremely high ethylene selectivity as well as a reversible chain transfer nature has made it possible to produce these unique polymers. Therefore, both Ti- and Zr-FI catalysts are at the forefront of the commercial production of polyolefinic block copolymers.

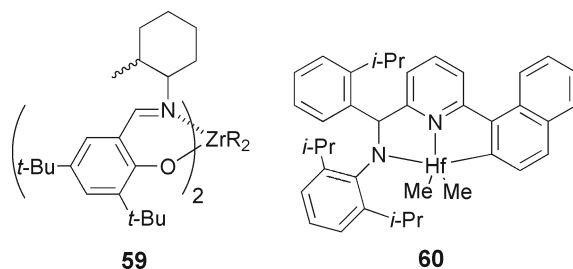


Fig. 38 Structures of Zr-FI catalyst **59** and Hf complex **60**

7 Summary

The ligand oriented catalyst design concept has resulted in the discover of a number of families of high-activity catalysts, represented by bis(phenoxo-imine) early transition metal complexes (now known as FI catalysts). FI catalysts not only show exceptional activity for ethylene polymerization but also have created a wide range of polyolefinic materials with a wide variety of microstructures. The polyolefinic materials include selective vinyl- and Al-terminated PEs, ultrafine particle PEs, ultra-high molecular weight (co)polymers, regio- and stereoirregular high molecular weight poly(higher α -olefin)s, and a variety of polyolefinic block copolymers. Many of these FI polymers are either difficult or impossible to synthesize using conventional Ziegler–Natta catalysts.

Additionally, research on FI catalysts has provided useful information on high catalytic activity, the formation of highly syndiotactic PPs with C_2 -symmetric catalysts, the origin of highly controlled living olefin polymerization, and the high incorporation capability for higher α -olefins.

The above achievements depend highly on both the recent advances in rational catalyst design with the aid of computational science represented by DFT calculations and the wide range of catalyst design possibilities that are afforded by FI catalysts. These possibilities are derived from the readily varied steric and electronic properties of the phenoxo-imine ligands. It is expected that future research on FI catalysts will provide opportunities to produce additional polyolefin-based materials with unique microstructures and a chance to study catalysis and mechanisms for olefin polymerization.

References

1. Bochmann M (1996) *J Chem Soc Dalton Trans* 1996:255
2. Brintzinger HH, Fisher D, Müllhaupt R, Rieger B, Waymouth RM (1995) *Angew Chem Int Ed* 34:1143
3. McKnight AL, Waymouth RM (1998) *Chem Rev* 98:2587

4. Bolton PD, Mountford P (2005) *Adv Synth Catal* 347:355
5. Britovsek GJP, Gibson VC, Wass DF (1999) *Angew Chem Int Ed* 38:428
6. Gibson VC, Spitzmesser SK (2003) *Chem Rev* 103:283
7. Gibson VC, Redshaw C, Solan GA (2007) *Chem Rev* 107:1745
8. Ittel SD, Johnson LK, Brookhart M (2000) *Chem Rev* 100:1169
9. Stephan DW (2005) *Organometallics* 24:2548
10. Suzuki Y, Terao H, Fujita T (2003) *Bull Chem Soc Jpn* 76:1493
11. Matsugi T, Fujita T (2008) *Chem Soc Rev* 37:1264
12. Makio H, Kashiwa N, Fujita T (2002) *Adv Synth Catal* 344:477
13. Matsui S, Fujita T (2001) *Catal Today* 66:63
14. Mitani M, Saito J, Ishii S, Nakayama Y, Makio H, Matsukawa N, Matsui S, Mohri J, Furuyama R, Terao H, Bando H, Tanaka H, Fujita T (2004) *Chem Rec* 4:137
15. Nakayama Y, Saito J, Bando H, Fujita T (2006) *Chem Eur J* 12:7546
16. Yoshida Y, Matsui S, Takagi Y, Mitani M, Nakano T, Tanaka H, Kashiwa N, Fujita T (2001) *Organometallics* 20:4793
17. Yoshida Y, Mohri J, Ishii S, Mitani M, Saito J, Matsui S, Makio H, Nakano T, Tanaka H, Onda M, Yamamoto Y, Mizuno A, Fujita T (2004) *J Am Chem Soc* 126:12023
18. Yoshida Y, Matsui S, Fujita T (2005) *J Organomet Chem* 690:4382
19. Matsugi T, Matsui S, Kojoh S, Takagi Y, Inoue Y, Nakano T, Fujita T, Kashiwa N (2002) *Macromolecules* 35:4880
20. Suzuki Y, Inoue Y, Tanaka H, Fujita T (2004) *Macromol Rapid Commun* 25:493
21. Suzuki Y, Tanaka H, Oshiki T, Takai K, Fujita T (2006) *Chem Asian J* 1:878
22. Saito J, Tohi Y, Matsukawa N, Mitani M, Fujita T (2005) *Macromolecules* 38:4955
23. Terao H, Ishii S, Saito J, Matsuura S, Mitani M, Nagai N, Tanaka H, Fujita T (2006) *Macromolecules* 39:8584
24. Tohi Y, Makio H, Matsui S, Onda M, Fujita T (2003) *Macromolecules* 36:523
25. Tohi Y, Nakano T, Makio H, Matsui S, Fujita T, Yamaguchi T (2004) *Macromol Chem Phys* 205:1179
26. Ishii S, Saito J, Matsuura S, Suzuki Y, Furuyama R, Mitani M, Nakano T, Kashiwa N, Fujita T (2002) *Macromol Rapid Commun* 23:693
27. Saito J, Suzuki Y, Makio H, Tanaka H, Onda M, Fujita T (2006) *Macromolecules* 39:4023
28. Furuyama R, Saito J, Ishii S, Mitani M, Matsui S, Tohi Y, Makio H, Matsukawa N, Tanaka H, Fujita T (2003) *J Mol Cat A* 200:31
29. Mitani M, Yoshida Y, Mohri J, Tsuru K, Ishii S, Kojoh S, Matsugi T, Saito J, Matsukawa N, Matsui S, Nakano T, Tanaka H, Kashiwa N, Fujita T (2001) *WO Patent 01/55231 A1* (filed Jan 2000)
30. Mitani M, Furuyama R, Mohri J, Saito J, Ishii S, Terao H, Nakano T, Tanaka H, Fujita T (2003) *J Am Chem Soc* 125:4293
31. Prasad AV, Makio H, Saito J, Onda M, Fujita T (2004) *Chem Lett* 33:250
32. Saito J, Onda M, Matsui S, Mitani M, Furuyama R, Tanaka H, Fujita T (2002) *Macromol Rapid Commun* 23:1118
33. Furuyama R, Mitani M, Mohri J, Mori R, Tanaka H, Fujita T (2005) *Macromolecules* 38:1546
34. Kojoh S, Matsugi T, Saito J, Mitani M, Fujita T, Kashiwa N (2001) *Chem Lett* 30:822
35. Mitani M, Mohri J, Yoshida Y, Saito J, Ishii S, Tsuru K, Matsui S, Furuyama R, Nakano T, Tanaka H, Kojoh S, Matsugi T, Kashiwa N, Fujita T (2002) *J Am Chem Soc* 124:3327
36. Bott R K J, Hammond M, Horton P N, Lancaster S J, Bochmann M, Scott P (2005) *Dalton Trans* 2005:3611
37. Bryliakov K P, Kravtsov E A, Pennington D A, Lancaster S J, Bochmann M, Brintzinger H H, Talsi E P (2005) *Organometallics* 24:5660
38. Cherian R A E, Lobkovsky E B, Coates G W (2005) *Macromolecules* 38:6259
39. Dawson D M, Walker D A, Pett M T, Bochmann M (2000) *J Chem Soc, Dalton Trans* 2000:459
40. Johnson A L, Davidson M G, Lunn M D, Mahon M F (2006) *Eur J Inorg Chem* 15:3088

41. Lamberti M, Consolmagno M, Mazzeo M, Pellicchia C (2005) *Macromol Rapid Commun* 26:1866
42. Milano G, Cavallo L, Guerra G (2002) *J Am Chem Soc* 124:13368
43. Parssinen A, Luhtanen T, Klinga M, Pakkanen T, Leskela M, Repo T (2007) *Organometallics* 26:3690
44. Pennington DA, Coles SJ, Hursthouse MB, Bochmann M, Lancaster SJ (2005) *Chem Commun* 2005:3150
45. Severn JR, Chadwick JC (2004) *Macromol Rapid Commun* 25:1024
46. Strauch J, Warren TH, Erker G, Fröhlich R, Saarenketo P (2000) *Inorg Chim Acta* 300–302:810
47. Talarico G, Busico V, Cavallo L (2003) *J Am Chem Soc* 125:7172
48. Van Meurs M, Britovsek GJP, Gibson VC, Cohen SA (2005) *J Am Chem Soc* 127:9913
49. Weiser M-S, Mülhaupt R (2006) *Macromol Rapid Commun* 27:1009
50. Inoue Y, Nakano T, Tanaka H, Kashiwa N, Fujita T (2001) *Chem Lett* 30:1060
51. Matsui S, Tohi Y, Mitani M, Saito J, Makio H, Tanaka H, Nitabaru M, Nakano T, Fujita T (1999) *Chem Lett* 28:1065
52. Matsui S, Mitani M, Saito J, Tohi Y, Makio H, Tanaka H, Fujita T (1999) *Chem Lett* 28:1263
53. Matsui S, Mitani M, Saito J, Matsukawa N, Tanaka H, Nakano T, Fujita T (2000) *Chem Lett* 29:554
54. Matsui S, Mitani M, Saito J, Tohi Y, Makio H, Matsukawa N, Takagi Y, Tsuru K, Nitabaru M, Nakano T, Tanaka H, Kashiwa N, Fujita T (2001) *J Am Chem Soc* 123:6847
55. Matsukawa N, Matsui S, Mitani M, Saito J, Tsuru K, Kashiwa N, Fujita T (2001) *J Mol Catal A* 169:99
56. Ishii S, Saito J, Mitani M, Mohri J, Matsukawa N, Tohi Y, Matsui S, Kashiwa N, Fujita T (2002) *J Mol Catal A* 179:11
57. Ishii S, Furuyama R, Matsukawa N, Saito J, Mitani M, Tanaka H, Fujita T (2003) *Macromol Rapid Commun* 24:452
58. Ishii S, Mitani M, Saito J, Matsuura S, Furuyama R, Fujita T (2003) *Stud Surf Sci Catal* 145:49
59. Saito J, Mitani M, Matsui S, Tohi Y, Makio H, Nakano T, Tanaka H, Kashiwa N, Fujita T (2002) *Macromol Chem Phys* 203:59
60. Nakayama Y, Bando H, Sonobe Y, Kaneko H, Kashiwa N, Fujita T (2003) *J Catal* 215:171
61. Nakayama Y, Bando H, Sonobe Y, Suzuki Y, Fujita T (2003) *Chem Lett* 32:766
62. Nakayama Y, Bando H, Sonobe Y, Fujita T (2004) *J Mol Catal A* 213:141
63. Nakayama Y, Bando H, Sonobe Y, Fujita T (2004) *Bull Chem Soc Jpn* 77:617
64. Makio H, Fujita T (2005) *Bull Chem Soc Jpn* 78:52
65. Makio H, Tohi Y, Saito J, Onda M, Fujita T (2003) *Macromol Rapid Commun* 24:894
66. Tian J, Coates GW (2000) *Angew Chem Int Ed* 39:3626
67. Saito J, Mitani M, Matsui S, Kashiwa N, Fujita T (2000) *Macromol Rapid Commun* 21:1333
68. Furuyama R, Saito J, Ishii S, Makio H, Mitani M, Tanaka H, Fujita T (2005) *J Organomet Chem* 690:4398
69. Suzuki Y, Oshiki T, Tanaka H, Takai K, Fujita T (2005) *Chem Lett* 34:1458
70. Reinartz S, Mason AF, Lobkovsky EB, Coates GW (2003) *Organometallics* 22:2542
71. Saito J, Mitani M, Yoshida Y, Matsui S, Mohri J, Ishii S, Kojoh S, Kashiwa N, Fujita T (2001) *Angew Chem Int Ed* 40:2918
72. Makio H, Fujita T (2004) *Macromol Symp* 213:221
73. Makio H, Oshiki T, Takai K, Fujita T (2005) *Chem Lett* 34:1382
74. Sakuma A, Weiser M-S, Fujita T (2007) *Polym J* 39:193
75. Mitani M, Nakano T, Fujita T (2003) *Chem Eur J* 9:2396
76. Nakayama Y, Mitani M, Bando H, Fujita T (2003) *J Synth Org Chem* 61:1124
77. Chan MCW, Kui SCF, Cole JM, McIntyre GJ, Matsui S, Zhu N, Tam K-H (2006) *Chem Eur J* 12:2607

78. Kui SCF, Zhu N, Chan MCW (2003) *Angew Chem Int Ed* 42:1628
79. Saito J, Mitani M, Mohri J, Ishii S, Yoshida Y, Matsugi T, Kojoh S, Kashiwa N, Fujita T (2001) *Chem Lett* 30:576
80. Talarico G, Busico V, Cavallo L (2004) *Organometallics* 23:5989
81. Mason AF, Tian J, Hustad PD, Lobkovsky EB, Coates GW (2002) *Isr J Chem* 42:301
82. Coates GW, Tian J, Hustad PD (2003) US Patent 6562930 (filed Sept 2001)
83. Nakayama Y, Saito J, Bando H, Fujita T (2005) *Macromol Chem Phys* 206:1847
84. Mason AF, Coates GW (2004) *J Am Chem Soc* 126:16326
85. Ono SS, Matsugi T, Matsuoka O, Kojoh S, Fujita T, Kashiwa N, Yamamoto S (2003) *Chem Lett* 32:1182
86. Tian J, Hustad PD, Coates GW (2001) *J Am Chem Soc* 123:5134
87. Weiser M-S, Wesolek M, Mülhaupt R (2006) *J Organomet Chem* 691:2945
88. Weiser M-S, Thomann Y, Heinz L-C, Pasch H, Mülhaupt R (2006) *Polymer* 47:4505
89. Mitani M, Mohri J, Furuyama R, Ishii S, Fujita T (2003) *Chem Lett* 32:238
90. Arriola DJ, Carnahan EM, Hustad PD, Kuhlman RL, Wenzel TT (2006) *Science* 312:714

Hafnocene-Based Olefin Polymerizations

T. Diesner, C. Troll, and B. Rieger

Abstract Zirconocenes have been used for a long time in the field of olefin polymerization using MAO as cocatalyst. The equivalent hafnocenes were seldom used due to a lack of productivity while using MAO activation. In the last few years borane and borate activation has come into the focus of research for olefin polymerization. A variety of different hafnocenes were used to investigate the polymerization mechanism and the different cocatalysts.

Differences in the polymer microstructures prepared with MAO and borate as cocatalysts are especially noted. While using TIBA/borate for building the active species, activities increase dramatically. Activities exceeded those of comparable Zr/MAO systems, obtaining high and ultrahigh molecular weight polypropylenes with molecular weights of up to 5,000,000 g mol⁻¹ and tacticities of 10–80% depending on the structure of the catalyst.

Keywords Borate activation, Hafnocene catalysts, Olefin polymerization, Ultrahigh M_w polyolefins

Contents

1	Introduction	48
2	Catalyst Characterization	49
2.1	Overview	49
2.2	Mechanism	50
3	Cocatalysts	54
3.1	Methylaluminumoxane (MAO)	54
3.2	Borane and Borate	56
4	Polymerization Experiments	57
4.1	Polymerization Procedure	57
4.2	Activities, Molecular Weights, and Stereoselectivity	57
5	Conclusion	60
	References	61

T. Diesner, C. Troll, and B. Rieger(✉)

WACKER-Chair of Makromolekular Chemistry, Technische Universität München
Lichtenbergstraße 4, 85748 Garching bei München, Germany
e-mail: rieger@tum.de

1 Introduction

Propylene, a light olefin, is like ethylene one of the most important feedstocks for the petrochemical industry. In recent years the main way to obtain propylene and ethylene has been via cracking of naphtha. For this reason the cost of the corresponding polymers, mainly polypropylene and polyethylene, depends on the international oil price. One big challenge for modern chemistry is to look for an alternative production of feedstocks that is independent of the oil-industry.

Much research has been done, and in the last few years the production process of propene out of natural gas or coal via methanol (methanol-to-propylene, MTP) has become more important and is already commercially used. The following transformation of cheap, easily available propene into high molecular weight polypropylene with unique, tailor-made material properties is a research field with an enormous potential. The key to tailoring polymer properties such as stiffness, mechanical strength, or transparency is to control the molecular architecture. For the polymerization of olefins, the development of metallocene catalysts gave access to new polymer microstructures. One significant advantage in metallocene polymerization catalysis [1, 2] is that the polymer microstructures and the corresponding material properties can be easily designed by variation of the catalyst. This enables the production of metallocene-catalyzed polypropylene with various types and degrees of stereoregularity [1–4], from highly stereoregular isotactic or syndiotactic polypropylenes to amorphous or low crystalline ones.

An important step in the field of investigation of metallocenes was the design of zirconocene catalysts. These made it possible to produce polypropylenes with a great variation in tacticity [5]. Although the ligands of the catalysts were varied, the molecular weights mostly did not exceed $300,000 \text{ g mol}^{-1}$.

To reach high and ultrahigh molecular weight polypropylenes, investigation took place by exchanging zirconium by hafnium in isostructural complexes. Literature provides a few examples showing that this exchange of the central metal leads to up to a threefold increase in molecular weight. Unfortunately, the activity of the hafnium complexes was reported to be negligible compared to the zirconium analogs while using standard MAO (methylaluminumoxane) activation [6]. Research work by Rieger et al. showed the same low activity for HfCl_2 complexes after MAO activation. The situation changed the first time that Rieger et al. activated a hafnium-dimethyl complex with trityl-tetrakis(pentafluorophenyl) borate. The activity increased to be equivalent to the zirconium complexes and even higher. For the first time it was possible to obtain polypropylenes with molecular weights up to $5,000,000 \text{ g mol}^{-1}$ and tacticities of 10–80%. Investigations during the following years showed that polypropylenes can be produced through hafnocene catalysts with high activities by using borate instead of MAO activation [5, 7].

In a time when prices for oil are continuously rising, hafnocene catalysts enable production of “high-tech” materials in a relatively cheap way. Hafnocenes are the key to a family of high and ultrahigh molecular weight polypropylenes whose material properties can be individually and simply varied. To help comprehend the importance

and the development of hafnocene catalysts in recent years, the following chapters show the function, polymerization mechanism, and the resulting polypropylenes of representative hafnocenes.

2 Catalyst Characterization

2.1 Overview

Collins et al. reported in 1995 that catalysts based on hafnium are desirable for the production of elastomeric polypropylene in that they polymerize propylene to a high molecular weight polymer and are indefinitely stable under typical polymerization conditions [8]. Based on the theory that hafnium as a catalytic center leads to a significant increase of molecular weight in propene polymerization compared with the zirconium-based catalyst, Rieger et al. searched for hafnocene systems to obtain polymers with new properties.

The exchange of zirconium in isostructural complexes leads to a new family of asymmetric metallocenes (Fig. 1) bearing a 2-methyl substituent and varied substituents in positions 5, 6, and 7 of the indenyl moiety. After borate activation all catalysts show an unexpected high and constant activity toward the polymerization of propylene and lead to significantly increased molecular weight products compared to the zirconocene species [9–11].

The explanation is based on the ability of these “dual-side” complexes to combine an isoselective side with one side leading predominantly to single stereoerrors within one particular species. This nonselective side can be exposed to migratory insertion reactions depending on the monomer concentration. This provides a new tool to control the amount and the distribution of single stereoerrors along an isotactic chain [5]. With catalyst **1**, depending on the reaction parameters, polypropylenes with tacticities of $17\% \leq [\text{mmmm}] \leq 34\%$ can be obtained with molecular weights up to $4.9 \times 10^6 \text{ g mol}^{-1}$.

To find more information about the influence of steric effects on the polymerization performance, catalyst **2** (5,6 triptycene indenyl hafnocene dichloride) was developed.

Besides the investigations into polymerization mechanisms and steric effects, a matter of particular interest was to extend the portfolio of material properties toward isotactic plastomers (higher stiffness materials). Therefore, hafnocene catalyst **3** (2-methyl-benzo-indeno [6,7] thiophen) bearing a substituted indenyl fragment derived from dibenzothiophene was synthesized. It was intended to look for other structural motifs that maintained the excellent performance of the asymmetric catalyst **1** but might afford higher tacticity values. Rigid substituents in the 6,7-positions of the 2-methylinden-1-yl fragment created a situation with a similar enantiofacial discrimination of the prochiral propylene monomer on either complex side in the migratory polyinsertion reaction [5, 10]. With the help of catalyst **3**, flexible

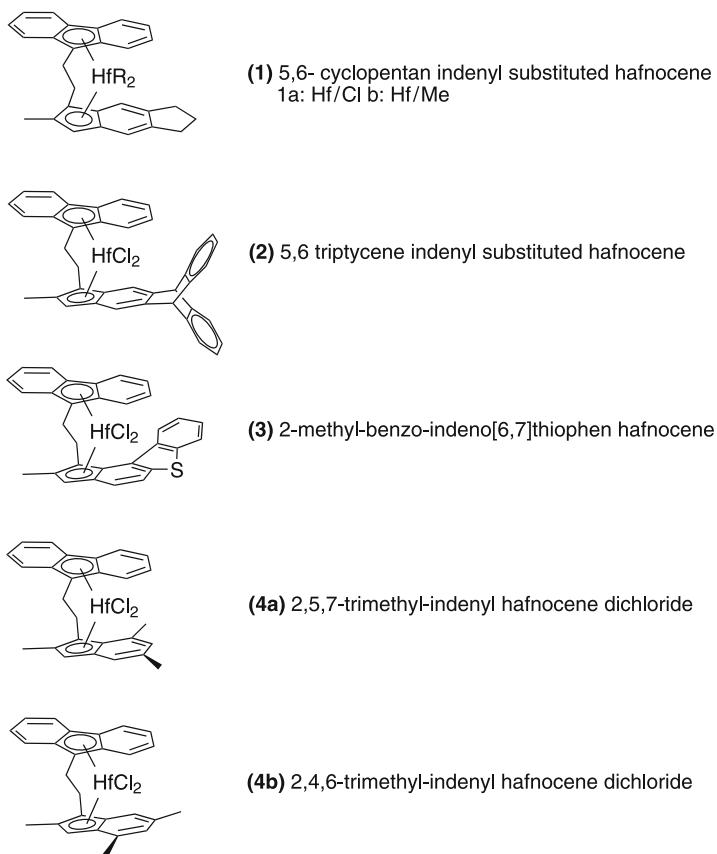


Fig. 1 Catalysts overview

polypropene plastomers with isotacticities in the range 65–85% and again ultrahigh molecular weights (up to 1.5×10^6 g mol⁻¹) could be achieved [5, 10]. This nicely fills the gap between “soft” elastomers and stiffer polypropene plastomers.

Since plastomeric polypropylenes were insufficiently investigated, further improvement of catalyst activity correlated with an easy synthetic approach was required. Therefore, the two asymmetric hafnocene dichloride complexes, each bearing a 2,5,7- and 2,4,6-trimethyl substituted indenyl moiety (**4a**, **4b**) were developed.

2.2 Mechanism

In the early stages of the metallocene-catalyzed olefin polymerizations the focus of research lay on C_2 - and C_s -symmetric complexes [3, 12, 13]. Since the beginning of the 1990s C_1 -symmetric catalysts have had more and more impact. The reason is

based on the different substituted coordination sides of these systems, which allow creation of new and auspicious polymer structures.

By using the asymmetric titanocene $[\text{MeHC}(\text{Me}_4\text{-Cp})(\text{Ind})]\text{TiCl}_2$ (Fig. 2), Chien obtained the first elastic polypropylene with a narrow molecular weight distribution [14–17].

Based on Chien's research results, Collins et al. modified the basic structure of the catalysts and also achieved elastic material [8, 18, 19]. In both cases the elastic properties of the polymers are justified in a block structure with isotactic and atactic sequences. In 1999 Rieger et al. presented a couple of asymmetric, highly active metallocene catalysts, e.g., the “dual-side” catalyst *rac*-[1-(9- η^5 -fluorenyl)-2-(5,6-cyclo-penta-2-methyl-1- η^5 -indenyl)ethane]zirconium dichloride (Fig. 3). These catalysts allowed building of isolated stereoerrors in the polymer chain to control the tacticity and therefore the material properties of the polymers [9].

2.2.1 C_2 Polymerization Mechanism

Looking at C_2 -symmetric catalysts, there exist in principle two different metallocene–olefin complexes (Fig. 4). Structure **a** is energetically favored because the methyl group of the propene is in *trans*-position relative to the β -methyl structure of the polymer chain. Both methyl groups in structure **b** are in *cis* position to each

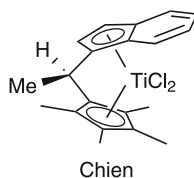


Fig. 2 C_1 -symmetric complex for synthesis of elastic polypropylene

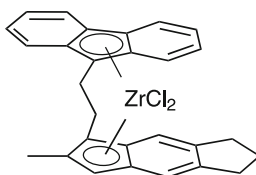


Fig. 3 “Dual-side” catalyst for variable material properties

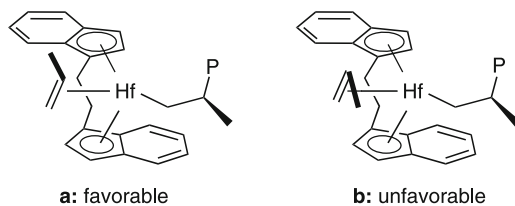


Fig. 4 Possible C_2 -symmetric metallocene complexes

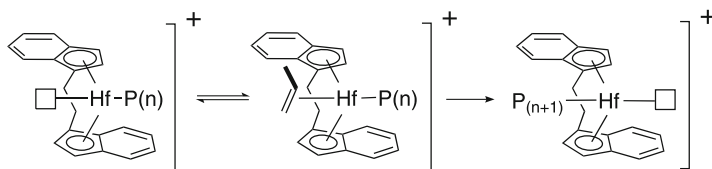


Fig. 5 Coordination cycle by C_2 -symmetric complexes

other, which is energetically unfavorable [1, 3, 20]. The coordinated monomer is therefore geometrically fixed. After the polymer changes place, a new monomer will find the same steric surrounding for insertion due to the C_2 symmetry of the complex. By repeating this coordination–insertion cycle an isotactic polymer structure will be achieved (Fig. 5).

2.2.2 “Chain Back” Polymerization Mechanism

The polymerization mechanism for the “dual-side” catalysts is totally different from the C_2 -symmetric complexes. Due to their geometry, the “dual-side” complexes show different stereoselectivities for monomer coordination and insertion. It was shown that the introduction of the stereoerror formation by the 5-substituted asymmetric catalysts originates predominately from the kinetic competition between chain back-skip and monomer coordination at the aspecific side of the catalyst [9].

As a consequence of the dependence of the polymer stereoregularity on monomer concentration and polymerization temperature, the mechanism shown in Fig. 6 was established.

Chien already postulated that C_1 -symmetric *ansa*-bridged complexes exist in two isomeric states, which interconvert during the course of the polymerization reaction [14, 15, 21, 22]. Different stereoselectivities for monomer coordination and insertion are found for the two coordination sites of the asymmetric metallocene catalysts (Fig. 6, **I** and **IV**). The migration of the polymer chain to the monomer, coordinated at the isoselective site (**I**→**II**), followed by a consecutive chain back-skip (at higher temperatures) to the sterically less hindered side (**II**→**III**) leads to isotactic [mmmm] sequences [11].

By the time the concentration of monomer is low, the back-skip of the polymer chain to the less-hindered site is faster than the formation of the high-energy alkene coordinated intermediate (**IV**). For this reason, at low propene concentrations and elevated temperatures isotactic sequences are formed. The probability of monomer coordination at the aspecific site (**IV**) is enhanced when the propene concentration increases. The consequence is that single stereoerrors [mrrm] are introduced in the isotactic polymer chain. ^{13}C -NMR was able to prove the mechanism because a

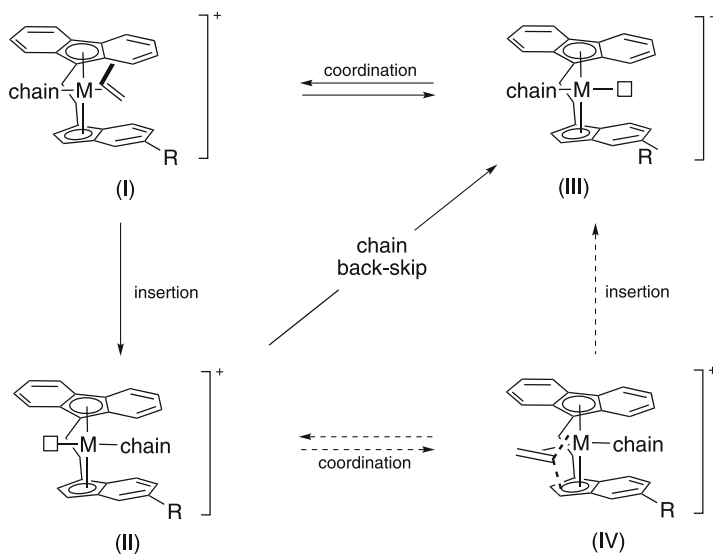


Fig. 6 Proposed mechanisms for the formation of isotactic polypropylenes I-IV with isolated stereoerrors obtained from C_1 -symmetric catalysts [9]

[mrrm] pentade would be observable from two consecutive misinsertions and is missing in the spectra derived from the latter polymers.

2.2.3 “ C_2 -Symmetric-Like” Polymerization Mechanism

A special case of the “chain back skip polymerization mechanism” and therefore an entirely different polymerization behavior was observed for differently substituted asymmetric complexes (for example catalyst **3**). Although asymmetric in structure, these catalysts follow the trend observed for C_2 -symmetric metallocenes [20]. Chien et al. [23] reported a similar behavior for *rac*-[1-(9- η^5 -fluorenyl)-2-(2,4,7-trimethyl-1- η^5 -indenyl)ethane]zirconium dichloride and attributed this difference in the stereoerror formation to the fact that both sides of the catalyst are stereoselective; thus isotactic polypropylene is obtained in the same manner as in the case of C_2 -symmetric metallocene catalysts.

In the case of catalyst **3**, the thiophene substitution in the 6,7 position controls the gap aperture between fluorenyl and indenyl ligands by repulsing steric interactions at the complex backside [10, 11]. This leads to increased stereoselectivities [9] and is responsible for a “ C_2 -symmetric-like” polymerization mechanism, characterized by increasing isotacticities when the polymerization temperature is reduced [5, 11] (Fig. 7).

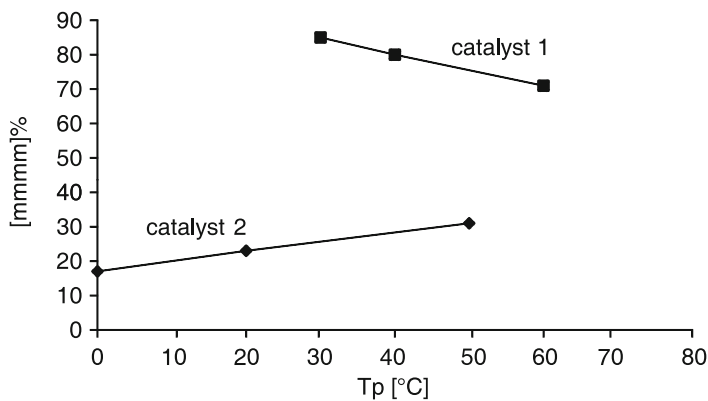


Fig. 7 Polypropylene stereoregularity versus polymerization temperature (catalyst **1**: chain back-skip mechanism, catalyst **2**: C_2 -symmetric-like mechanism) [11]

3 Cocatalysts

The key to highly active metallocene catalysts is the use of cocatalysts. In an activation step, the cocatalyst creates out of the metallocene a polymerization-active species. At first, methylaluminumoxane (MAO) was usually used to activate metallocenes. Nowadays an alternative activation via borane and borate is becoming more and more important [20, 24, 25].

3.1 Methylaluminumoxane (MAO)

Alkylaluminumoxanes, oligomeric compounds consisting of $-Al(R)-O-$ subunits, have been known to be active for polymerization of monomers such as oxiranes since the early 1960s [26]. Methylaluminumoxane $[-Al(Me)-O-]_n$ (MAO) prepared by controlled hydrolysis of $AlMe_3$ and typically having $n \approx 5-20$, affords highly active catalysts for polymerizing ethylene, propylene, and higher α -olefins when combined with group 4 metallocenes.

Although the structure of MAO was analyzed by different methods, such as IR and NMR spectroscopy, mass spectroscopy and lots more, the exact composition and structure of MAO are still not entirely clear or well-understood [27, 28]. It is assumed that the structures of MAO include one-dimensional linear chains, cyclic rings that contain tricoordinated Al centers, and three-dimensional clusters with tetracoordinated aluminum [24] (Fig. 8).

In metallocene-catalyzed polymerization reactions the active species is built through the reaction of a metallocene dichloride with the Lewis acid MAO. In the first step, a monomethyl-monochloro complex is formed and with an excess of MAO a dimethyl complex is created. In a fast equilibrium reaction through an

abstraction of a methyl group, the polymerization-active 14-valence electron cationic species $\text{Cp}_2\text{M}(\text{CH}_3)^+$ ($\text{M} = \text{Ti}, \text{Zr}, \text{Hf}$) is generated. $(\text{MAO}-\text{CH}_3)^-$ acts as soft coordinated counterion (Fig. 9).

In another slow balance reaction the active cation changes to an inactive dimeric species. This species is converted with the help of surplus MAO continuously back [29]. The transformation is connected with the property of alkylmetallocene cations, to react with a lot of CH-groups by elimination of CH_4 [30, 31].

As inactive species, a binuclear complex with a CH_3 bridge between the metal and Al center is existent (Fig. 10) [20]. For the regeneration of the binuclear inactive products to the active hafnocene cations, alkyl-exchange reactions are assumed between the $\text{M}-\text{CH}_2-\text{Al}$ - unit and MAO.

Therefore, the cocatalyst is expended by the building of $\text{Hf}-\text{CH}_3$ - and $\text{Al}-\text{CH}_2-\text{Al}$ -units and has to be used in a big overage to assure a high polymerization activity.

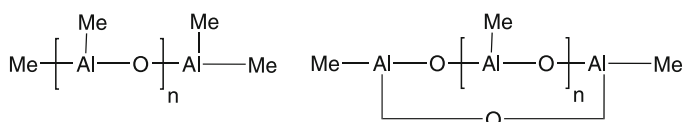


Fig. 8 Oligomer structures of MAO with $n = 5-20$ (linear/cyclic)

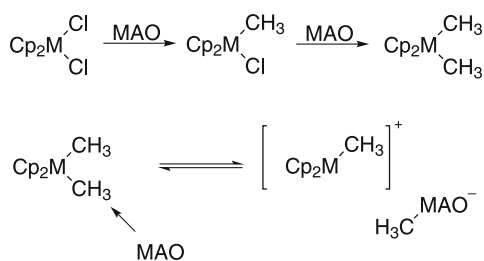


Fig. 9 Creation of the active species by MAO activation

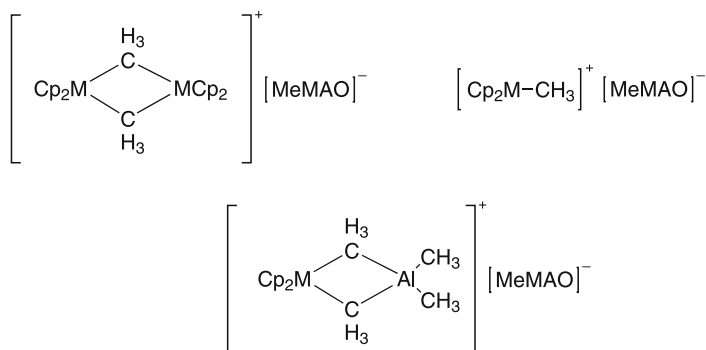


Fig. 10 Hypothetical products of the reaction between MAO and metallocene

3.2 Borane and Borate

An alternative to MAO activation is the formation of the active species via introduction of borate counterions by using borane or borate cocatalysts [32–34]. Relatively strong Lewis acidic organoboranes, such as $B(C_6F_5)_3$, or organoborates, such as $[PhNMe_2H]^+ [B(C_6F_5)_4]^-$ and $[PH_3C]^+ [B(C_6F_5)_4]^-$ (Fig. 11) could be used. With the help of the activation with borate it was possible for the first time to isolate alkylzirconocene cations (e.g., $\{[(CH_3)_2C_5H_3]ZrCH_3\}^+ [H_3CB(C_6F_5)_3]^-$) and investigate them with single-crystal X-ray analysis [35, 36].

An advantage of borate activation is that the boron-containing substances are used in a 1:1 proportion, in contrast to MAO, which is used in overage. Landis was able to show with the help of kinetic research that all centers are activated in the case of borate activation, whereas in activation with MAO only a fraction exists in the active form [36].

A considerably higher polymerization activity is reached by using borate and borane. Furthermore, molecular weights increase because the chain termination (compared to MAO activation) via transfer to aluminum is not possible.

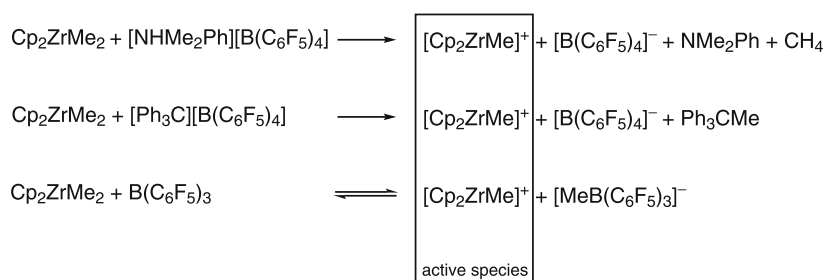


Fig. 11 Borate/borane activation

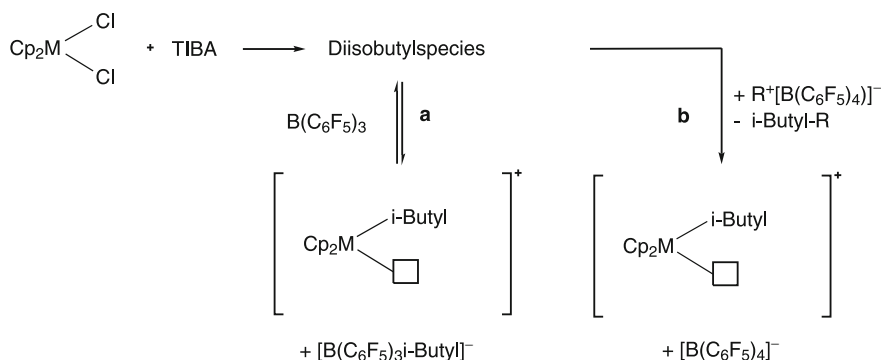


Fig. 12 “In situ” activation with borane (a) or borate (b)

A disadvantage of borane and borate systems is that the alkylmetallocene cations are more instable and more sensitive to impurities and water. To overcome this higher sensitivity, a dialkyl species can be built by an “in situ” reaction with triisobutylaluminum (TIBA). TIBA acts as alkylation reagent and as a scavenger and stabilizes the dialkyl species in solution; it is used as stock solution for the polymerization experiments (Fig. 12).

4 Polymerization Experiments

The synthesis of the catalysts **1**, **2**, **3** and **4** have been reported previously [9–11, 25, 37].

4.1 Polymerization Procedure

The polymerization reactions were performed in a 0.5- or 1-L Büchi steel autoclave at constant pressure and temperature. The steel reactor was charged with 200–300 mL of toluene and with the desired amount of cocatalyst and hafnocene (MAO activation, entries 1 and 2, Table 1) or with the desired amount of preactivated catalyst solution (borate activation, entries 12–16, 19–21; Table 1). Subsequently, the polymerization temperature was adjusted and the reactor was charged with propene up to the desired pressure. For borate activation the cocatalyst solution was injected into the autoclave via a pressure burette. The monomer consumption was followed using a calibrated gas flow meter (Bronkhorst F111C-HA-33P) and the pressure was kept constantly during the entire polymerization period (Bronkhorst pressure controller F-111C-HAP-602C-EA-33P). Pressure, temperature, and monomer consumption were monitored and recorded online [38].

Some experiments (entries 3–10, 17, 18, 22–25; Table 1) were performed in liquid propene, which was condensed at $-10\text{ }^{\circ}\text{C}$ up to the desired volume in the autoclave. Using liquid propene, the catalyst and cocatalyst solutions were both injected into the autoclave via a pressure burette.

Both in liquid propene or in toluene the polymerization reactions were quenched with MeOH, and the polymer products were precipitated by pouring the toluene solution into an excess of MeOH. The product was filtered, washed with acidified methanol, and dried in vacuum at $60\text{ }^{\circ}\text{C}$ overnight [39].

4.2 Activities, Molecular Weights, and Stereoselectivity

The experimental data of the polymerization reactions of propylene performed with the hafnocene compounds **1–4** after MAO or $[(\text{C}_6\text{H}_5)_3\text{C}^+][(\text{C}_6\text{F}_5)_4\text{B}^-]$ activation are summarized in Table 1.

Table 1 Selected polymerization results obtained with the catalysts 1–4 after MAO or borate activation

Entry	Catalyst	Activator	T_p (°C)	$[C_3]$ (mol L ⁻¹)	Activity ^a (kg mol ⁻¹ h ⁻¹)	M_w (g mol ⁻¹)	M_w/M_n	[mmmm] (%)
1	1a	MAO	30	3.1	150	55,000	2	31
2		MAO	50	2.2	320	27,000	2.1	40
3	1b	Borate	0	C ₃ H ₆ (l)	6000	4,900,000	6.9	17
4		Borate	20	C ₃ H ₆ (l)	23,000	1,600,000	2.6	24
5		Borate	50	C ₃ H ₆ (l)	50,000	700,000	3.5	34
6	1a	TIBA (RT)/ borate	30	C ₃ H ₆ (l)	100,000	1,000,000	2.7	25
7		TIBA (60 °C)/ borate	30	C ₃ H ₆ (l)	350,000	1,300,000	2.6	27
8	2	Borate	30	C ₃ H ₆ (l)	1300	260,000	2.2	20
9		Borate	30	C ₃ H ₆ (l)	2400	300,000	2.5	19
10	3	Borate	30	C ₃ H ₆ (l)	15,900	254,000	2.6	77.7
11		Borate	0	C ₃ H ₆ (l)	5300	1,524,000	3.8	75.4
12	4a	Borate	30	2.1	80,000	200,000	2.8	76
13		Borate	30	2.9	138,000	350,000	2.4	74
14		Borate	30	3.9	166,000	380,000	2.9	72
15		Borate	40	2.4	151,000	130,000	2.5	78
16		Borate	50	1.9	214,000	50,000	2.6	82
17		Borate	10	C ₃ H ₆ (l)	39,000	960,000	3.3	63
18		Borate	40	C ₃ H ₆ (l)	321,000	300,000	3.2	72
19	4b	Borate	20	4.2	50,000	360,000	2.9	60
20		Borate	30	2.9	45,000	160,000	2.6	60
21		Borate	40	2.4	25,000	70,000	2.4	60
22		Borate	10	C ₃ H ₆ (l)	1500	600,000	2.6	48
23		Borate	20	C ₃ H ₆ (l)	21,500	500,000	3.8	47
24		Borate	30	C ₃ H ₆ (l)	6400	300,000	3.7	46
25		Borate	40	C ₃ H ₆ (l)	100	300,000	3	58

^akg PP per mmol Hf [C₃] per h

The asymmetric 5,6-cyclopentyl-substituted metallocene **1a/MAO** shows a very low activity in toluene solution (around 150–320 kg PP mol⁻¹ Hf h⁻¹). In addition, the molecular weight is quite low (entry 1, M_w 5.5 × 10⁴ g mol⁻¹). By increasing the temperature to 50 °C the activity more than doubled, but on the other hand the molecular weight decreased to 2.7 × 10⁴ g mol⁻¹ [5, 7, 11].

Compared to the previously studied complex **1a/MAO**, the catalyst **1b/borate** proved to be highly active (up to 50,000 kg PP mol⁻¹ Hf h⁻¹). The excellent catalytic performance of **1b/borate** is complemented by the high molecular weight of the polymer products. At 0 °C polymer chains with ultrahigh molecular weight (entry 3, M_w 4.9 × 10⁶ g mol⁻¹) are accessible. The broad molecular weight distribution results most likely from the insolubility of the ultrahigh molecular weight products in liquid propene at 0 °C [7].

Increasing the temperature leads to a decline of the molecular weight (e.g., entry 3, 20 °C, M_w 1.6×10^6 g mol⁻¹). However, even at technical process temperatures elastic homopolypropylenes with very high molecular weights (entry 9, 50 °C, M_w 7×10^5 g mol⁻¹) are produced. According to the data from Table 1, there was a strong influence of the polymerization temperature on the substituted catalyst **1b**, for which the isotacticity is increased from 17% (at 0 °C) to 34% (50 °C).

Incredibly increased activities could be observed using the in situ activation method for the catalyst **1a** (up to 350,000 kg PP mol⁻¹ Hf h⁻¹). The resulting polypropylenes have ultrahigh molecular weight (entries 6 and 7, M_w 1,000,000 g mol⁻¹) and tacticities round 25% (30 °C).

For further investigations on the influence of steric effects on the polymerization performance of dual-side catalysts, Rieger et al. examined the incorporation of the sterically demanding triptycene ligand in several bridged hafnocenes **2** (Table 1.) [25]. In comparison to the sterically less demanding 5,6-cyclopentyl substitution, the triptycene unit leads to significantly lower activities (up to 2400 kg PP mol⁻¹ Hf h⁻¹) and molecular weights (M_w 150,000–300,000 g mol⁻¹) whereas tacticities stayed within the range of catalyst **1**.

In the case of **3/borate** the highest activity was obtained at T_p 30 °C (1.59×10^4 kg PP mol⁻¹ Hf h⁻¹, entry 9). As shown by different investigations, a sufficiently high molecular weight and isotacticities above 60% are a prerequisite for the appearance of plastomeric properties. In polymerization experiments with the 6,7-substituted complex **3**, isotactic polypropylenes with [mmmm] pentad concentrations ranging around 75–78% were obtained, with molecular weights up to 1.5×10^6 g mol⁻¹ (entry 10), properties that fall into the expected range for plastomers. The polymerization experiments in liquid propene show that the molecular weight could be highly increased. This is in accordance with recent observations that significantly higher molecular masses could be obtained for borate-activated dimethyl complexes due to the absence of the chain transfer to aluminum [5].

Compared to the previously studied complex **3**, the catalyst **4a/borate** shows much higher activity (Table 1, 12–18). Increasing the polymerization temperature affords the highest productivity at 50 °C in toluene solution (up to 2.14×10^5 kg PP mol⁻¹ Hf h⁻¹). The activity of catalyst **4a** even reaches values up to 3.21×10^5 kg PP mol⁻¹ Hf h⁻¹ in liquid monomer. Evidently, the catalytically active species has not been deactivated by the sulfur function **3** via an intramolecular mechanism, but might take part in intermolecular coordination processes that facilitate chain growth. This assumption could explain the activities (up to 14 times higher) achieved with each of the catalysts mentioned. So far the trend for asymmetric metallocene catalyst is that higher molecular weights of the polypropylenes could be reached at lower polymerization temperatures [9–11, 20]. Following the same trend, ultrahigh molecular weight plastomeric polypropylenes (M_w 9.6×10^5 g mol⁻¹) were obtained with **4a/borate** at low polymerization temperature (20 °C). One explanation could be that the backward oriented 5,7-dialkyl substitution effectively suppress the chain-end isomerization process [11] (source of

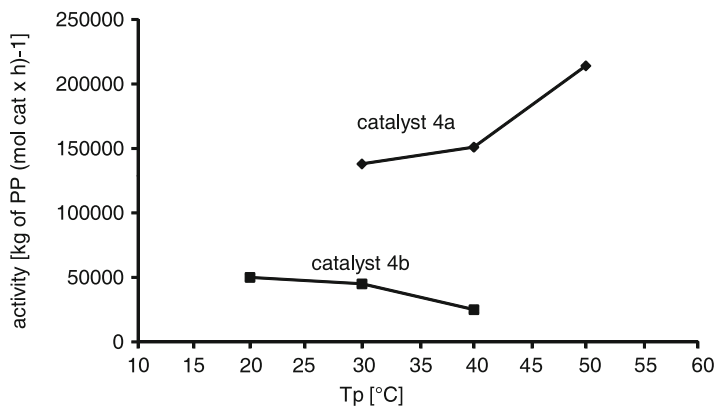


Fig. 13 Polypropylene activity vs. polymerization temperature (catalyst **4a**: chain back-skip mechanism, catalyst **4b**: C_2 -symmetric-like mechanism)

stereoerrors in C_2 -symmetric catalysts) and hinders at the same time a subsequent chain termination reaction, leading to higher molecular weight products (C_2 -symmetric-like polymerization mechanism).

The catalyst **4b/borate** was tested under similar conditions as in the case of **4a** (toluene solution and liquid propylene) in propylene polymerization experiments after preactivation with TIBA (Table 1). According to the data from Table 1, the catalytic properties of **4b** are inferior to those of **4a**. The behavior of **4b** is similar to that of asymmetric catalysts with a forward orientation of the 4-substituted indene unit [10]. The effect of the substitution position is remarkable. While the 5,7-substituted hafnocene **4a** shows higher activities (up to 3.2×10^5 kg PP mol⁻¹ Hf h⁻¹ at 40 °C) with increasing temperatures, substantially lower or almost no activities were found for the 4,6-substituted hafnocene **4b** at the same temperature (Fig. 13).

Tacticities of the polypropylenes above 60% [mmmm] highlights the tendency of the backward oriented substitution (**4a**) to produce plastomeric materials. During experiments in liquid propylene, no similarity is observed between the two isomeric catalysts. Catalyst **4b/borate** does not follow the same trend in the catalytic performance as previously mentioned, but leads to polypropylenes with sufficient amount of isotactic sequences and relatively high molecular weight for the design of plastomeric polypropylenes.

5 Conclusion

The combination of structural studies and polymerization experiments of a series of hafnocene catalysts has provided greater insight into the polymerization mechanism and the possibilities of tailoring polymer microstructures.

Depending on the hafnocene catalyst, it is possible to obtain polypropylenes with different tacticities in a range from 10 to 80%. Taking into consideration the

correlation between polymer tacticity and material properties it was demonstrated that hafnocene catalysts possess a high potential for tailoring the polymer microstructures, leading to new materials with properties ranging from thermoplastic elastomers to highly isotactic plastomers with ultrahigh molecular weights.

Independent of the ligand system, two different activation methods have been used in performing the propylene polymerization experiments. In both cases, the catalytic activities and molecular weights of the polymers are a sensitive function of the aluminum content provided by the activators. This dependence suggested an additional reversible chain transfer to aluminum when activating with MAO. As lower contents of Al are provided in the polymerization system in the case of in situ activation with TIBA/borate, the only mechanism occurring is the chain back-skip. Furthermore, the differences in the polymer microstructures prepared with MAO and borate as cocatalysts are reflected. They sustain the proposed reversible chain transfer.

The long-existing theory that the activity of hafnocene catalysts is negligible compared to the zirconium analogs can now be abandoned. The deciding point is not hafnium; it is more the way of activation! While using TIBA/borate for building the active species, activities increase dramatically and exceed those of comparable Zr/MAO systems, obtaining high and ultrahigh molecular weight polypropylenes.

Based on the current situation that oil prices are continuously rising and the industrial process of natural gas to methanol, methanol to propylene, propylene to polypropylene becomes more important, it will be interesting to see what importance hafnocene-catalyzed polypropylenes will have in future daily life.

References

1. Brintzinger HH, Fink G, Mühlhaupt R (1995) Ziegler catalysts. Springer, Berlin Heidelberg New York
2. Resconi L, Cavallo L, Fait A, Pietmontesi F (2000) Selectivity in propene polymerization with metallocene catalysts. *Chem Rev* 100:1253–1345
3. Brintzinger HH, Fischer D, Mühlhaupt R, Rieger B, Waymouth RM (1995) Stereospezifische Olefinpolymerisation mit chiralen Metallocenkatalysatoren. *Angew Chem Int Ed Engl* 107:1255–1283
4. Kaminsky W (1996) New polymers by metallocene catalysis. *Macromol Chem Phys* 197:3907
5. Rieger B, Troll C, Hild S, Cobzaru C (2006) “Dual-side” catalysts for high and ultrahigh molecular weight homopolypropylene elastomers and plastomers. *Coord Chem Rev* 250:189–211
6. Kaminsky W, Engehausen R, Zoumis K (1992) Standardized polymerizations of ethylene and propene with bridged and unbridged metallocene derivatives: a comparison. *Makromol Chem* 193:1643–1651
7. Rieger B, Troll C, Preuschen J (2002) Ultrahigh molecular weight polypropylene elastomers by high activity “dual-side” hafnocene catalysts. *Macromolecules* 35:5742–5743
8. Collins S, Gauthier WJ, Corrigan JF, Nicholas NJ (1995) Elastomeric poly(propylene): influence of catalyst structure and polymerization conditions on polymer structure and properties. *Macromolecules* 28:3771–3778

9. Rieger B, Dietrich U, Hackmann M, Klinga M, Leskelä M (1999) Control of stereoerror formation with high-activity “dual-side” zirconocene catalysts: a novel strategy to design the properties of thermoplastic elastic polypropenes. *J Am Chem Soc* 121:4348–4355
10. Rieger B, Deisenhofer S, Feifel T, Kukral J, Klinga M, Leskelä M (2003) Asymmetric metallocene catalysts based on dibenzothiophene: a new approach to high molecular weight polypropylene plastomers. *Organometallics* 22:3495–3501
11. Rieger B, Troll C, Hild S, Cobzaru C, Deisenhofer S, Hearley A (2005) Novel high and ultrahigh molecular weight poly(propylene) plastomers by asymmetric hafnocene catalysts. *Macromol Chem Phys* 206:1231–1240
12. Kaminsky W, Arndt M (1997) Metallocenes for polymer catalysis. *Adv Polym Sci* 127:143–187
13. Kaminsky W, Scheir J (1999) Metallocene-based polyolefins. Preparation, properties and technology. Wiley, New York
14. Chien JCW, Rausch MD, Mallin DT, Lin YG, Dong SH (1990) *rac*-Ethylidene(1- η 5-tetramethylcyclopentadienyl)(1- η 5-indenyl)dichlorotitanium and its homopolymerization of propylene to crystalline-amorphous block thermoplastic elastomers. *J Am Chem Soc* 112:2030–2031
15. Chien JCW, Rausch MD, Llinas GH, Lin Y, Winter HH (1991) Two-state propagation mechanism for propylene polymerization catalyzed by *rac-anti*-ethylidene(1- η 5-tetramethylcyclopentadienyl)(1- η 5-indenyl)dimethyltitanium. *J Am Chem Soc* 113:8569–8570
16. Llinas GH, Dong SH, Mallin DT, Rausch MD, Lin YG, Winter HH, Chien JCW (1992) Crystalline-amorphous block polypropylene and nonsymmetric *ansa*-metallocene catalyzed polymerization. *Macromolecules* 25:1242–1253
17. Chien JCW, Llinas GH, Day RO, Rausch MD (1993) Ethylidene(1- η 5-tetramethylcyclopentadienyl)(1- η 5-indenyl)dichlorozirconium: synthesis, molecular structure, and polymerization catalysis. *Organometallics* 12:1283–1288
18. Collins S, Gauthier WJ (1995) Elastomeric poly(propylene): propagation models and relationship to catalyst structure. *Macromolecules* 28:3779–3786
19. Collins S, Bailey L, Pigeon M (1998) Synthesis of elastomeric poly(propylene) using unsymmetrical zirconocene catalysts: marked reactivity differences of “rac”- and “meso”-like diastereomers. *Macromolecules* 31:1000–1009
20. Deffieux A, Cramail A, Radharkrishnen K, Pedetour JN (2001) Reactivity of metallocene catalysts for olefin polymerization: influence of activator nature and structure. *Macromol Rapid Commun* 22:1095–1123
21. Chien JCW, Babu GN, Newmark RA, Cheng HH, Llinas GH (1992) Microstructure of elastomeric polypropylenes obtained with nonsymmetric *ansa*-titanocene catalysts. *Macromolecules* 25:7400–7402
22. Chien JCW, Llinas GH, Rausch MD, Lin YG, Winter HH, Atwood JL, Bott SG (1992) Metallocene catalysts for olefin polymerizations. XXIV. Stereoblock propylene polymerization catalyzed by *rac-anti*-ethylidene(1- η 5-tetramethylcyclopentadienyl)(1- η 5-indenyl)dimethyltitanium: A two-state propagation. *J Polym Sci A* 30:2601–2617
23. Rausch MD, Chien JCW, Thomas EJ (2000) Substituent effects on the stereospecificity of propylene polymerization by novel asymmetric bridged zirconocenes. A mechanistic discussion. *Macromolecules* 33:1546–1552
24. Chen EY, Marks TJ (2000) Cocatalysts for metal-catalyzed olefin polymerization: activators, activation process, and structure–activity relationships. *Chem Rev* 100:1391–1434
25. Deisenhofer S (2002) Entwicklung neuer Zirkonocen- und Hafnocen-Katalysatorarchitekturen und deren Verwendung in der metallocenkatalysierten Olefinpolymerisation. Dissertation, Ulm
26. Vandenberg EJ (1960) Elastomers, synthetic (polyethers). *J Polym Sci* 47:486–489
27. Sinn H, Kaminsky W, Hoker H (eds) (1995) Alumoxanes, macromolecular symposia 97. Huthig & Wepf, Heidelberg
28. Sivaram S, Srinivasa RS (1995) Homogeneous metallocene-methylaluminoxane catalyst systems for ethylene polymerization. *Prog Polym Sci* 20:309–367

29. Mühlhaupt R, Fischer D, Jüngling S (1993) Donor- and acceptor-modified metallocene-based homogeneous Ziegler–Natta catalysts. *Makromol Chem Macromol Symp* 66:191–202
30. Jordan RF, Bajgur CS, Dasher WE, Rheingold AL (1987) Hydrogenation of cationic dicyclopentadienylzirconium(IV) alkyl complexes. Characterization of cationic zirconium(IV) hydrides. *Organometallics* 6:1041–1051
31. Jordan RF, LaPointe RE, Bradley PK, Baenziger N (1989) Synthesis and chemistry of cationic alkyl, alkenyl, and allyl complexes derived from the soluble, cationic hydride $(CH_3)_2Zr(H)(THF)^+$. *Organometallics* 8:2892–2903
32. Bochmann M, Lancaster SJ (1995) Cationic group IV metal alkyl complexes and their role as olefin polymerization catalysts: The formation of ethyl-bridged dinuclear and heterodinuclear zirconium and hafnium complex. *J Org Chem* 49:55–59
33. Marks TJ, Yang S, Stern CL, Chen YXE (1996) Organo-Lewis acids as cocatalysts in cationic metallocene polymerization catalysis. Unusual characteristics of sterically encumbered Tris(perfluorobiphenyl)borane. *J Am Chem Soc* 118:12451–12452
34. Marks TJ, Stern CL, Chen YXC (1997) Very large counteranion modulation of cationic metallocene polymerization activity and stereoregulation by a sterically congested (perfluoroaryl) fluoroaluminate. *J Am Chem Soc* 119:2582–2583
35. Marks TJ, Yang W, Stern CL (1991) Models for organometallic molecule-support complexes. Very large counterion modulation of cationic actinide alkyl reactivity. *Organometallics* 10:840–842
36. Schlögl M (2003) *Metallocen Polymerisationskatalyse in kompartimentierten Systemen*. Dissertation, Ulm
37. Cobzaru C (2006) *Asymmetric metallocene catalysts design of ultrahigh molecular weight polypropylene plastomers*. Dissertation, Ulm
38. Hild S, Rieger B, Troll C, Cobzaru C (2006) Elastomeric poly(propylene) from “dual-side” metallocenes: reversible chain transfer and its influence on polymer microstructure. *Macromol Chem Phys* 207:665–683
39. Rieger B, Cobzaru C (2006) Control of ultrahigh molecular weight polypropylene microstructures via asymmetric “dual-side” catalysts. *Macromol Symp* 236:151–155

Chain Shuttling Catalysis and Olefin Block Copolymers (OBCs)

Timothy T. Wenzel, Daniel J. Arriola, Edmund M. Carnahan,
Phillip D. Hustad, and Roger L. Kuhlman

Abstract Olefin block copolymers (OBCs) with new-to-the-world properties have recently been made via a process called chain shuttling polymerization. These systems comprise two or more catalysts with differing affinities for comonomer combined with a chain shuttling agent (CSA), which distributes the growing polymer chains among the various catalysts. The result is a unique block copolymer, with statistically distributed block sizes and numbers of blocks per chain. A unique property of the materials is that the melting temperature is nearly independent of the comonomer incorporation, which breaks a seemingly immutable relationship that was long held to be true.

Keywords Catalyzed olefin polymerization, Chain shuttling catalysis, Chain transfer, Olefin block copolymers, Thermoplastic elastomers

Contents

1	Introduction.....	67
2	Block Copolymers from Olefins.....	69
3	Chain Transfer to Metal in Olefin Polymerization.....	69
3.1	Coordinative Chain Transfer Polymerization.....	69
3.2	Reversible Chain Transfer in Dual-Catalyst Systems.....	71
4	High Throughput Method for the Discovery of Chain Shuttling Catalyst Systems.....	74
4.1	Mathematical Simulation of Single Catalyst Batch Reactions.....	74
4.2	Selection of Chain Shuttling Agent and Catalysts.....	81
4.3	Investigations of Chain Shuttling Using Deuterium Labeling.....	86

D.J. Arriola and T.T. Wenzel
The Dow Chemical Company, Bld 1776, Midland, MI 48674, USA
e-mail: djarriola@dow.com
e-mail: wenzeltt@dow.com

E.M. Carnahan, P.D. Hustad, and R.L. Kuhlman
The Dow Chemical Company, 2301 Brazosport, Freeport, TX 77541, USA
e-mail: ecarlahan@dow.com
e-mail: pdhustad@dow.com
e-mail: kuhlmarl@dow.com

5	Chain Shuttling in a Continuous Reactor.....	89
5.1	Olefin Block Copolymer Production in a Continuous Reactor	89
6	Properties of OBCs Made by Chain Shuttling Catalysis	91
6.1	Melting Temperature.....	91
6.2	Crystallinity and Solid-State Morphology.....	91
6.3	Solubility Properties	94
6.4	Performance.....	95
7	OBCs by CCTP.....	97
7.1	Comparison of Batch, Semi-Batch, and Continuous Processes	97
7.2	Synthesis of Diblock OBCs in a Continuous Process	97
7.3	Properties of Diblock OBCs from CCTP	98
8	Comparison of Polymer Architectures from Living Polymerization, Chain Shuttling, and Continuous CCTP.....	100
9	Summary.....	102
	References.....	103

Abbreviations

CSA	Chain shuttling agent
OBC	Olefin block copolymer
LDPE	Low density polyethylene
LLDPE	Linear low density polyethylene
VLDPE	Very low density polyethylene
ULDPE	Ultra-low density polyethylene
HDPE	High density polyethylene
PE	Polyethylene
PP	Polypropylene
iPP	Isotactic polypropylene
aPP	Atactic polypropylene
sPP	Syndiotactic polypropylene
LAO	Linear alpha olefin
f-PVC	Flexible polyvinylchloride
TPU	Thermoplastic polyurethane
TPV	Thermoplastic vulcanizate
CCG	Catalyzed chain growth
CTA	Chain transfer agent
CCTP	Coordinative chain transfer polymerization
TiBA	Triisobutylaluminum
TMA	Trimethylaluminum
TEA	Triethylaluminum
MAO	Methylalumoxane
MMAO	Modified methylalumoxane
DEZ	Diethylzinc
oct	Octyl
poly	Polymeryl

HS	Hard segment
SS	Soft segment
GPC	Gel-permeation chromatography
M_n	Number-average molecular weight
M_w	Weight-average molecular weight
M_w/M_n	Molecular weight distribution
DSC	Differential scanning calorimetry
CRYSTAF	Crystallization analysis fractionation
TREF	Temperature rising elution fractionation

1 Introduction

Polyolefins are the most ubiquitous synthetic polymers in the world [1]. High density polyethylene (HDPE), low-density polyethylene (LDPE), and linear low density polyethylene (LLDPE) are found in a myriad of applications in high volume, in part because the properties can be varied so widely. Many modifications to the performance of polyolefins can be effected by changing catalysts (traditional Ziegler–Natta catalysts [2], metallocenes [3] and post metallocene [4] catalysts), changing the molecular weight, incorporating linear alpha olefin (LAO) comonomers, or by blending with other polyolefins.

For instance, HDPE contains little or no comonomer and is made by a low-pressure, catalyzed process. It is high melting (ca. 135 °C), relatively stiff (high modulus) and difficult to stretch (high tensile strength) [5]. LDPE is typically made without comonomer using a non-catalyzed high pressure radical process [6]. The resulting polymer has a lower melting point than HDPE, primarily because the chains are so branched that they disrupt crystallization. Lower crystallinity results in decreased density, modulus, and tensile strength. However, the long chain branches in LDPE impart high melt strength, which leads to processing advantages.

LLDPE, like HDPE, is made in a low pressure catalyzed process [7]. It is a copolymer containing various levels of LAO, primarily 1-butene, 1-hexene, or 1-octene. Because it comprises a linear backbone with side chains (ethyl, butyl, or hexyl), lamellar crystallization is increasingly reduced at higher LAO levels, leading to decreased density, modulus, and tensile strength. Like LDPE, it can contain long-chain branches (depending on the catalyst and reaction conditions) that affect the melt rheology and solid-state properties.

Despite this tremendous versatility, there is still a fundamental limitation for these random copolymers: *melting point and modulus (stiffness) are inextricably coupled to the density* (or percentage short-chain branching from LAO comonomer) as shown in Fig. 1. The same method employed to lower modulus (incorporation of comonomer) results in a thinning of the polyethylene crystals, concomitant with a lowering of the melting point, according to a relationship established by Flory [8].

Because commercial grades of polyethylene are made with coordination catalysts, and incorporation of comonomer is dictated by statistical processes, none can violate this seemingly immutable relationship.

To illustrate this relationship, consider a random ethylene copolymer of a density 0.856 g cm^{-3} containing about 19 mol% 1-octene comonomer. At room temperature,

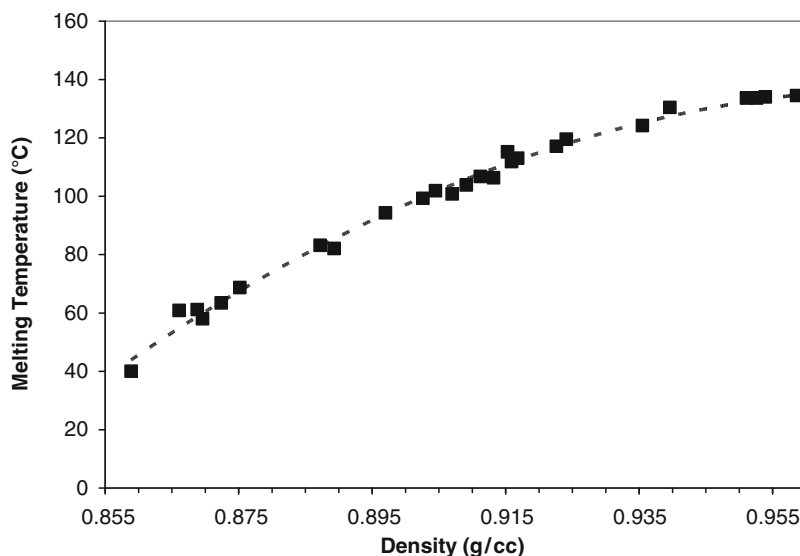


Fig. 1 Relationship between melting point and density for random ethylene-LAO copolymers

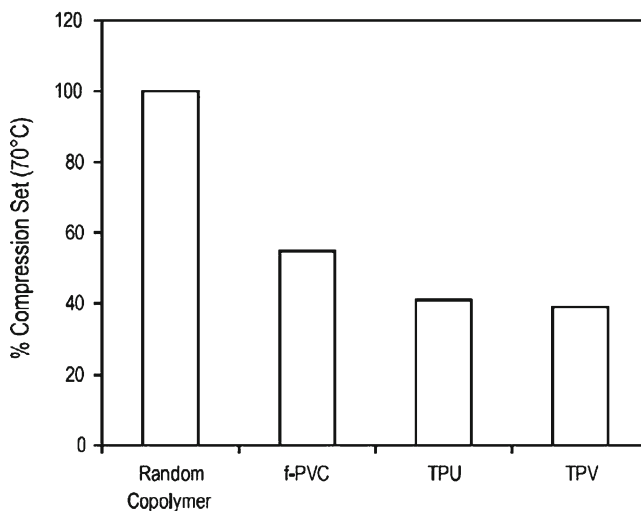


Fig. 2 Compression set (elastic recovery under compressive deformation) at 70 °C for an ethylene-LAO random copolymer, flexible polyvinylchloride (f-PVC) thermoplastic polyurethanes (TPUs), and thermoplastic vulcanizates (TPVs)

the material is an elastomer. However, the copolymer loses the desirable properties of an elastomer at higher temperatures; for example, the material has a compression set (a measure of elastic recovery under compressive deformation) of 100% at 70 °C (Fig. 2).

The ability to make PE with properties that fall outside these limitations would lead to a tremendous expansion of uses for this polymer, for example replacing flexible polyvinylchloride (f-PVC), which cannot be incinerated or recycled, thermoplastic polyurethanes (TPUs), or thermoplastic vulcanates (TPVs).

2 Block Copolymers from Olefins

One approach towards expanding the use of polyolefins is to control its microstructure, i.e., the orientation and distribution of comonomer along the polymer backbone. In particular, block copolymers constraining much of the alpha olefin (short chain branching) to certain blocks of the chain while leaving other blocks linear (no short chain branches) take on many of the best characteristics of HDPE and LLDPE. The melting point can be controlled by the HDPE region (“hard” polymer) whereas the elasticity or modulus can be controlled by the LLDPE portion (“soft” polymer). This occurs because the HDPE regions of different polymer chains can co-crystallize, while the elastomeric LLDPE regions still provide the rubber-like properties. In a sense, the material acts as a cross-linked rubber, but, unlike normal vulcanized rubber, the cross links can be reversed by melting. Therefore such a material can be melted and re-formed many times (or recycled) unlike vulcanized rubber, which, once cross-linked, retains its initial shape indefinitely. In general, these types of rubbers are referred to as thermoplastic elastomers [9].

3 Chain Transfer to Metal in Olefin Polymerization

3.1 Coordinative Chain Transfer Polymerization

We recently introduced an alternative to the “one-catalyst per polymer chain” approach to prepare a new type of olefin block copolymer (OBC) [10]. We refer to this process as *chain shuttling* polymerization, where a chain shuttling agent (CSA) is used to pass a growing polymer chain between two different catalysts. When the two catalysts are selected such that one makes a high density polyethylene and the other makes an elastomer, chain shuttling can enable the catalytic production of olefin block copolymers. We have also demonstrated that OBCs can be made using CCTP [11] with a single precatalyst by changing reactor conditions or monomer composition.

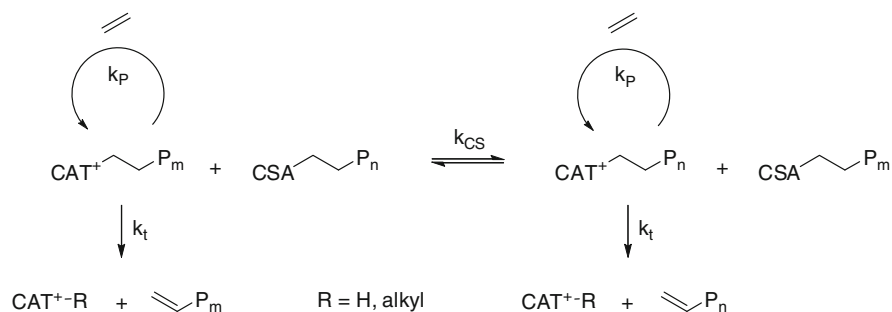
For these processes to work, fast and reversible chain transfer between the catalysts and the CSA is necessary. Such reversible chain transfer has been called variously

catalyzed chain growth (CCG) or coordinative chain transfer polymerization (CCTP). In CCTP, the vast majority of chains lie in a dormant state while attached to the CSA. These chains become active only when exchanged with the growing chain from a live catalyst (Scheme 1).

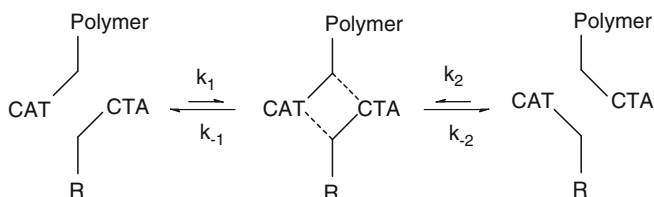
As stated above, a necessary precondition for CCTP and chain shuttling is reversible chain transfer with a chain transfer agent. We distinguish CCTP from chain shuttling in that the former is reversible exchange of polymer chains between like catalysts whereas the latter is reversible exchange of polymer chains between two or more different kinds of catalysts.

Irreversible transfer of polymer chains to metal-based chain transfer agents (CTAs) by heterogeneous titanium-based Ziegler–Natta catalysts has been reported in the literature as early as 1959 [12]. The proposed mechanism of alkyl exchange involves alkyl-bridged heterobimetallic dimer intermediates. To achieve efficient CCTP while maintaining optimal polymerization rates, binding with the chain transfer agent must not be so strong that the inactive bimetallic dimer is the dominant species, yet there must be sufficient binding to effect alkyl/polymeryl exchange (Scheme 2). Not only is the equilibrium constant important, but the actual rate constants for complexation and decomplexation should be as fast as possible (Scheme 3).

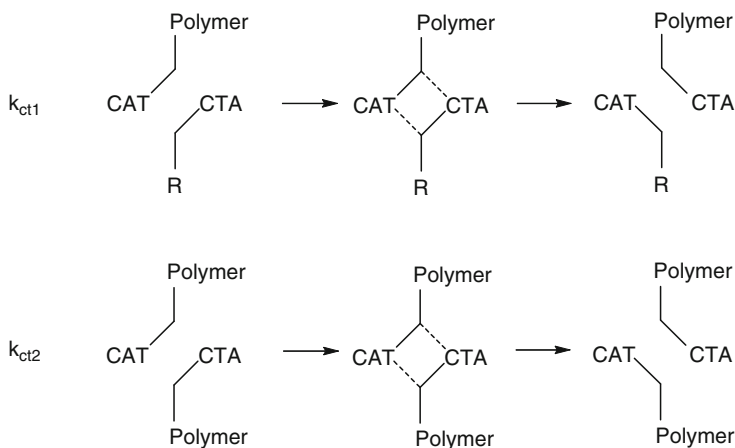
The first report of catalyzed chain growth on aluminum was presented by Samsel et al., using metallocenes of actinides [13] or hafnium [14, 15]. Gibson et al. described a detailed study of chain growth using the bis(imino)pyridyl iron complex **1** in combination with several metal alkyls [16]. Other systems reported to



Scheme 1 Activation of dormant chains by exchange with the growing chain from a live catalyst AU9



Scheme 2 Fully reversible binding of the chain transfer agent is required



Scheme 3 Relationship between alkyl exchange and reversibility (k_{ct1} , k_{ct2})

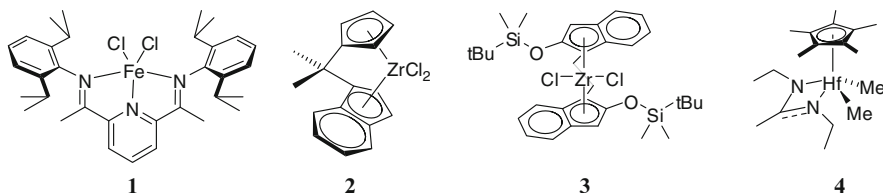


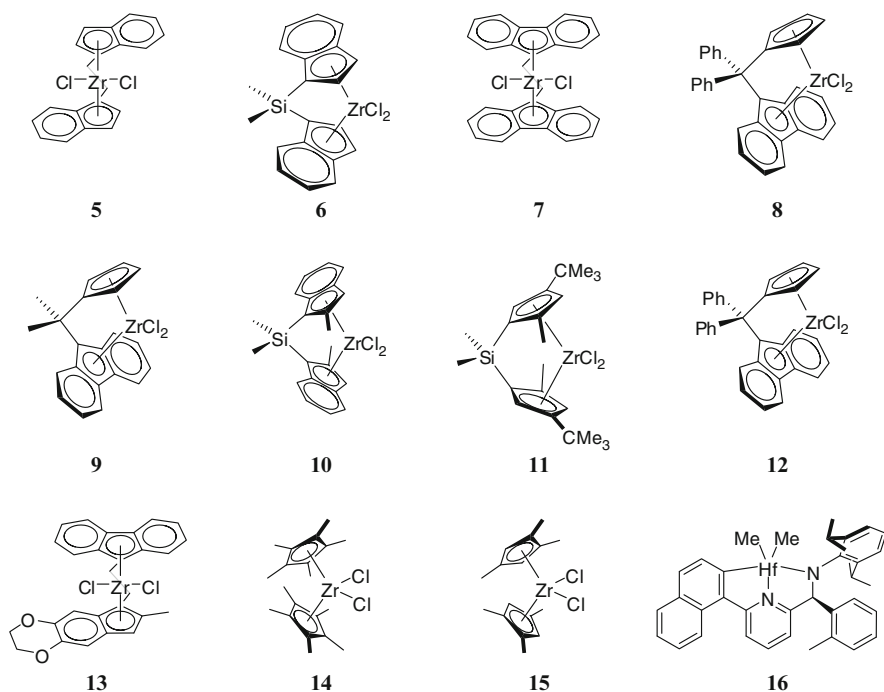
exhibit this behavior were recently reviewed by Kempe [17]. Brintzinger et al. claim that CCTP occurs in ethylene-norbornene copolymerizations using metallocenes **2** and **3** [18]. Sita has also recently demonstrated reversible chain transfer using the hafnium amidinate precatalyst **4** with diethylzinc (DEZ) [19].

3.2 Reversible Chain Transfer in Dual-Catalyst Systems

As stated above, we postulated that fast, reversible chain transfer between two different catalysts would be an excellent way to make block copolymers catalytically. While CCTP is well established, the use of main-group metals to exchange polymer chains between two different catalysts has much less precedent. Chien and coworkers reported propylene polymerizations with a dual catalyst system comprising either of two isospecific metallocenes **5** and **6** with an aspecific metallocene **7** [20]. They reported that the combinations gave polypropylene (PP) alloys composed of isotactic polypropylene (iPP), atactic polypropylene (aPP), and a small fraction (7–10%) claimed by ^{13}C NMR to have a stereoblock structure. Chien later reported a product made from mixtures of isospecific and syndiospecific polypropylene precatalysts **5** and **8** [21] (detailed analysis using WAXS, NMR, SEC/FT-IR, and AFM were said to be done and details to be published in *Makromolekulare Chemie*

but at this writing (Aug. 2008) no such paper has appeared). As in the above examples, the resulting polymer was largely a blend of isotactic and syndiotactic PP (sPP) with a small stereoblock fraction. The mechanism for formation of the stereoblock fraction was proposed to involve the exchange of propagating chains between the two different catalyst sites.

Przybyla and Fink reported that a 1:1 combination of the syndiospecific precatalyst **9** and the isospecific precatalyst **6** on MAO-impregnated silica using either TiBA or TEA gave a polymer with decreased ^{13}C NMR pentad ratios ($[mmmm]/[mmmr]$ and $[rrrr]/[rrrm]$) claimed to be indicative of a block structure [22]. This is of interest because the previous report by Chien et al. stated that a similar supported system showed no evidence of chain exchange [23, 24]. However, it should be noted that other stereoerror ratios, unrelated to block junctions, changed as well, suggesting other factors can affect the stereoselectivity. This was especially apparent when the catalysts were supported on a different type of silica. Here, the $[mmmm]/[mmmr]$ and $[rrrr]/[rrrm]$ ratios increased beyond those expected for the polymer blend, providing further support for the notion that factors other than block formation can change the apparent ratios of those errors.



Lieber and Brintzinger reported a detailed study using mixtures of precatalysts with different stereospecificities [25]. Isospecific precatalyst **10** undergoes facile chain transfer to TMA, as revealed by an increase in isopropyl end groups and a sharp reduction in molecular weight in the presence of TMA (there was no exchange with TiBA). An aspecific precatalyst **7** was affected similarly by TMA

(again, no effect with TiBA). The dual precatalyst system **7** + **10** at high [MAO] produced an ether-soluble atactic fraction and an insoluble isotactic fraction as expected for these catalysts. However, the polymer samples also contained as much as 27% of a third fraction that was soluble in hexane. A blend of polymer obtained from individual polymerizations using **7** and **10** contained no such hexane-soluble fraction (subsequent to ether extraction). The *[mmmm]* content of this fraction was about half that of the insoluble isotactic fraction, consistent with a 50/50 blend or block copolymer. The latter was proposed based on the unique solubility. The authors proposed that efficient polymer chain exchange between active catalyst sites and the aluminum centers of the cocatalyst were required for formation of stereoblock copolymer.

The authors conducted a similar investigation of precatalysts **7** and **11** using TiBA and trityl tetrakis(pentafluorophenyl)borate as the cocatalyst. They concluded that this material contained no fraction that could be characterized as blocky. It was therefore proposed that reversible chain transfer occurred only with MAO or TMA and not with TiBA. This stands in contrast to the work of Chien et al. [20] and Przybyla and Fink [22] (*vide supra*), who claim reversible chain transfer with TiBA in similar catalyst systems. Lieber and Brintzinger also investigated a mixture of isospecific **11** and syndiospecific **12** in attempts to prepare iPP/sPP block copolymers. Extraction of such similar polymers was acknowledged to be difficult and even preparative temperature rising elution fractionation (TREF) [26, 27] was only partially successful.

Rieger et al. described a heteroatom-containing C_1 symmetric metallocene **13** whose stereoselectivity depended on the activator [28, 29]. The resulting PP contained fewer stereoerrors when activated with a combination of TiBA and trityl tetrakis(pentafluorophenyl)borate than with MAO. In addition, the molecular weight was lower with MAO. To explain this, it was proposed that some of the stereoerrors arise by reversible chain transfer to aluminum.

Rytter et al. reported polymerizations with the dual precatalyst system **14/15** in presence of MAO [30]. Under ethylene-hexene copolymerization conditions, **14**/MAO produced a polymer with 0.7 mol% hexene, while the **15**/MAO gave a copolymer with ca. 5 mol% hexene. In the mixed catalyst system, the activity and comonomer incorporation were approximate averages of what would be expected for the two catalysts. Using crystallization analysis fractionation (CRYSTAF) and differential scanning calorimetry (DSC) analysis, it was concluded in a later paper by Rytter that the material was a blend containing no block copolymer [31].

Later Rytter et al. reported possible polymer chain exchange with polypropylene produced with a combination of **8** and **11** with TMA [32]. The number of stereoerrors increased in the binary system at higher TMA levels. As discussed in the case of Przybyla and Fink (*vide supra*), pentad analysis is less compelling evidence for reversible chain transfer. In addition, the gel permeation chromatography (GPC) data showed bimodal peaks, indicating very limited reversible transfer.

Busico et al. reported in 2007 the first conclusive ^{13}C NMR evidence for polypropylene chain shuttling between enantiomeric catalysts derived from the pyridylamide precatalyst

16, as evidenced by presence of $m_x(r)m_y$ stereoerrors [33]. In contrast, these stereoerrors were absent in iPPs made with the enantiopure catalyst. According to the authors: “this is the first ^{13}C NMR evidence of chain shuttling for polyolefins in general. For polypropylene in particular, in previously claimed cases the microstructural analysis of the polymer was inconclusive, and fractionation results revealed that the samples were largely physical blends, with at most a minor fraction of stereoblock chains.”

4 High Throughput Method for the Discovery of Chain Shuttling Catalyst Systems

Our work [10] began with the intention of discovering efficient, entirely new polymerization catalyst systems capable of cleanly synthesizing new-to-the-world olefin block copolymers. We surmised that a polymer comprising alternating blocks with high or low levels of short chain branching might function as a thermoplastic elastomer. Such a molecule might be made by chain shuttling polymerization using a catalyst that does not incorporate LAO, a “poor incorporator”, and a catalyst that does, a “good incorporator”.

As discussed above, there were reports in the literature at that time claiming reversible chain transfer between catalysts, but only to make stereoblock materials. In addition, the amount of block copolymer made was low, if indeed blocky polymer was made at all. We reasoned that a good approach would be to utilize high throughput tools to identify single catalyst/CSA pairs. If we understood the effect of reversible chain transfer on the molecular structure of the polymer, we could quickly screen large numbers of catalyst/CSA pairs. While some effects of reversible chain transfer on polymer microstructure were inferred, we soon realized that the complexity of the system required a kinetic model. This semi-batch mathematical model confirmed our hypothesis that the greatest reduction in molecular weight should be observed at early monomer conversion. Unexpectedly, the model also revealed that the conversion dependence of the molecular weight distribution provided a powerful clue as to the reversibility of the chain transfer reaction!

4.1 Mathematical Simulation of Single Catalyst Batch Reactions

Our approach to polymer chain growth modeling is based on population balances for the various polymer species participating in and resulting from chain growth and transfer [34]. The kinetics scheme is written below in mathematical fashion and is a precursor to the derivation of population balances. Monomer units are represented as M , and growing polymer chains are represented by the symbol P_n , where n is the number of repeat units attached to the active catalyst. Dormant polymer is represented by A_n where n is the number of repeat units attached to the CTA. “Dead” polymer chains, which arise from chain termination events such as hydrogenolysis

and β -hydride eliminations, are represented by D_n , where n is the number of repeat units in the free polymer chain (Scheme 4).

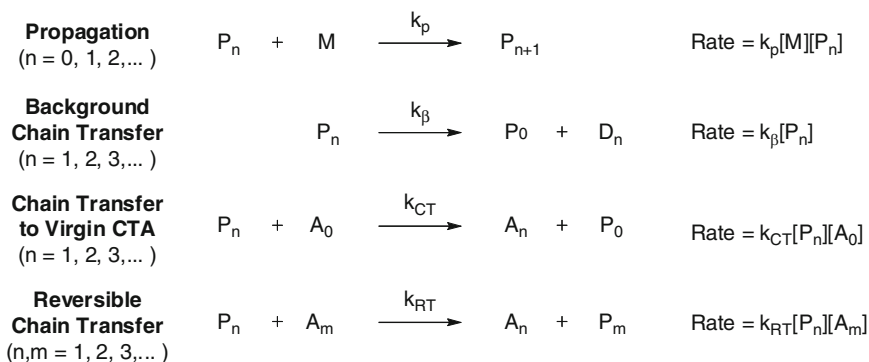
The simplest scenario to simulate is a homopolymerization during which the monomer concentration is held constant. We assume a constant reaction volume in order to simplify the system of equations. Conversion of monomer to polymer, X_p , defined as the mass ratio of polymer to free monomer, is used as an independent variable. Use of this variable simplifies the model by combining several variables, such as catalyst load, turnover frequency, and degradation rate, into a single value. Also, by using conversion instead of time as an independent variable, the model only requires three dimensionless kinetics parameters.

Three kinetics parameters in particular give estimates of the relative rates of chain transfer and shuttling to propagation:

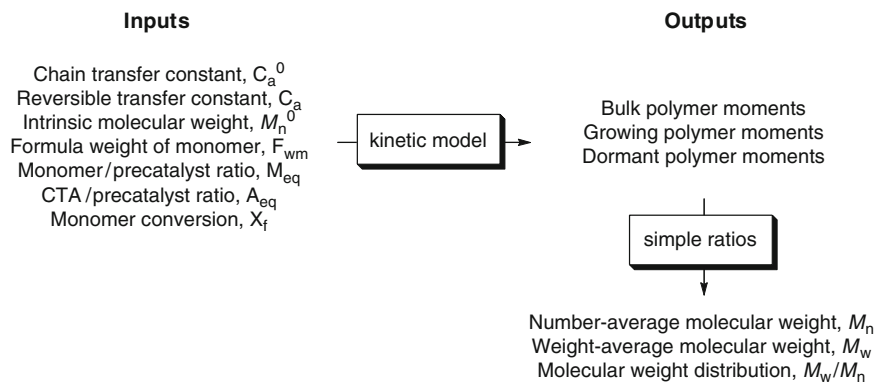
1. The chain transfer constant for sites bearing the original alkyl moiety (virgin CTA sites), C_a^0 , where $C_a^0 = k_{CT}/k_p$
2. The reversible chain transfer constant, C_a , where $C_a = k_{RT}/k_p$
3. The molar ratio of shuttling agent sites to catalyst (A_{eq})

A more rigorous treatment for a chain shuttling agent with multiple alkyl substituents would require more chain transfer constants (ancillary substituents may be alkyl or polymeryl), but we felt that this description was sufficient for initial investigations. The only other kinetic parameter required is the intrinsic molecular weight (M_n^0), which is used to indirectly account for background chain transfer. Differential and algebraic equations for the moments of the molecular weight distribution (M_w/M_n) have been derived from population balances on the above kinetics scheme and are described in detail elsewhere [35]. Separate moments for bulk, growing, and dormant polymer chains were defined, and ratios of these moments were used to express properties such as molecular weights, with F_{wm} as the repeat unit formula weight of the monomer (e.g., 28 g mol⁻¹ for ethylene). The workflow of the model, with inputs and outputs, is depicted in Scheme 5

A series of simulations was performed to investigate the effects of reaction parameters on polymer M_n and M_w/M_n . These values depend on several variables,



Scheme 4 Mathematical depiction of the kinetics scheme



Scheme 5 Workflow of the kinetic model, with inputs and outputs

and fortunately many of them are measurable or determined experimentally. These known inputs include M_n^0 , which is determined by catalyst selection (and H_2 concentration); M_{eq} , the molar ratio of monomer to precatalyst and A_{eq} , the molar ratio of CTA to precatalyst, which are determined by the experimental design; and X_f , which is directly related to the experimentally measured polymer yield. The only dependent variables are the chain transfer and shuttling constants, C_a^0 and C_a . For all the simulations described here, the intrinsic molecular weight and monomer/catalyst ratio were fixed such that $M_n^0 = 1000 \text{ kg mol}^{-1}$ and $M_{eq} = 1,000,000$, while the other inputs were varied to determine their influence on M_n and M_w .

A number of interesting and non-obvious insights into molecular weight distributions can be gained from these simulations. For example, Fig. 3 demonstrates the effect of X_f on M_w/M_n as a function of C_a^0 for irreversible chain transfer where $C_a = 0$. One can consider the horizontal axis in this plot as reaction time. Early in the reaction (i.e., low X_f), the M_w/M_n quickly rises above 2.0 due to the fast initial chain transfer, which generates a number of dead chains on the CTA with M_n much lower than M_n^0 . As the reaction proceeds, the concentration of virgin CTA is depleted and normal chain transfer and termination events begin to dominate. The dead chains residing on the CTA eventually become outnumbered by eliminated chains that are “fully grown.” Therefore, the M_n approaches M_n^0 and the M_w/M_n approaches 2.0 at higher X_f . The magnitude of the increase in M_w/M_n and the location of the maximum is a function of C_a^0 , with higher values producing higher and earlier maximum M_w/M_n . The M_w/M_n is greater than 2.0 at all conversions examined in the simulation for this scenario. Thus, the expected polymer from any olefin polymerization in a batch reaction with irreversible chain transfer to metal must have $M_w/M_n \geq 2.0$. This effect is a result of the batch nature of the reaction, in which the concentration of virgin CTA decreases to near zero as conversion increases.

As an opposite extreme, cases of fully reversible chain transfer ($C_a^0 = C_a$) were simulated. The effect of conversion on M_w/M_n is plotted in Fig. 4 as a function of C_a with $A_{eq} = 50$. Early in the reaction, or low X_f , the M_w/M_n quickly plunges below 2.0, followed by a steady convergence back to 2.0 at higher X_f . Faster reversible chain

transfer produces a lower minimum M_w/M_n and also moves this minimum to lower conversion. One interesting trend is that the M_w/M_n is less than 2.0 at all simulated conversions for reversible chain transfer with $C_a^0 = C_a$, regardless of the absolute

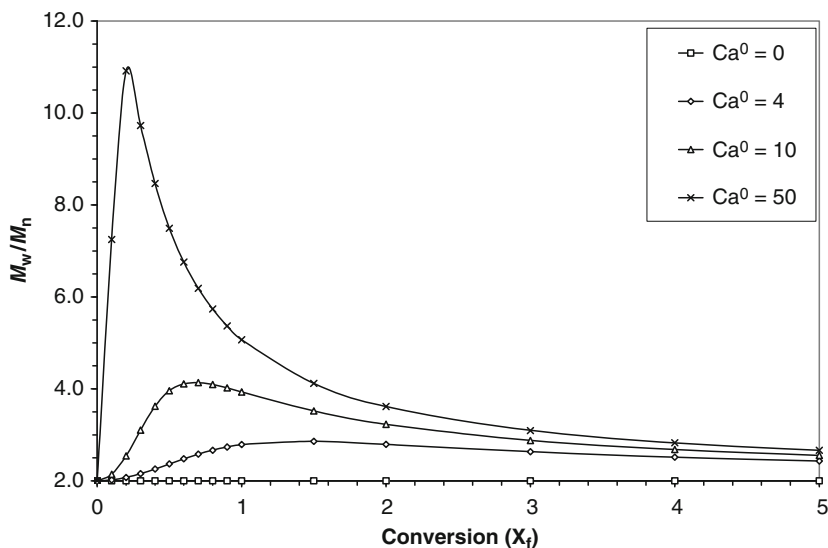


Fig. 3 Simulated M_w/M_n vs. conversion as a function of chain transfer constant for irreversible chain transfer, where $C_a^0 = 0$

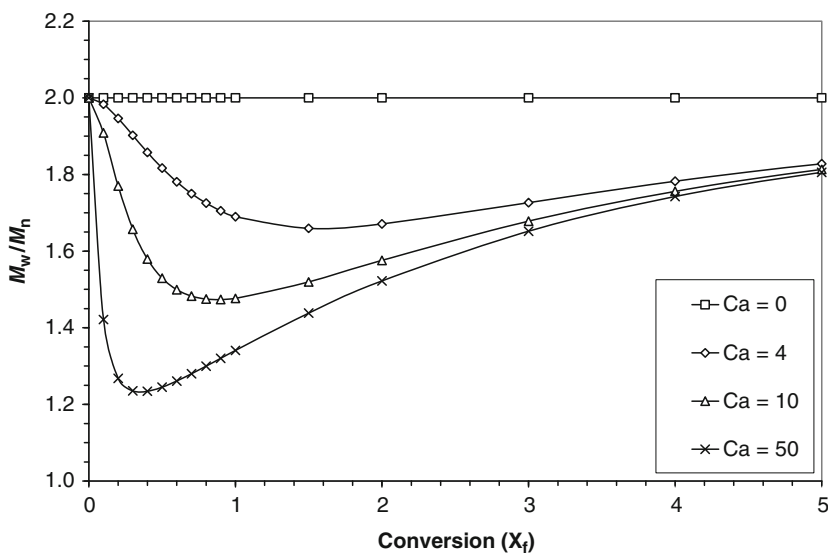


Fig. 4 Simulated M_w/M_n vs. conversion as a function of chain shuttling constant for reversible chain transfer, with $C_a^0 = C_a$

value of C_a . This is in sharp contrast to the case of irreversible chain transfer, where $M_w/M_n \geq 2.0$ at all conversions.

Investigation of the effect of fully reversible chain transfer on the M_n is also informative. Figure 5 depicts the relationship of M_n vs. X_f as a function of C_a . As may be expected, higher chain transfer constants give lower M_n at low conversions. In all cases, M_n increases monotonically toward M_n^0 at higher conversions. Under the model conditions used for this simulation, C_a has very little influence on M_n for $X_f > 2.0$. As one might expect, plots of M_n vs. X_f generally follow this pattern of monotonic increase toward M_n^0 . One consequence of high C_a is the linear increase in M_n at lower conversion. When $C_a \geq 50$, the M_n increases nearly linearly up to $X_f \sim 0.5$ with a y-intercept near zero (see insert in Fig. 5). At lower values of C_a , the near linearity extends to much higher conversions, but the apparent intercepts from linear fits of M_n for $X_f < 0.4$ increase steadily with decreasing C_a . The positive intercept reflects the competition of chain growth vs. chain transfer. These trends suggest that this intercept may be a better measure of shuttling rate than the goodness-of-fit for the line. At higher C_a , the initial chain transfer occurs very early in the reaction when M_n is very low. As C_a approaches zero, the ratio of propagation to transfer increases and the chains grow to higher M_n before chain transfer takes place. In the extreme of $C_a = C_a^0 = 0$ (no chain transfer or shuttling), M_n vs. conversion is perfectly linear, with a slope of zero and apparent intercept of M_n^0 .

The plot in Fig. 6 depicts the response of both M_n and M_w/M_n as a function of conversion for a realistic case of fast reversible chain shuttling, with $C_a^0 = C_a = 50$ and $A_{eq} = 200$. In the fast reversible chain transfer regime, these reactions have some

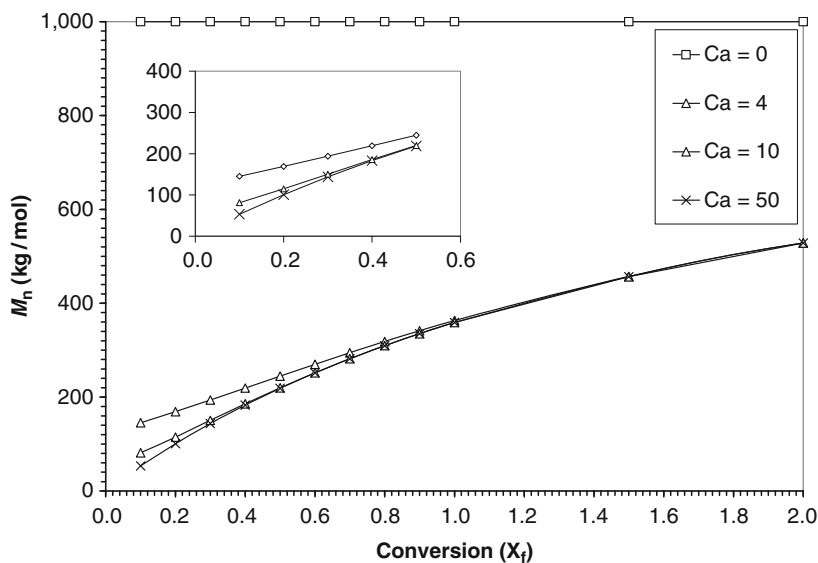


Fig. 5 Simulated M_n vs. conversion by chain shuttling constant for reversible chain transfer, where $C_a^0 = C_a$

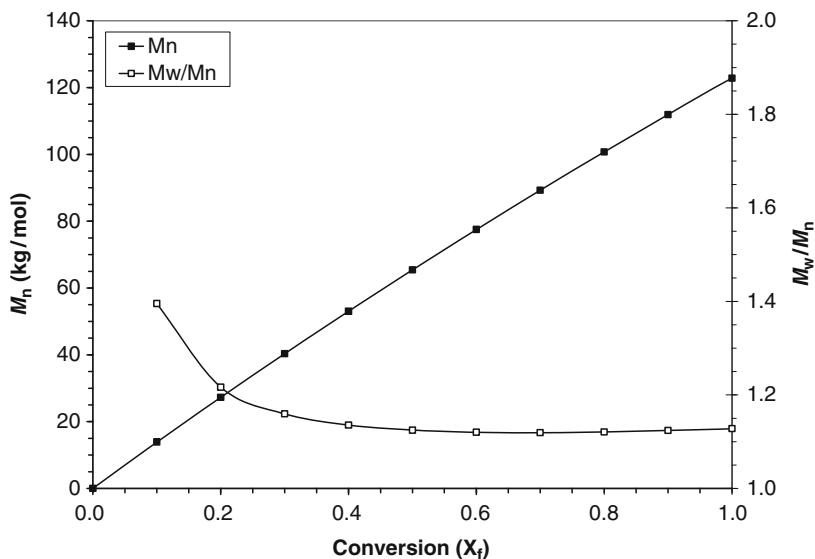


Fig. 6 Simulated M_n and M_w/M_n vs. conversion for polymerization with reversible chain transfer when $C_a^0 = C_a = 50$ and $A_{eq} = 200$

kinetic resemblance to controlled or living free radical processes. Although many chains are growing simultaneously, only a small fraction of them are alive at any given moment, while most of the chains lie dormant on the chain transfer agent. This behavior is also importantly not limited to the low molecular weights normally associated with “catalyzed chain growth” reactions [17] but can extend to very high molecular weight polymers if the value of M_n^0 is sufficiently high.

Each of the cases simulated above consider reactions for which the rate constants for the initial transfer from the virgin CTA and subsequent polymeryl transfer are at most equal, with $C_a^0 \geq C_a$. The magnitude of the difference in k_{CT} and k_{RT} is most likely a function of the nature of the transferable group and the growing polymer chain. If the initiating group is not a good model of the growing polymer chain, initiation is likely to be slower than propagation. On the other hand, “living” behavior can often be realized by selecting an initiating species that closely resembles the polymer chain.

One interesting observation is revealed in an estimation of the relative rates of propagation (R_p) to reversible transfer (R_{RT}) in these systems. Since the rates are both functions of catalyst concentration, this important ratio can be estimated for the above case using M_{eq} , A_{eq} and C_a with the following equation:

$$R_p / R_{RT} = \frac{k_p[M][P]}{k_{RT}[P][A]} = \frac{k_p[M]}{k_{RT}[A]} = \frac{[M]}{C_a[A]}$$

In the above case, with $M_{eq} = 1,000,000$, $A_{eq} = 200$, and $C_a = 50$, the rate of propagation is 100 times faster than the rate of reversible chain transfer. Nevertheless, the

simulation above clearly shows characteristics normally associated with CCTP, with a linear increase in M_n and M_w/M_n near 1.1.

The situation becomes more complex for semi-reversible chain transfer, where k_{CT} and k_{RT} are both positive, but $k_{CT} > k_{RT}$. As demonstrated in Fig. 7, M_w/M_n can be greater than, less than, or equal to 2.0, depending on the conversion and the magnitudes of the chain transfer constants. The M_n of the polymer is simply a function of C_a^0 ; the value of C_a has no effect on M_n up to $C_a = C_a^0$. However, M_w is dramatically affected by lower values of C_a . If $C_a^0 \gg C_a > 0$, then the initial increase in M_w/M_n is dramatic, and M_w/M_n does not dip below 2 until high conversion. However, as C_a approaches C_a^0 , the initial increase in M_w/M_n is negligible, and M_w/M_n drops below 2.0 at low conversion. In any case, if $C_a > 0$, then M_w/M_n asymptotically approaches two from the low side.

The effect of the ratio of chain transfer agent to catalyst (A_{eq}) was also investigated for semi-reversible chain transfer. Figure 8 demonstrates the predicted effect on M_w/M_n of varying the CTA concentration when $C_a^0 = 50$ and $C_a = 4$. Remarkably, nearly identical plots are obtained for three different A_{eq} at conversions less than $X_f = 0.5$. The only difference is a slight increase in the maximum value of M_w/M_n with increasing A_{eq} . However, there is a pronounced influence of A_{eq} on M_w/M_n at conversions higher than the “crossover point” at which M_w/M_n falls below 2.0. Similar simulations with different values of C_a and C_a^0 show the same trend, with very little effect of A_{eq} on M_w/M_n before this point. However, the position of the crossover point is affected by the values of C_a and C_a^0 . Once again, these predicted trends are not intuitively obvious.

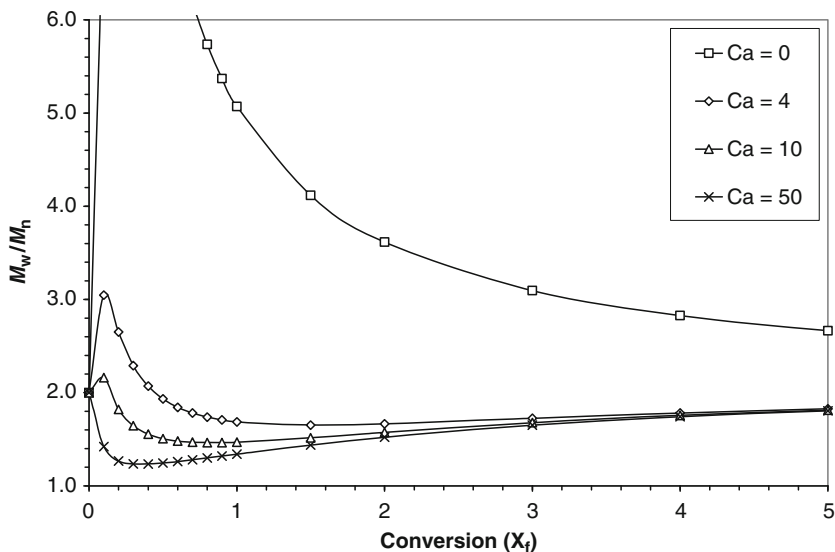


Fig. 7 M_w/M_n vs. conversion for semi-reversible chain transfer in simulations with $C_a^0 = 50$

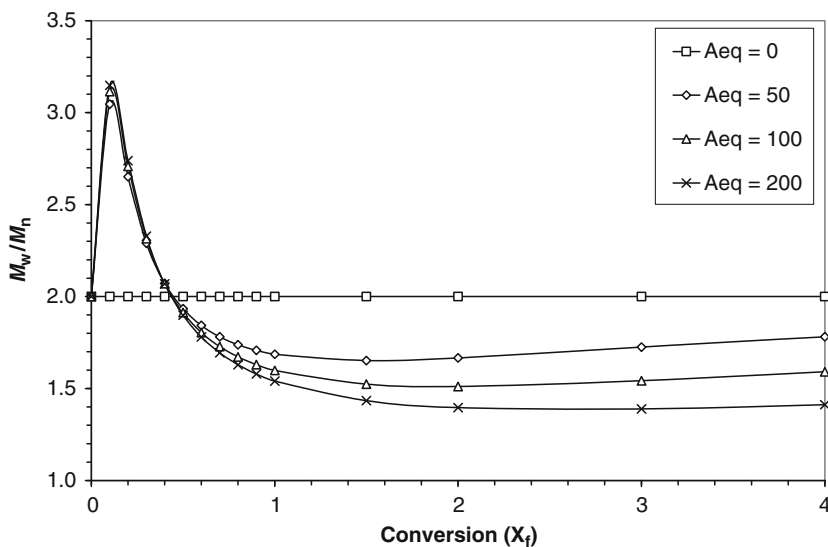


Fig. 8 Effect of A_{eq} on M_w/M_n as a function of conversion for semi-reversible chain transfer, in simulations where $C_a^0 = 50$ and $C_a = 4$

4.2 Selection of Chain Shuttling Agent and Catalysts

The kinetic model simulations described above reveal straightforward methods of determining reversibility in chain transfer. In the cases simulated above, a reduction in M_n in connection with narrowing of the distribution such that $M_w/M_n < 2.0$ indicates reversible chain transfer. These criteria provide a test for finding suitable combinations of catalyst and chain transfer agent for use in our two-catalyst system.

Given the multitude of olefin polymerization catalysts, it was daunting to identify a pair of catalysts with significantly different monomer selectivities that are also capable of chain shuttling. Furthermore, the chosen system should preferably operate at a high solution reaction temperature ($T \geq 120$ °C) to prevent undesired polymer precipitation. We therefore adopted a high-throughput method to expedite this discovery process. The technique outlined in Fig. 9 employs a parallel screen of the effects of metal alkyl reagents on the molecular weight and molecular weight distributions of polyethylene produced by catalyst/CSA combinations.

To begin the selection process, we first selected representative examples from a broad variety of catalyst structure types known to have high polymerization rates. Ethylene copolymerizations were then carried out with these catalysts in combination with a number of potential chain shuttling agents using high-throughput screening techniques [36]. Using an array of robotically manipulated individual polymerization reactors combined with rapid polymer characterization methods, we conducted and evaluated more than 1600 individual polymerization reactions over a 3-week period, a feat that would have taken several months using conventional techniques.

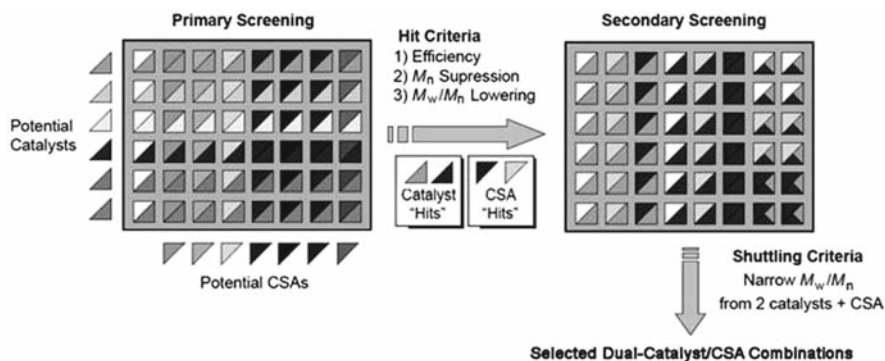


Fig. 9 High-throughput screening protocol for the chain shuttling screen

Catalyst efficiency, estimated by polymer yield, eliminated several of the potential CSAs due to their inhibition of polymerization. For those combinations that produced a sufficient amount of polymer for characterization, the molecular weights and molecular weight distributions of the polyethylene samples were then compared to control polymers prepared with no added CSA. A reduction in the M_n in combination with a narrowing of the M_w/M_n indicated a “hit” for chain shuttling behavior.

Another criterion for catalyst selection is relative comonomer incorporation. The proposed material design is one in which the soft segment (SS) is amorphous and the hard segment (HS) contains as little comonomer as possible. To achieve this combination, the chain shuttling catalysts must have very different reactivity ratios.

Olefin polymerization catalysts systems typically experience higher reactivity toward ethylene (monomer 1) than LAOs (monomer 2), resulting in $r_1 \gg 1 \gg r_2$ [37]. For our purposes, let us consider a hypothetical example where the catalysts have the following reactivity ratios:

Catalyst	r_1	r_2
Good incorporator (makes SS)	5	0.1
Poor incorporator (makes HS)	200	0.02

The copolymer composition produced by these two catalysts can be estimated using the Mayo–Lewis equation [38] and these values of r_1 and r_2 . Figure 10 depicts the hypothetical comonomer content in the polymer (F_2) as a function of the mole fraction of comonomer in the reactor (f_2). The good incorporator produces a material with higher F_2 as f_2 increases. In contrast, the composition from the poor incorporator is relatively flat across a broad range and increases only at very high values of f_2 . The F_2 required to render the copolymer amorphous is comonomer-dependent; for 1-octene, this value is near 0.19. In this hypothetical system, the good incorporator produces that composition at $f_2 = 0.57$, at which the poor incorporator incorporates very little comonomer ($F_2 = 0.01$).

To identify catalysts with this type of difference in comonomer reactivity, we performed copolymerizations of ethylene and 1-octene at relatively high f_2 . Several different families of catalysts were evaluated under these conditions. The resulting copolymer

compositions revealed information about the relative comonomer reactivities; a rigorous definition of the reactivity ratios was not necessary. This screening protocol allowed us to rapidly classify catalysts into the good or poor incorporator categories.

The molecular weight distribution of a polymer produced with a chain shuttling catalyst/CSA system is highly dependent on reaction conditions. The extent of reversibility with the catalyst/CSA pairs was therefore further explored through a series of polymerizations over a range of monomer conversions (i.e., yield). A representative example from this secondary screening process is described below for precatalyst **17**. Several members from this well-studied bis(phenoxyimine)-based catalyst family [39] were identified as poor incorporators in the primary screen. A series of ethylene/octene copolymerizations using **17** was performed across a

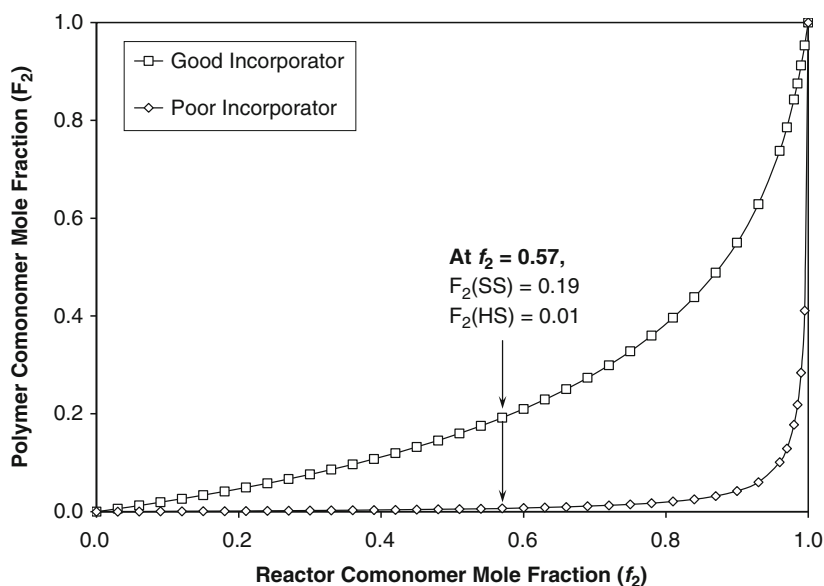


Fig. 10 Polymer composition as a function of reactor composition for hypothetical good and poor incorporators

Table 1 Ethylene polymerization with **17** in presence of DEZ^a

Sample	CSA	Time (s)	Yield (g)	M_n^b (kg mol ⁻¹)	M_w/M_n^b
1	DEZ	16	0.059	6.48	1.38
2	DEZ	36	0.085	9.59	1.29
3	DEZ	58	0.117	13.2	1.26
4	DEZ	92	0.142	17.4	1.23
5	DEZ	146	0.192	23.7	1.23
6	DEZ	227	0.275	32.2	1.27

^aGeneral polymerization conditions: ethylene pressure 100 psi, 120 °C

^bDetermined using GPC relative to polystyrene standards and converted to polyethylene equivalents

range of polymer yields using diethylzinc (DEZ) as CSA (Table 1). The effects of polymer yield on the molecular weight characteristics are depicted in Fig. 11.

Polymerization with **17** without CSA shows no trend in molecular weight response and allows estimation of M_n^0 of ~ 260 kg mol $^{-1}$. Addition of 29 equivalents DEZ (10 μ mol) results in a linear increase in M_n to 32 kg mol $^{-1}$ and M_w/M_n below 1.4 for each sample. In this case, the M_n is well below M_n^0 even at the highest yield examined, and therefore the M_w/M_n remains relatively narrow. This plot of experimental data looks remarkably similar to the simulation depicted in Fig. 6 for fast reversible chain transfer.

Similar studies performed with pyridylamide pre-catalysts [40] such as **18** [41] revealed fast polymeryl chain exchange with DEZ, much like catalyst **17**. This particular class of catalyst readily incorporates LAO in general. We then designed dual-catalyst experiments to probe the possibility of making linear block copolymers using this technology. Figure 12 shows an overlay of GPC traces obtained

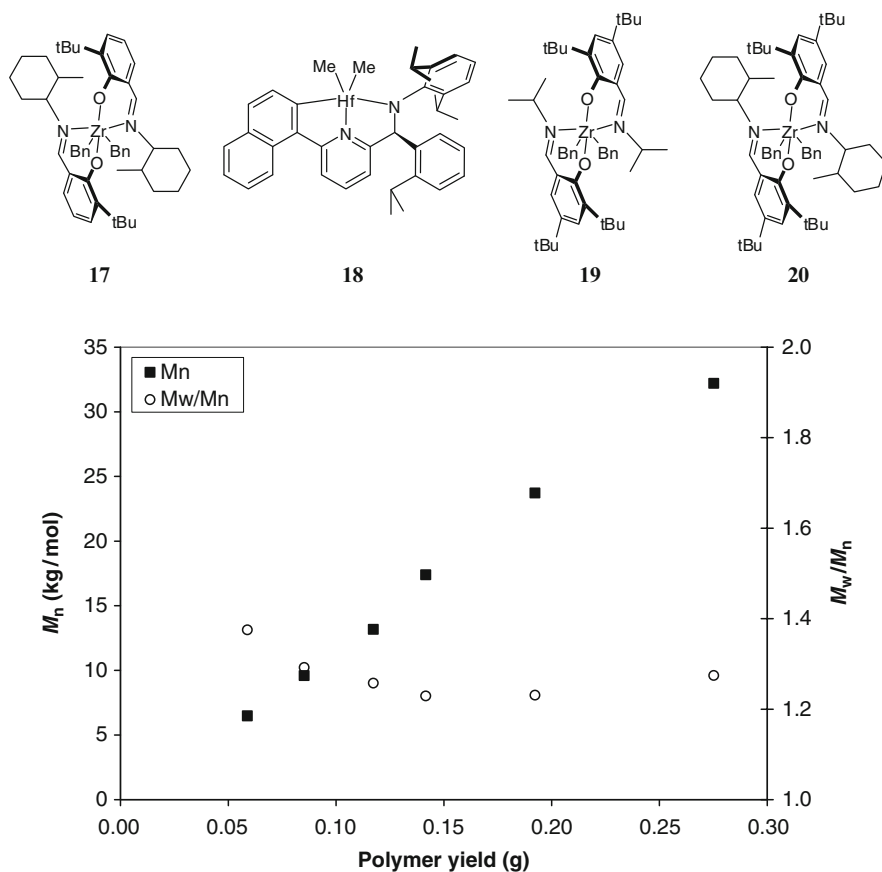


Fig. 11 Molecular weight (M_n) and molecular weight distribution, M_w/M_n , of polyethylene prepared with **17** using DEZ as CSA as a function of polymer yield

from runs comprising only **18**/MMAO, only **19**/MMAO, and a combination of **18** and **19** with MMAO and cocatalyst. As expected, the GPC trace for the dual catalyst experiment roughly comprises those of the single component traces.

The GPC trace is dramatically different when a CSA is added in the mixed catalyst system in that a simple composite GPC is not obtained (Fig. 13). Inclusion of either TEA or DEZ in the polymerization produces a single peak in the GPC,

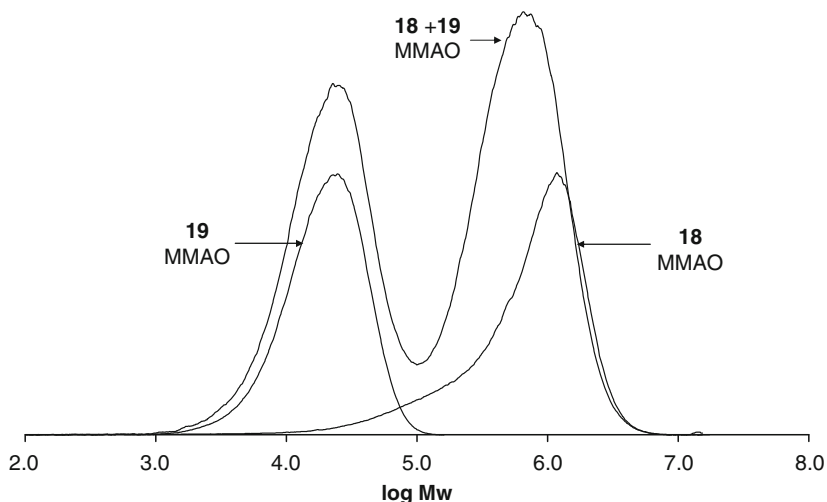


Fig. 12 GPC traces for **18**, **19**, and combination of the two catalysts without CSA

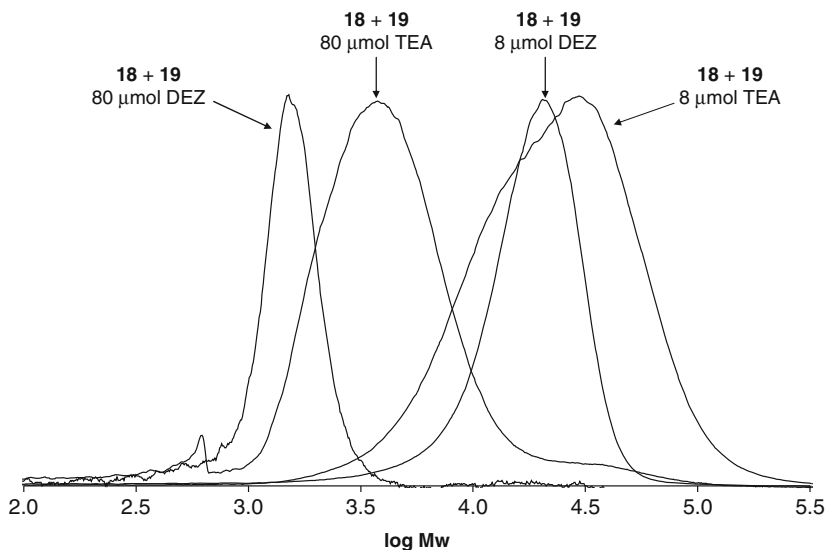


Fig. 13 GPC traces for **18/19** system with DEZ or TEA as CSA

reflecting low M_n , and narrow M_w/M_n (see Table 2). The octene incorporation data for runs with 8 μmol of CSA indicate an intermediate incorporation level between those found for polymers made by **18** and **19** individually. Incorporation levels for the runs using 80 μmol CSA are very high as measured by IR, but there is some question about the accuracy of this technique for such extremely low molecular weight polymers ($M_n < 3100$). These analyses indicate that both catalysts are active and undergoing rapid chain shuttling. It was therefore our conclusion that linear block copolymers were being produced, as predicted.

4.3 Investigations of Chain Shuttling Using Deuterium Labeling

It occurred to us that simply quenching of the polymerization reactions with D_2O could provide some insight into the details of a chain shuttled polymerization [42]. Specifically, a series of semi-batch polymerization reactions using a known chain shuttling catalyst/CSA pair were conducted, systematically varying yield and CSA loading. Furthermore, quenching the polymerization with D_2O labels the chains that reside on the CSA (or catalyst), providing a measure of the extent of chain transfer (i.e., the fraction of potential CSA sites bearing polymeryl chains). This ^2H label also allows for characterization of the polymer terminus using ^2H and ^{13}C NMR, providing information about the relative rate of chain transfer after insertion of ethylene relative to LAO.

Because we had previously recognized its participation in fast chain shuttling and ready incorporation of LAO, we selected **18** as our precatalyst for these experiments. For the CSA, we chose Oct_3Al because it allows us to easily quantify the relatively non-volatile product of its reaction with D_2O , 1-d-octane. This measurement in turn allows us to measure the overall distribution of chain types at the end of the reaction, and serves as an internal check for the validity of our measurements.

Table 2 Ethylene polymerization with **18** and **19** in presence of DEZ and TEA CSAs^a

Sample	Catalyst	CSA	CSA		M_n^b (kg mol^{-1})	M_w/M_n^b	C_8^c
			(μmol)	(g)			
1	18	na ^d	0.8	0.136	262	1.76	6.5
2	19	na ^d	0.8	0.164	14.8	1.63	2.0
3	18+ 19	na ^d	0.8	0.203	32.9	13.6	4.3
4	18+ 19	DEZ	8	0.128	15.2	1.33	5.1
5	18+ 19	DEZ	80	0.093	1.49	1.08	15
6	18+ 19	TEA	8	0.211	15.9	1.98	4.3
7	18+ 19	TEA	80	0.250	3.08	1.84	13

^aGeneral polymerization conditions: ethylene pressure 200 psi, 130 °C, 1.1 equiv. cocatalyst to total catalyst

^bDetermined using GPC relative to polystyrene standards

^c1-Octene content in the polymer determined by infrared (IR) spectroscopy

^dNot applicable, MMAO was added as a scavenger

We began our study with a relatively simple series of experiments, varying the level of CSA, and holding polymer yield nearly constant (runs 1–5, Table 3). As expected for chain shuttling, M_w/M_n was generally less than two. The M_n and M_w/M_n both decrease markedly and monotonically as the CSA loading is increased. Interestingly, less than half of the available aluminum sites are filled in these experiments, according to GPC analysis. Thus, the effects of chain shuttling are observed in this system prior to complete conversion of alkyls to polymeryl on the CSA, indicating that chain shuttling is kinetically competitive with chain transfer in this system.

Several ethylene-hexene copolymerization experiments were performed, varying either CSA loading or polymer yield (Table 3, runs 6–15). Mass balance for the experiments was remarkably good, as demonstrated by a nearly perfect accounting of the fates of all Oct₃Al sites as either 1-d-octane or Poly-D. In addition, good agreement was observed between M_n 's determined by GPC and ²H NMR, implying minimal chain termination mechanisms other than transfer to aluminum. There is a clear relationship between CSA fill ratio and polymer yield (conversion), as shown in Fig. 14. The data can be fit to a simple first-order (exponential) decay of CSA concentration, but the actual chain transfer constant cannot

Table 3 Batch polymerization results

Run no.	Oct ₃ Al (mmol)	Yield (g)	M_n^a		Oct-D ^b (mmol)	Poly-D ^c + Oct-D			CSA fill ratio ^e (² H NMR)	M_n^f (NMR)
			(kg mol ⁻¹)	M_w/M_n^a		(mmol)	(mmol)	(mmol)		
1	0.25	5.9	15.4	2.03	nd	nd	nd	0.85	0.45 ^e	nd
2	0.50	5.2	8.68	1.92	nd	nd	nd	1.6	0.37 ^e	nd
3	1.0	6.1	4.56	1.70	nd	nd	nd	3.1	0.43	nd
4	2.0	6.4	2.78	1.61	nd	nd	nd	6.1	0.38 ^e	nd
5	4.0	5.1	1.76	1.47	nd	nd	nd	12.1	0.24 ^e	nd
6 ^g	0.25	11.4	33.9	2.95	0.54	0.37	0.90	0.85	0.44	30.8
7 ^g	0.50	10.8	16.0	2.07	1.01	0.66	1.68	1.6	0.41	16.4
8 ^g	1.0	9.5	6.56	2.10	1.99	1.29	3.28	3.1	0.42	7.36
9 ^g	2.0	9.1	3.35	2.04	4.39	2.22	6.61	6.1	0.36	4.10
10 ^g	4.0	7.7	1.24	2.59	9.52	3.18	12.7	12.1	0.26	2.42
11 ^g	8.0	6.8	0.794	2.25	21.5	4.38	25.9	24.1	0.18	1.55
12 ^g	2.0	8.7	3.45	1.97	nd	1.73	nd	6.1	0.28	5.03
13 ^g	2.0	28.8	5.14	1.96	nd	4.02	nd	6.01	0.67	7.16
14 ^g	2.0	36.1	5.85	1.92	nd	4.57	nd	6.01	0.76	7.90
15 ^g	2.0	51.0	9.71	2.07	nd	5.05	nd	6.01	0.84	10.1

Polymerizations were performed at 80 °C with 100 psig C₂H₄ using 2.0 μmol precatalyst **18**, and 2.0 μmol [R₂NMeH][B(C₆F₅)₄]nd not determined

^aDetermined using GPC

^bDetermined by GC integration relative to nonane internal standard. All samples were exclusively monodeuterated as determined by GC/MS

^cDetermined by ²H NMR integration relative to C₆D₆ internal standard

^dTotal aluminum alkyl functionality (3 × Oct₃Al + 1 × MMAO)

^eRatio of polymeryl chains to total aluminum alkyl functionality determined by ²H NMR

^fDetermined using NMR

^gCopolymerizations with 40 g 1-hexene added

be derived since the active catalyst concentration changes during the experiment due to initiation and deactivation reactions. Using ^2H and ^{13}C NMR, the label was clearly identified attached to a linear endgroup, consistent with earlier indications that chain transfer after ethylene insertion is much faster than after LAO insertion (Fig. 15).

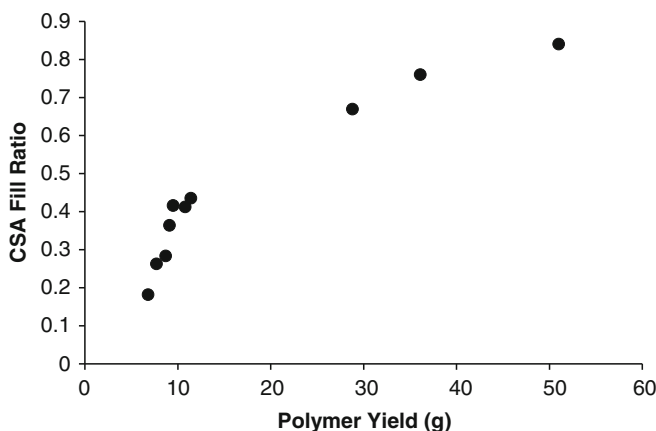


Fig. 14 Relationship between CSA fill ratio and polymer yield. The CSA fill ratio is the fraction of Al sites bearing a polymer chain at the end of the polymerization

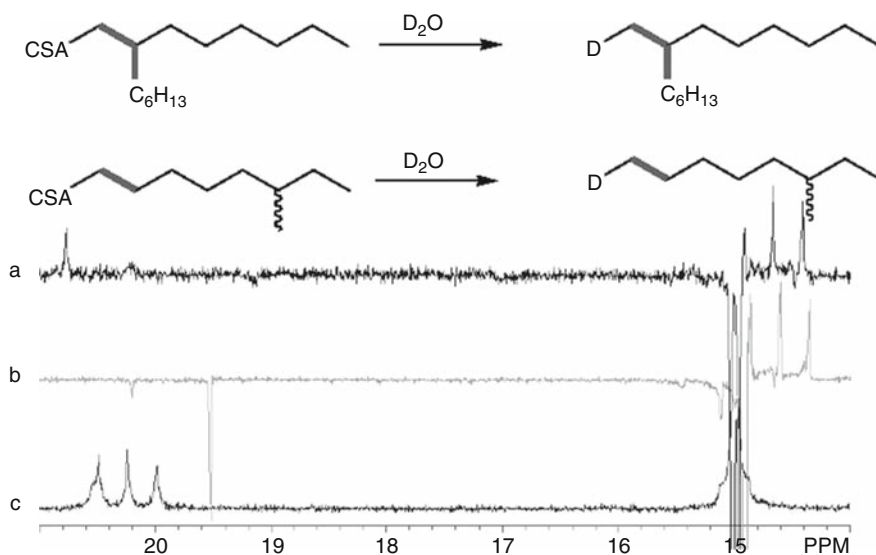


Fig. 15 $^{13}\text{C}\{^1\text{H}\}$ NMR spectra for end-functionalized polymer and model compounds: polymer- CH_2D (a), *n*-heptyl- CH_2D (b), and 7- CH_2D -pentadecane (c). The *top two* spectra were acquired using the APT pulse sequence to more clearly show the deuterated methyl peak

5 Chain Shuttling in a Continuous Reactor

5.1 Olefin Block Copolymer Production in a Continuous Reactor

Experiments were conducted with a dual catalyst chain shuttling system in a continuous solution polymerization reactor. A series of ethylene-octene copolymers of similar melt index were produced with a composition of ca. 30% (by weight) hard and 70% soft blocks. The level of DEZ was systematically varied to study the effects of CSA ratio on polymer microstructure.

Individual catalyst experiments confirmed the difference in reactivity ratios for the catalyst pair, as precatalyst **18** and **20** gave copolymer with density (ρ) of 0.860 and 0.936 g cm⁻³, respectively (Table 4). These two baseline polymerizations provided an estimate of the catalyst ratio necessary to achieve the desired composition for the dual catalyst products. An overall density of ~0.88 g cm⁻³ was targeted to give the desired copolymer composed of 30% high density material (the reciprocal density relationship $\rho = 1/(f_1/\rho_1 + f_2/\rho_2)$ was used to estimate the resulting overall density of the desired polymer composition). A series of products was produced at four different levels of blockiness, including a blend sample prepared in the absence of DEZ. The blockiness, or average block length and number of blocks per chain, was adjusted by varying the ratio of concentrations of DEZ to ethylene ($[\text{Zn}]/[\text{C}_2\text{H}_4]$).

The copolymer prepared without DEZ is clearly shown to be bimodal by GPC, with $M_w/M_n = 13.8$ (Fig. 16). The GPC trace was deconvoluted into components of $M_w \sim 240,000$ and ~ 9600 g mol⁻¹ reflecting the differing propensities for hydrogen-induced termination between the two catalysts. The molecular weight distribution narrows as DEZ is added, as expected for an efficient chain shuttling polymerization;

Table 4 Process details for production of olefin block copolymers using precatalysts **18** and **20** in presence of DEZ

Sample	Catalytic package	$[\text{Zn}]/[\text{C}_2\text{H}_4]^a$ ($\times 10^3$)	Density (g cm ⁻³)	I_2 (dg min ⁻¹)	M_w^b (g mol ⁻¹)	M_w/M_n^b	Chains/ Zn ^c	Chains/ (Hf + Zr) ^c
1 (soft PE)	18 + DEZ	1.87	0.862	1.5	110,000	1.97	2.7	230
2 (hard PE)	20 + DEZ	2.07	0.938	2.6	65,000	1.95	4.6	2200
3 (blend)	18 + 20	–	0.890	0.92	137,300	13.8	–	3600
4 (low CSA)	18 + 20 + DEZ	0.56	0.883	0.90	129,000	3.22	12	820
5 (mid CSA)	18 + 20 + DEZ	1.40	0.883	1.0	118,500	2.23	3.6	630
6 (high CSA)	18 + 20 + DEZ	2.39	0.879	0.93	104,600	1.97	1.9	260

^a $[\text{Zn}]/[\text{C}_2\text{H}_4]$ ratio is defined as the molar ratio of chain shuttling agent to ethylene in the reactor

^bDetermined by GPC relative to polystyrene standards

^cChains/Zn was calculated using the zinc feed and polymer production rates and the number-average molecular weight of the resulting copolymer corrected for comonomer content. Similarly, chains/(Hf + Zr) was estimated using the total catalyst metal feed

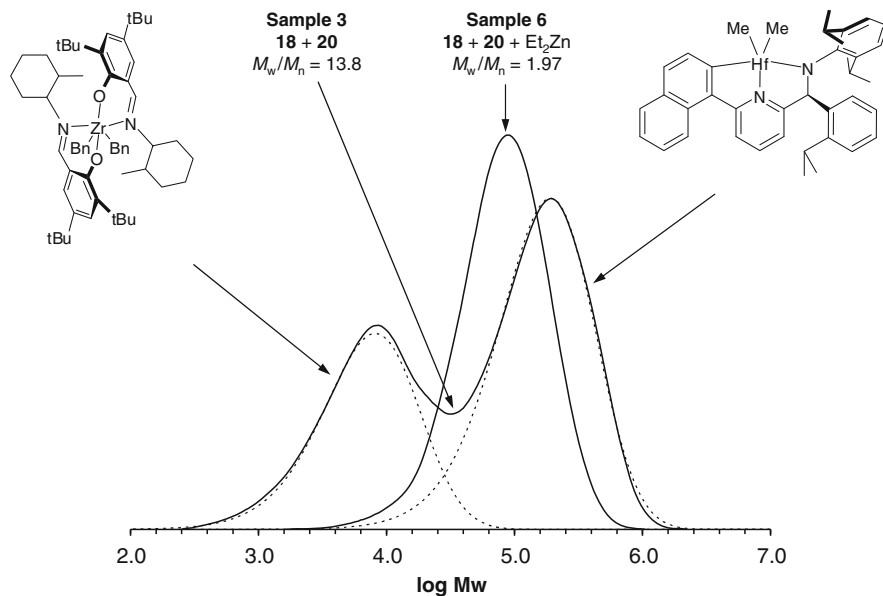


Fig. 16 GPC traces for **18/20** system with and without DEZ as CSA. Reproduced by permission from [10]

the $M_w/M_n = 1.97$ at the highest DEZ level examined. This narrow molecular weight distribution is normally associated with a single catalytic species and is indicative of the multiblock nature of the copolymer, since several shuttling events are required to generate such a homogeneous molecular weight distribution.

This molecular weight response clearly indicates that chain-shuttled ethylene-octene block copolymers, rather than blends, are formed upon introduction of DEZ. The M_n can also be used in conjunction with the DEZ feed and polymerization rate to calculate the number of chains produced per Zn molecule. The low DEZ level of sample 4 results in the production of ca. 12 chains/Zn. However, the reaction is practically stoichiometric at higher DEZ (no H_2), with production of sample 6 resulting in 1.9 chains/Zn (or ca. one chain per Zn-alkyl moiety). This example indicates that nearly every polymer chain exited the reactor bound to the CSA, with very little chain termination, demonstrating the efficiency of the chain shuttling reaction.

Despite the potentially stoichiometric nature of the reaction with the CSA, a similar calculation of the number of chains per catalyst molecule reveals that the polymerization is highly catalytic in the hafnium and zirconium species. The chain shuttling methodology is capable of generating unlimited olefin block copolymer chains per catalyst. For example, the synthesis of sample 6 results in formation of ~260 chains per total catalyst!

The chain shuttling process offers a high level of control over the resulting OBC microstructure. The average number of blocks per chain can be adjusted by modifying the ratio of CSA to monomer; higher values of $[Zn]/[C_2H_4]$ result in shorter

Table 5 Production of OBCs with varying hard/soft ratio

Sample	Density (g cm ⁻³)	HS content ^a (wt%)	Precat. ratio ^b (18/20)	[Zn]/[C ₂ H ₄] ^c (×10 ³)	M _w ^d (g mol ⁻¹)	M _w /M _n ^d
7	0.865	18	3.5	2.40	112,100	1.97
8	0.880	27	2.3	1.61	124,000	2.06
9	0.893	40	1.0	1.41	110,300	2.11
10	0.902	57	0.61	1.38	107,600	1.95
11	0.910	67	0.49	1.46	99,800	1.90
12	0.920	82	0.18	1.11	102,300	1.93

^aHard segment (HS) content is estimated by ¹³C NMR spectroscopy

^b18/20 is the molar ratio of precatalyst **18** to **20** in the reactor feed

^c[Zn]/[C₂H₄] is defined as the molar ratio of chain shuttling agent to ethylene in the reactor

^dDetermined by GPC relative to polystyrene standards

block lengths. The hard/soft composition (i.e., density) can be easily varied by adjusting the ratio of the two catalysts in the reactor feed (Table 5). The overall molecular weight can be controlled through a combination of [Zn]/[C₂H₄] ratio, hydrogen feed, and the reactor temperature.

6 Properties of OBCs Made by Chain Shuttling Catalysis

6.1 Melting Temperature

Production of OBCs by chain shuttling catalysis can result in a copolymer with a melting point more than 50 °C higher than that expected for a statistically random copolymer prepared at equivalent density. Figure 17 shows the typical relationship between density and melting point for random ethylene-LAO copolymers. The circled symbols are several OBCs prepared by chain shuttling catalysis [10]. While a typical random copolymer with density of 0.88 g cm⁻³ would melt at ~60 °C, the OBCs made by chain shuttling do not melt until almost 120 °C.

6.2 Crystallinity and Solid-State Morphology

Melting point alone cannot uniquely identify an OBC. For example, blends of high and low density polyolefins also exhibit an elevated melting point at equivalent density. Sample 3 in Fig. 17 (small circle) is a 70:30 physical blend of 0.86 and 0.94 g cm⁻³ ethylene-octene copolymers, and the melting point is similar to the OBCs. Physical blends of polymers of such disparate densities are not phase-continuous, however, and segregate into domains of the high and low density polymers. Figure 18 reveals differences in appearance of pressed plaques of the polymer samples

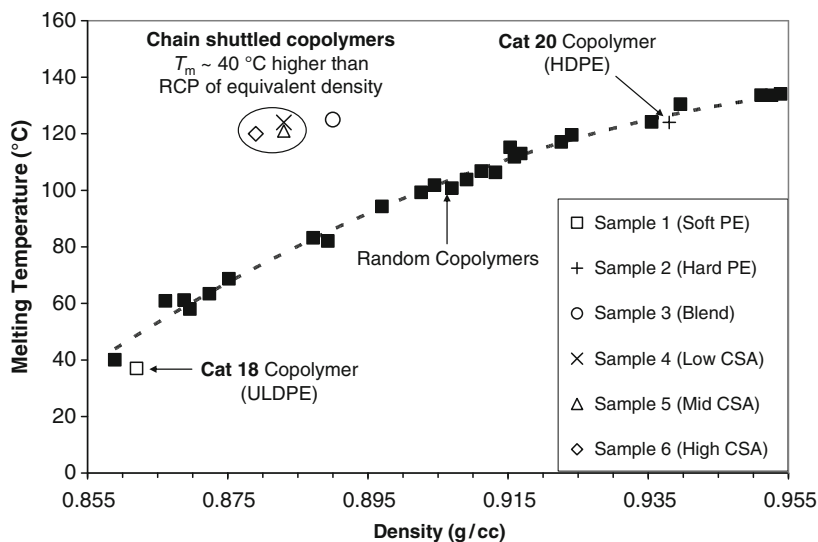


Fig. 17 OBCs have melting points much higher than the corresponding random copolymers at equivalent density. *Circled symbols* are OBCs prepared by chain shuttling catalysis Reproduced by permission from [10]



Fig. 18 Several samples of ethylene-octene copolymers having similar comonomer content, crystallinity, and melt index. *Sample 3* is a physical blend of high and low density copolymers. *Samples 4–6* are OBCs prepared with several different levels of chain shuttling agent. Reproduced by permission from [10]

3–6. Note that sample 3, the physical blend, is completely opaque, while the OBC samples have differing degrees of clarity. These differences can be explained by examining the distribution of crystallinity in the sample.

Figure 19 reveals optical micrographs of the above samples through plane-polarized light, as well as reference samples including a random copolymer of equivalent density and HDPE. Random copolymers in this density range exhibit only fringe micelle crystallinity [43, 44]. HDPE shows patterns of spherulitic crystallinity filling the image. Remarkably, OBCs also show spherulites at a density range where none should be evident for a random copolymer. Moreover, the relative size and distribution of these spherulites can be influenced by the amount of chain shuttling agent employed to produce the polymer. At higher $[CSA]/[C_2H_4]$ ratios, shuttling is fast with respect to propagation, and shorter ethylene blocks are produced which result in smaller spherulites. Conversely, longer ethylene runs at lower $[CSA]/[C_2H_4]$ ratios result in fewer, larger spherulites. All samples (with the exception of the HDPE) are at approximately the same density and crystallinity! (Figure 19)

A detailed study of the crystallinity of OBCs was published by Hiltner and Baer working in collaboration with researchers at Dow Chemical [45]. The authors

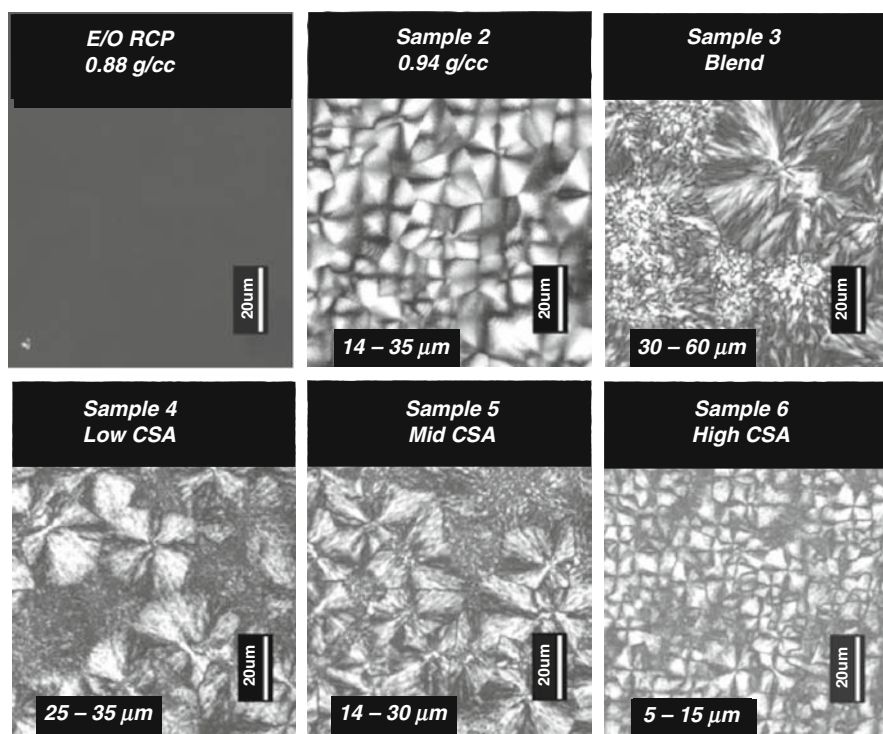


Fig. 19 Polarized optical micrographs of several polymers. From *top left to lower right*: a random ethylene-octene copolymer; high density polyethylene; samples 3–6

indeed found the crystallizable ethylene sequences of the OBCs were long enough to form lamellar crystals organized into the space-filling spherulites shown above. They further found that the polyethylene crystals were orthorhombic, and the morphology was consistent with crystallization from a miscible melt.

6.3 Solubility Properties

OBCs also show very unusual solution dissolution behavior. Figure 20 shows the analytical TREF chromatogram for an OBC, a blend of high and ultra-low density polyethylene, and a random copolymer, all of equivalent crystallinity. A random copolymer at this density and crystallinity dissolves and elutes from the column when the solvent reaches a temperature of ~ 55 °C. The blend fractionates into the two components: the amorphous fraction comes out in the purge at room temperature, whereas the high density component elutes at ~ 95 °C. The OBC, however, elutes at a temperature much higher than that predicted for a random copolymer at equivalent crystallinity, but lower than that of the high density fraction of the blend. In addition, the OBC shows a very low purge fraction compared to either the random copolymer or the blend. These phenomena can be explained by the block structure of the OBC. Each polymer molecule has regions of high comonomer and low comonomer content. For each polymer molecule of the OBC, the long ethylene runs of the low commoner regions keep some of the amorphous regions from dissolving, while the amorphous regions help solubilize the crystalline regions.

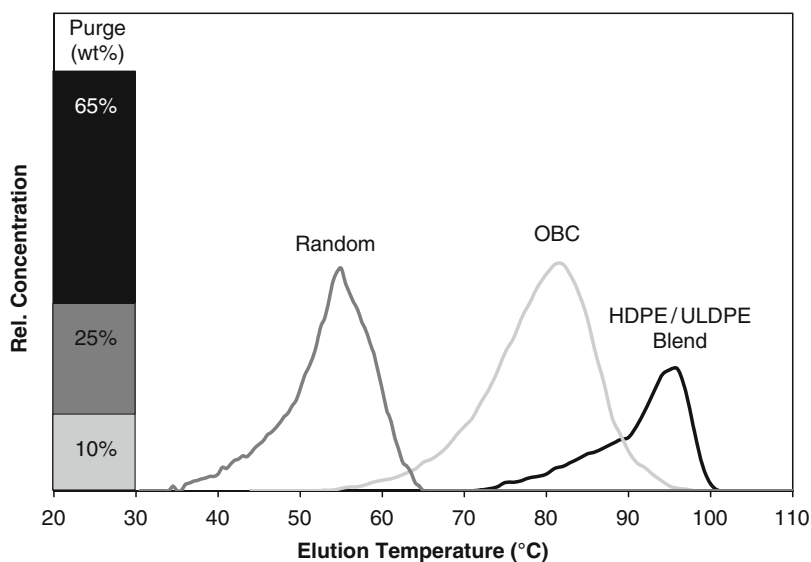


Fig. 20 Analytical TREF profiles of a random copolymer, an OBC, and a blend of HDPE with ultra-low density polyethylene (ULDPE) of similar overall densities [46]

To support this hypothesis, the OBC sample can be fractionated by the TREF experiment. TREF fractionation of the OBC, followed by evaluation of the octene content by ^{13}C NMR, reveals the data shown in Fig. 21. For a polymer blend, each molecule dissolves and elutes according to its comonomer content. The results invariably fall on the line in Fig. 21 labeled “random copolymer line.” The triangles reveal the comonomer content of the TREF fractions from an OBC. At any given temperature, the polymer eluting has much more comonomer than would be expected for a random distribution. The only explanation is that the comonomer is blocked, as expected from the chain shuttling mechanism. The extent of deviation can even be quantified, and a new method was recently invented to determine the “block index” for a given polyolefin [46].

6.4 Performance

The results above show how OBCs made by chain shuttling between catalysts incorporating large and small amounts of comonomer, respectively, can produce polymer microstructures that block the comonomer, thus generating crystallization behavior differentiated from that of random copolymers of equivalent crystallinity. The net effect of these new microstructures is a newly accessible regime of elasticity and heat balance for olefin-based thermoplastic elastomers. Figure 22 reveals a plot of storage modulus versus temperature for several olefin-based elastomers. An ethylene/LAO random copolymer with density of $\sim 0.88 \text{ g cm}^{-3}$ will have a low glass transition temperature (T_g) and a relatively flat modulus up to near the melting point of the polymer. Random propylene-ethylene copolymers at similar crystallinity

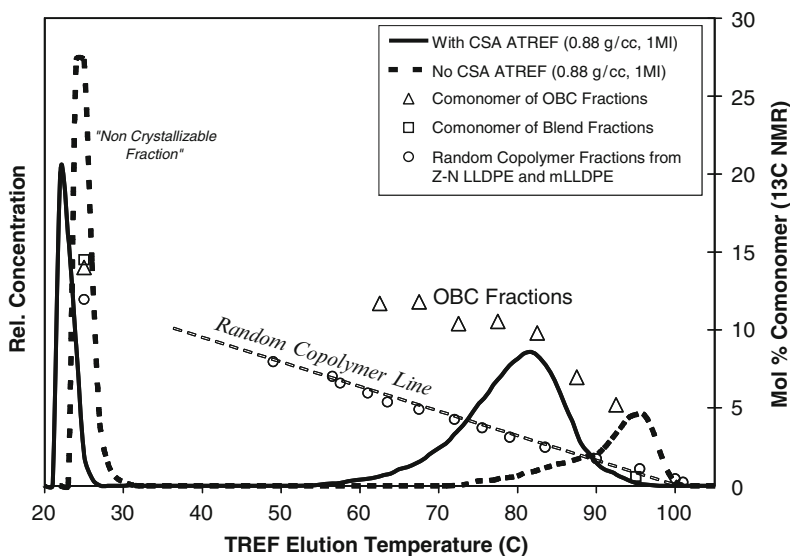


Fig. 21 Comonomer content vs. TREF elution temperature for an OBC and a blend of two random copolymers [46]

behave in an analogous way, although the T_g is higher. OBCs, however, show a relatively flat plateau modulus from the T_g all the way to the melting of the high crystallinity parts of the OBC molecules.

The use temperature of an elastomer is determined by the range between the T_g and the T_m . These new OBCs have increased the use temperature range of olefin-based elastomers by > 40 °C, enabling the introduction of these polymers to many new markets and applications where a simple olefin-based solution was previously unavailable. This performance translates to better high temperature elastomeric properties for the OBCs. For example, the 70 °C compression set of an OBC is much lower than that of a comparable ethylene/LAO random copolymer and is closer to that of f-PVC, TPU, or TPV materials [47] (Fig. 23).

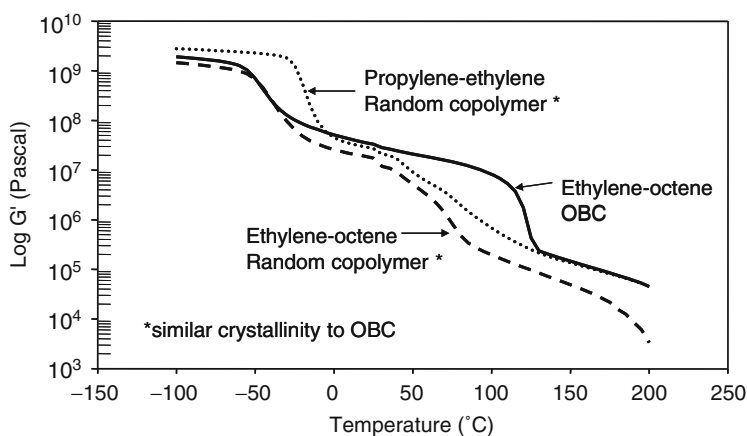


Fig. 22 Storage modulus vs. temperature for statistically random ethylene-octene and propylene-ethylene copolymers compared to an ethylene-octene OBC

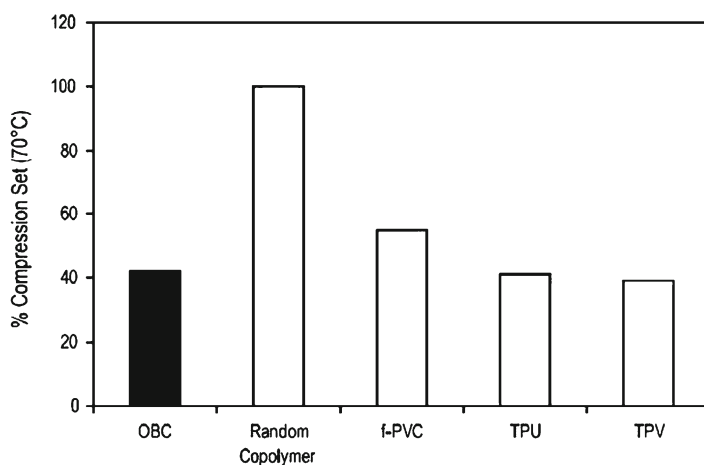


Fig. 23 Compression set at 70 °C for an OBC and competitive materials

7 OBCs by CCTP

In addition to the dual-catalyst chain shuttling system, we also reasoned that synthesis of OBCs using a single catalyst might also be possible using CCTP. Most of the CCTP systems described in [13–17] lose their “living-like” properties before desirable high molecular weight polymers can be achieved, typically around $M_n = 4000 \text{ g mol}^{-1}$ [17]. This restriction unfortunately severely limits their use in one of the most attractive applications of a living polymerization: formation of olefin-based block copolymers via sequential monomer addition. In contrast, the catalysts used in our dual catalyst chain shuttling system operate in high-temperature processes ($> 100 \text{ }^\circ\text{C}$) and overcome the M_n^0 limitations of systems reported in the literature [17]. With these systems, it is possible to form OBCs from a single catalyst through sequential monomer addition.

7.1 Comparison of Batch, Semi-Batch, and Continuous Processes

Block copolymer synthesis from living polymerization is typically carried out in batch or semi-batch processes. In the simplest case, one monomer is added, and polymerization is carried out to complete conversion, then the process is repeated with a second monomer. In batch copolymerizations, simultaneous polymerization of two or more monomers is often complicated by the different reactivities of the two monomers. This preferential monomer consumption can create a composition drift during chain growth and therefore a tapered copolymer composition.

In contrast, a continuous reactor process is controlled at steady state, thereby ensuring a homogeneous copolymer composition. Therefore, a diblock prepared in a series of CSTRs has precise block junctions and homogeneous compositions of each block. In this case, effective CCTP gives a polymer with precisely two blocks per chain, instead of the statistical multiblock architecture afforded by dual catalyst chain shuttling systems.

7.2 Synthesis of Diblock OBCs in a Continuous Process

The advantages provided by the continuous reactor prompted us to explore CCTP in a reactor with two CSTRs connected in series [11]. This reaction scheme depicted in Scheme 6 provides a highly flexible process for production of a wide range of diblock OBC compositions. The block composition can easily be varied by changing the production rate in either reactor. The comonomer content of either block can also be independently tailored by varying the feed compositions because the process operates in two independent reactors. This CCTP scheme also produces multiple chains per catalyst, an advantage over stoichiometric living polymerization systems, but is necessarily stoichiometric in CSA. The reaction produces

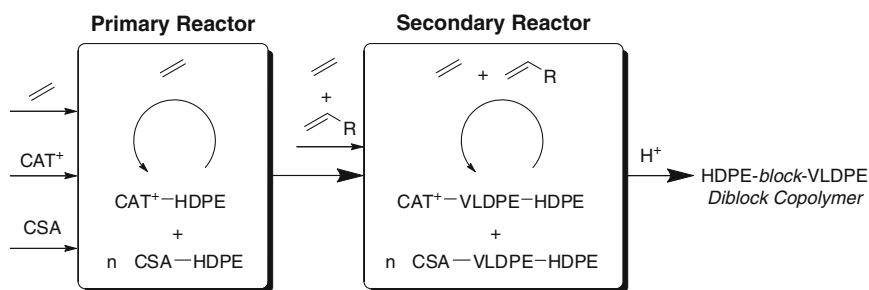
approximately one chain per CSA alkyl functionality, so the overall molecular weight can be controlled by adjusting the CSA feed.

To demonstrate this technology, we targeted a copolymer with blocks of both high density polyethylene (HDPE, density $\sim 0.94 \text{ g cm}^{-3}$) and very low density polyethylene (VLDPE, density $\sim 0.88 \text{ g cm}^{-3}$). Process and product characterization details are given in Table 6. We chose the pyridylamide precatalyst **18** [41] for this study due to its high comonomer reactivity, high M_n^0 , and demonstrated CCTP ability.

The two reactor feeds were controlled to give copolymers with the desired densities, and a physical blend and a diblock OBC were produced. DEZ was added to the first reactor to achieve the desired melt index ($I_2 = 20 \text{ dg min}^{-1}$, equivalent to a M_n of $\sim 15\text{--}20 \text{ kg mol}^{-1}$). This material was fed to the second reactor, and production was continued under different conditions. The material collected after the second reactor had a lower melt index ($I_2 = 3.9 \text{ dg min}^{-1}$), indicating a higher molecular weight consistent with the chain extension reaction from the CCTP process.

7.3 Properties of Diblock OBCs from CCTP

A number of methods provide data consistent with the diblock nature of this new copolymer, including molecular weight, thermal, and solution solubility behavior.



Scheme 6 CCTP in a reactor with two CSTRs connected in series

Table 6 Product and process details for production of a diblock OBC using CCTP in a series of continuous reactors

Sample	Density (g cm^{-3})	I_2 (dg min^{-1})	M_n^a (g mol^{-1})	M_w/M_n^a	Chains per Zn ^b	Chains per Hf ^b
Blend	0.899	1.0	25,900	4.42	–	191
Diblock OBC	0.899	3.9	44,500	1.67	2.5	380

^aMeasured by GPC relative to polystyrene standards and converted to polyethylene equivalents

^bChains per Zn was calculated by using the zinc feed and polymer production rates and the number-average molecular weight of the resulting copolymer corrected for comonomer content. Similarly, chains per Hf was estimated by using the total catalyst metal feed

The GPC traces in Fig. 24 reveal a broad molecular weight distribution, $M_w/M_n = 4.42$, for the dual reactor blend sample. On the other hand, the diblock OBC displays an overall M_w/M_n of 1.67. The narrowing of the distribution indicates that the polymerization has CCTP characteristics. The theoretical molecular weight distribution from an ideal “living” polymerization in a series of two CSTR reactors is given by the following equation, where f_1 and f_2 are the mass fractions of polymer comprising the two blocks [11]:

$$M_w / M_n = 2(1 - f_1 f_2).$$

The theoretical lower limit of the molecular weight distribution for the diblock OBC is 1.58. The observed M_w/M_n of 1.67 indicates that the sample contains a very large fraction of polymer chains with the anticipated diblock architecture. The estimated number of chains per zinc and hafnium are also indicative of a high level of CCTP. The M_n of the diblock product corresponds to just over two chains per zinc but 380 chains per hafnium. This copolymer also provides a highly unusual example of a polyolefin produced in a continuous process with a molecular weight distribution less than that expected for a polymer prepared with a single-site catalyst (in absence of chain shuttling).

The comonomer composition distributions of these two materials are also indicative of the block architecture of the OBC. A comparison of solution solubility characteristics as revealed by TREF is shown in Fig. 25. The physical blend displays a peak at 96 °C with a soluble fraction of 56 wt%, consistent with a physical blend of HDPE and VLDPE. The trace from the diblock OBC reveals a peak at a slightly lower temperature, 93 °C, with no evidence of a shoulder at higher temperature that could be attributed to uncoupled HDPE. In contrast to the blend, the majority of this sample, 84 wt%, elutes at this high temperature, while only 13 wt%

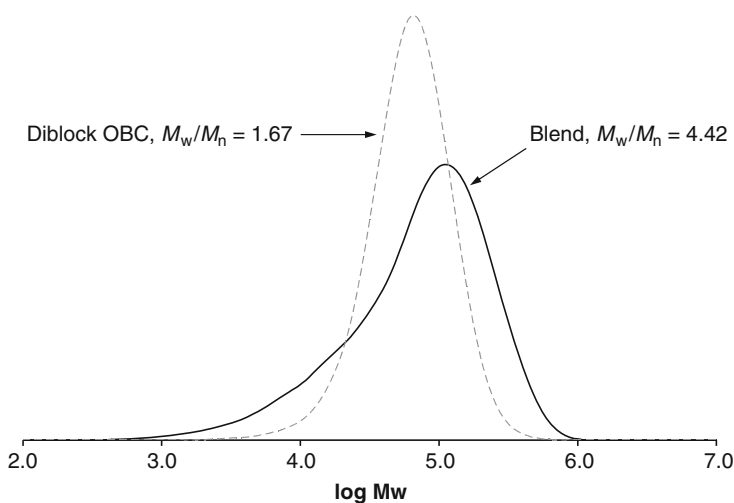


Fig. 24 Comparison of GPC traces of the blend and diblock OBC

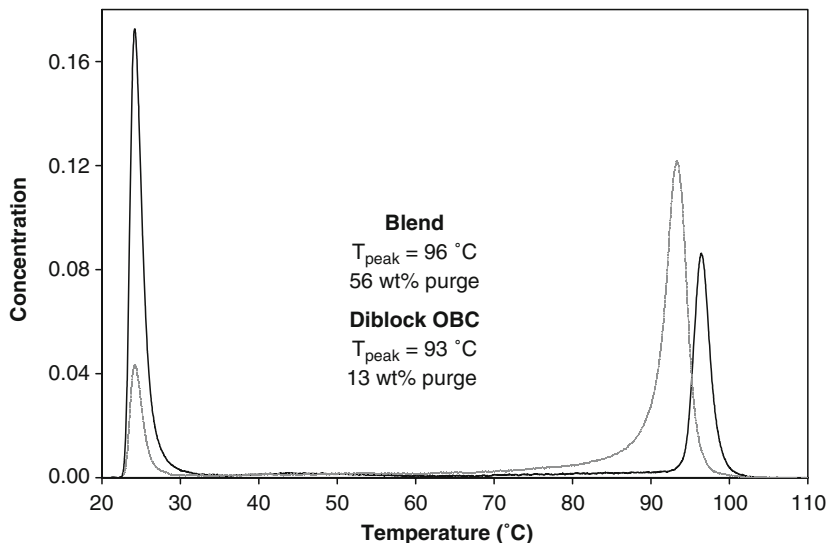


Fig. 25 Comparison of solution solubility by analytical TREF of the blend and diblock OBC

of the sample is soluble at room temperature (since crystallization is an equilibrium process, even samples of HDPE have a small fraction, typically 5–10 wt%, that remains soluble under the employed TREF conditions). This TREF behavior can only result from an OBC architecture with a very homogeneous block structure.

The melting behavior of the two resins also reveals structural differences. The physical blend has a peak melting temperature (T_m) of 126 °C with a heat of fusion of 104 J g⁻¹, consistent with the high density fraction of the sample. The diblock sample has similar crystallinity, with heat of fusion of 104 J g⁻¹, reflecting the similar compositions of the two samples. However, the diblock sample displays a lower peak melting temperature, with $T_m = 122\text{ }^{\circ}\text{C}$. This depression of peak melting temperature is also consistent with OBC architecture.

8 Comparison of Polymer Architectures from Living Polymerization, Chain Shuttling, and Continuous CCTP

Several differences in the block copolymer microstructure and architectures distinguish OBCs prepared using chain shuttling and continuous CCTP from block copolymers afforded by living polymerization systems. Figure 26 depicts some typical polymer chains to illustrate these differences. Block copolymers from living polymerization systems have very narrow molecular weight distributions, with M_w/M_n approaching 1.0 for both the overall chains and blocks within chains. The number of blocks per chain is clearly defined by the process conditions. As discussed previously, precise block junctions are difficult to obtain, and copolymer

blocks normally have tapered compositions from the differences in reactivity if two monomers are polymerized simultaneously in batch polymerizations.

Multiblock OBCs from chain shuttling polymerization have very different architectures. The overall chains and blocks within chains have distributions of molecular weights, with M_w/M_n approaching 2.0. The statistical shuttling process produces chains with a distribution in the number of blocks per chain. The block junctions are precise since each block is grown on a different catalyst, and the compositions are homogeneous since the OBCs are produced at steady-state in a continuous reactor.

Diblock OBCs from continuous CCTP are different from either of the previous two families of copolymers. The continuous process produces blocks lengths with M_w/M_n approaching 2.0. However, the CCTP process in a series of reactors results in a narrower overall distribution, with M_w/M_n approaching 1.5 in the case of a symmetric diblock. The number of blocks per chain is determined by the number of reactors connected in series. Finally, the dual reactor scheme ensures precise block junctions with homogeneous copolymer compositions.

These differences in block architecture of the multiblock and diblock OBCs are apparent in a comparison of the solubility characteristics. Figure 27 shows analyti-

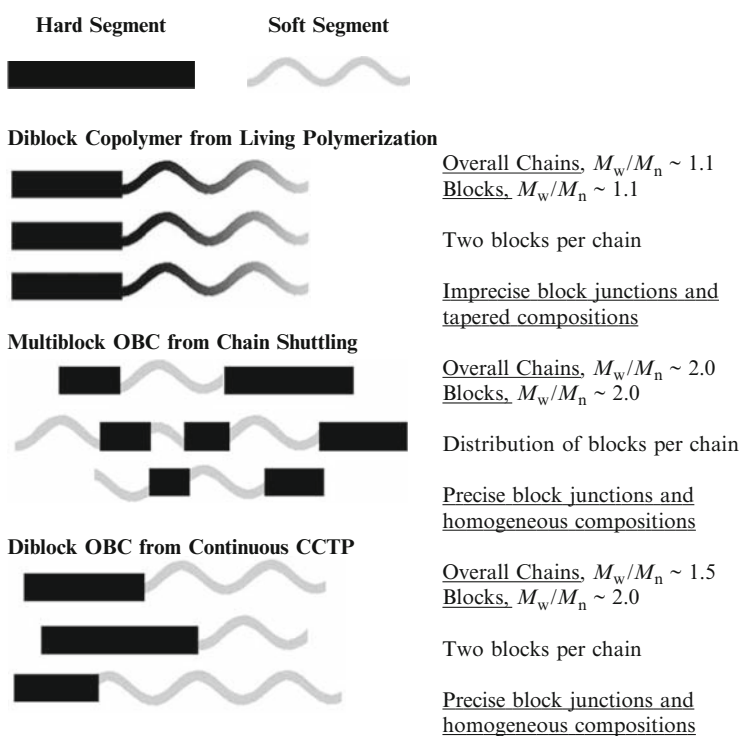


Fig. 26 Comparison of block copolymer architectures from living polymerization, chain shuttling, and continuous CCTP

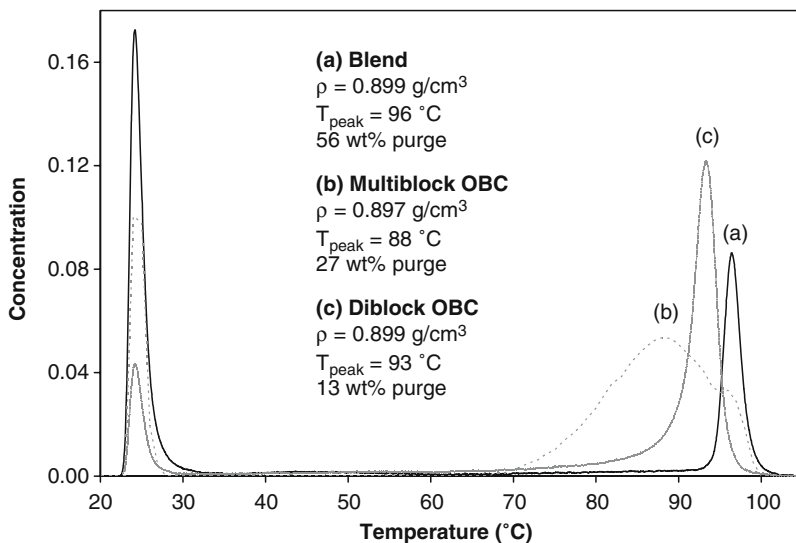


Fig. 27 Comparison of solution solubility by analytical TREF of a blend, diblock, and multiblock OBC with similar overall density ($\sim 0.90 \text{ g cm}^{-3}$)

cal TREF traces for a physical blend, multiblock OBC, and diblock OBC with similar composition. Both OBCs have lower purge fractions and elute at lower temperatures than the high density fraction of the blend. However, the multiblock OBC elutes at a lower temperature and over a broader temperature range than the diblock OBC.

9 Summary

The production of olefin block copolymers has been an aspiration of academic researchers and polymer manufacturers alike. Tremendous progress toward this end has been achieved in recent years with the discovery of several designer catalysts capable of living olefin polymerization. However, the stoichiometric nature of the living process, coupled with related process limitations of low polymerization temperatures and slow batch processes, have precluded these approaches from widespread application.

The chain shuttling and CCTP systems described above overcome these challenges, providing means for production of new polyolefins that display advantaged combinations of physical properties. Chain shuttling polymerization catalysis offers a remarkable variety of OBC compositions, whose properties are almost infinitely tunable. For example, the average number of hard and soft segments per chain can be tuned by changing concentrations of CSA, monomer, comonomer, or

H₂, or by using a catalyst with different M_n^0 . Similarly, the dual-reactor CCTP scheme offers high flexibility in product design. The split can easily be varied by changing the production rate in either reactor, while the comonomer content of either block can be tailored by varying the feed compositions or even introducing another catalyst into one reactor (as long as the new catalyst also does CCTP).

The properties of these new OBCs break the long-held modulus/density relationship, thereby allowing the creation of elastomers with higher use temperatures. The technology has been developed to such a degree that The Dow Chemical Company has introduced a new family of materials under the trade-name INFUSE Olefin Block Copolymers. While this technology introduces a solution to a long-standing challenge, it also poses several new questions. We anticipate future efforts will lead to further elucidation of the kinetic and mechanistic intricacies of chain shuttling reactions, discoveries of catalysts with improved performance, and application of this technology to other polymer systems.

Acknowledgments We thank David Devore, David Graf, Pamela Stirn, Marilyn Bokota, Daryoosh Beigzadeh, Robert Froese, Chris Schultz, Mike Allen, Curt Theriault, Gordon Roof, Tom Karjala, Min Zhang, Lindsey Miller, Jan Bazen, Colin Li Pi Shan, Wilson Cheung, James Stevens, Ben Poon, and Gary Marchand for their hard work and many helpful discussions.

References

1. Vasile C (2000) Handbook of polyolefins, 2nd edn. Marcel Dekker, New York
2. Boor JJ (1979) Ziegler–Natta catalysts and polymerizations. Academic, New York
3. Kaminsky W (2004) *J Poly Sci A Poly Chem* 42:3911–3921
4. Gibson VC, Spitzmesser SK (2003) *Chem Rev* 103(1):283–315
5. Benjam E, McDaniel M (2006) Polyethylene, high density (HDPE). In: Kirk–Othmer encyclopedia of chemical technology, vol 20, 5th edn. Wiley, New York, pp 149–179
6. Maraschin N (2006) Polyethylene, low density (LDPE). In: Kirk–Othmer encyclopedia of chemical technology, vol 20, 5th edn. Wiley, New York, pp 211–239
7. Kissin YV (2006) Polyethylene, linear low density (LLDPE). In: Kirk–Othmer encyclopedia of chemical technology, vol 20, 5th edn. Wiley, New York, pp 179–211
8. Flory PJ (1956) *Science* 124:53–60
9. Holden G (2000) Thermoplastic elastomers and their applications. In: Craver C, Carraher C (eds) *Applied polymer science: 21st century*. Elsevier, Amsterdam, pp 231–256
10. Arriola DJ, Carnahan EM, Hustad PD, Kuhlman RL, Wenzel TT (2006) *Science* 312:714–719
11. Hustad PD, Kuhlman RL, Arriola DJ, Carnahan EM, Wenzel TT (2007) *Macromolecules* 40:7061–7064
12. Natta G, Pasquon I, *Adv Catal* (1959) 11:1–65
13. Samsel EG, Eisenberg DC (1994) US patent 5,276,220
14. Samsel EG (1993) US patent 5,210,338
15. Samsel EG, Brooks FN (2002) US patent 6,444,867
16. Britovsek GJP, Cohen SA, Gibson VC, Van Meurs M (2004) *J Am Chem Soc* 126:10701–10712
17. Kempe R (2007) *Chem Eur J* 13:2764–2773
18. Bhriain NN, Brintzinger H-H, Ruchatz D, Fink G (2005) *Macromolecules* 38:2056–2063
19. Wei Z, Sita LR (2008) *J Am Chem Soc* 130:442–443

20. Chien JCW, Iwamoto Y, Rausch MD, Wedler W, Winter HH (1997) *Macromolecules* 30:3447–3458
21. Chien JCW, Iwamoto Y, Rausch MD (1999) *J Polym Sci Part A Poly Chem* 37:2439–2445
22. Przybyla C, Fink G (1999) *Acta Polym* 50:77–83
23. Song W, Uy Z, Chien JCW (1996) *J Organomet Chem* 512:131–140
24. Song W, Yu Z, Chien JCW (1998) *J Organomet Chem* 558:223–226
25. Lieber R, Brintzinger H-H *Macromolecules* (2000) 33:9192–9199
26. Hazlitt LG, Moldovan DG (1989) US patent 4,798,081
27. Hazlitt LG (1990) *J Appl Polym Sci Appl Polym Symp* 45:25–37
28. Kukral J, Lehmus P, Klinga M, Leskelä M, Rieger B (2002) *Eur J Inorg Chem* 2002:1349–1356
29. Hild S, Cobzaru C, Troll C, Rieger B (2006) *Macromol Chem Phys* 207:665–683
30. Bruaseth I, Rytter E (2003) *Macromolecules* 36:3026–3034
31. Bruaseth I, Soares JBP, Rytter E (2004) *Polymer* 45:7853–7861
32. Tynys A, Eilertsen JL, Seppala JV, Rytter E (2007) *J Poly Sci A Poly Chem* 45:1364–1376
33. Alfano F, Boone HW, Busico V, Cipullo R, Stevens JC (2007) *Macromolecules* 40:7736–7738
34. Ray WH (1972) *J Macromol Sci-Revs Macromol Chem C8*:1–56
35. Hustad PD, Kuhlman RL, Carnahan EM, Wenzel TT, Arriola DJ (2008) *Macromolecules* 41:4081–4089
36. Murphy V, Bei X, Boussie TR, Brummer O, Diamond GM, Goh C, Hall KA, Lapointe AM, Leclerc M, Longmire JM, Shoemaker JAW, Turner H, Weinberg WH (2002) *Chem Rec2*:278–289
37. Odian G (2004) *Principles of polymerization*, 4th edn. Wiley, Hoboken, NJ
38. Mayo FR, Lewis FM (1944) *J Am Chem Soc* 66:1594–1601
39. Makio H, Kashiwa N, Fujita T (2002) *Adv Synth Cat* 344:477
40. Boussie TR, Diamond GM, Goh C, Hall KA, LaPointe AM, Leclerc MK, Murphy V, Shoemaker JAW, Turner H, Rosen RK, Stevens JC, Alfano F, Busico V, Cipullo R, Talarico G (2006) *Angew Chem Int Ed* 45:3278–3283
41. Frazier KA, Boone HW, Vosejka PC, Stevens JC (2004) US patent 2004/0220050
42. Kuhlman RL, Wenzel TT (2008) *Macromolecules* 41:4090–4094
43. Minick J, Moet A, Hiltner A, Baer E, Chum SP (1995) *J Appl Polym Sci* 58:1371–1384
44. Bensason S, Stepanov EV, Chum S, Hiltner A, Baer E (1997) *Macromolecules* 30:2436–2444
45. Wang HP, Khariwala DU, Cheung W, Chum SP, Hiltner A, Baer E (2007) *Macromolecules* 40:2852–2862
46. Li Pi Shan C, Hazlitt LG (2007) *J Macromol Symp* 257:80–93
47. Karande SV, Chueng YW, Diehl CF, Levinson MJ (2006) In: *Proceedings 64th SPE annual technical conference*, 7–11 May 2006, Charlotte, NC. Society of Plastics Engineers, Brookfield, CT

Iron-Based and Cobalt-Based Olefin Polymerisation Catalysts

Vernon C. Gibson and Gregory A. Solan

Abstract This chapter describes the brief history of iron or cobalt catalysts for olefin polymerisation and oligomerisation. Since the discovery in 1998 that 2,6-bis(imino)pyridine iron and cobalt halides, on activation with MAO, can convert ethylene to highly linear polyethylene, numerous reports have been concerned with ligand modification, mechanisms for precatalyst activation, identifying the active species and understanding the mode of propagation/chain transfer. In addition, heterogenisation of this class of catalysts, their incorporation into macrocycles/polymers and their use in reactor blending/tandem catalysis has seen some important developments; alternative ligand architectures that can support active iron and cobalt catalysts are also discussed as are different types of olefinic monomer.

Keywords 2–6-Bis(arylimino)pyridine, Cobalt catalysts, Iron catalysts, Olefin polymerisation, Polyethylene

Contents

1	Introduction.....	109
2	Synthesis of 2,6-Bis(imino)pyridine Iron(II) and Cobalt(II) Halides.....	110
2.1	Ligand Preparation.....	110
2.2	Complexation with MX_2 (M = Fe, Co).....	117
3	2,6-Bis(imino)pyridine Iron Halide/MAO and Cobalt Halide/MAO Catalysts.....	120
3.1	Catalytic Evaluation.....	120
3.2	MAO-Generated “Active Species”.....	125
3.3	Propagation and Chain Transfer Pathways/Theoretical Studies.....	128

V.C. Gibson(✉)

Department of Chemistry, Imperial College, South Kensington Campus, London, SW7 2AZ UK
e-mails: v.gibson@imperial.ac.uk

G.A. Solan(✉)

Department of Chemistry, University of Leicester, University Road, Leicester, LE1 7RH UK
e-mails: gas8@leicester.ac.uk

3.4 Other Co-catalysts/Activators	130
3.5 Well-Defined Iron and Cobalt Alkyls.....	132
4 Supported Catalysts	135
5 Macrocyclic and Polymeric Derivatives	138
6 Tandem Catalysis.....	143
7 Alternative Iron and Cobalt Catalysts.....	143
8 Conclusions.....	152
References.....	153

Abbreviations

Acac	Acetylacetonate
Ar	Aryl
Bn	Benzyl
Cy	Cyclohexyl
DEAC	Diethylaluminium chloride
DFT	Density functional theory
DRIFT	Diffuse reflectance infrared fourier transform
EPR	Electron paramagnetic resonance
ESI-MS	Electrospray ionisation tandem mass spectrometry
Et	Ethyl
Et ₂ O	Diethyl ether
Fc	Ferrocenyl
g (mmol h bar) ⁻¹	Grams per millimole (of precatalyst) per hour per bar
HDPE	High density polyethylene
<i>i</i> -Bu	<i>iso</i> -Butyl
<i>i</i> -Pr	Isopropyl
IR	Infra red
LLDPE	Linear low density polyethylene
MAO	Methylaluminoxane
Me	Methyl
MeCN	Acetonitrile
Mesityl or Mes	2,4,6-Trimethylphenyl
MMAO	Modified methylaluminoxane, AlMeO:Al- <i>i</i> -BuO = 3:1
NMR	Nuclear magnetic resonance
Ph	Phenyl
PS	Polystyrene
Py	Pyridine
<i>t</i> -Bu	<i>tert</i> -Butyl
TEA	Triethylaluminium
THF	Tetrahydrofuran
ULDPE	Ultra low density polyethylene

1 Introduction

A decade has now passed since mixtures of 2,6-bis(arylimino)pyridine-iron(II) halide/MAO and 2,6-bis(arylimino)pyridine-cobalt(II) halide/MAO were first found to impart exceptionally high activities (comparable with metallocenes) for the conversion of ethylene to HDPE (Fig. 1) [1, 2, 3, 4, 5, 6, 7]. The discovery was of particular interest since these late transition metal centres had no track record at the time for olefin polymerisation applications. Through straightforward manipulation of the ligand frame, exceedingly efficient oligomerisation catalysts were also developed allowing access to highly linear α -olefins with Schulz–Flory distributions. When compared with metallocenes and other types of early transition metal single-site Ziegler–Natta catalysts, their relative ease of manipulation, the cost-effectiveness of the metal centres employed coupled with their limited environmental impact makes these systems particularly attractive to study. Indeed in the last 10 years a proliferation of studies has been documented on a variety of topics connected with this class of catalyst and structure–activity relationships have become apparent.

In this chapter we highlight some of the key developments in iron and cobalt polymerisation catalysis that have emerged in the literature since the original discovery that was made independently by Brookhart, Bennett and ourselves [1, 2, 3, 4, 5, 6, 7]. In particular, we focus on 2,6-bis(arylimino)pyridine iron(II) and 2,6-bis(arylimino)pyridine cobalt(II) systems with regard to the impact of steric and electronic properties of the ligand framework on catalyst performance. In addition, studies devoted to identifying the active catalyst, the mode of propagation/chain transfer and to the role played by co-catalysts in the polymerisations will be examined. Immobilisation of the systems on solid supports and incorporation into macrocyclic frameworks represents an area of on-going development that will be reviewed as will the use of this catalyst class as a component in reactor blending/tandem catalysis. New ligand systems that

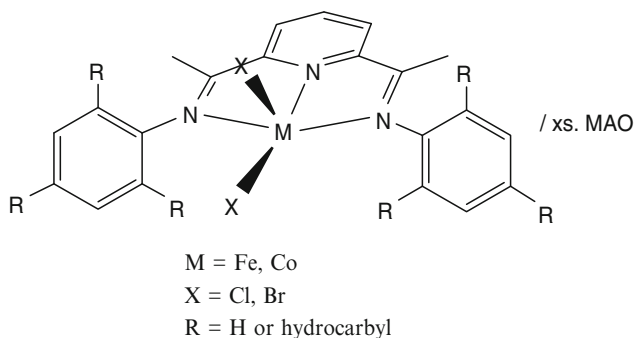


Fig. 1 Original iron and cobalt catalysts developed for ethylene polymerisation and oligomerisation [1, 2, 3, 4, 5, 6, 7]

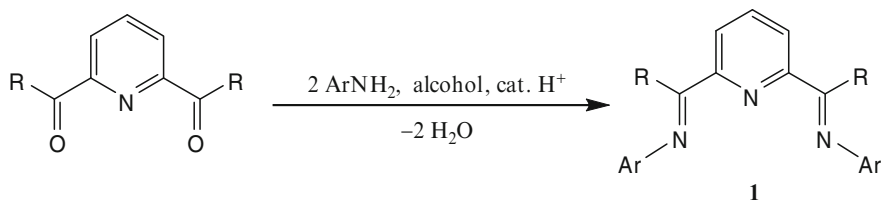
do not fall under the class of 2,6-bis(arylimino)pyridines have started to emerge as compatible supports for iron and cobalt catalysts and these will be summarised and compared with the prototype systems.

For more general overviews of post-metallocene α -olefin polymerisation catalysts, the reader is referred to a series of reviews [8, 9, 10, 11, 12], while recent reviews pertaining to the importance of 2,6-bis(imino)pyridines and to iron and cobalt systems per se have also been documented [13, 14].

2 Synthesis of 2,6-Bis(imino)pyridine Iron(II) and Cobalt(II) Halides

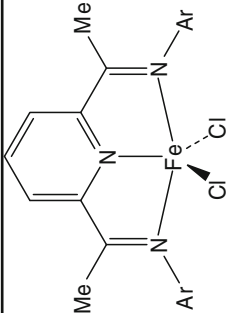
2.1 Ligand Preparation

The bis(arylimino)pyridine ligands, [2,6-(ArN=CR)₂C₅H₃N] (**1** R = H, Me, Ar = aryl group), can be made in good yield from the condensation reaction of either 2,6-pyridinedicarboxaldehyde or 2,6-diacetylpyridine with the corresponding aniline in a 1:2 molar ratio using an alcohol as solvent (e.g. ethanol, propanol, methanol) and usually in the presence of an acid catalyst (e.g. formic acid, acetic acid, *p*-toluene sulfonic acid) (Scheme 1). Generally for a given aniline, the condensation reaction occurs more readily for 2,6-pyridinedicarboxaldehyde than for 2,6-diacetylpyridine, while 2,6-dibenzoylpyridine is much less reactive under these conditions. Using this simple approach a wide variety of symmetrical examples of **1** have been prepared in which the steric bulk and electronic properties of the aryl groups have been systematically varied (see Tables 1 and 2 for complexed examples [1, 2, 3, 4, 5, 6, 7, 8, 9, 10, 11, 12, 13, 14, 15, 17, 20, 21, 24, 26, 27, 29, 28, 32, 33, 36, 37, 38, 39, 40, 41, 42, 44, 48, 18, 16, 19, 22, 23, 25, 30, 31, 34, 35, 45, 43, 46, 47, 49, 50, 51, 52, 53, 54, 55, 56, 57, 58, 59, 60, 61, 62, 63, 64, 65, 66, 67]). The less reactive 2,6-dibenzoylpyridine can be activated towards condensation by a templating/de-metallation route [22] or by the acid catalysed condensation of the 2,6-dibenzoylpyridine under azeotropic reflux in toluene [49]. Supported catalysts such as those based on silica-alumina have been useful for promoting condensation reactions of 2,6-, 2,5-, and 2,4-difluoroanilines [68]. Bis(arylimino)pyridines (**1** R = OR, SR; Ar = aryl group) containing non-hydrocarbyl substituents on the imino carbons, can also be readily prepared [52, 53] as can derivatives of the type



Scheme 1 General route to 2,6-bis(arylimino)pyridines

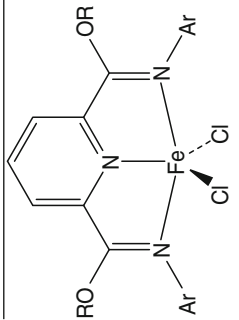
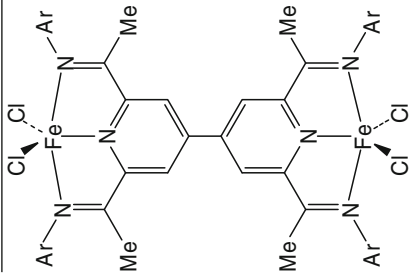
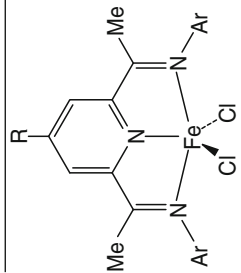
Table 1 2,6-Bis(arylimino)pyridine iron(II) chloride complexes reported

Complex	Ar group	References ^a	Ar group	References ^a
	2-Methylphenyl	[1, 15]	2,4-Difluorophenyl	[16]
	4-Methylphenyl	[17]	2,6-Difluorophenyl	[18, 19]
	2,3-Dimethylphenyl	[15, 20, 21]	2-(Trifluoromethyl)phenyl	[22, 23]
	2,4-Dimethylphenyl	[15, 24]	4-(Trifluoromethyl)phenyl	[25]
	2,5-Dimethylphenyl	[26, 27]	2-(Trifluoromethyl)-4-fluorophenyl	[23]
	2,6-Dimethylphenyl	[6, 24]	2-(Trifluoromethyl)-6-fluorophenyl	[23]
	2,4,6-Trimethylphenyl	[6]	3-Bromo-2,4,6-trimethylphenyl	[27, 28]
	2,6-Dimethyl-4-ferrocenylphenyl	[29]	4-Bromo-2,6-dimethylphenyl	[30]
	2-Ethylphenyl	[1]	3,5-Dibromo-4-methylphenyl	[31]
	2,6-Diethylphenyl	[28]	2-Chloro-4-methylphenyl	[16]
	2-Isopropylphenyl	[1]	2-Fluoro-4-methylphenyl	[16]
	2,6-Diisopropylphenyl	[6]	2-Methoxy-6-methylphenyl	[22]
	2,4,6-Triisopropylphenyl	[32]	4-Bromo-2,6-diisopropylphenyl	[32]
	2,6-Diisopropyl-4-ferrocenylphenyl	[29]	2-Bromo-4,6-diisopropylphenyl	[32]
	2,6-Diisopropyl-4-allylphenyl	[33]	2-Methyl-4-nitrophenyl	[34, 35]
	2-Isopropyl-6-methylphenyl	[36]	2-Methyl-3-nitrophenyl	[34, 35]
	2- <i>tert</i> -Butylphenyl	[6, 17, 24]	2-Methyl-4-diethylaminophenyl	[34]
	2,5-Di- <i>tert</i> -butylphenyl	[37, 38]	4-Methoxyphenyl	[25]
2,6-Dicycloalkylphenyl	[39, 40, 41, 42]	2-Benzylphenyl	[43]	
2-Bromophenyl	[44]	Naphthyl	[43, 45]	
2-Chlorophenyl	[44]	Anthracenyl	[46]	
2,6-Dichlorophenyl	[44]	Tetrahydronaphthyl	[47]	
2-Cyanophenyl	[48]	4-Cyano-2-methylphenyl	[48]	
2-Fluorophenyl	[44, 18]	Pyrenyl	[43]	

(continued)

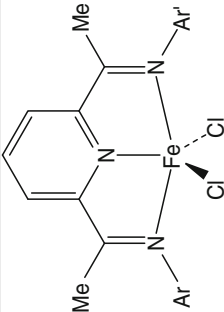
Table 1 (continued)

Complex	Ar group	References ^a	Ar group	References ^a
	2-Methylphenyl 2,6-Dimethylphenyl 2,4,6-Trimethylphenyl 2-Phenylphenyl	[15] [1] [1, 6] [15]	2,6-Diethylphenyl 2,6-Diisopropylphenyl 2,6-Diphenylphenyl Naphthyl	[6] [6] [15] [15]
	2,6-Diisopropylphenyl 2,6-Dimethylphenyl	[49] [28]	2,4,6-Trimethylphenyl	[50]
	2,6-Diisopropylphenyl (R = <i>i</i> -Pr, Et, CH ₂ CH ₂ Ph, CH(CH ₂ Ph) ₂) 2,4,6-Trimethylphenyl (R = <i>i</i> -Pr, Et, CH ₂ CH ₂ Ph, CH(CH ₂ Ph) ₂)	[51] [51]	2,6-Dimethylphenyl (R = Et, PhCH ₂ CH ₂)	[28]

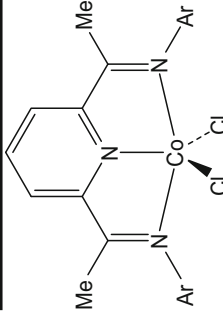
 <p>2,4,6-Trimethylphenyl (R = 2,4,6-Me₃C₆H₃O, 2,4,6-Me₃C₆H₂S, MeS, MeO)</p>	[52]	2,6-Diisopropylphenyl (R = Me, Et)	[53]
 <p>2,6-Diisopropylphenyl</p>	[54]	4- <i>t</i> -Butylphenyl (R = <i>t</i> -Bu)	[55]
 <p>2,6-Dimethylphenyl (R = <i>t</i>-Bu), 2,6-Diisopropylphenyl (R = Cl)</p>	[55]	2,6-Diisopropylphenyl (R = OCH ₂ CH=CH ₂ , OCH ₂ CH ₂ CH ₂ CH=CH ₂)	[57, 58]
	[56]	2,6-Dimethylphenyl (R = OCH ₂ CH=CH ₂)	[57]

(continued)

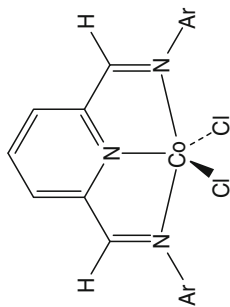
Table 1 (continued)

Complex	Ar group	References ^a	Ar group	References ^a
	2-Fluoro-6-methyl (Ar), 2-methyl (Ar')	[59]	2-Fluoro-6-methyl (Ar), 2,4-dimethyl (Ar')	[59]
	2- <i>tert</i> -Butylphenyl (Ar), 2,6-dimethylphenyl (Ar')	[36]	2- <i>tert</i> -Butylphenyl (Ar), 2,6-diisopropylphenyl (Ar')	[36]
	2,6-Dimethylphenyl (Ar), 2,6-diisopropylphenyl (Ar')	[36]	2,6-Diisopropylphenyl (Ar), 2-methyl-6-isopropylphenyl (Ar')	[36]
	2,6-Diisopropylphenyl (Ar), 2-methylphenyl (Ar')	[60]	2,6-Diisopropylphenyl (Ar), phenyl (Ar')	[60]
	2,4,6-Trimethylphenyl (Ar), 4-cyano (Ar')	[48]		

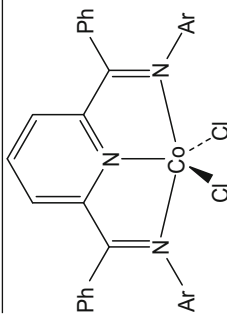
^a Only original reports given**Table 2** 2,6-Bis(arylimino)pyridine cobalt(II) chloride complexes reported

Complex	Ar group	References ^a	Ar group	References ^a
	2-Methylphenyl	[15]	2-Chlorophenyl	[44]
	4-Methylphenyl	[61]	2,6-Dichlorophenyl	[44]
	2,3-Dimethylphenyl	[26]	2-Fluorophenylphenyl	[44, 18]
	2,4-Dimethylphenyl	[26]	2,4-Difluorophenyl	[19]
	2,5-Dimethylphenyl	[26]	2,6-Difluorophenyl	[19]
	2,6-Dimethylphenyl	[26, 37]	2-(Trifluoromethyl) phenyl	[37, 23] (Br derivative)
	2,4,6-trimethylphenyl	[3, 6]	2-(Trifluoromethyl)-4-Fluorophenyl	[23] (Br derivative)
	2,6-Dimethyl-4-ferrocenylphenyl	[29]	2-(Trifluoromethyl)-6-Fluorophenyl	[23] (Br derivative)
	2-ethylphenyl	[62]	4-Bromo-2,6-dimethylphenyl	[37]
	2,6-Diethylphenyl	[63]	4-Bromo-2,6-diisopropylphenyl	[32]
	2-Isopropylphenyl	[62]	2-Bromo-4,6-diisopropylphenyl	[32]

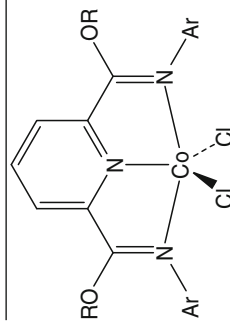
2,6-Diisopropylphenyl	[4, 6]	4-Methoxyphenyl	[64]
2,4,6-Trisopropylphenyl	[32]	2-Benzylphenyl	[43]
2,6-Diisopropyl-4-ferrocenylphenyl	[29]	Naphthyl	[43]
2- <i>tert</i> -Butylphenyl	[2, 3, 6]	Tetrahydronaphthyl	[47]
2,5-di- <i>tert</i> -Butylphenyl	[37, 38]	Pyrenyl	[43]
2-Bromophenyl	[44]		
2-Methylphenyl	[15]	2,6-Diisopropyl	[61]
2,4,6-trimethyl	[3, 6]	Naphthyl	[65]



2,6-Diisopropylphenyl	[46]	2,4,6-Trimethylphenyl	[47]
2,6-Dimethylphenyl	[66]		

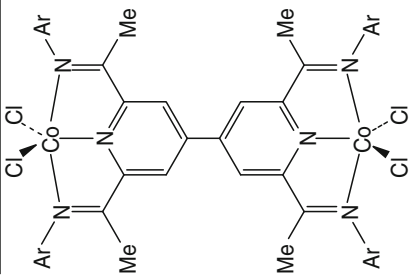
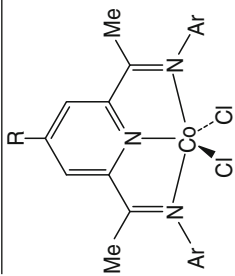


2,6-Diisopropylphenyl (R = Me, Et)	[46]		
------------------------------------	------	--	--



(continued)

Table 2 (continued)

Complex	Ar group	References ^a	Ar group	References ^a
	2,6-Diisopropylphenyl	[50]		
	2,6-Diisopropylphenyl (R = Cl)	[54]	2,6-Diisopropylphenyl (R = OCH ₂ CH=CH ₂)	[67]

^aOnly original reports given

[2,6-(ArN=CMe)₂-4-R-C₅H₂N] (**1** R = *t*-butyl [55]), allyl [69], O(ω -alkenyl) [57, 58], benzyl [69], Cl [56], 2-methyl-2-phenylpropyl [69]) in which the 4-position of the central pyridine unit in **1** can be varied; this latter site also being used to facilitate the linking of two bis(imino)pyridine units [54].

Unsymmetrical 2,6-bis(arylimino)pyridines (Fig. 2), [2-(ArN=CMe)-6-(Ar'N=CMe)C₅H₃N] (**2**), are prepared by the successive condensation reactions of 2,6-diacetylpyridine with two different anilines [36, 22, 34, 59, 60, 70]. For example, the mixed mesityl/*m*-xylyl derivative is prepared by firstly treating 2,6-diacetylpyridine with 2,4,6-trimethylaniline and the reacted the mono-imino intermediate with 2,6-dimethylaniline [22]. The unsymmetrical 2-(arylimino)-6-(alkylimino)pyridine **3**, containing a stereogenic centre (Fig. 2), has been prepared by a related route [71]. Symmetrical 2,6-bis(alkylimino)pyridines, [2,6-(R'N=CR)₂C₅H₃N] (**4** R' = alkyl), can be prepared using the general route employed for **1** [22, 45, 72, 73].

X-ray structures of **1** (R = H or Me) reveal that, in the solid state, the imino nitrogen atoms prefer to be configured *trans* with respect to the central pyridine nitrogen [36, 44, 31, 74, 75, 76, 77, 78] (Yap and Gambarotta, CSD private communication) with the *N*-aryl groups essentially orthogonal to the pyridyl-imine planes (Fig. 3). Notably, with the more bulky Ph-ketimine derivative of **1**, [2,6-((2,6-*i*-Pr₂C₆H₃)N=CPh)₂C₅H₃N], some distortions of this *trans* arrangement are apparent [49].

The ability of bis(imino)pyridines to undergo a broad range of chemistries in their own right such as deprotonation [80, 81, 82, 83], alkylation [82, 83, 84, 85, 86, 87, 88] and reduction [89, 90] has been the subject of numerous reports and has been reviewed elsewhere [13, 14, 91].

2.2 Complexation with MX₂ (M = Fe, Co)

Typically, the synthesis of the precursor iron(II) and cobalt(II) halide complexes proceeds by treatment of an anhydrous or hydrated divalent iron or cobalt halide (e.g. MX₂·*x*H₂O or MX₂; X = Cl or Br) with **1** (and also **2–4**) in

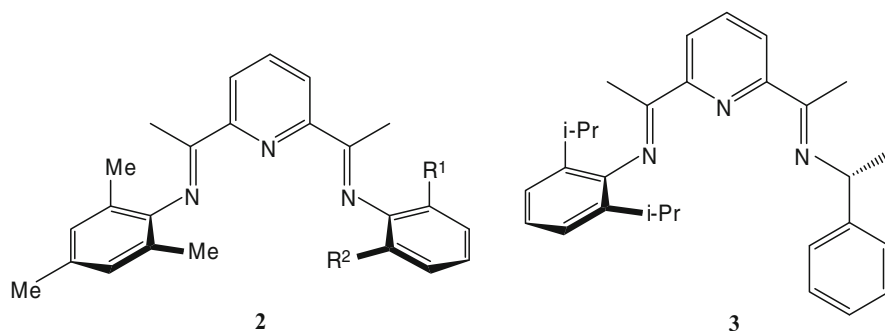


Fig. 2 Unsymmetrical **2** (R¹ = R² = *i*-Pr; R¹ = *t*-Bu, R² = H; R¹ = CF₃, R² = H) and **3**

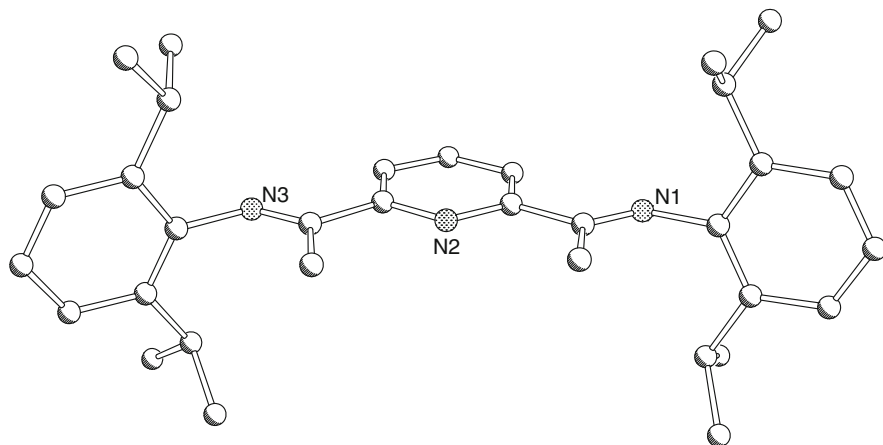
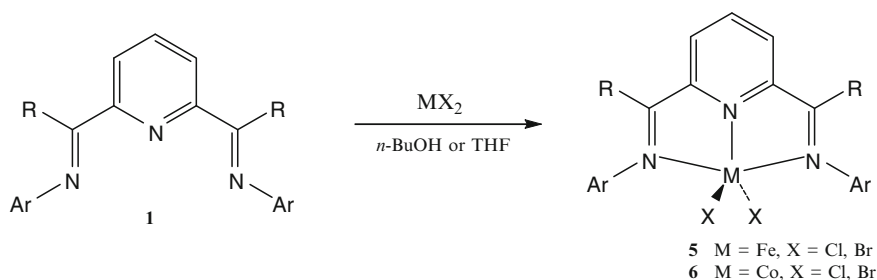


Fig. 3 Molecular structure of **1** (R = Me, Ar = 2,6-*i*-Pr₂C₆H₃) (data from Yap and Gambarotta was used to generate the figure)



Scheme 2 Synthesis of bis(arylimino)pyridine iron(II) and cobalt(II) halides

tetrahydrofuran or *n*-butanol affording [2,6-(ArN=CR)₂C₅H₃N]MX₂ (**5** M = Fe; **6** M = Co; X = Cl or Br) (Scheme 2) [1, 2, 3, 4, 5, 6, 7] in good yields. The importance of solvent polarity in the formation of the desired five-coordinate complexes was recognised by Qian and co-workers, with solvents of lower polarity than acetonitrile being recommended [44, 19]. If the aryl groups in **1** are insufficiently bulky, bis(ligand) salts of the type [{2,6-(ArN=CR)₂C₅H₃N}₂M][MX₄] (**7**) can be formed [44, 19]. Tables 1 and 2 list the comprehensive range of examples of **5** and **6** that have now been prepared and well characterised using this simple synthetic approach.

Both the iron and cobalt complexes are paramagnetic adopting high spin configurations consistent with four [*S* = 2 (**5**)] and three unpaired electrons [*S* = 3/2 (**6**)], respectively. In their IR spectra, shifts of ca. 40 cm⁻¹ (when compared with the free ligand) for the ν(C=N)_{imine} band to lower wavenumber are characteristic of metal coordination. Even though the complexes are paramagnetic in nature, ¹H NMR spectroscopy has also been useful in complex characterisation. Fig. 4 shows three representative spectra in which the proton signals (A–F) are paramagnetically

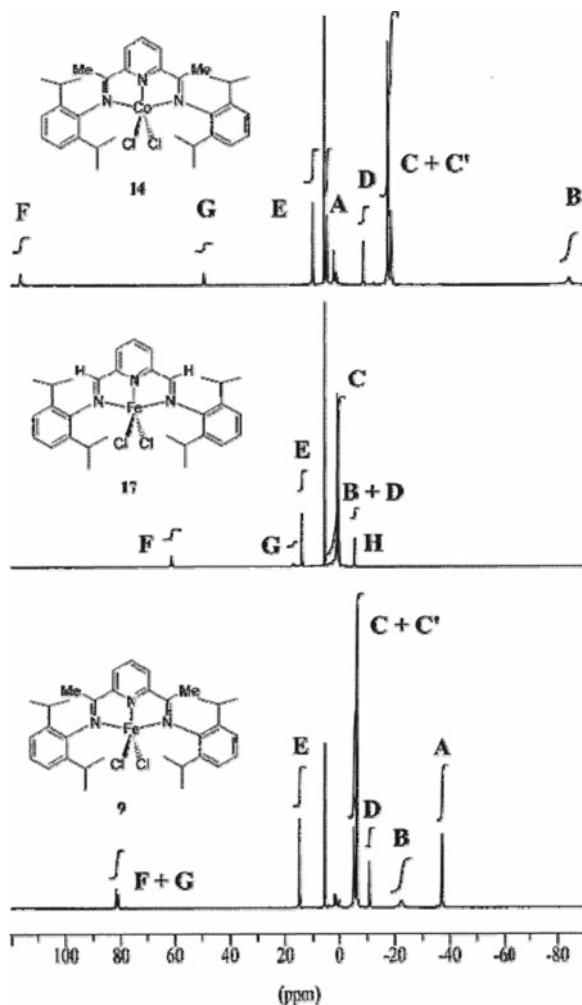


Fig. 4 ¹H NMR spectra of isostructural **6** (R = Me, Ar = 2,6-*i*-Pr₂C₆H₃) and **5** (R = Me, Ar = 2,6-*i*-Pr₂C₆H₃) along with the corresponding iron aldimine complex **5** (R = H, Ar = 2,6-*i*-Pr₂C₆H₃) in CD₂Cl₂ at 293 K. Peak A = NCMe, B = CHMe₂, C and C' = CHMe₂, D = Ar-H_p, E = Ar-H_m, F = Py-H_m, G = Py-H_p, H = CH=N (figure was reproduced from [6], with permission of the copyright holders)

shifted. On the basis of integration and proximity to the paramagnetic centre, full assignment was possible [6].

Nearly 50 crystal structure determinations of examples of **5** and **6** have now been determined and reveal that the geometry at the five-coordinate metal centres can be anywhere between square-pyramidal and trigonal bipyramidal (CSD search April 2008). For example, in [2,6-(ArN=CMe)₂C₅H₃N]FeCl₂ (**5** Ar = 2,6-*i*-Pr₂C₆H₃) a distorted square-pyramidal geometry at the metal is exhibited with the arylimino groups almost perpendicular to the plane of the bis(imino)pyridine backbone (Fig. 5) [5, 6]. The overall result is that the metal centre is protected both above and below

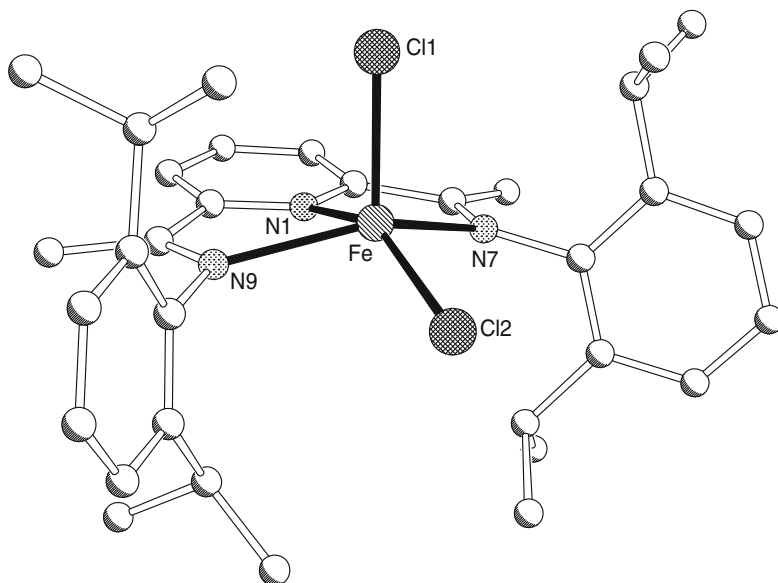


Fig. 5 Molecular structure of **5** ($R = \text{Me}$, $\text{Ar} = 2,6\text{-}i\text{-Pr}_2\text{C}_6\text{H}_3$, $\text{X} = \text{Cl}$) (data from [5], with permission of the copyright holders, was used to generate the figure)

the M-N-N-N plane by the bulky *ortho* substituents on the imino aryl rings. On the other hand, when the aryl group is 2,3-dimethylphenyl or biphenyl ($M = \text{Fe}$), the geometry at the metal centre is a distorted trigonal bipyramid with the pyridyl nitrogen and two halides forming the equatorial plane [15]. This same geometry is also adopted at cobalt for the 2,6-Me₂C₆H₃ derivative [92]. Interestingly in the case of [2,6-(ArN=CR)₂C₅H₃N]FeCl₂ (**5** $R = i\text{-Pr}$, $\text{Ar} = 2,4,6\text{-Me}_3\text{C}_6\text{H}_2$), both square pyramidal and trigonal bipyramidal geometries were found in one structure determination, suggesting a weak energetic bias for one geometry over the other in these systems [51]. For 2,4- or 2,6-difluoro-phenyl derived ligands, complexation with iron dichloride in acetonitrile yielded only the ion-pair complexes [$\{2,6\text{-}(2,4\text{-F}_2\text{C}_6\text{H}_3\text{N}=\text{CMe})_2\text{C}_5\text{H}_3\text{N}\}_2\text{Fe}\}[\text{Cl}_3\text{FeOCl}_3]$ (**8**) and [$\{2,6\text{-}(2,6\text{-F}_2\text{C}_6\text{H}_3\text{N}=\text{CMe})_2\text{C}_5\text{H}_3\text{N}\}_2\text{Fe}\}[\text{FeCl}_4]$ (**9**), respectively [19].

3 2,6-Bis(imino)pyridine Iron Halide/MAO and Cobalt Halide/MAO Catalysts

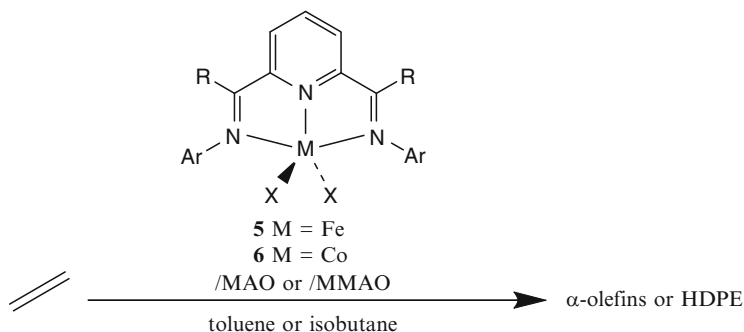
3.1 Catalytic Evaluation

The capacity of bis(arylimino)pyridine iron(II) (**5**) and cobalt(II) halides (**6**) to act as precatalysts for the polymerisation and oligomerisation of ethylene was first demonstrated when toluene solutions of **5** or **6** were treated with excess MAO

(or MMAO = containing 20–25% Al(*i*-Bu)₃) and the resultant catalysts exposed to an ethylene atmosphere (Scheme 3) [1, 2, 3, 4, 5, 6, 7]. Under similar conditions bis(arylimino)pyridine iron(III) halides also serve as active precatalysts [6].

The early studies revealed that the productivities of the iron catalysts (**5**/MAO) are in general an order of magnitude higher than for cobalt (**6**/MAO) and that the steric properties of the 2,6-*ortho* positions of the *N*-aryl groups are crucial in determining whether the catalyst performed as a polymerisation or an oligomerisation catalyst. With two bulky substituents at the 2,6-positions [*i*-Pr (**a**), Me (**b**)] access to high-molecular weight high density polyethylene was achievable for both iron and cobalt systems (Fig. 6) [2, 4, 5, 6], with the less bulky 2,6-Me₂ derivative giving relatively lower molecular weight polymer for iron (**5b**). When a single *ortho*-substituent is present [Me (**c**)], the iron and cobalt systems perform as selective oligomerisation catalysts forming highly linear α -olefins with Schulz–Flory distributions [1, 15]. However, if the steric bulk of the *ortho*-position is too large [*t*-Bu (**d**)], the catalysts generate only polymer [1, 2, 3, 4, 5, 6, 7]. The important role played by electronic properties was first recognised when a methyl group was added to the *para*-position of iron-containing **5b** to give **5e**; a significant increase in the activity of the polymerisation catalyst was observed [2, 5, 6]. On changing from the ketimine (R = Me) to the aldimine (R = H) derivative (for a given aryl group) of either **5** or **6**, a reduction in polymer molecular weight was observed along with a lowering in the activity of the catalyst (e.g. **5e** vs. **5f**) [1, 2, 3, 4, 5, 6, 7].

In subsequent studies, emphasis was placed on examining the electronic variations of the aryl group substitution pattern with the result that a number of additional structure/activity trends have become apparent. Studies on iron systems with different combinations of H, halide and methyl in the *ortho*, *meta* and *para* positions have established that optimal activities are obtained when a chloro substituent is *ortho* and a methyl is either *meta* or *para* (**5g**) (Fig. 6); all are oligomerisation catalysts affording mostly linear α -olefins [16]. Difluoro substituted ligands (**h**, one F always *ortho*) have also been evaluated (with MMAO) for both iron and cobalt, and high oligomerisation activities were found for the iron systems (**5h**), whereas the cobalt systems (**6h**) were inactive [16, 19]. Introduction of a *para*-bromo group (**5i**) raises the activity from 3750 to 5900 g (mmol h bar)⁻¹, with a concomitant decrease



Scheme 3 Catalytic evaluation of **5** and **6** in the presence of MAO or MMAO

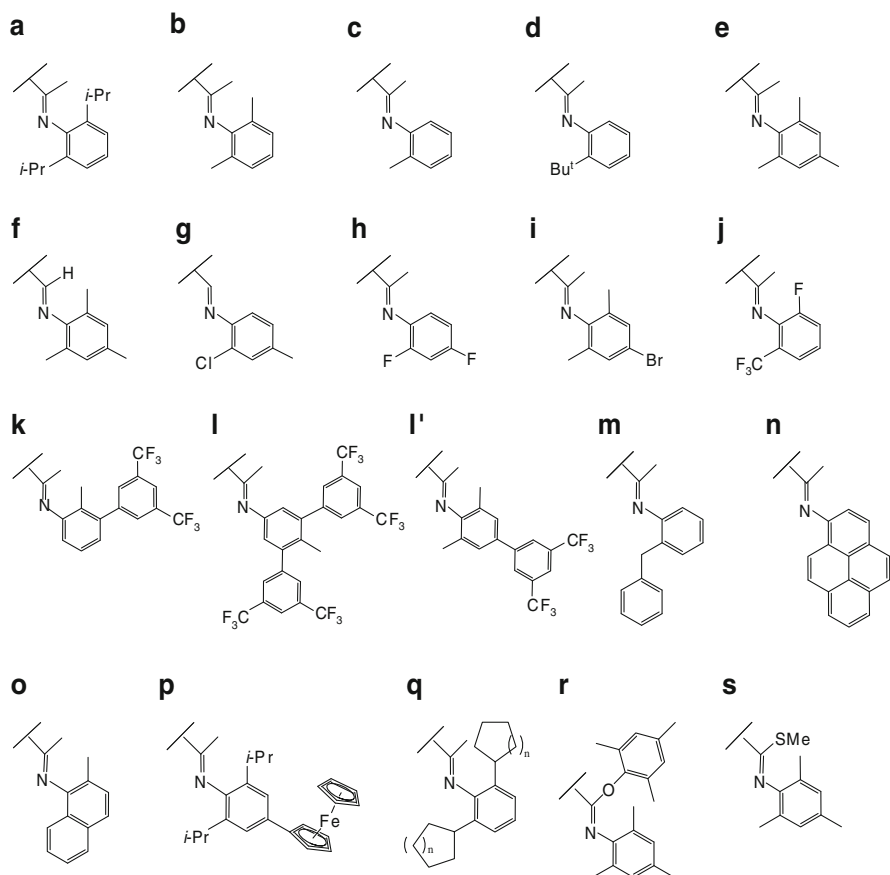


Fig. 6 Selected iminoaryl units (a–s) in precatalysts 5 and 6

in polymer molecular weight [30]. The effect of the *para*-bromo group has been compared to that of *para*-isopropyl, and results suggest electronic effects are beneficial for increased activity for iron systems whereas steric effects appear more dominant for cobalt [32].

The use of an *ortho*-aryl CF_3 group in the cobalt systems can lead to substantial increases in activity (and catalyst lifetimes) upon activation with MAO [23]. Notably, the cobalt-based catalyst bearing an *ortho*- CF_3 group in combination with an *ortho*-F substituent (j) displays an activity greater than $100,000 \text{ g (mmol h bar)}^{-1}$, which is comparable in performance to the most active iron catalysts. A number of substitution patterns involving *ortho*-methyl groups and *meta*-fluorinated aryls (F or CF_3 groups) have been investigated by Ionkin et al. [31]. Ligands involving a 2,3-pattern of *ortho*-methyl and *meta*-aryl (k) or with two *meta*-aryls on one side and two *ortho*-methyls (l and l') on the other yield highly active iron oligomerisation

systems with more ideal Schulz–Flory distributions than related systems containing no *meta*-aryl groups [31]. In the absence of *ortho*-methyl substituents, but with two *meta*-fluorinated aryl groups on each imino aryl ring, inactive ion-pair complexes of the form $[L_2Fe][FeCl_4]$ are generated.

Incorporating *ortho*-benzyl groups (**m**) has been reported to give a very high activity iron catalyst (40,800 g (mmol h bar)⁻¹ cf. 1655 g (mmol h bar)⁻¹ for the original 2,6-diisopropylphenyl derivative under the same catalytic conditions), producing linear polyethylene. Related ligands possessing either an *ortho*-phenyl or *ortho*-myrtanyl group are far less active [43]. Use of a pyrenyl group (**n**) gave an iron catalyst exhibiting an activity of 13,480 g (mmol h bar)⁻¹ and is reported to yield (for first time) branched polyethylene [43]. For iron systems based on naphthyl groups, introduction of an *ortho*-methyl group (**o**) greatly enhances the activity of the system [45].

An electrochemically active ferrocenyl group can be attached at the *para*-position of the *N*-aryl group, with the iron system (**5p**) displaying an activity of 6300 g (mmol h bar)⁻¹ [cf. 440 g (mmol h bar)⁻¹ for the cobalt analogue (**6p**)] and affording a polymer with a molecular weight of 900,000 [29]. Such iron and cobalt systems when oxidised with ferrocenium hexafluorophosphate afford smoothly $[2,6-(2,6-i-Pr_2-4-FcArNCMe)_2C_5H_3N]MCl_2(PF_6)_2$ (**10p**, M = Fe; **11p**, M = Co). However, no difference in polymerisation performance has been observed between **10p** and **11p** when compared with the reduced species treated with MAO; this has been attributed to reduction of the dicationic ferrocenium species by the alkylaluminum co-catalyst.

The presence of cycloalkyl substituents in the 2,6-positions of the aryl groups (**5q**) has been found to increase the temperature stability of the iron catalysts over their alkyl analogues (e.g., **5b** or **5c**); these results are further supported by a quantum mechanical study [39].

Complexes $[2,6-\{(2,4,6-Me_3C_6H_2)N=CR\}_2C_5H_3N]FeCl_2$ [**5rR** = 2,4,6-Me₃C₆H₂O; **5s R** = MeS], possessing ether and thioether groups as the imino carbon substituents, are highly active catalysts for ethylene polymerisation on treatment with MAO (Fig. 6). Interestingly, replacement of the mesityl aryloxy in **5r** with an O–Me group leads to an inactive system [52].

Bis(hydrazone)pyridyl complexes $[2,6-(R'N=CMe)_2C_5H_3N]FeCl_2$ [**12 R'** = NPhMe; **R'** = NPh₂, NMe₂; **13 R'** = 2,5-dimethylpyrrolyl] have been tested in combination with MAO (Fig. 7) [93, 94, 95]. For small *R'* groups, toluene-soluble α -olefins are obtained, whereas larger *R'* groups afford low molecular weight solid polyethylene; the catalytic activity of the 2,5-dimethylpyrrolyl derivative **13** (up to ca. 3000 g (mmol h bar)⁻¹) is at least an order of magnitude greater than those of the other hydrazones [93].

The C₁-symmetric complex $[2-\{2,6-i-Pr_2C_6H_3\}N=CMe]-6-\{(PhCH(Me))N=CMe\}C_5H_3N]FeCl_2$ (**14**), upon activation with MAO, has been found to promote simultaneous polymerisation and oligomerisation (Schulz–Flory distribution) of ethylene (Fig. 7) [60]. Complexes $[2,6-(R'N=CMe)C_5H_3N]FeCl_2$ (**15 R'** = Ph₂CH; **16 R'** = fluorenyl), bearing *N*-alkyl substituents, exhibit contrasting behaviour with **15** being inactive but **16** forming a highly active iron system for ethylene oligomerisation to give C₄–C₁₀ olefins [96]; deprotonation of the N–CH bond in **16** by the activating MAO has been proposed as an explanation for the different behaviour.

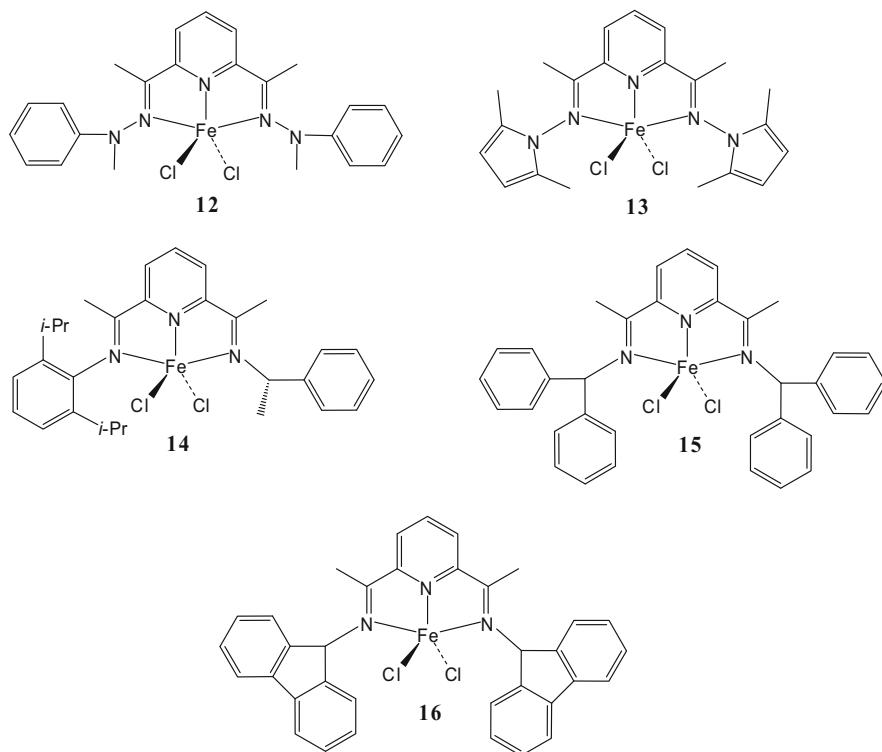
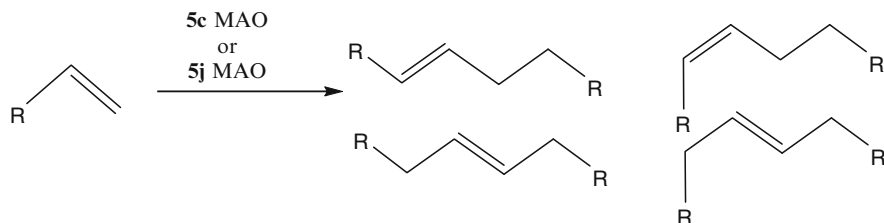


Fig. 7 Bishydrazone (**12**, **13**), C_1 -symmetric (**14**) and bisalkyl precatalysts (**15**, **16**)

α -Olefins have also been employed as monomers in the catalytic evaluation of **5**/MAO and **6**/MAO. In general, significantly lower productivities are observed for the polymerisation of propylene [36, 97, 98] and this reflects the inability of the ethylene polymerisation catalysts to incorporate higher α -olefins into the growing polymer chains. Fink et al. have shown that the low activities can be considerably increased by using $\text{CPh}_3\text{B}(\text{C}_6\text{F}_5)_4/\text{AlR}_3$ ($\text{R} = i\text{-Bu, Et}$) as the co-catalyst; the combination of [2,6- $\{(2\text{-}i\text{-Pr-6-MeC}_6\text{H}_3)\text{N}=\text{CMe}\}_2\text{C}_5\text{H}_3\text{N}\}\text{FeCl}_2$ (**5t**)/ $\text{CPh}_3\text{B}(\text{C}_6\text{F}_5)_4/\text{Al}(i\text{-Bu})_3$ proving the most active system [99].

Use of less sterically hindered examples of **5** in combination with MAO allows for active catalysts for the linear (head-to-head) dimerisation of α -olefins such as 1-butene, 1-hexene, 1-decene and Chevron Phillips' C20–24 α -olefin mixture (Scheme 4) [47]. The mechanism for dimerisation is thought to involve an initial 1,2-insertion into an iron-hydride bond followed by a 2,1-insertion of the second alkene and then chain transfer to give the dimers. Structurally related cobalt systems have also been shown to promote dimerisation albeit with lower activities [62]. Oligomerisation of the α -olefins propene, 1-butene and 1-hexene has additionally been achieved with the CF_3 -containing iron and cobalt systems **5j** and **6j** yielding highly linear dimers [23].



Scheme 4 Use of **5c**/MAO or **5j**/MAO to mediate the head-to-head dimerisation of α -olefins

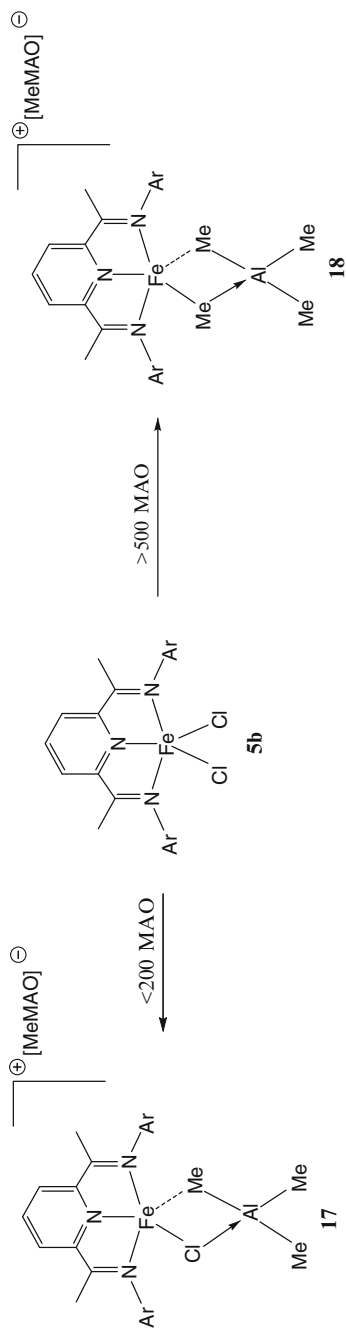
5/MAO has also been reported to promote the conversion of acrylates to polyacrylates [63, 100, 101]. In the case of *tert*-butylacrylate, the *N*-alkyl catalyst [2,6-((1-*cis*)-myrtanyl)N=CMe)₂C₅H₃N]FeCl₂/MAO was found to give the highest activities and the highest molecular weight polymer [100]; some activity was also reported using this system for methyl methacrylate and *n*-vinylcarbazole.

3.2 MAO-Generated “Active Species”

The active species generated when bis(arylimino)pyridine iron (**5**) and cobalt (**6**) halides are activated with MAO was, by analogy with metallocene catalysts, initially considered to be a highly reactive mono-methylated cobalt(II) or iron(II) cation of the form LM–Me⁺ bearing a weakly coordinating counter-anion such as [X–MAO][–] (X = halide, Me). To examine this theory a number of spectroscopic investigations have been directed towards identifying the active species (*vide infra*).

Both ¹H NMR and ²H NMR spectroscopy have been employed to study intermediates formed via activation of ferrous-based polymerisation catalysts with MAO (also studied were AlMe₃, AlMe₃/B(C₆F₅)₃ and AlMe₃/CPh₃B(C₆F₅)₄) [102]. With **5b**/MAO, the ion-pairs of the type [2,6-((2,6-Me₂C₆H₃)N=CMe)₂C₅H₃N]Fe^{II}(μ-Cl)(μ-Me)AlMe₂]⁺[Me-MAO][–] (**17**) (at Al/Fe < 200) and [2,6-((2,6-Me₂C₆H₃)N=CMe)₂C₅H₃N]Fe^{II}(μ-Me)₂AlMe₂]⁺[Me-MAO][–] (**18**) (at Al/Fe > 500) (Scheme 5) are evident. On the other hand with the (**5b**)/AlMe₃ system, neutral species of the type [2,6-((2,6-Me₂C₆H₃)N=CMe)₂C₅H₃N]Fe^{II}(Cl)(μ-Me)₂AlMe₂ (**19**) or [2,6-((2,6-Me₂C₆H₃)N=CMe)₂C₅H₃N]Fe^{II}(Me)(μ-Me)₂AlMe₂ (**20**) are observed [102, 103, 104, 105]. An EPR spectroscopic study by the same group suggested that the iron centre remains in the ferrous state throughout the activation [104]. The latter observation contrasts with an investigation by Gibson et al. using Mössbauer and EPR spectroscopy of the **5a**/MAO system, which indicated 100% conversion to a species exhibiting a +3 oxidation state [89].

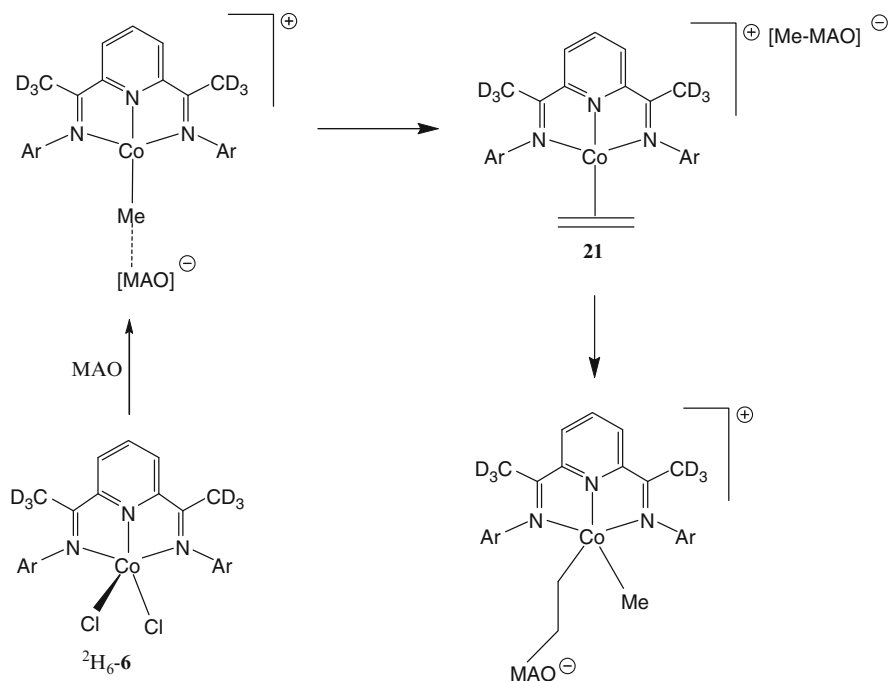
ESI mass spectrometry has been used to probe the activation of **5a** with MAO in THF and has shown the presence of both a four coordinate [2,6-((2,6-*i*-Pr₂C₆H₃)N=CMe)₂C₅H₃N]FeMe⁺ cation and an iron hydride species [2,6-((2,6-*i*-Pr₂C₆H₃)N=CMe)₂C₅H₃N]FeH⁺ [106]. Using low Fe/MAO ratios, the activation reaction of



Scheme 5 Effects of Al/Fe ratio on activation of **5b** with MAO (Ar = 2,6-Me₂C₆H₃)

5a by MAO does not reach completion, with a cationic monochloride complex $[2,6-\{(2,6-i\text{-Pr}_2\text{C}_6\text{H}_3\text{N}=\text{CMe})_2\text{C}_5\text{H}_3\text{N}\}\text{FeCl}]^+$ being the only species observed. In addition, UV–visible spectroscopic studies revealed that the alkyl and hydride cations exist as THF adducts. UV–visible spectral changes associated with an MAO-activated bis(imino)pyridine iron complex have also been investigated by Schmidt et al., in which it was shown that changes in the spectra are strongly dependent on the elapsed time after MAO addition and MAO concentration [107].

Studies conducted to examine the mode of activation of MAO with bis(imino)pyridine cobalt halide systems have shown some intriguing findings. With regard to **6a**/MAO, initial reduction of the cobalt(II) precatalyst to cobalt(I) halide followed by conversion to a cobalt(I) methyl and ultimately to a cobalt(I) cationic species has been demonstrated (see Sect. 2.6) [108, 109]. Addition of ethylene affords an ethylene adduct $[\{2,6-\{(2,6-i\text{-Pr}_2\text{C}_6\text{H}_3\text{N}=\text{CMe})_2\text{C}_5\text{H}_3\text{N}\}\text{Co}(\eta^2\text{-C}_2\text{H}_4)\}\text{[MeMAO]}]^+$ (**21**), which is considered as the immediate precursor to the active species (Scheme 6). Using ^1H NMR and ^2H NMR spectroscopy it has been shown that the “non-coordinating” $[\text{Me-MAO}]^-$ anions are incorporated at the saturated ends of the polymers consistent with an activation mechanism that involves nucleophilic attack by an abstracted alkyl group on the cationic ethylene species [109].



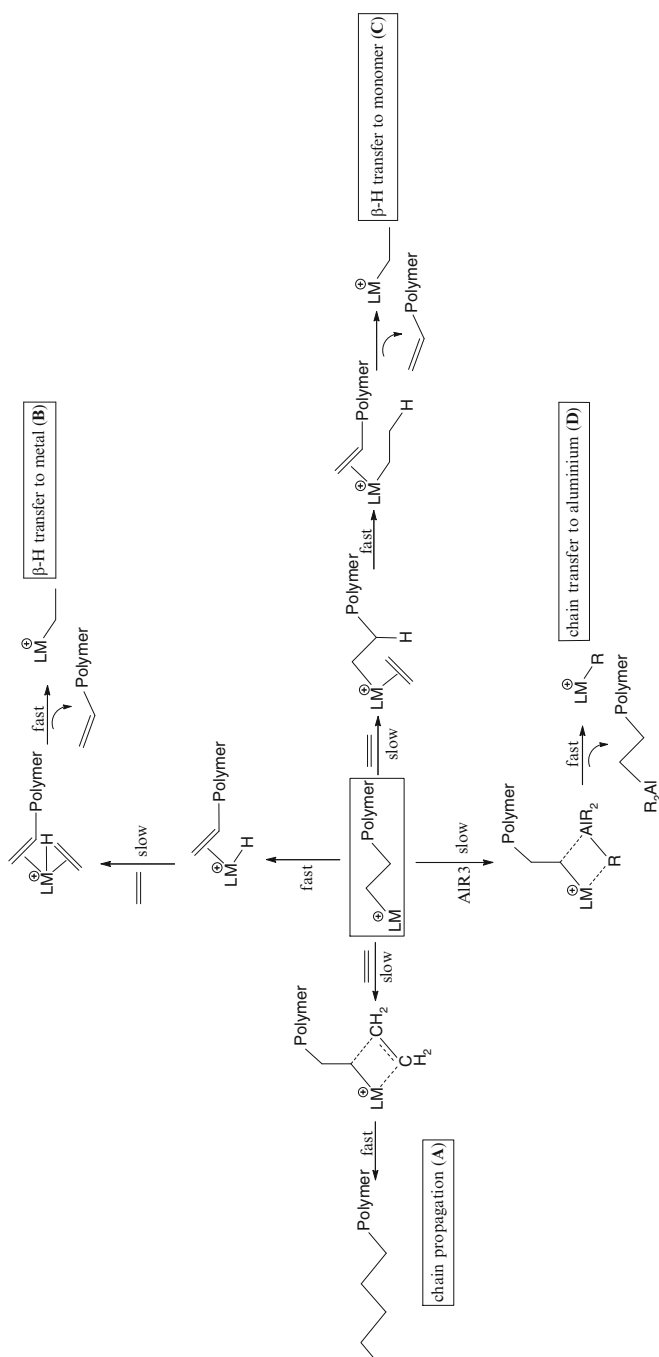
Scheme 6 Proposed mechanism for activation **6a** with MAO [109]

3.3 *Propagation and Chain Transfer Pathways/Theoretical Studies*

For both the iron (**5**/MAO) and cobalt (**6**/MAO) catalysts a Cossee-type propagation mechanism [110] is assumed (pathway A in Scheme 7), in which a repetition of steps involving ethylene coordination and migratory insertion of the bound ethylene into a metal alkyl bond occur in succession until at some point propagation ceases and chain transfer occurs. Support for the Cossee-type propagation was provided by a first-order rate dependence on ethylene pressure/concentration [6]. The molecular weight, however, was found to remain constant, with variation in ethylene pressure in accordance with the overall rate of chain transfer being first order in ethylene. Based on these results it was concluded that β -H by transfer to metal (pathway B) or to monomer (pathway C) (kinetically indistinguishable) represents the dominant chain-transfer process [6]. Uniquely for iron, broad molecular weight distributions can be observed, which in some cases take the form of bimodal distributions (see Fig. 9). Using ^1H NMR spectroscopy to monitor the chain ends in the lower molecular weight peak, it was shown that both end groups are fully saturated. Based on the latter findings it was concluded that chain transfer to aluminium (pathway D) can also be an operative termination mechanism with iron-based catalysts. The preference for cobalt systems to undergo uniquely β -H transfer has been the basis of a combined experimental and theoretical study [111].

To supplement the experimental observations, a number of theoretical studies have been performed to probe the mode of propagation and chain transfer. In an initial full ab initio study on the diisopropylphenyl catalysts derived from **5a**, Gould and co-workers [112] computed the key structures operating for the first monomer insertion and showed that intermediates along the reaction coordinate have low spin ($S = 0$) configurations. Ziegler et al. have carried out DFT and DFT/molecular mechanics for an ethylene polymerisation process initiated by cationic alkyl species based on the bis(imino)pyridine iron model system **22** (Fig. 8), and the iron-alkyl cation derived from **5a**. In this study they find that the rate-determining step for both termination and propagation is the capture of ethylene by the iron alkyl cation. The steric properties imposed by the *N*-Ar group (2,6-*i*-Pr₂C₆H₃) group was found to inhibit ethylene capture for the termination step and increase the rate of insertion [113]. Using the cationic alkyl complex derived from **5a**, similar calculations reveal that the activity is inhibited by steric crowding [114].

Musaev, Morokuma and co-workers have been concerned with understanding the mechanisms of chain propagation and β -hydride transfer termination for a series of iron catalysts [115]. By varying the steric bulk of the systems studied, it was found that two axial ligands are required in order for the d_{z^2} orbital to be destabilised (with the tridentate bis(imino)pyridine ligand defining the equatorial xy plane) and for the singlet to be the ground state, a situation found for the β -hydride termination species. In contrast, only one axial ligand is present for chain propagation. The calculations for the two extremes of steric bulk are in agreement with the observed suppression of β -hydride transfer termination upon increasing the steric bulk of the ligand **1**. For cobalt(I) alkyl



Scheme 7 Proposed chain propagation and transfer process in bis(imino)pyridine iron and cobalt catalysts

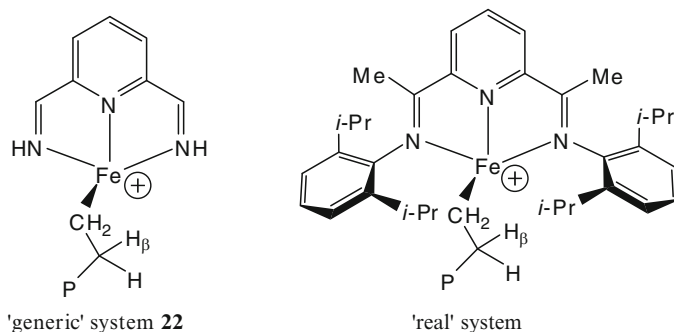


Fig. 8 Cationic alkyl “generic” model system **22** and “real” system derived from **5a**

Table 3 Other co-catalysts that have been employed to activate bis(arylimino)pyridine iron dihalides (**5**)

Co-catalyst	References	Co-catalyst	References
AlMe ₃	[102, 103, 116, 119]	AlMe ₃ /B(C ₆ F ₅) ₃	[102]
AlEt ₃	[117, 118]	AlMe ₃ /CPh ₃ B(C ₆ F ₅) ₄	[102]
Al(<i>i</i> -Bu) ₃	[103, 116, 117, 119, 180]	AlEt ₃ /CPh ₃ B(C ₆ F ₅) ₄	[99]
Al(<i>n</i> -octyl) ₃	[103, 117]	Al(<i>i</i> -Bu) ₃ /CPh ₃ B(C ₆ F ₅) ₄	[99]
AlEt ₂ Cl	[116]	Et ₂ AlOAlEt ₂	[118]
Al(<i>n</i> -hexyl) ₃	[117]	(<i>i</i> -Bu) ₂ AlOAl(<i>i</i> -Bu) ₂	[116, 118]
AlMe ₃ /Al(<i>i</i> -Bu) ₃	[117]		

complexes, experiment and theory have been shown to be in agreement and support a stepwise pathway for the reaction of the alkyl complexes with 1-alkenes, reacting by β -hydride transfer via a cobalt hydride intermediate [115]. Such cobalt alkyls have also been shown to contain low-spin cobalt(II) antiferromagnetically coupled to a ligand radical anion. The lowest triplet state is thermally accessible and accounts for observed ¹H NMR chemical shifts at room temperature [66].

3.4 Other Co-catalysts/Activators

In general, MAO or MMAO (MAO containing 25% isobutyl groups) has been the co-catalyst/activator most employed with bis(imino)pyridine iron(II) halide (**5**) and cobalt(II) halide (**6**) precatalysts. Nevertheless, a range of alternative activators have also been screened (Table 3). Early in the development of the iron and cobalt catalysts the important role played by the co-catalyst on catalyst performance was recognised. For example, as has already been mentioned (see Sect. 2.5), the molar Al:Fe ratio can be highly influential on the molecular weight distribution of the polyethylene formed with large excesses of MAO, leading to broad bimodal distributions (see L and H in Fig. 9) [6, 10].

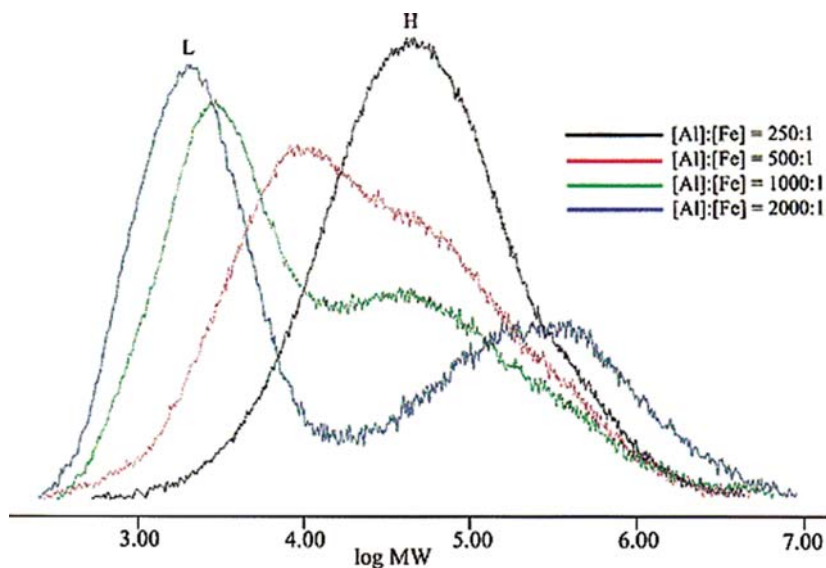


Fig. 9 Effect of MAO concentration on modality of polymer formed using **5a** (figure was reproduced from [6], with permission of the copyright holders)

A similar bimodal molecular weight distribution containing large fractions of low molar mass products can be obtained using **5a** in combination with AlMe_3 [116, 117]. On studying a range of trialkylaluminiums as activators it was found that the catalytic activity followed the order $\text{AlMe}_3 < \text{Al}(n\text{-Oct})_3 < \text{Al}(i\text{-Bu})_3 < \text{AlEt}_3 < \text{Al}(n\text{-Hex})_3$, with MAO-based systems still displaying the highest activity. Notably, the polyethylene obtained using $\text{Al}(i\text{-Bu})_3$ as the co-catalyst displayed a relatively narrow and unimodal molecular weight distribution [116]. By mixing AlMe_3 with $\text{Al}(i\text{-Bu})_3$ the catalytic activity was found to be higher than that obtained by taking each activator individually [117]. Using the tetraethylaluminumoxane, $\text{Et}_2\text{AlOAlEt}_2$ in combination with **5a** the activity of the catalyst is higher than using AlEt_3 or $\text{Al}(i\text{-Bu})_3$ [118]. The bis(imino)pyridine cobalt precatalyst/co-catalyst systems have also been examined with regard to co-catalyst variation. For example, **6b**/ AlMe_3 shows similar activities to MAO-based systems whereas **6b**/ $\text{Al}(i\text{-Bu})_3$ was almost inactive at a molar ratio $\text{Al}:\text{Co} = 500$ [119]. As a general feature, the activities exhibited by these cobalt systems are less than their iron counterparts.

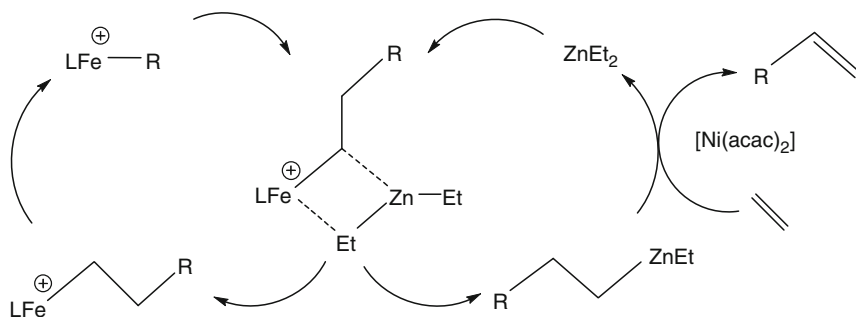
The introduction of metal alkyls to an MAO-activated bis(imino)pyridine iron catalyst has also been the subject of a number of studies. Both AlMe_3 and AlEt_3 have been added to **5a**/MAO-based polymerisation catalysts leading to polyethylene displaying a bimodal distribution similar to that observed using **5a**/MAO_{large excess} (see Fig. 9) [120]. Conversely, the use of excess $\text{Al}(i\text{-Bu})_3$ gives a monomodal distribution in a manner similar to that seen using $\text{Al}(i\text{-Bu})_3$ alone (vide supra). Indeed in early catalytic studies, $\text{Al}(i\text{-Bu})_3$ was used as a scavenger for **5**/MAO-mediated polymerisations and as result polymers were obtained containing isopropyl end groups, indicative of chain transfer to aluminium [6]. As observed when using

AlEt₂Cl as the sole co-catalyst [116], addition of AlEt₂Cl to **5a**/MAO deactivates the catalyst system. Analysis of the polymer end groups reveals that chain transfer to aluminium is the operative mechanism for termination. To examine whether this particular chain transfer mechanism can occur with other metals, addition of a range of metal alkyls [e.g. *n*-BuLi, Mg(*n*-Bu)₂, BEt₃, GaR₃ (R = Me, Et, *n*-Bu), SnMe₄, PbEt₄, ZnEt₂] to **5a**/MAO was also reported. Significantly, in the case of ZnEt₂, **5a**/MAO is shown to catalyse polyethylene chain growth at zinc (Scheme 8) [120, 121, 122]. The grown alkyl chains can then be displaced from the zinc centres by an olefin exchange reaction catalysed by, for example, [Ni(acac)₂] to give linear α -olefins with a Poisson distribution of chain lengths.

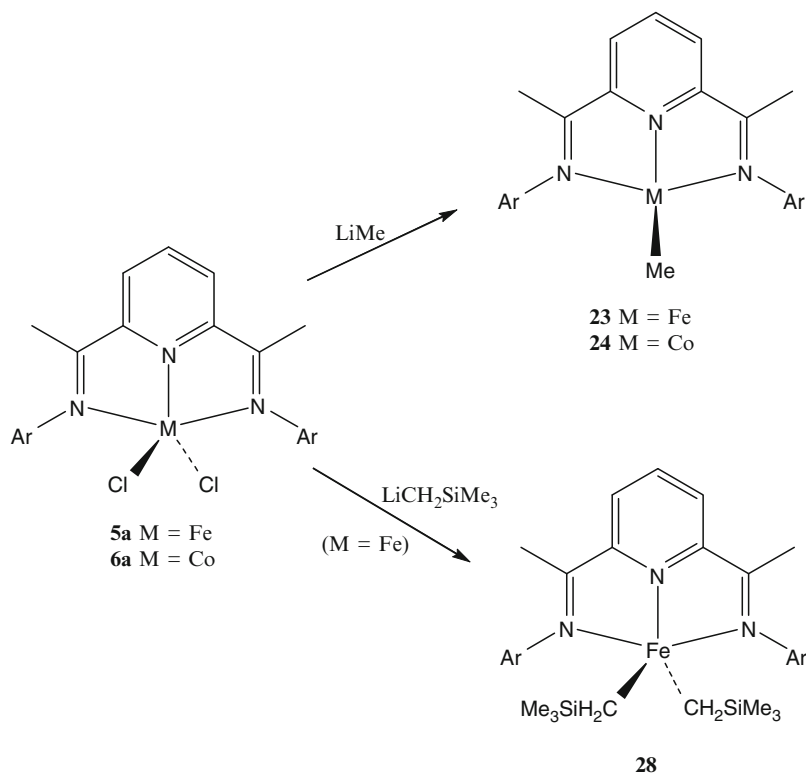
3.5 Well-Defined Iron and Cobalt Alkyls

Since the initial discovery of bis(arylimino)pyridine iron/cobalt catalysts, a significant goal has been to prepare well-defined alkyl complexes as it was viewed that these could serve as precursors for single component olefin polymerisation catalysts and also help shed some light on the nature of the propagating species (see Sect. 3.3). Hence the alkylation chemistry of dihalide-containing **5** and **6** has been thoroughly investigated.

For example, interaction of **5a** or **6a** with LiMe results in reduction to give the alkylated M(I) species [2,6-(ArN=CMe)₂C₅H₃N]MCH₃ [**23** M = Fe; **24** M = Co; Ar = 2,6-*i*-Pr₂C₆H₃] (Scheme 9). Alternatively, **23** or **24** can be prepared from the corresponding monovalent metal halide species [2,6-(ArN=CMe)₂C₅H₃N]MCl (**25** M = Fe; **26** M = Co) on reaction with LiMe [49, 108, 109, 123, 124, 125]. In a similar way, the Ph-ketimine cobalt(II) complex, [2,6-{ArN=CR}₂C₅H₃N]CoCl₂ (**6** R = Ph, Ar = 2,6-*i*-Pr₂C₆H₃), has been reduced to afford the cobalt(I) chloride [2,6-{(2,6-*i*-Pr₂C₆H₃)N=CPh}₂C₅H₃N]CoCl (**27**), which can then be alkylated with LiMe to afford the corresponding cobalt(I) methyl complex. Activation of the latter complex with Li[B(C₆F₅)₄] gave low activity ethylene polymerisation catalysts [49]. Grignard reagents have also been used to generate reduced alkylated species of the form [2,6-(ArN=CMe)₂C₅H₃N]CoMe (**24**) [126].



Scheme 8 Chain growth on zinc by **5a**/MAO and proposed mechanism for the process

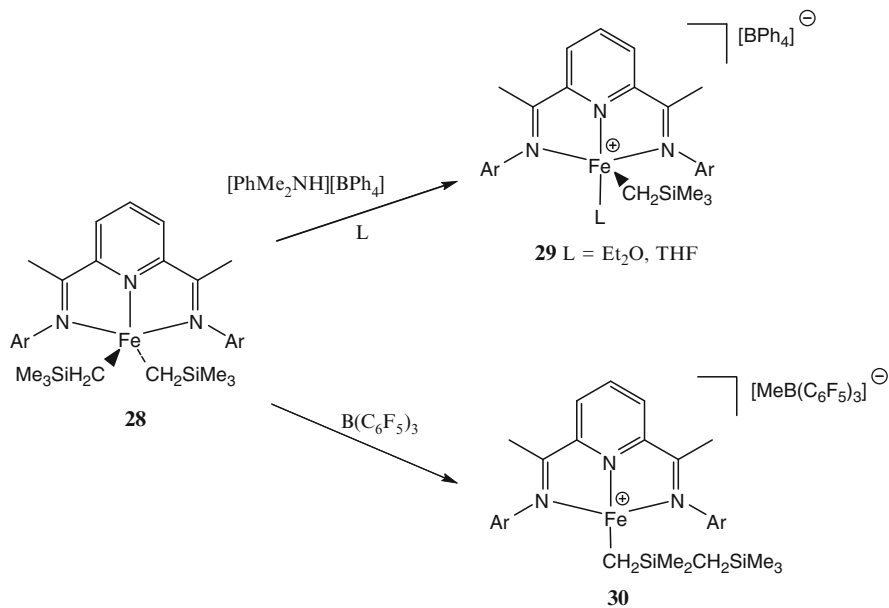


Scheme 9 Reactions of **5a** and **6a** with lithium alkyls (Ar = 2,6-*i*-Pr₂C₆H₃)

Unlike the reaction of **5a** with LiMe, treatment of **5a** with the more bulky LiCH₂SiMe₃ gave the crystallographically characterised dialkyl ferrous species [2,6-(ArN=CMe)₂C₅H₃N]Fe(CH₂SiMe₃)₂ (**28** Ar = 2,6-*i*-Pr₂C₆H₃) (Scheme 9) [125]. On the other hand, alkylation with LiCH₂CMe₃ or LiPh does result in reduction to give the monoalkylated derivatives [2,6-(ArN=CMe)₂C₅H₃N]FeR (**23'** R = CH₂CMe₃; **23''** R = Ph); the X-ray structure of **23'** reveals a distorted square planar geometry [127].

Whilst the nature of the active species for MAO-activated iron species continues to be the subject of some discussion (see Sect. 2.3), it has been shown that iron(II) alkyl cations can act as propagating species. For example, treatment of **28** with [PhMe₂NH][BPh₄] in the presence of diethylether or THF gives [{2,6-(ArN=CMe)₂C₅H₃N}M(CH₂SiMe₃)(L)] [BPh₄] (**29** L = Et₂O or THF, Ar = 2,6-*i*-Pr₂C₆H₃), respectively (Scheme 10); the base free species [{2,6-(ArN=CMe)₂C₅H₃N}M(CH₂SiMe₂CH₂SiMe₃)] [MeB(C₆F₅)₃] (**30** Ar = 2,6-*i*-Pr₂C₆H₃) is accessible on reaction of **28** with B(C₆F₅)₃. Although **29** gives very low activity for ethylene polymerisation, the base free species **30**, with the weaker coordinating anion, shows productivities approaching the MAO-activated catalyst [128]; the molecular structure of the cationic unit in **30** is shown in Fig. 10.

Gambarotta and Budzelaar have re-examined the reaction of **5a** with LiCH₂SiMe₃ under a number of different conditions. Reaction of in situ generated **5a** with two



Scheme 10 Dealkylation of **28** with $[PhMe_2NH][BPh_4]$ or $B(C_6F_5)_3$ ($Ar = 2,6\text{-}i\text{-}Pr_2C_6H_3$)

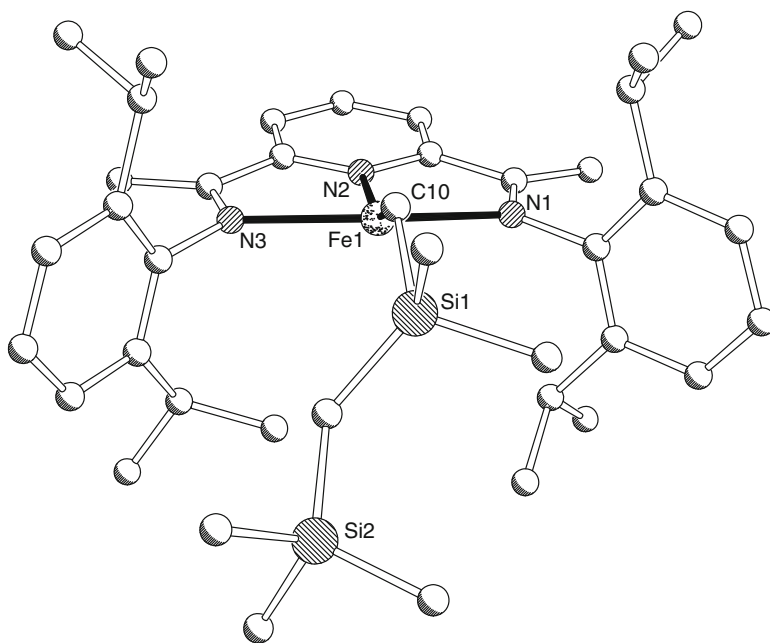


Fig. 10 Molecular structure of cationic unit in active catalyst **30** (data from [128], with permission of the copyright holders, was used to generate the figure)

equivalents of $\text{LiCH}_2\text{SiMe}_3$ gave as the major product the expected dialkyl complex **28** together with the minor products $\{[2,6-((2,6-i\text{-Pr}_2\text{C}_6\text{H}_3)\text{N}=\text{CMe})_2-2\text{-CH}_2\text{SiMe}_3\}\text{C}_5\text{H}_3\text{N}[\text{Fe}(\text{CH}_2\text{SiMe}_3)]$ (**31**) and $\{2-[(2,6-i\text{-Pr}_2\text{C}_6\text{H}_3)\text{N}=\text{CMe}]-6-[(2,6-i\text{-Pr}_2\text{C}_6\text{H}_3)\text{NCMe}(\text{CH}_2\text{SiMe}_3)]\text{C}_5\text{H}_3\text{N}[\text{Fe}(\text{CH}_2\text{SiMe}_3)]$ (**32**), for which alkylation had occurred at either the pyridine ring 2-position or the imine C atom, respectively. Interestingly, use of analytically pure **5a** yielded **28** together with a new alkylated product, namely $[2,6-[(2,6-i\text{-Pr}_2\text{C}_6\text{H}_3)\text{NC}=(\text{CH}_2)]_2\text{C}_5\text{H}_3\text{N}[\text{Fe}(\mu\text{-Cl})\text{Li}(\text{THF})_3]$ (**33**). Reductive coupling of the two ligand frameworks through the methyl carbon wings can occur during these alkylation reactions and indeed the dinuclear iron(I) complex **34** has been structurally characterised (Fig. 11). All the species (**43**, **31–34**) display, on activation with MAO, high activities for olefin polymerisation, forming two types of polymer, the natures of which are related to the formal oxidation state of the metal centre [129].

Dialkyl iron(II) species of the type **28**, can be more conveniently prepared from the reaction of **1** with the precursor complex $[\text{FeR}_2(\text{py})_2]$ ($\text{R} = \text{CH}_2\text{Ph}$, $\text{CH}_2\text{CMe}_2\text{Ph}$ and CH_2SiMe_3) [130]. However, extension of this approach to $[\text{Fe}(\text{CH}_2\text{CMe}_3)_2(\text{py})_2]$ gave a range of products including the result of neopentyl attack at the 4-position on the pyridyl unit of the ligand [127].

As with the free ligands, bis(imino)pyridine-containing iron and cobalt halides can undergo a range of chemistries at the ligand itself including deprotonation [129, 131]. In addition, several studies have involved the reduction of **5** or **6** in the presence of nitrogen as a means of generating dinitrogen-containing complexes [53, 132, 133, 134].

4 Supported Catalysts

The application of various inorganic and organic media as supports, through covalent and non-covalent interactions, for 2,6-bis(imino)pyridine iron and cobalt complexes (or ligands) has been extensively investigated. This has, in part, been stimulated by the desire to circumvent problems such as reactor fouling and high polymerisation exothermicities that have been encountered in continuous flow processes using these systems. Some examples in the area have also been included in a review article [135].

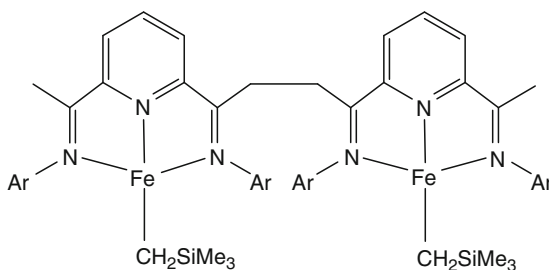
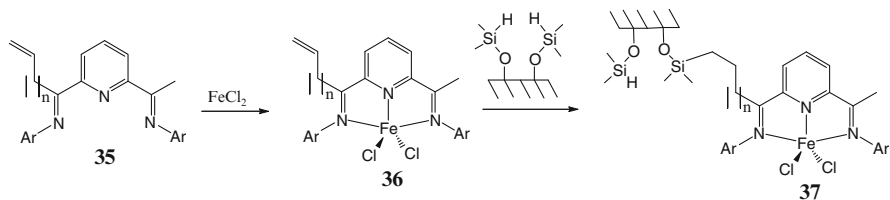


Fig. 11 Dinuclear iron complex **34** ($\text{Ar} = 2,6-i\text{-Pr}_2\text{C}_6\text{H}_3$)



Scheme 11 Immobilisation of **36** on silica via the imino-carbon group

Herrmann and co-workers reported the immobilisation of bis(imino)pyridine iron-type precatalysts on silica. By introduction of an alkenyl group onto the alkyl substituent of the imino carbon of the ligand, [2-{(2,6-*i*-Pr₂C₆H₃)N=CMe}, 6-{(2,6-*i*-Pr₂C₆H₃)N=C(CH₂)_nCH=CH₂}C₅H₃N] (**35**, *n* = 1–3) [136], the resultant iron dichloride complex [2-{(2,6-*i*-Pr₂C₆H₃)N=CMe}, 6-{(2,6-*i*-Pr₂C₆H₃)N=C(CH₂)_nCH=CH₂}C₅H₃N] FeCl₂ (**36**) could be readily tethered covalently to give **37** by hydrosilylation (Scheme 11). This family of heterogeneous systems is less active (with MAO) for ethylene polymerisation than its homogeneous analogues; notably the activity increases with tether chain length. High molecular weight fractions dominate with the highest molecular weight produced by the system with the shortest tethering chain. Self-immobilisation, by using **36** as a comonomer in the polymerisation, is also possible with the resultant polyethylene-supported catalysts being less active than the silica-supported systems.

The use of alkenyl-substituted *N*-aryl groups on the catalyst has been used by two groups as a potential means of anchoring the catalysts to a support [33, 124]. Thus *para*-allyl substituted precatalyst **5**, [2,6-{(4-(CH₂CHCH₂)-2,6-*i*-Pr₂C₆H₃)N=CMe}₂C₅H₃N] FeCl₂, can be co-polymerised with styrene in the presence of a radical initiator to afford polystyrene-supported iron catalysts **38** (Fig. 12); the MMAO-activated systems display high activities affording high molecular weight HDPE.

The 4-position on the central pyridyl ring has also been employed as the site for supporting iron catalysts [57, 58, 137]. For example, Kim et al. have used the 4-substituted *O*-allyl group in **1** (Ar = 2,6-Me₂C₆H₃) as a means of generating silica-supported iron and cobalt systems (**39**) (Scheme 12) [58]. On activation with MAO these systems exhibited about 100-fold lower activity than the analogous homogeneous catalysts. This lowering in activity has been attributed to either diffusion limitation of monomer into the interior pores of the supported catalyst or to the result of reduced active sites present in the heterogeneous variant. *O*-allyl substituted derivatives of **1** have also been supported on SBA-15 mesoporous material [67].

In addition to other polystyrene [138] and silica supports [139, 140, 141, 142, 143, 144], iron and cobalt precatalysts have been immobilised on calcosilicate [145], magnesium dichloride [146, 147, 148, 149], MCM-41 zeolite [150, 151], clay [152] and fluorotetrasilicic mica [153]. Supported systems have also been examined using alternative activators [154, 155, 156, 157, 158, 159]. For example, silica- and alumina-supported samples **5** have been activated with Al(*i*-Bu)₃ to afford highly active, thermally robust catalysts [154]. IR spectroscopy in DRIFT mode

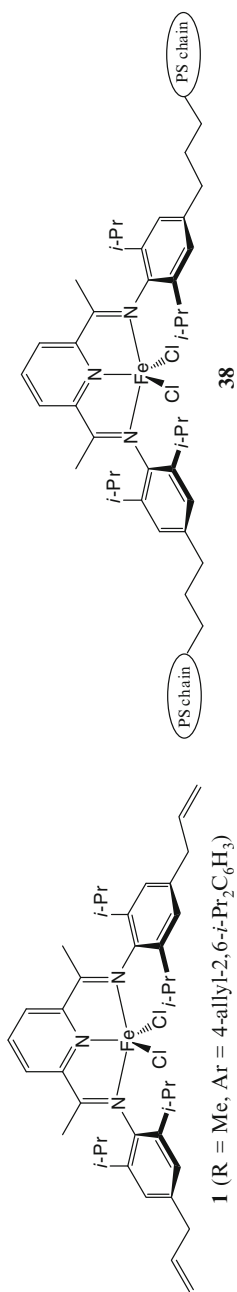
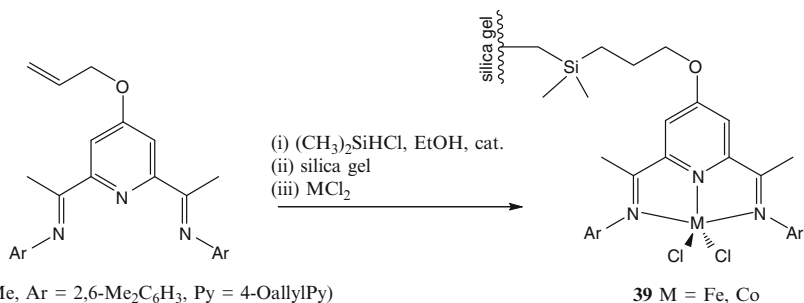


Fig. 12 *para*-Allyl substituted **1** and its polystyrene-immobilised **38**



Scheme 12 Use of 4-pyridyl position as means of supporting **1** to give **39**

indicates that only a few of the silica hydroxyl groups are used, leading to supported catalysts with low iron content. Higher iron content is achievable using alumina for which IR studies using CO as a probe indicate that there are two types of iron species present. A heterogenised co-catalyst (consisting of partially hydrolysed trimethylaluminium on silica gel) has also been used to activate iron catalysts [160].

Incorporation of iron catalysts into dendrimers has also proved an active research direction. For example, the *para*-allyl unsymmetrical bis(imino)pyridine ligand **2** (R = Me, Ar = 2,6-*i*-Pr₂C₆H₃, Ar' = 4-CH₂CHCH₂-2,6-*i*-Pr₂C₆H₂) can be reacted with tetra- and octasilanes, in the presence of [PtCl₆]²⁻, to afford the carbosilane ligands **40** and **41**, respectively (Fig. 13). Activation of the resultant peripherally bound iron dendrimers with MMAO affords active catalysts for ethylene polymerisation and, notably in the case of low Al/Fe molar ratios, they display much higher catalytic activities and produce much higher molecular weight polyethylenes than the corresponding mononuclear complex [161].

Attachment of dendritic wedges of either the carbosilane or benzylphenyl ether type to the *para*-hydroxy aryl site in [2,6-(ArN=CMe)₂C₃H₃N] (**1** R = Me, Ar = 2-Me-4-OHC₆H₃), has been shown to proceed in good yield [162]. Complexation with iron(II) chloride allows access to dendrimer-supported precatalyst **42** (Scheme 13). Using MAO as a co-catalyst, it was shown that **42** are active in the oligomerisation of ethylene; the activity of these new catalysts is not, however, related to the type of dendritic wedge employed.

5 Macrocyclic and Polymeric Derivatives

Prior to the development of polymerisation catalysts based on the bis(imino)pyridine framework, the bis(imino)pyridine moiety was widely incorporated into macrocycles [163, 164]. As an extension of this design strategy to polymerisation applications, several groups have been attempting to incorporate sterically bulky bis(arylimino)pyridine units into macrocycles. In a similar fashion, the introduction of the bis(imino)pyridine unit into polymeric chains in which polymerisation-active metal centres are bound has been the subject of study.

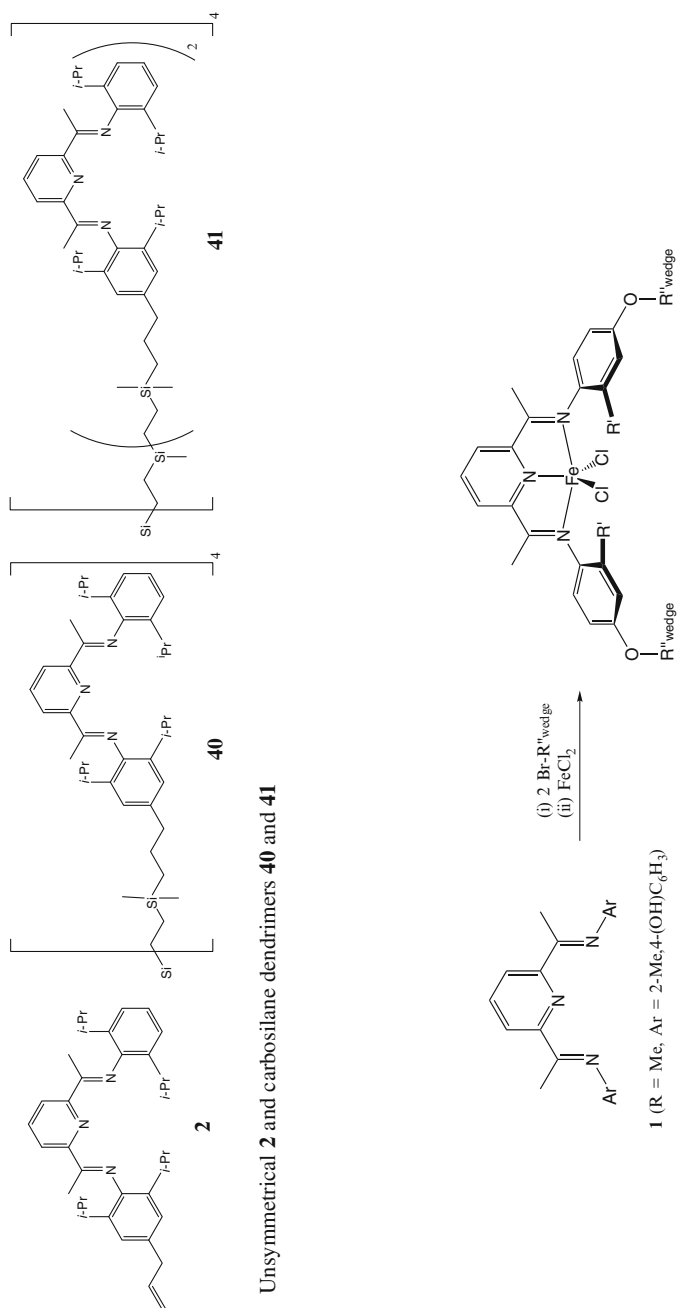
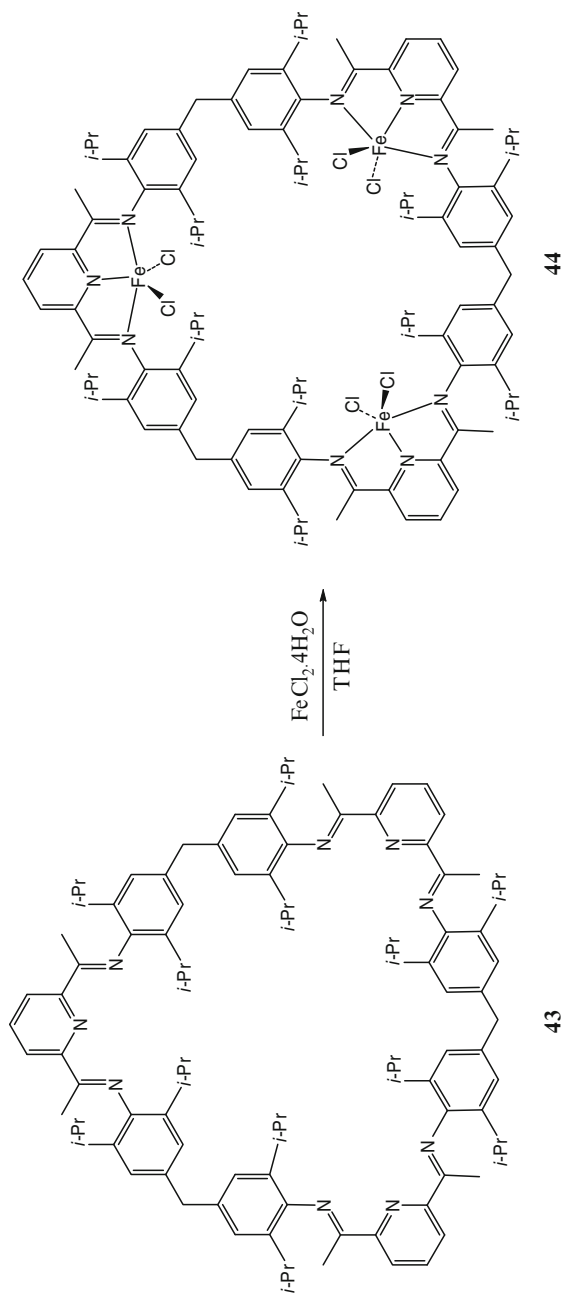


Fig. 13 Unsymmetrical **2** and carbosilane dendrimers **40** and **41**

Scheme 13 Use of *para*-hydroxy **1** as a means of linking to dendritic wedges and complexation with iron(II) chloride

**Scheme 14** Use of macrocycle **43** to support the formation of triiron **44**

The sterically encumbered macrocyclic ligand **43** has been reported to be formed on reaction of 2,6-diacetylpyridine with the diamine [(3,5-*i*-Pr₂C₆H₂-4-NH₂)₂CH₂] under high-dilution conditions (Scheme 14) [165]. Interaction of **43** with iron(II) chloride tetrahydrate in THF gives the trinuclear macrocyclic complex **44** in high yield. High activities for the polymerisation of ethylene have been reported on activation of **43** with MAO; notably the lifetime of the catalyst is reported to be enhanced when compared with its mononuclear analogue **5**/MAO.

In contrast, the related diamines **45** and **46** [cf. (3,5-*i*-Pr₂C₆H₂-4-NH₂)₂CH₂ above] give, on treatment with 2,6-diacetylpyridine, oligomeric polyimines that can be readily complexed with iron dichloride to afford **47** and **48**, respectively (Fig. 14). Notably, on activation with MAO, **47** and **48** are active catalysts for ethylene polymerisation and indeed perform more efficiently at elevated temperatures than those of the original bis(imino)pyridine iron precatalyst **5** [166].

Polymeric frameworks incorporating the bis(imino)pyridine motif and units derived from *ortho*-, *meta*- or *para*-phenylenediamines can be prepared and used to generate metallopolymers (**49**, **50** and **51**) containing varying levels of iron(II) chloride (Fig. 15). Increased accessibility of the coordination sites in the “*meta*” system has been revealed from calculations, consistent with the greater iron content observed experimentally. Following activation with MAO, observed activities and polymer properties are found to be highly dependent upon the ligand backbone [167].

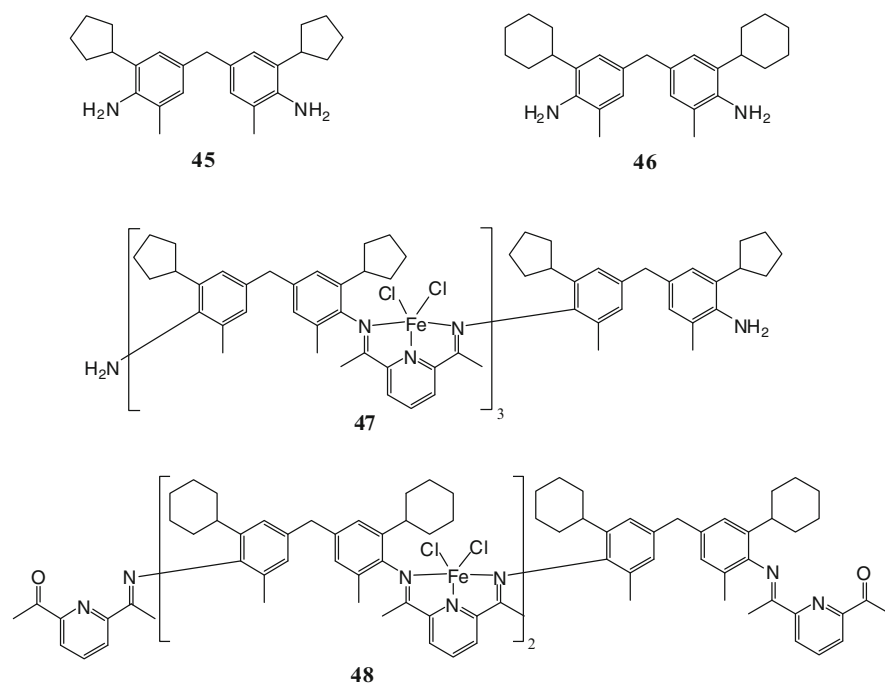


Fig. 14 Diamines **45** and **46** used to make polymeric iron-containing **47** and **48**

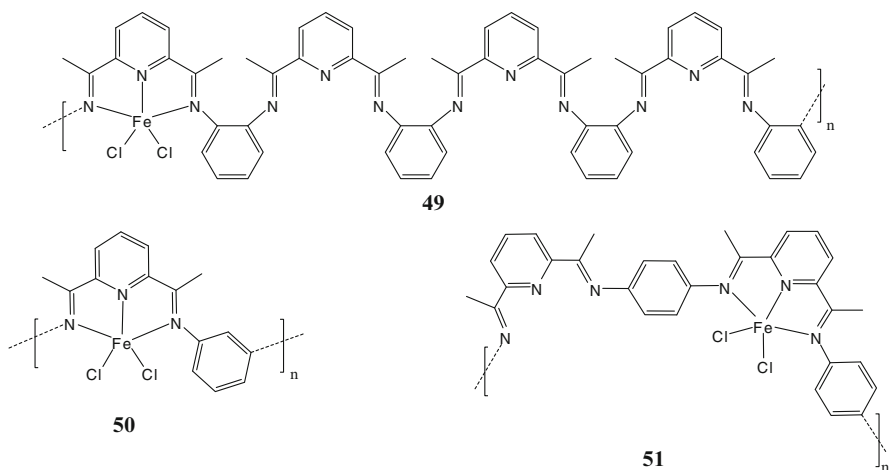


Fig. 15 Polymeric **49**, **50** and **51** differing in iron content

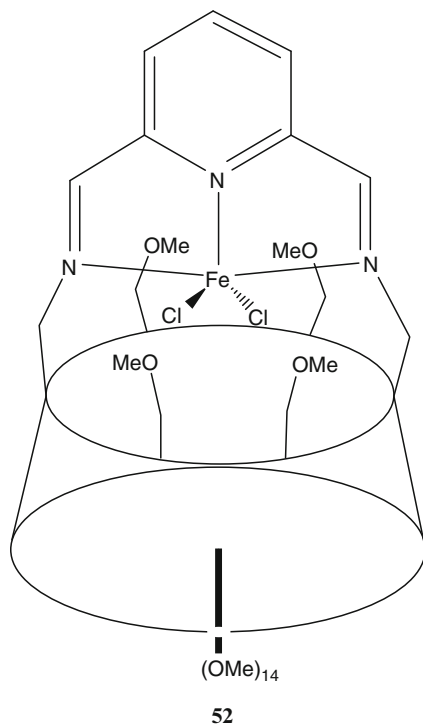


Fig. 16 Cyclodextrin-supported iron precatalyst **52**

In addition, cyclodextrins incorporating a 2,6-bis(imino)pyridine unit have been used to support active iron polymerisation catalysts. Using the β -cyclodextrin-based system **52**, in the presence of a large excess of MAO, ethylene can be converted into HDPE (Fig. 16). Only low activities are, however, observed, which

has been attributed to an over-protective cyclodextrin, which tightly wraps around the metal centre thereby inhibiting any potential chain growth [168].

6 Tandem Catalysis

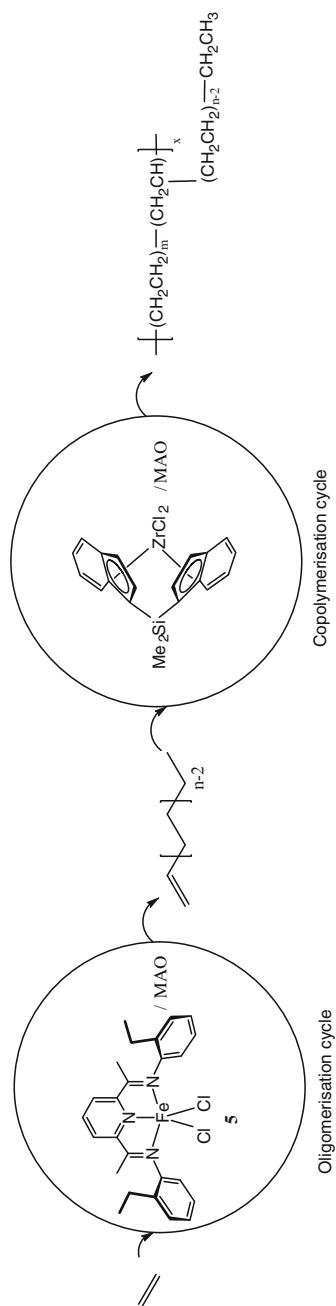
The use of two or more different catalysts in the same reactor, sometimes known as *in situ* reactor blending or *tandem catalysis*, has been widely employed industrially as means of controlling the properties of a polyolefin (e.g. molecular weight and the molecular weight distribution). Recent years have seen a variety of reports emerge on the use of bis(imino)pyridine iron/cobalt systems as one component of the process [169, 170, 171, 172, 173, 174, 175, 176, 177, 178, 179].

By combining **5a**/MAO with an α -diimine nickel(II) halide/MAO catalyst, access to blended polymers consisting of a mixture of linear and branched polyethylenes are obtainable from a single ethylene feed [169]. On the other hand, use of **5a**/MAO with a metallocene can give rise to blends of polyethylenes with different molecular weights [169]. When an iron catalyst that selectively forms α -olefins is combined with a metallocene copolymerisation catalyst, LLDPE and in some cases ULDPE can be obtained from a single ethylene feedstock [172, 173, 174, 175, 176]. For example, using $[2,6-(\text{ArN}=\text{CMe})_2\text{C}_5\text{H}_3\text{N}]\text{FeCl}_2$ (**5** Ar = 2-EtC₆H₄)/MAO in combination with $[\text{Me}_2\text{Si}(\text{Ind})_2]\text{ZrCl}_2/\text{MAO}$ or $[\text{Et}(\text{Ind})_2]\text{ZrCl}_2/\text{MAO}$ in the same reactor affords branched polyethylenes with ethyl, butyl, and longer chain branches (Scheme 15) [174]. Bis(imino)pyridine cobalt catalysts have also been employed in tandem polymerisations to generate LLDPE [177].

Heterogeneous tandem catalysis involving at least one of the components being supported has also been reported [178, 179]. For example, calcosilicate has recently been used as an effective carrier for simultaneous immobilisation of a dual-functional system based on a bis(imino)pyridine iron compound and a zirconocene to form a heterogeneous catalyst precursor. On activation with triethylaluminium, ethylene was converted to LLDPE; the layered structure of the calcosilicate was used to account for the improved thermal stability and higher molecular weights of the LLDPE formed [179].

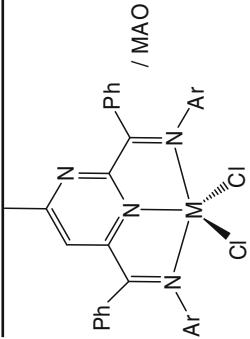
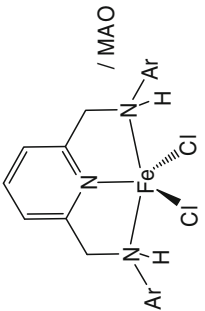
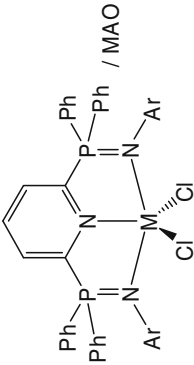
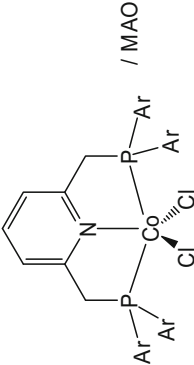
7 Alternative Iron and Cobalt Catalysts

While the 2,6-bis(imino)pyridine ligand frame has continued to lead the way, the past 10 years has also seen the development of alternative ligand sets that can act as compatible supports for iron and cobalt ethylene oligomerisation/polymerisation catalysts (Table 4) [46, 50, 181, 182, 183, 184, 185, 186, 187, 188, 189, 190, 191, 192, 193, 194, 195, 196, 197, 198, 199, 200, 201, 202, 203, 204, 205, 206, 207, 208, 209]; active catalysts based on bimetallic iron and cobalt precatalysts have also started to emerge (Table 5) [54, 210, 211, 212, 213, 214, 215]. In the main, these systems show lower activities than the prototype bis(imino)pyridine-based catalysts, although several of these systems have significantly started to approach their catalytic performances (e.g. **65**/MAO [46, 188], **69**/MAO [191, 192, 193], **70**/MAO [194], **71**/MMAO [195]).

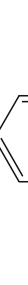

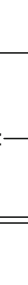


Scheme 15 Use of **5**/MAO in tandem catalysis to form LLDPE

Table 4 Selected non-bis(imino)pyridine iron and cobalt precatalyst/activator combinations for ethylene oligomerisation/polymerisation

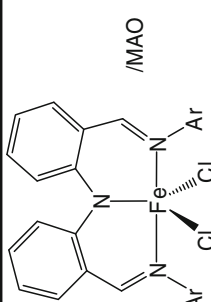
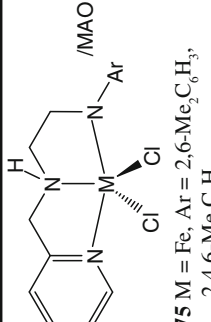
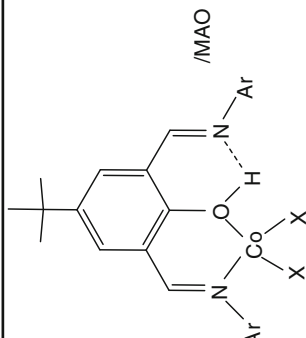
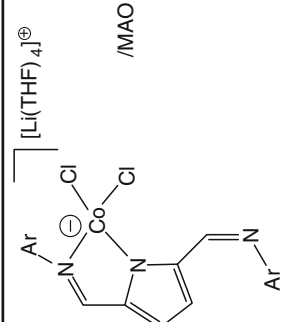
Precatalyst/activator	Product (oligomer/polymer)	References	Precatalyst/activator	Product (oligomer/polymer)	References
 <p>55 M = Fe, Ar = 2,6-Me₂C₆H₃ or 2,4,6-Me₃C₆H₂ 56 M = Co, Ar = 2,4,6-Me₃C₆H₂</p>	Polymer	[50]	 <p>57 Ar = 2,6-<i>i</i>-Pr₂C₆H₃</p>	Polymer	[181]
 <p>58 M = Fe, Ar = 2,6-<i>i</i>-Pr₂C₆H₃ or 2,4,6-Me₃C₆H₂ 59 M = Co, Ar = 2,6-<i>i</i>-Pr₂C₆H₃ or 2,4,6-Me₃C₆H₂</p>	Polymer	[182, 183]	 <p>60 Ar = 2-MeC₆H₄, 2,4,6-Me₃C₆H₂</p>	Polymer	[184]

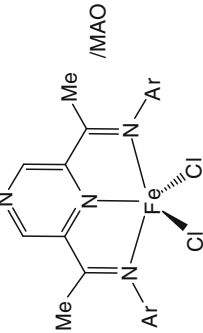
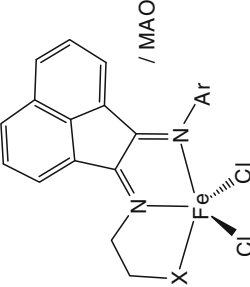
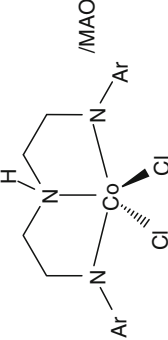
(continued)

[189]	Polymer (66); Oligomer (67)		[190]	Polymer
[191, 193, 194]	Short chain α -olefins		[194]	Short chain α -olefins (mainly 1-butene and 1-hexene)
[195, 196, 198]	Low molecular weight polymer (71); short chain oligomer (72)		[199]	Polymer

(continued)

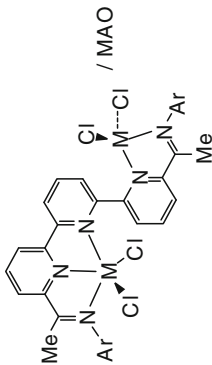
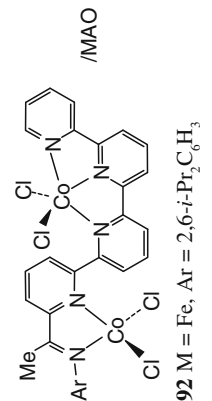
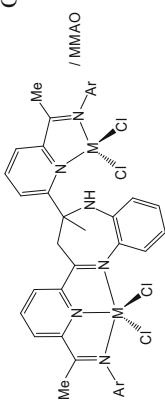
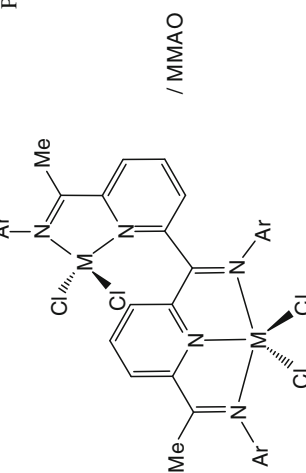
Table 4 (continued)

Precatalyst/activator	Product (oligomer/polymer)	References	Precatalyst/activator	Product (oligomer/polymer)	References
 74 Ar = 2,6-Me ₂ C ₆ H ₃ , 2,6- <i>i</i> -Pr ₂ C ₆ H ₃	Polymer	[200]	 75 M = Fe, Ar = 2,6-Me ₂ C ₆ H ₃ , 2,4,6-Me ₃ C ₆ H ₂ 76 M = Co, Ar = 2,6-Me ₂ C ₆ H ₃ , 2,4,6-Me ₃ C ₆ H ₂	Oligomer	[201]
 77 Ar = 2,6-Me ₂ C ₆ H ₃ , 2,6- <i>i</i> -Pr ₂ C ₆ H ₃	Oligomer	[201]	 78 Ar = 2,6- <i>i</i> -Pr ₂ C ₆ H ₃	Oligomer (linear and branched products)	[203]

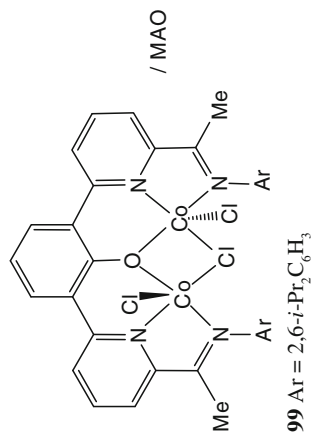
[204, 205]	Polymer	 <p>79 M = Fe, Ar = 2,6-Me₂C₆H₃, 2,6-<i>i</i>-Pr₂C₆H₃</p>	[203]	Polymer and oligomer (80); Oligomer (81)
[207]	Oligomer	 <p>80 M = Fe, Ar = 2,6-<i>i</i>-Pr₂C₆H₃, 2,4,6-Me₃C₆H₂</p> <p>81 M = Co, Ar = 2,6-<i>i</i>-Pr₂C₆H₃, 2,4,6-Me₃C₆H₂</p>	[208]	Polymer
[201]	Oligomer	 <p>89 Ar = 2,6-Me₂C₆H₃, 2,4,6-Me₃C₆H₂</p>		
		<p>83 X = 2-pyridyl, Ar = 2,6-Me₂C₆H₃</p> <p>84 X = NMe₂, Ar = 2,6-Me₂C₆H₃</p> <p>85 X = PPh₂, Ar = 2,6-Me₂C₆H₃</p> <p>86 X = S(3,5-Me₂C₆H₃)₂, Ar = 2,6-Me₂C₆H₃</p>		
		<p>87 M = Fe, X = N or P</p> <p>88 M = Co, X = N or P</p>		

(continued)

Table 5 Selected non-bis(imino)pyridine diiron and dicobalt precatalyst/activator combinations for ethylene oligomerisation/polymerization

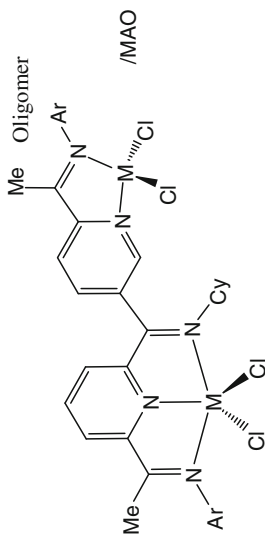
Precatalyst/activator	Product (oligomer/polymer)	References	Precatalyst/activator	Product (oligomer/polymer)	Ref.
 90 M = Fe, Ar = 2,6- <i>i</i> -Pr ₂ C ₆ H ₃ 91 M = Co, Ar = 2,6- <i>i</i> -Pr ₂ C ₆ H ₃	Oligomer (α-olefins)	210, 211	 92 M = Fe, Ar = 2,6- <i>i</i> -Pr ₂ C ₆ H ₃	Oligomers	212
 93 M = Fe, Ar = 2,6- <i>i</i> -Pr ₂ C ₆ H ₃ 94 M = Co, Ar = 2,6- <i>i</i> -Pr ₂ C ₆ H ₃	Oligomer/polymer	212, 213	 95 M = Fe, Ar = 2,4,6-Me ₃ C ₆ H ₃ 96 M = Co, Ar = 2,4,6-Me ₃ C ₆ H ₃	Polymer	54

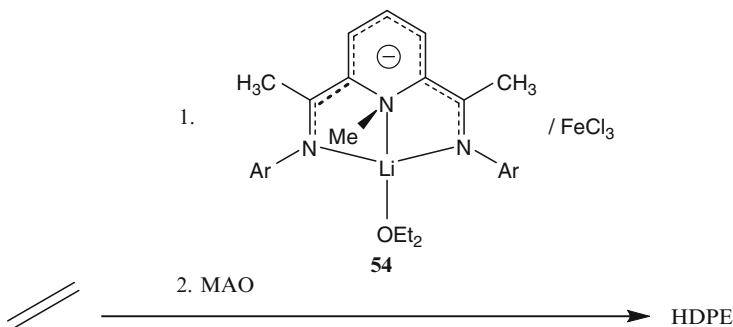
Oligomer 216



214

Oligomer





Scheme 16 Use of **54**/FeCl₃ and MAO as a highly active catalyst system

Furthermore, a number of non-halide-containing precatalysts have been developed that either contain a bis(imino)pyridine chelate or possess one that is generated during the activation process. For example, [Fe(acac)₃] in the presence of **1** (R = Me, Ar = 2,6-*i*-Pr₂C₆H₃) and MAO promotes the formation of HDPE [216]. Similarly, the well-defined cationic iron-acac complex [{2,6-{(2,6-*i*-Pr₂C₆H₃N=CMe)₂C₅H₃N}Fe(acac)](SbF₆) (**53**) on activation with MAO forms polyethylene [217]. *N*-Methylated anionic forms of bis(imino)pyridine **1** such as, [2,6-{(2,6-*i*-Pr₂C₆H₃)NCMe)₂C₅H₃NMe]Li(OEt₂) (**54**), in combination with a metal halide and MAO have also been shown to generate an active catalyst. For example, the treatment of **54** with successively [FeCl₃] and MAO affords an active catalyst that polymerises ethylene with an activity comparable with **5a**/MAO (Scheme 16) [67].

8 Conclusions

The discovery in 1998 of cobalt- and iron-based complexes bearing sterically bulky tridentate 2,6-bis(imino)pyridine ligands that can act as highly active catalysts for the conversion of ethylene to high density polyethylene triggered a remarkable phase in the development of late transition metal polymerisation catalysis. In this chapter we have tried to highlight some of the key advances in the field that have appeared in the literature in the intervening years. While considerable research time has been spent on elaborating the 2,6-bis(imino)pyridine ligand motif and new structure–activity correlations have become apparent, significant breakthroughs have been disclosed regarding the role of MAO. These in turn have shed some light on the active species and intricacies of the polymerisation/oligomerisation pathway. The susceptibility of the precursor iron(II) and cobalt(II) halide species to redox changes during alkylation, coupled with some conflicting spectroscopic studies have raised some intriguing questions as to the oxidation state of the active catalyst in a MAO-activated system. The potential for electron transfer processes to occur

within the metal-ligand unit of the active catalysts no doubt further clouds a precise assignment of oxidation state. The amenability of these systems to heterogenisation along with their compatibility to tandem catalysis/reactor blending has signposted further industrial possibilities of these systems. Of considerable industrial significance is the discovery of highly efficient reversible chain transfer of growing polymer chains to zinc, which forms the basis of potentially commercially significant chain shuttling processes. While the main emphasis has been placed on the development of the bis(imino)pyridine ligand framework, new ligand frames capable of supporting iron and cobalt catalyst have now come to the fore. By a range of inventive ligand design strategies, novel precatalysts are being developed that can incorporate not only one but two polymerisation-active metal centres.

References

1. Small BL, Brookhart M (1998) *J Am Chem Soc* 120:7143
2. Small BL, Brookhart M, Bennett AMA (1998) *J Am Chem Soc* 120:4049
3. Bennett AMA (EI Du Pont de Nemours and Co, USA) (1998) *PCT Int. Appl. WO 9827124* [(1998) *Chem Abstr* 129:122973x]
4. Bennett AMA (1999) *CHEMTECH* 29:24–28
5. Britovsek GJP, Gibson VC, Kimberley BS, Maddox PJ, McTavish SJ, Solan GA, White AJP, Williams DJ (1998) *Chem Commun* 1998:849
6. Britovsek GJP, Bruce M, Gibson VC, Kimberley BS, Maddox PJ, Mastroianni S, McTavish SJ, Redshaw C, Solan GA, Strömberg S, White AJP, Williams DJ (1999) *J Am Chem Soc* 121:8728
7. Britovsek GJP, Dorer BA, Gibson VC, Kimberley BS, Solan GA (1999) (BP Chemicals Ltd, UK) *PCT Int Appl WO 9912981* [*Chem Abstr* 130:252793]
8. Gibson VC, Spitzmesser SK (2003) *Chem Rev* 103:283
9. Britovsek GJP, Gibson VC, Wass DF (1999) *Angew Chem Int Ed* 38:428
10. Ittel SD, Johnson LK, Brookhart M (2000) *Chem Rev* 100:1169
11. Mecking S (2001) *Angew Chem Int Ed* 40:534
12. Park S, Han Y, Kim SK, Lee J, Kim HK, Do Y (2004) *J Organomet Chem* 689:4263
13. Gibson VC, Redshaw C, Solan GA (2007) *Chem Rev* 107:1745
14. Bianchini C, Giambastiani G, Rios GI, Mantovani G, Meli A, Segarra AM (2006) *Coord Chem Rev* 250:1391
15. Britovsek GJP, Mastroianni S, Solan GA, Baugh SPD, Redshaw C, Gibson VC, White AJP, Williams DJ, Elsegood MRJ (2000) *Chem Eur J* 6:2221
16. Zhang Z, Chen S, Zhang X, Li H, Ke Y, Lu Y, Hu Y (2005) *J Mol Catal A: Chem* 230:1
17. Granifo J, Bird SJ, Orrell KG, Osborne AG, Sik V (1999) *Inorg Chim Acta* 295:56
18. Zhang Z, Zou J, Cui N, Ke Y, Hu Y (2004) *J Mol Catal A: Chem* 219:249
19. Chen Y, Qian C, Sun J (2003) *Organometallics* 22:1231
20. Schmidt R, Hammon U, Gottfried S, Welch MB, Alt HG (2003) *J Appl Polym Sci* 88:476
21. Schmidt R, Welch MB, Knudsen RD, Gottfried S, Alt HG (2004) *J Mol Catal A: Chem* 219:9
22. Esteruelas MA, Lopez AM, Mendez L, Oliván M, Onate E (2003) *Organometallics* 22:395
23. Tellmann KP, Gibson VC, White AJP, Williams DJ (2005) *Organometallics* 24:280
24. Cetinkaya B, Cetinkaya E, Brookhart M, White PS (1999) *J Mol Catal A: Chem* 142:101
25. Bluhm ME, Folli C, Doring M (2004) *J Mol Catal A: Chem* 212:13
26. Kim I, Han BH, Ha YS, Ha CS, Park DW (2004) *Catal Today* 93–95:281
27. Schmidt R, Welch MB, Knudsen RD, Gottfried S, Alt HG (2004) *J Mol Catal A: Chem* 222:9

28. Schmidt R, Welch MB, Palackal SJ, Alt HG (2002) *J Mol Catal A: Chem* 179:155
29. Gibson VC, Long NJ, Oxford PJ, White AJP, Williams DJ (2006) *Organometallics* 25:1932
30. Paulino IS, Schuchardt U (2004) *J Mol Catal A: Chem* 211:55
31. Ionkin AS, Marshall WJ, Adelman DJ, Fones BB, Fish BM, Schiffhauer MF (2006) *Organometallics* 25:2978
32. Liu JY, Zheng Y, Li YG, Pan L, Li YS, Hu NH (2005) *J Organomet Chem* 690:1233
33. Liu C, Jin G (2002) *New J Chem* 26:1485
34. Ionkin AS, Marshall WJ, Adelman DJ, Shoe AL, Spence RE, Xie T (2006) *J Polym Sci A: Polym Chem* 44:2615
35. Adelman DJ, Ionkin SA (EI Du Pont de Nemours and Co, USA) (2007) *PCT Int. Appl WO* 2007021955
36. Small BL, Brookhart M (1999) *Macromolecules* 32:2120
37. Pelascini F, Peruch F, Lutz PJ, Wesolek M, Kress J (2005) *Eur Polym J* 41:1288
38. Chen J, Huang Y, Li Z, Zhang Z, Wei C, Lan T, Zhang W (2006) *J Mol Catal A: Chem* 259:133
39. Ivanchev SS, Yakimansky AV, Rogozin DG (2004) *Polymer* 45:6453
40. Oleinik II, Oleinik IV, Abdrakhmanov IB, Ivanchev SS, Tolstikov GA (2004) *Russ J Gen Chem* 74:1575
41. Ivanchev SS, Tolstikov GA, Badaev VK, Oleinik II, Ivancheva NI, Rogozin DG, Oleinik IV, Myakin SV (2004) *Kinet Catal* 45:176
42. Oleinik II, Oleinik IV, Abdrakhmanov IB, Ivanchev SS, Tolstikov GA (2004) *Russ J Gen Chem* 74:1423
43. Ma Z, Qui J, Xu D, Hu Y (2001) *Macromol Rapid Commun* 22:1280
44. Chen Y, Chen R, Qian C, Dong X, Sun J (2003) *Organometallics* 22:4312
45. Abu-Surrah AS, Lappalainen K, Piironen P, Lehmus P, Repo T, Leskelä M (2002) *J Organomet Chem* 648:55
46. Kaul FAR, Puchta GT, Frey GD, Herdtweck E, Herrmann WA (2007) *Organometallics* 26:988
47. Small BL, Marcucci AJ (2001) *Organometallics* 20:5738
48. Ionkin AS, Marshall WJ, Adelman DJ, Fones BB, Fish BM, Schiffhauer MF, Soper PD, Waterland RL, Spence RE, Xie T (2007) *J Polym Sci Part A: Polym Chem* 46:585
49. Kleigrewe N, Steffen W, Blömker T, Kehr G, Fröhlich R, Wibbeling B, Erker G, Wasilke JC, Wu G, Bazan GC (2005) *J Am Chem Soc* 127:13955
50. Britovsek GJP, Gibson VC, Hoarau OD, Spitzmesser SK, White AJP, Williams DJ (2003) *Inorg Chem* 42:3454
51. McTavish S, Britovsek GJP, Smit TM, Gibson VC, White AJP, Williams DJ (2007) *J Mol Catal A: Chem* 261:293
52. Smit T, Tomov AK, Gibson VC, White AJP, Williams DJ (2004) *Inorg Chem* 43:6511
53. Archer AM, Bouwkamp MW, Cortez MP, Lobkovsky E, Chirik PJ (2006) *Organometallics* 25:4269
54. Barbaro P, Bianchini C, Giambastiani G, Rioja IG, Meli A, Oberhauser W, Segarra AM, Sorace L, Toti (2007) *Organometallics* 26:4639
55. Nüchel S, Burger P (2001) *Organometallics* 20:4345
56. Pelascini F, Wesolek M, Peruch F, Lutz PJ (2006) *Eur J Inorg Chem* 2006:4309
57. Seitz M, Milius W, Alt HG (2007) *J Mol Catal A: Chem* 261:246
58. Kim I, Heui Han B, Ha C-S, Kim J-K, Suh H (2003) *Macromolecules* 36:6689
59. Ionkin AS, Marshall WJ, Adelman DJ, Fones BB, Spence RE, Xie T (2008) *Organometallics* 27:1147
60. Bianchini C, Giambastiani G, Guerrero IR, Meli A, Passaglia E, Gragnoli T (2004) *Organometallics* 23:6087
61. Daisuke T, Kouhei A, Kohtaro O (2005) *Bull Chem Soc Jpn* 87:1868
62. Small BL (2003) *Organometallics* 22:3178
63. Kim II, Hwang J-M, Lee JK, Ha CS, Woo SI (2003) *Macromol Rapid Commun* 24:508
64. Edwards DA, Edwards SD, Pringle TJ, Thornton P (1992) 11: 1569
65. Lappalainen K, Yliheikkilä K, Abu-Surrah AS, Polamo M, Lekelläe M, Repo T (2005) *Zeit Anorg Allg Chem* 631:763

66. Knijnenburg Q, Hetterschied D, Kooistra TM, Budzelaar PHM (2004) *Eur J Inorg Chem* 2004:1204
67. Kim II, Byeong H, Kim JS, Ha C-S (2005) *Catal Lett* 101:249
68. Qian C, Gao F, Chen Y, Gao L (2003) *Synlett* 2003:1419
69. Campora J, Perez CM, Rodriguez-Delgado A, Naz AM, Palma P, Alvarez E (2007) *Organometallics* 26:1104
70. Small BL, Carney MJ, Holman DM, O'Rourke CE, Halfen JA (2004) *Macromolecules* 37:4375
71. Bianchini C, Mantovani G, Meli A, Migliacci F, Zanobini F, Laschi F, Sommazzi A (2003) *Eur J Inorg Chem* 2003:1620
72. Nakayama Y, Sogo K, Yasuda H, Shiono T (2005) *J Polym Sci A: Pol Chem* 43:3368
73. Lappalainen K, Yliheikkilä K, Abu-Surrah AS, Polamo M, Leskelä M Repo T (2005) *Z Anorg Allg Chem* 631:763
74. Yuan-Biao H, Xiu-Ling M, Si-Ning Z, Jian-Xin C, Chun-Xia W (2006) *Acta Crystallogr Sect E* 62:o3044
75. Vance AL, Alcock NW, Heppert JA, Busch DH (1998) *Inorg Chem* 37:6912
76. Menten A, Fawcett J, Kemmitt RDW (2001) *Acta Crystallogr Sect E* 57:o424
77. Meehan PR, Alyea EC, Ferguson G (1997) *Acta Crystallogr Sect C* C53:888
78. Agrifoglio G, Reyes J, Atencio R, Briceno A (2008) *Acta Crystallogr Sect E* 64:28
79. Moody LS
80. Sugiyama H, Korobkov I, Gambarotta S, Möller A, Budzelaar PHM (2004) *Inorg Chem* 43:5771
81. Sugiyama H, Gambarotta S, Yap GPA, Wilson DR, Thiele SK-H (2004) *Organometallics* 23:5054
82. Clentsmith GKB, Gibson VC, Hitchcock PB, Kimberley BS, Rees CW (2002) *Chem Commun* 2002:1498
83. Blackmore IJ, Gibson VC, Hitchcock PB, Rees CW, Williams DJ, White AJP (2005) *J Am Chem Soc* 127:601
84. Khorobkov I, Gambarotta S, Yap GPA (2002) *Organometallics* 21:3088
85. Milione S, Cavallo G, Tedesco C, Grassi A (2002) *J Chem Soc Dalton Trans* 2002:1839
86. Bruce M, Gibson VC, Redshaw C, Solan GA, White AJP, Williams DJ (1998) *Chem Commun* 1998:2523
87. Knijnenburg Q, Smits JMM, Budzelaar PHM (2004) *CR Chim* 7:865
88. Knijnenburg Q, Smits JMM, Budzelaar PHM (2006) *Organometallics* 25:1036
89. Britovsek GJP, Clentsmith GKB, Gibson VC, Goodgame DML, McTavish SJ, Pankhurst QA (2002) *Catal Commun* 3:207
90. Enright D, Gambarotta S, Yap PA, Budzelaar PHM (2002) *Angew Chem Int Ed* 41:3873
91. Knijnenburg Q, Gambarotta S, Budzelaar PHM (2006) *Dalton Trans* 2006:5442
92. Kooistra TM, Hekking KFW, Knijnenburg Q, de Bruin B, Budzelaar PHM, de Gelder R, Smits JMM, Gal AW (2003) *Eur J Inorg Chem* 2003:648
93. Britovsek GJP, Gibson VC, Kimberley BS, Mastroianni S, Redshaw C, Solan GA, White AJP (2001) *J Chem Soc Dalton Trans* 2001:94, 1639
94. Moody LS, Mackenzie PB, Killan CM, Lavoie GG, Pansik Jr JA, Barrett AGM, Smith TW, Pearson JC (Eastman Chemical Company) (2000) WO0050470 [Chem Abstr 133:208316]
95. Amort C, Malaun M, Krajete A, Kopačka H, Wurst K, Christ M, Lilge D, Kristen MO (2002) *Appl Organometal Chem* 16:506
96. Ma Z, Sun W-H, Li Z-L, Shao C-X, Hu Y-L, Li X-H (2002) *Polym Int* 51:994
97. Brookhart MS, Small BL (1998) (Dupont/UNC) WO 9830612 [Chem Abstr 129:149375r]
98. Pellecchia C, Mazzeo M, Pappalardo D (1998) *Macromol Rapid Commun* 19:651
99. Babik ST, Fink G (2002) *J Mol Catal A: Chem* 188:245
100. Abu-Surrah AS, Qaroush AK (2007) *Eur Polym J* 43:2967
101. Castro PM, Lappalainen K, Ahlgren M, Leskela M, Repo T (2003) *J Polym Sci Part A: Polym Chem* 41:1380

102. Talsi EP, Babushkin DE, Semikolenova NV, Zudin VN, Panchenko VN, Zakharov VA (2001) *Macromol Chem Phys* 202:2046
103. Bryliakov KP, Semikolenova NV, Zakharov VA, Talsi EP (2004) *Organometallics* 23:5375
104. Bryliakov KP, Semikolenova NV, Zudin VN, Zakharov VA, Talsi EP (2004) *Catal Commun* 5:45
105. Talsi EP, Bryliakov KP, Semikolenova NV, Zakharov VA, Bochmann M (2007) *Kinet Catal* 48:490
106. Castro PM, Lahtinen P, Axenov K, Viidanoja J, Kotiaho T, Leskela M, Repo T (2005) *Organometallics* 24:3664
107. Schmidt R, Das PK, Welch MB, Knudsen RD (2004) *J Mol Catal A: Chem* 222:27
108. Kooistra TM, Knijnenburg Q, Smits JMM, Horton AD, Budzelaar PHM, Gal AW (2001) *Angew Chem Int Ed* 40:4719
109. Humphries MJ, Tellmann KP, Gibson VC, White AJP, Williams DJ (2005) *Organometallics* 24:2039
110. Cossee P (1964) *J Catal* 3:80
111. Tellmann KP, Humphries MJ, Rzepa HS, Gibson VC (2004) *Organometallics* 23:5503
112. Griffiths EAH, Britovsek GJP, Gibson VC, Gould IR (1999) *Chem Commun* 1999:1333
113. Deng L, Margl P, Ziegler T (1999) *J Am Chem Soc* 121:6479
114. Margl P, Deng L, Ziegler T (1999) *Organometallics* 18:5701
115. Khoroshun DV, Musaev DG, Vreven T, Morokuma K (2001) *Organometallics* 20:2007
116. Kumar KR, Sivaram S (2000) *Macromol Chem Phys* 201:1513
117. Radhakrishnan K, Cramail H, Deffieux A, Francois P, Momtaz A (2003) *Macromol Rapid Commun* 24:251
118. Wang Q, Yang H, Fan Z (2002) *Macromol Rapid Commun* 23:639
119. Semikolenova NV, Zakharov VA, Talsi EP, Babushkin DE, Sobolev AP, Echevskaya LG, Khusniyarov MM (2002) *J Mol Catal A: Chem* 182:283
120. Britovsek GJP, Cohen SA, Gibson VC, van Meurs M (2004) *J Am Chem Soc* 126:10701
121. Britovsek GJP, Cohen SA, Gibson VC, Maddox PJ, Van Meurs M (2002) *Angew Chem Int Ed* 41:489
122. Van Meurs M, Britovsek GJP, Gibson VC, Cohen SA (2005) *J Am Chem Soc* 127:9913
123. Scott J, Gambarotta S, Korobkov I, Budzelaar PHM (2005) *Organometallics* 24:6298
124. Steffen W, Blömker T, Kleigrewe N, Kehr G, Fröhlich R, Erker G (2004) *Chem Commun* 2004:1188
125. Boukamp MW, Bart SC, Hawrelak EJ, Trovitch RJ, Lobkovsky E, Chirik PJ (2005) *Chem Commun* 2005:3402
126. Gibson VC, Humphries MJ, Tellmann KP, Wass DF, White AJP, Williams DJ (2001) *Chem Commun* 2001:2252
127. Trovitch RJ, Lobkovsky E, Bill E, Chirik PJ (2008) *Organometallics* 27:109
128. Boukamp MW, Lobkovsky E, Chirik PJ (2005) *J Am Chem Soc* 127:9660
129. Scott J, Gambarotta S, Korobkov I, Budzelaar PHM (2005) *J Am Chem Soc* 127:13019
130. Campora J, Naz AM, Palma P, Alvarez E, Reyes ML (2005) *Organometallics* 24:4878
131. Bouwkamp MW, Lobkovsky E, Chirik PJ (2006) *Inorg Chem* 45:2
132. Bart SC, Lobkovsky E, Chirik PJ (2004) *J Am Chem Soc* 126:13794
133. Bart SC, Lobkovsky E, Bill E, Chirik PJ (2006) *J Am Chem Soc* 128:5302
134. Scott J, Vidyaratne I, Korobkov I, Gambarotta S, Budzelaar PHM (2008) *Inorg Chem* 47:896
135. Mastroilli P, Nobile CF (2004) *Coord Chem Rev* 248:377
136. Kaul FAR, Puchta GT, Schneider H, Bielert F, Mihalios D, Hermann WA (2002) *Organometallics* 21:74
137. Goerl C, Alt HG (2007) *J Mol Catal A: Chem* 273:118
138. Bouilhac C, Cloutet E, Cramail H, Deffieux A, Taton D (2005) *Macromol Rapid Commun* 26:1619
139. Ray S, Sivaram S (2006) *Polym Int* 55:854
140. Zheng Z, Liu J, Li Y (2005) *J Catal* 234:101

141. Li L, Wang Q (2004) *J Polym Sci Part A: Polym Chem* 42:5662
142. Guo C, Jin G-X, Wang F (2004) *J Polym Sci Part A: Polym Chem* 42:4830
143. Ma Z, Ke Y, Wang H, Guo C, Zhang M, Sun W-H, Hu Y (2003) *J Appl Polym Sci* 88:466
144. Ma Z, Sun W-H, Zhu N, Li Z, Shao C, Hu Y (2002) *Polym Int* 51:349
145. Xu H, Guo C, Xue C, Ma Z, Zhang M, Dong J, Wang J, Hu Y (2006) *Eur Polym J* 42:203
146. Huang R, Koning CE, Chadwick JC (2007) *J Polym Sci Part A: Polym Chem* 45:4054
147. Huang RB, Koning CE, Chadwick JC (2007) *Macromolecules* 40:3021
148. Xu R, Liu D, Wang S, Mao B (2006) *Macromol Chem Phys* 207:779
149. Huang R, Liu D, Wang S, Mao B (2004) *Macromol Chem Phys* 205:966
150. Paulino IS, Schuchardt U (2004) *Catal Commun* 5:5
151. Zhang M, Xu H, Guo C, Ma Z, Dong J, Ke Y, Hu Y (2005) *Polym Int* 54:274
152. Ray S, Galgali G, Lele A, Sivaram S. (2004) *J Polym Sci Part A: Polym Chem* 43:304
153. Kurokawa H, Matsuda M, Fujii K, Ishihama Y, Sakuragi T, Ohshima M, Miura H (2007) *Chem Lett* 36:1004
154. Semikolenova NV, Zakharov VA, Paukshtis EA, Danilova IG (2005) *Top Catal* 32:77
155. Zakharov VA, Semikolenova NV, Mikenas TB, Barabanov AA, Bukatov GD, Echevskaya LG, Mats'ko MA (2006) *Kinet Catal* 47:303
156. Mikenas TB, Zakharov VA, Echevskaya LG, Matsko MA (2005) *J Polym Sci Part A: Polym Chem* 43:2128
157. Mikenas TB, Zakharov VA, Echevskaya LG, Matsko MA (2007) *J Polym Sci Part A: Polym Chem* 45:5057
158. Huang R, Kukalyekar N, Koning CE, Chadwick JC (2006) *J Mol Catal A: Chem* 260:135
159. Huang R, Liu D, Wang S, Mao B (2005) *J Mol Catal A: Chem* 233:91
160. Schmidt R, Welch MB, Palackal SJ, Alt HG (2002) *J Mol Catal A: Chem* 179:155
161. Zheng ZJ, Chen J, Li YS (2004) *J Organomet Chem* 689:3040
162. Overett MJ, Meijboom R, Moss JR (2005) *Dalton Trans* 2005:551
163. Nelson SM, McCann M, Stevenson C, Drew MGB (1979) *J Chem Soc Dalton Trans* 1979:1477
164. Nelson SM, Knox CV, McCann M, Drew MGB (1981) *J Chem Soc Dalton Trans* 1981:1669
165. Liu J, Li Y, Liu J, Li Z (2005) *Macromolecules* 38:2559
166. Tolstikov GA, Ivanchev SS, Oleinik II, Ivancheva NI, Oleinik IV (2005) *Doklady Phys Chem* 404:182
167. Seitz M, Alt HG (2006) *J Mol Catal A: Chem* 257:73
168. Armspach D, Matt D, Peruch F, Lutz P (2003) *Eur J Inorg Chem* 2003:805
169. Mecking S (1999) *Macromol Rapid Commun* 20:139
170. Bennett AMA, Coughlin EB, Citron JD, Wang L (1999) (E.I. Du Pont de Nemours and Co., USA) WO 99/50318
171. Pan L, Zhang KY, Li YG, Bo SQ, Li YS (2007) *J Appl Polym Sci* 104:4188
172. Ivanchev SS, Badaev VK, Ivancheva NI, Sviridova EV, Rogozina DG, Khaikin SY (2004) *Vysokomolekulyarnye Soedineniya, Seriya A i Seriya B* 46:1959
173. Quijada R, Rojas R, Bazan G, Komon ZJA, Mauler RS, Galland GB (2001) *Macromolecules* 34:2411
174. Galland GB, Quijada R, Rojas R, Bazan G, Komon ZJA (2002) *Macromolecules* 35:339
175. Lu Z, Zhang Z, Li Y, Wu C, Hu Y (2006) *J Appl Poly Sci* 99:2898
176. Wang R, Zheng Y, Cui N, Zhang Z, Ke Y, Hu Y (2005) *Gaofenzi Xuebao* 132:204
177. Wang H, Ma Z, Ke Y, Hu Y (2003) *Polym Int* 52:1546
178. Zhang Z, Lu Z, Chen S, Li H, Zhang X, Lu Y, Hu Y (2005) *J Mol Catal A: Chem* 236:87
179. Xu H, Guo C-Y, Zhang M, Y and H-J, Dong J, Yuan G (2007) *Catal Commun* 8:2143
180. Barabanov AA, Bukatov GD, Zakharov VA, Semikolenova NV, Echevskaya LG, Matsko MA (2005) *Macromol Chem Phys* 206:2292
181. Britovsek GJP, Gibson VC, Mastroianni S, Redshaw C, Solan GA, White AJP, Williams DJ (2001) *Eur J Inorg Chem* 2001:431

182. Al-Benna S, Sarsfield MJ, Thornton-Pett M, Ormsby D, Maddox PJ, Bres P, Bochmann M (2000) *J Chem Soc Dalton Trans* 2000:4247
183. Kreisher K, Kipke J, Bauerfeind M, Sundermeyer J (2001) *Z Anorg Allg Chem* 627:1023
184. Müller G, Klinga M, Leskelä M, Rieger B (2002) *Z Anorg Allg Chem* 628:2839
185. Nomura K, Warit S, Imanishi Y (1999) *Macromolecules* 32:4732
186. Nomura K, Warit S, Imanishi Y (2000) *Bull Chem Soc Jpn* 73:599
187. Sun W-H, Hao P, Zhang S, Shi Q, Zuo W, Tang X, Lu X (2007) *Organometallics* 26:2720
188. Fernandes S, Bellabarba RM, Ribeiro DF, Gomes PT, Ascenso JR, Mano JF, Dias AR, Marques MM (2002) *Polym Int* 51:1301
189. Sun W-H, Tang X, Gao T, Wu B, Zhang W, Ma H (2004) *Organometallics* 23:5037
190. Gibson VC, Redshaw C, Solan GA, White AJP, Williams DJ (2007) *Organometallics* 26:5119
191. Bianchini C, Mantovani G, Meli A, Migliacci F, Laschi F (2003) *Organometallics* 22:2545
192. Bianchini C, Giambastiani G, Mantovani G, Meli A, Mimeau D (2004) *J Organomet Chem* 689:1356
193. Bianchini C, Gatteschi D, Giambastiani G, Guerrero Rios I, Ienco A, Laschi F, Mealli C, Meli A, Sorace L, Toti A, Vizza F (2007) *Organometallics* 26:726
194. Britovsek GJP, Baugh SPD, Hoarau O, Gibson VC, Wass DF, White AJP, Williams DJ (2003) *Inorg Chim Acta* 345:279
195. Sun WH, Jie S, Zhang S, Zhang W, Song Y, Ma H, Chen J, Wedeking K, Fröhlich R (2006) *Organometallics* 25:666
196. Jie S, Zhang S, Sun WH (2007) *Eur J Inorg Chem* 2007:5584
197. Jie SY, Zhang S, Sun WH, Kuand X, Liu T, Guo J (2007) *J Mol Catal A: Chem* 269:85
198. Pelletier JDA, Champouret YDM, Cadarso J, Clowes L, Gaete M, Singh K, Thanarajasingham V, Solan GA (2006) *J Organomet Chem* 691:4114
199. Nakayama Y, Baba Y, Yasuda H, Kawakita K, Ueyama N (2003) *Macromolecules* 36:7953
200. Matsui s, Nitabaru M, Tsuru K, Fujita T, Suzuki Y, Takagi Y, Tanaka H (1999) (Mitsui Chemicals Inc., Japan) PCT Int., Japan) PCT Int. Appl W09954364 [Chem Abstr 131:310946
201. Cowdell C, Davies CJ, Hilton SJ, Marechal J-D, Solan GA, Thomas O, Fawcett J (2004) *Dalton Trans* 2004:3231
202. Wang L, Sun W-H, Han L, Li Z, Hu Y, He C, Yan C (2002) *J Organomet Chem* 650:59
203. Dawson DM, Walker DA, Thornton-Pett M, Bochmann M (2000) *J Chem Soc Dalton Trans* 2000:459
204. Beaufort L, Benvenuti F, Noels AF (2006) *J Mol Catal A: Chem* 260:210
205. Beaufort L, Benvenuti F, Noels AF (2006) *J Mol Catal A: Chem* 260:215
206. Sun WH, Hao P, Li G, Zhang S, Wang W, Yi J, Asma M, Tang N (2007) *J Organomet Chem* 692:4506
207. Small BL, Rios R, Fernandez ER, Carney MJ (2007) *Organometallics* 26:1744
208. Karam A, Tenia R, Martinez M, Lopez-Linares F, Albano C, Diaz-Barrios A, Sanchez Y, Catari E, Casa E, Pekerar S, Albornoz A (2007) *J Mol Catal A: Chem* 265:127
209. Solan GA, Pelletier JDA (2004) (ExxonMobil Chemical) PCT Int. Appl., WO2005118605
210. Champouret YDM, Maréchal JD, Dadhiwala I, Fawcett J, Palmer D, Singh K, Solan GA (2006) *Dalton Trans* 2350
211. Armitage A, Champouret YDM, Grigoli H, Pelletier JDA, Singh K, Solan GA (2008) *Eur J Inorg Chem* 4597
212. Zhang S, Sun WH, Kuang X, Vystorop I, Yi J (2007) *J Organomet Chem* 692:5307
213. Zhang S, Vystorop I, Tang ZH, Sun W-H (2007) *Organometallics* 26:2456
214. Bianchini C, Giambastiani G, Rios IG, Meli A, Oberhauser W, Sorace L, Toti A (2007) *Organometallics* 26:5066
215. Champouret YDM, Fawcett J, Nodes WJ, Singh K, Solan GA (2006) *Inorg Chem* 45:9890
216. Wang LC, Ren H, Sun JQ (2008) *J Appl Polm Sci* 108:167
217. Britovsek GJP, Gibson VC, Spitzmesser SK, Tellmann KP, White AJP, Williams DJ (2002) *Dalton Trans* 2002:1159

Late Transition Metal Catalysts for the Copolymerization of Olefins and Polar Monomers

Brian L. Goodall

Abstract The evolution of olefin polymerization catalysis since Karl Ziegler's and Giulio Natta's Nobel Prize-winning discoveries in the mid-1950s has involved a prolific interplay of polymer science and organometallic chemistry and led to the development and commercial deployment of catalysts that rival the activities of enzymes and systems, yielding polyolefins possessing structures and physical properties that allow them to be applied in countless applications worldwide. In contrast, commercial processes for the copolymerization of ethylene with polar monomers such as acrylate and vinyl acetate still exclusively employ free radical processes. This chapter reviews recent developments in the catalytic copolymerization of ethylene and these polar comonomers, including well-defined, single-component catalysts capable of copolymerizing (for example) acrylates and vinyl ethers to high molecular weight, linear, random copolymers.

Keywords Acrylate comonomers, Ethylene, Mechanism, Palladium catalysts, Polar groups, Polymerization catalysis, Random copolymers

Contents

1 Introduction.....	160
2 Copolymerization of Ethylene with Polar Comonomers.....	161
3 Linear, Random Copolymers of Ethylene and Polar Comonomers.....	168
4 Conclusion	176
References.....	176

B.L. Goodall
Sapphire Energy Inc., 3115 Merryfield Row, San Diego, CA 92121, USA
e-mail: brian.goodall@sapphirefuel.com

1 Introduction

Industry-wide a need exists for new molecular catalysts capable of polymerizing polar monomers in a controlled fashion and for copolymerizing the same monomers with olefins (e.g., ethylene, propylene) under mild reaction conditions and, where appropriate, in a stereoregular (“tactic”) fashion. Of the many approaches to modifying the properties of a polymer that are available, the incorporation of functional groups into an otherwise non-polar material is of vital importance [1, 2]. Polar groups exercise control over important properties such as toughness, adhesion, barrier properties, and surface properties, thus influencing the material properties of the polymer resin (such as solvent resistance, miscibility with other polymers and rheological properties) and product performance (such as paintability, printability, gloss, hardness, mar resistance, etc.). By incorporating polar groups into hydrocarbon polymers (such as polyethylene, polypropylene and polystyrene), not only would the important properties related to crystallinity be maintained, but these new properties would also be introduced. As Christopher Killian of Eastman Chemical recently stated [3]: “It has been a dream to copolymerize ethylene and other functional monomers” and, in the same article: “History teaches us that the more control you have over a system, the more probability there is to tailor a material to fit a certain application.”

It should be noted that the scope of this review is limited to the copolymerization of olefins (especially ethylene) with polar monomers. Polar monomers are defined as olefinic monomers bearing a polar group such as an ester, acid, nitrile or ether group, with the polar group either being directly attached to the olefin (e.g., acrylates, acrylonitrile) or remotely attached (e.g., polar norbornene monomers, alpha-olefins bearing terminal polar groups). It is also intended to focus primarily on developments since 2000 when two extensive reviews appeared in the literature [4, 5]. Hence no attempt has been made to review the copolymerization of ethylene with carbon monoxide (polyketone). Polyketone was successfully scaled up and commercialized by Shell under the name Carilon (driven by inventions and innovations of Eite Drent) in the 1990s using homogeneous palladium catalysts. Thorough reviews have appeared elsewhere [6]. Commercial production was halted by Shell in the 2000–2002 time-frame and the patent portfolio was donated to SRI International in 2002 [7] and recently licensed to Asahi Kasei Fibers Corporation [8]. Properties of the ethylene/carbon monoxide copolymer are also to be found on the SRI website [9].

Polyethylene was discovered on several different occasions over the last century or so, by accident or serendipity. It was first synthesized by Hans von Pechman in 1898 after heating diazomethane. Strictly speaking the waxy material that he isolated was polymethylene since it comprised repeat ($-\text{CH}_2-$) units, rather than ($-\text{CH}_2\text{CH}_2-$) units. The first synthesis of polyethylene starting from ethylene itself was carried out in 1933 when two organic chemists working for the Imperial Chemical Industries Research Laboratory were testing various chemicals under highly pressurized conditions. In their wildest fantasies, the two researchers Eric Fawcett and Reginald Gibson could have had no idea that the revolutionary substance that they had isolated – polyethylene – and the process (free radical polymerization of ethylene) would have such an enormous impact on the world. Eventually they discovered that trace oxygen

impurities had caused the polymerization to initiate, and in 1935 another ICI chemist (Michael Perrin) led the development of high pressure ethylene polymerization into what became the LDPE (low density polyethylene) process in 1939.

In 1951 Robert Banks and Paul Hogan of Phillips Petroleum discovered that ethylene could be polymerized under rather mild conditions of temperature and pressure to afford high molecular weight polyethylene using chromium trioxide as the catalyst. This invention laid the foundation for both the Phillips and Union Carbide processes for ethylene polymerization (both use heterogeneous chromium catalysts).

In the early 1950s Karl Ziegler and his group were exploring the oligomerization of ethylene to a mixture of ethylene oligomers (alpha-olefins and waxes) using triethylaluminum as the catalyst. This was the “Aufbau reaction” – the basis of the BP (formerly Albemarle) and Chevron olefin processes. They serendipitously discovered that trace amounts of nickel salts changed the reaction to give selectively 1-butene as the product (the “Nickel effect”). In searching for other metal salts to give similar selectivity they discovered that early transition metal salts (such as zirconium, vanadium, and titanium halides) caused the formation of high molecular weight, linear, crystalline polyethylene (HDPE or high density polyethylene). A complete, riveting review of all of these events, the characters involved, and the subsequent developments was written by Frank M. McMillan [10].

The evolution of olefin polymerization catalysis since Karl Ziegler’s Nobel Prize-winning discovery of the transition metal-catalyzed polymerization of ethylene on 26 October 1953 has involved a prolific interplay of polymer science and organometallic chemistry. Commercial successes include the development and deployment of catalysts that rival the activities of enzymes and systems, yielding polyolefins possessing structures and physical properties allowing them to be applied in countless applications worldwide. This discovery, and subsequent innovations, has provided the basis for an industry enjoying global sales of polyethylene and polypropylene exceeding 160 billion pounds by 2000, and still growing at 3–4% per annum [11].

Central to this sustained and expanding commercial exploitation has been (i) increased understanding of reaction mechanisms at the molecular level and (ii) translation of this understanding into morphological and architectural control of the resulting polymers through catalyst design [12]. The use of transition metal catalysts has significantly improved economics (low energy, low pressure processes), greatly improved product properties (just look at the strength of the ultrathin plastic bags at the produce counter), resulted in new products (new grades of polyethylene, elastomers, medical packaging), and even brand new polymers (e.g., isotactic polypropylene, syndiotactic polystyrene) by virtue of the molecular level control of polymer architecture endowed by these catalysts.

2 Copolymerization of Ethylene with Polar Comonomers

In contrast, commercial processes for the copolymerization of ethylene with polar monomers such as acrylate and vinyl acetate still exclusively employ free radical processes [13]. The use of free radical initiators across the entire acrylic polymer

market gives little or no control over polymer architecture (tacticity or crystallinity, blockiness, molecular weight and distribution thereof) and thus limits the range of materials and performances available. Furthermore, free radical processes result in branched (co-)polymers and relatively broad molecular weights; this results in lower crystallinity and typically (in the case of free radical polyethylene homopolymers, LDPE) performance inferior to the highly tailored single-site (metallocene) polyethylenes, which now account for all the growth in this enormous, and still growing, market. The acid or ester functionality may be converted to their respective salts, leading to polymers bearing ionic cross-links. These polyolefin ionomers are used in applications requiring extreme toughness (e.g., Surlyn for golf ball covers) or superior sealing properties (e.g., sealing challenging commodities such as in bacon packaging). Because these free radical processes require extreme pressures, they suffer from high capital investment and manufacturing costs.

However, despite nearly 50 years of intense activity and progress, there are no commercially viable catalysts for the polymerization of acrylates or the controlled copolymerization of simple olefins with polar functional monomers. The development of a catalytic system capable of such controlled copolymerization would constitute a quantum advance in the plastics industry.

In the early days of Ziegler catalysis (the 1960s) there was considerable effort expended, and a flurry of patents and papers on the copolymerization of ethylene with countless polar monomers. It is generally accepted that none of these attempts was successful, and at least some of the erroneous claims must be attributed to lack of sophisticated analytical methods in those pioneering days. For interested parties this work is best surveyed in the book of John Boor [14].

In the world of polyolefins, early transition metal Ziegler–Natta type complexes and metallocene catalysts are used extensively for the polymerization of ethylene and propylene. Early transition metals are those on the left side of the Periodic Table (e.g., Ti, Zr, Hf, Cr) and are usually active in high oxidation states. Their high oxophilicity (the tendency to react irreversibly with oxygen-containing molecules) makes them intolerant of water (and hence makes aqueous emulsion polymerization impractical) and causes them to be poisoned by most functionalized olefins, particularly the commercially available polar comonomers such as acrylates and vinyl acetate. However, there are examples of copolymerizations with special (protected in one way or another) substrates [e.g., 15 and references therein] or with very high levels of a Lewis acid incorporated into the polymerization system to protect the polar functionality through complexation [16–21]. Alternative routes to polar copolymers involving metathesis of cyclic olefins and functionalization of the resulting unsaturated polymer or metathesis of polar cycloolefins followed by hydrogenation to remove the resulting unsaturation have been published [22, 23]. The cost of these multistep routes would preclude commercialization of all but the most valuable polymers.

Late transition metals are found on the right of the Periodic Table (e.g. Ni, Pd, Pt, Co, Fe, Ru, Rh, Cu; active in low oxidation states) and are more tolerant of oxygen functionalities in the monomer and the polymer. This behavior stems from the preference of late transition metals for soft ligands (polarizable ligands, typically

P, N, O, S, or C based, which favor covalent bonding and stabilize low oxidation states) due to the metals' higher electronegativity and lower oxidation states [24]. In recent years, late transition metal catalysts [25–29] have attracted attention not only for the polymerization of α -olefins, but more importantly for the copolymerization of hydrocarbon monomers with readily available polar monomers such as acrylates, vinyl ethers, and vinyl acetate [27 and references therein].

However, the practical, direct synthesis of functionalized linear polyolefins via coordination copolymerization of olefins with polar monomers ($\text{CH}_2 = \text{CHX}$) remains a challenging and industrially important goal. In the mid-1990s Brookhart et al. [25, 27] reported that cationic (α -diimine)palladium complexes with weakly coordinating anions catalyze the copolymerization of ethylene with alkylacrylates to afford hyperbranched copolymers with the acrylate functions located almost exclusively at the chain ends, via a chain-walking mechanism that has been meticulously studied and elucidated by Brookhart and his collaborators at DuPont [25, 27]. Indeed, this seminal work demonstrated for the first time that the insertion of acrylate monomers into certain late transition metal alkyl species is a surprisingly facile process. It spawned almost a decade of intense research by several groups to understand and advance this new science and to attempt to exploit it commercially [30–33, 61].

In their simplest form, the Brookhart catalysts comprise neutral nickel (or palladium) complexes of bulky aryl α -diimine ligands bearing steric hindrance in the *ortho* positions of the aryl rings (Fig. 1) activated with typical Ziegler–Natta co-catalysts (e.g., diethyl aluminum chloride DEAC) or activators (e.g., methaluminoxane MAO). The α -diimine ligands have been widely used to stabilize organometallic complexes, and their synthesis is simply a condensation reaction between a diketone and two moles of an alkyl- or arylamine, giving a wide diversity of such ligands for catalytic study.

The resulting catalysts exhibit highly efficient homopolymerization of ethylene, with the nickel analogs showing much higher rates and productivities, to afford branched (nickel) or hyperbranched (palladium) polyethylenes. Interestingly, the chain-walking mechanism causes these catalysts to afford chain-straightened polyolefins starting with propylene and α -olefins (e.g., substantially less methyl groups than one to every two backbone carbons in the resulting “polypropylene”).

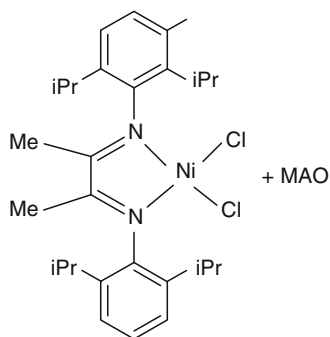


Fig. 1 “Brookhart catalyst”

The Lewis acidity and reactivity of these alkyl aluminum cocatalysts and activators with Lewis basic polar monomers such as acrylates make them impractical components in the copolymerization of ethylene with acrylates. To address this shortcoming, Brookhart et al. developed well-defined cationic species such as that shown in Fig. 2, in which the counterion (not illustrated) was the now-ubiquitous fluorinated arylborate family [34] such as tetrakis(pentafluorophenyl)borate. At very low methyl acrylate levels the nickel catalysts gave linear copolymers but with near-zero levels of acrylate incorporation.

More recently, the DuPont group [35] reported that it is possible to make linear copolymers of ethylene and acrylates using this catalyst family by increasing the ethylene pressure to 1000 psi and adding large excesses (200–300×) of the expensive Lewis acid, tris(pentafluorophenyl)borane, to the nickel catalysts. However, yields are poor and acrylate incorporation (<6 mol%) and molecular weights ($M_n < 8000$) are low. The high pressures required and enormous costs of the exotic Lewis acid used to overcome the “polymer back-biting” problem (Fig. 3) represent significant hurdles to commercialization. A similar approach was taken in the early days of Ziegler catalysis when 2 mol% acrylic acid was incorporated into isotactic polypropylene by protecting it with an inexpensive Lewis acid (diethylaluminum chloride) [36] in combination with a first generation Ziegler–Natta (TiCl_3) catalyst.

Given the higher stability of the palladium analogs, their easier synthetic availability, and their higher robustness to polar groups, most attention was given to the

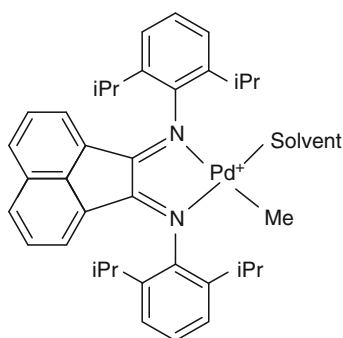


Fig. 2 Single-component, well-defined Brookhart catalyst

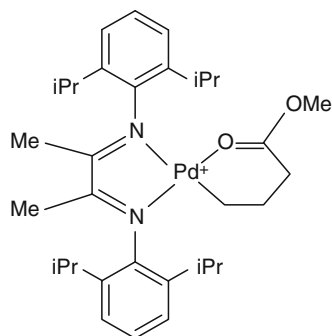


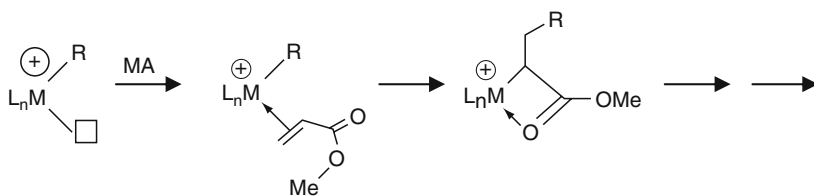
Fig. 3 Cationic palladium catalyst showing coordination of last inserted acrylate unit

palladium derivatives. The palladium α -diimine catalysts yield high MW polyethylene that is amorphous and highly branched, with topologies ranging from moderate branching to hyperbranched oily structures. The palladium catalysts are remarkably tolerant towards polar groups and ethylene polymerization can be carried out in the presence of moisture, air, ethers, esters and the like, although nitrile functionality typically inhibits these and most other late transition metal catalysts. The functional group tolerance also encompasses comonomers bearing polar groups such as acrylates and the like.

While relatively slow polymerization catalysts, they represented the first systems to directly copolymerize ethylene and acrylates. Scheme 1 shows a simplified reaction pathway for the insertion of methyl acrylate (MA) into these catalysts, with the first step being coordination of the olefinic moiety of MA monomer onto the cationic metal (palladium) center. This is followed by migratory insertion of the MA monomer into the palladium–carbon bond in a 2,1 fashion to form the resulting insertion product. However, the electrophilicity of the metal center and the resulting geometry results in a tight coordination of the carbonyl function of the inserted acrylate monomer essentially “short-stopping” further polymerization reaction by occupying the vacant site critical for coordination and subsequent insertion of the next monomer unit. However, it was found that chain-walking of the palladium center resulted in migration of the metal away from the ester function, and ring expansion to afford palladium species such as that shown in Scheme 1, which could be isolated as crystalline complexes. Although sluggish, these complexes proved to be effective catalysts for the copolymerization of ethylene and acrylates. Despite being capable of incorporating quite high levels (around 12 mol%) of acrylate, the chain-walking following every acrylate insertion (Scheme 1) resulted in the observed hyperbranched polyethylenes with acrylate end groups rather than the desired linear polyethylene with random incorporation of acrylate functionality.

These materials have possible utility in a number of specialty applications and are being explored by Guan et al. [37]. They have used these catalysts, and their unique chain-walking characteristics to synthesize a variety of dendritic materials (Fig. 4), which could find potential application as processing aids, rheological modifiers, and amphiphilic core-shell nanoparticles for drug delivery and dye formulation.

The same authors [38] further refined these catalysts by developing very bulky cyclophane diimine palladium(II) catalysts (Fig. 5), which show greater activity and stability than their acyclic analogs. The incorporation levels of acrylates (methyl and *tert*-butyl acrylate were exemplified) are unusually high (up to around 25



Scheme 1 Acrylate insertion into a Brookhart catalyst

mol%) compared to the corresponding acyclic catalyst. Mechanistic studies using low-temperature NMR spectroscopy revealed that the differences between the insertion barriers for ethylene and MA are similar for the acyclic and cyclophane catalysts. However, the equilibration of comonomers, fast on the experimental time scale for the acyclic catalyst, was below the measurement threshold for the cyclophane catalyst. It was argued that these results suggest that ligand substitution is significantly retarded by the bulky cyclophane ligand and that the reduction in the rate of monomer exchange with respect to monomer insertion greatly diminishes the catalyst's ability to discriminate between comonomers, resulting in the observed high incorporation levels of acrylates in the resulting ethylene copolymers.

There appear to be two fundamental reasons for the absence of truly efficient transition metal-based insertion polymerization catalysts for the copolymerization of acrylate monomers with ethylene or other olefins. The first reason is that, following insertion, the ester group of the acrylate coordinates to the metal as shown by

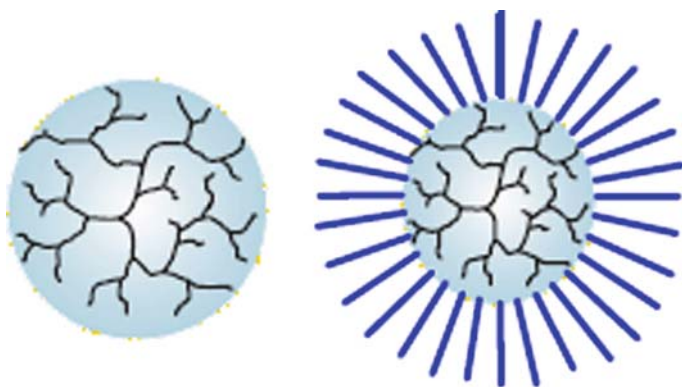


Fig. 4 Dendritic materials made via chain-walking mechanism. *Left:* processing aid, rheology modifier. *Right:* amphiphilic core-shell

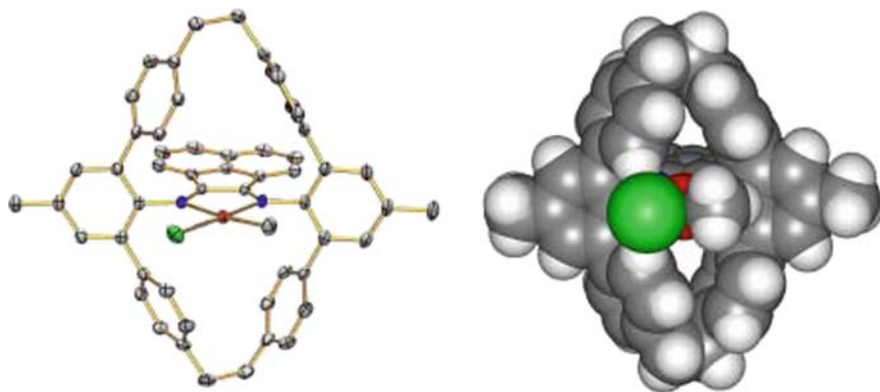


Fig. 5 X-ray crystal structure of cyclophane-palladium complex

Brookhart (Scheme 1). Since migratory insertion in these Pd(II) catalysts occurs through 4-coordinate intermediates, it has the effect of greatly diminishing the polymerization activity since the next incoming monomer unit can only coordinate after breaking the metal–oxygen bond. The second, seemingly less-appreciated, reason for the low activity of transition metal-based copolymerization systems involves the insertion step itself. For electronic reasons, acrylates have a strong preference for 2,1-insertion into metal–carbon bonds [39–41]. The resultant species has an electron-withdrawing ester group on the α -carbon. Since the insertion of an olefin into the metal–carbon bond is effectively an intramolecular nucleophilic attack by the alkyl group on the coordinated olefin, it is likely that this step is further retarded if the alkyl group (growing polymer chain) is less nucleophilic.

A possible route to circumventing these problems involves reducing the electrophilicity of the metal center by moving from a cationic metal center to a neutral one, so long as this does not too much reduce the coordination of the monomer itself since high incorporation of acrylate monomers require that these monomers compete effectively with the other olefins in the system. In a recent theoretical paper, Ziegler [41] argued that the interaction of the ester group of the acrylate with the metal center is weaker in neutral complexes than in the corresponding cationic species. On the other hand, the bonding of the olefinic functionality is not significantly affected because the weaker olefin-to-metal charge transfer in the neutral complex is compensated by stronger metal-to-olefin back-bonding. Grubbs reported a neutral nickel-based system [42] which, while tolerant of polar groups and capable of copolymerizing ethylene with monomers such as norbornenes bearing ester functionality, was ineffective for acrylates, presumably because coordination of the ester group is stronger with “harder” Ni(II) than Pd(II).

In addition to the use of less electrophilic, neutral metal complexes it is necessary to impose extreme steric crowding at the catalytic center by using bulky ligands. Crowding of the catalytic center can lead to two beneficial effects, the first of which is that binding of the last inserted ester functionality will likely either be reduced or prevented. In principle a second benefit (as yet apparently unobserved) might be the possible override of the electronic preference for 2,1-insertion of acrylates, resulting in a less sterically demanding 1,2-insertion. The resulting alkyl (growing polymer chain) will not have an ester functionality at the α -carbon, making it more nucleophilic and facilitating the next insertion step.

Again, calculations by Ziegler [40] on barriers for the 1,2- and 2,1-insertion of methyl acrylate into Brookhart-type diimine complexes show that for sterically unhindered catalysts 2,1-insertion is strongly favored, with the transition state for 2,1-insertion having a significantly lower energy (by 4.5 kcal mol⁻¹) than the corresponding 1,2 transition state. However, for a typical sterically encumbered catalyst 2,1-insertion is only marginally favored (by 0.5 kcal mol⁻¹) over 1,2-insertion.

Some of these approaches were attempted by Grubbs et al. [43–47]. In later studies [45, 46], the phenoxyimine ligands used in their initial study were replaced with nucleophilic heterocyclic carbene (NHC) ligands with the objective of pushing more electrons into the metal center to reduce the tendency of a last-inserted acrylate

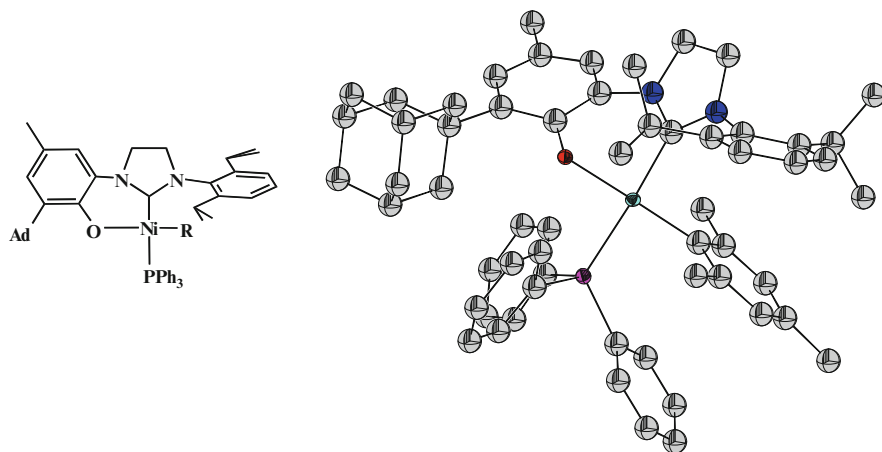


Fig. 6 Grubbs nickel complex bearing sterically encumbered nucleophilic heterocyclic carbene ligand

monomer to coordinate the catalyst and retard further reaction (as in Scheme 1). The synthesis of these chelating NHC ligands proved to be highly challenging, as was the synthesis of the metal complexes, since the carbenes decomposed through a novel ring-expansion pathway [46]. When the desired sterically bulky chelated NHC metal complexes (Fig. 6) were synthesized and tested, they were found to be inactive in olefin polymerization, indicating that the electron-donating power of the NHC ligand seemingly precludes coordination of ethylene by the metal center.

3 Linear, Random Copolymers of Ethylene and Polar Comonomers

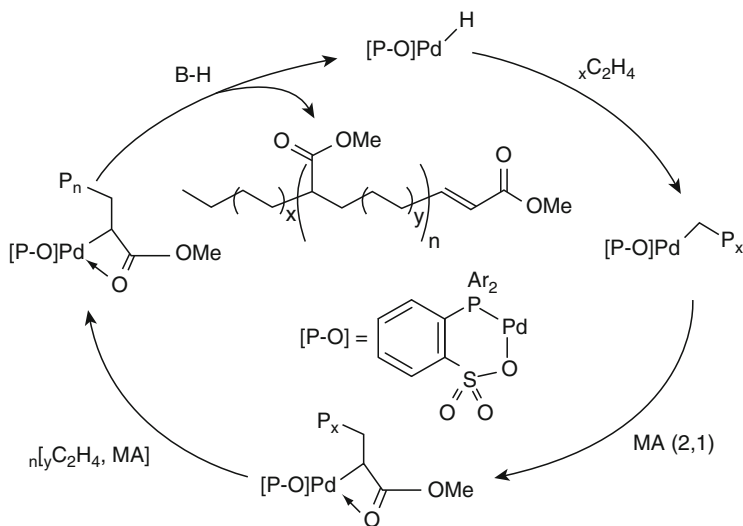
Only recently (2002) have the very first examples of the transition metal-catalyzed incorporation of acrylate monomers into linear polyethylene been demonstrated. In our opinion the most notable report is that of Drent and coworkers [48] who describe the use of a neutral palladium catalyst with a chelating P–O ligand to generate linear copolymers that included the incorporation of acrylate monomers (Drent's catalyst and proposed catalytic cycle are shown in Scheme 2). In these early results, there was only minor acrylate incorporation (limited to some 3–17 mol%) and the resulting polymers were of very low molecular weight (M_n 4000–15,000).

The catalyst reported by Drent [48] was generated in situ by mixing a palladium source with the ligand. A palladium source is broadly defined as a complex or any form of palladium metal whereby upon mixing with the ligand an active catalyst is formed. Many palladium sources are possible, but the sources exemplified by Drent are tris(dibenzylideneacetone)dipalladium(0) ($\text{Pd}_2(\text{dba})_3$), bis(dibenzylideneacetone)palladium(0) ($\text{Pd}(\text{dba})_2$), or palladium(II) acetate.

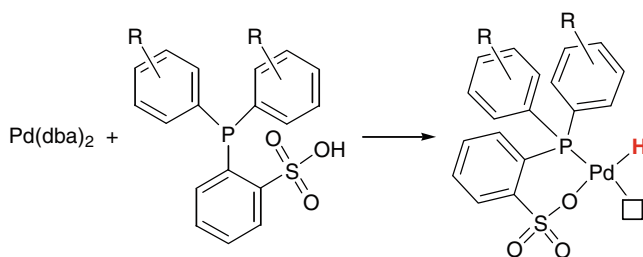
$\text{Pd}(\text{dba})_2$ [palladium(0)] generally affords the best results and thus an oxidation to the metal center must occur. The most likely mechanism for this to occur is by net oxidative addition of the acidic phosphonium P–H moiety (Scheme 3). This hypothesis is supported by the observation that the $\text{p}K_a$ of the phosphonium–hydrogen bond directly affects the activity of catalysts generated in situ with more basic ligands being inactive.

Reactivity patterns of this in situ method also support the hypothesis that Pd oxidation occurs via the acidic phosphonium. This initial reaction would involve initial formation of a palladium hydride. Such hydride intermediates are usually very reactive due to the weakness of the Pd–H bond, which in turn imparts instability.

The in situ method also appears to result in incomplete and inefficient use of palladium. As noted above, the ligand contains an acidic phosphonium hydrogen and can therefore also react with the initially formed Pd–H species to form a “bischelated complex” (two ligands per metal) as shown in Scheme 4. This bischelated palladium is inactive for polymerization. Indeed the formation of these



Scheme 2 Proposed mechanism for ethylene/methyl acrylate copolymerization



Scheme 3 Proposed mechanism for catalyst formation from Pd(0) compounds

bischelated catalyst sinks is a common problem with this general class of neutral, square-planar, late transition metal catalysts (“Keim-type” catalysts [49]). A recent example is found in the related work of Grubbs et al. [44] (Fig. 7), with nickel catalysts aimed at the same target of ethylene copolymerization with polar monomers.

The problems associated with the *in situ* approaches can be avoided by using a discrete catalyst. The presumed structure of the monometallic palladium catalyst contains the sulfonated phosphine ligand chelated to the palladium and a palladium–carbon bond (polymer), most probably in *cis* geometry with respect to the phosphorous (Fig. 8).

Thus, the requirements for a well-defined discrete complex are that:

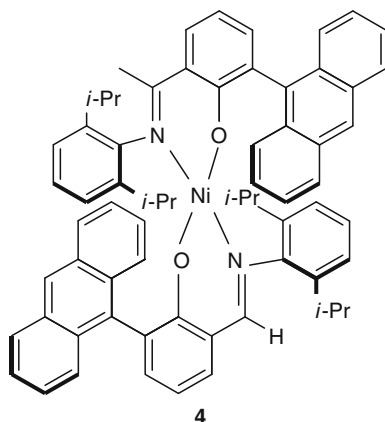
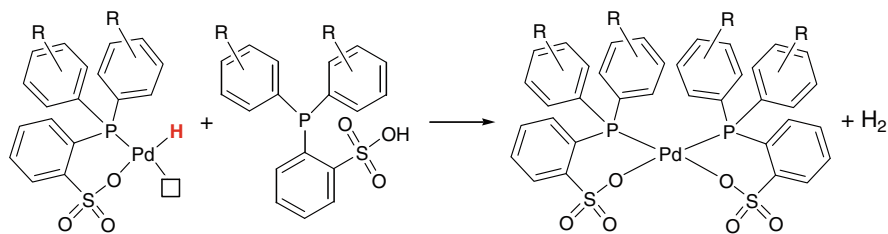


Fig. 7 Bis-chelated nickel complex



Scheme 4 Proposed reaction of Pd–H moiety reacting with excess ligand to form the inactive bis-chelated complex

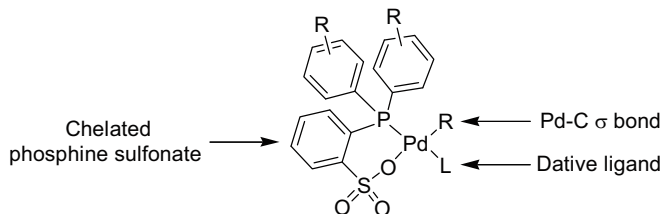


Fig. 8 Key features of well-defined neutral palladium complex

1. It is stable and isolable
2. It contains a palladium–carbon σ -bond (alkyl or aryl)
3. The sulfonated phosphine ligand is chelated to the metal center
4. It contains a weak dative auxiliary ligand that is readily replaced by incoming olefinic monomers (Fig. 8)

The free ligands as prepared are generally zwitterionic aryl phosphines (Fig. 9) and contain an acidic phosphonium moiety with a pK_a of approximately 3. Employing this acidic group to protonate off an alkyl or aryl group from palladium represents a clean method of synthesis [50] with tetramethylethyldiamine palladium(II) dimethyl, (TMEDA)PdMe₂, being a convenient and storage-stable palladium precursor. The resulting complex (catalyst) can be conveniently isolated as a stable, crystalline solid as the pyridine adduct (L, the auxiliary dative ligand in Fig. 8 is pyridine) by adding a stoichiometric amount of pyridine prior to drying and isolating the product.

The resulting complexes can be effectively employed as single component catalysts to homopolymerize ethylene or copolymerize ethylene with acrylates [50, 51] and a variety of other polar monomers including vinyl ethers, [51, 52] vinyl fluoride [53], *N*-vinyl-2-pyrrolidinone, and *N*-isopropylacrylamide [54]. In fact, the resulting catalysts are so robust that they can be used as single component catalysts in aqueous emulsion homo-polymerization of ethylene and copolymerization of ethylene with norbornenes and acrylates [55].

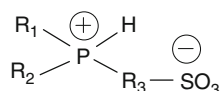


Fig. 9 Zwitterionic nature of the sulfonic acid phosphine ligand

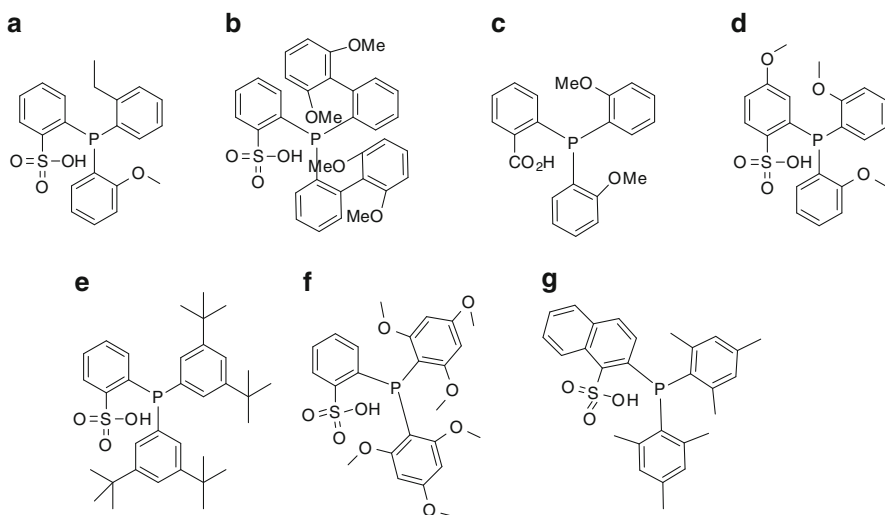
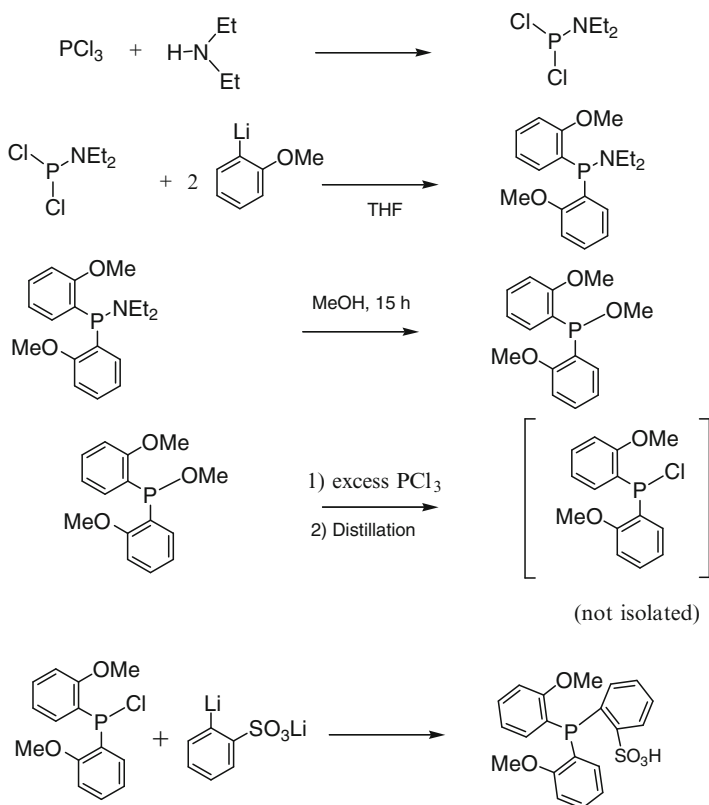


Fig. 10 Chelating phosphine ligands (a–g) with varying steric and electronic properties

In Drent's original publication the only ligands exemplified were 2-[bis(2-methoxy-phenyl)phosphanyl]-benzenesulfonic acid (Fig. 10a) and the simple biphenyl analog (no methoxy groups), with the latter being ineffective. One reason for this is probably that the synthetic methodology they followed and published for making the ligands involves multiple steps, requiring protection and deprotections, distillation and crystallization. The synthesis takes several days and typically affords poor overall yield (<20%) and is shown in Scheme 5.

My group at Rohm and Haas [56] came up with a relatively simple, direct, one-pot, high overall yield (>50%) synthesis as shown in Scheme 6. Using this procedure made it possible to synthesize a wide array of ligands, such as those shown in Fig. 10. Some of these ligands have also been described in subsequent publications giving crystal structures and polymerization performance [57]. From this patent and publication can be learnt that severely increasing the steric hindrance in the *ortho*-positions results in catalysts capable of delivering polymers with molecular weights one to two orders of magnitude higher than the simple *ortho*-methoxy ligand (Fig. 10a). In this regard, *ortho*-phenyl substituents such as the ligand shown in Fig. 10b give particularly high molecular weight polymers and copolymers [56,



Scheme 5 Multistep synthesis of sulfonic acid phosphine ligands

57]. The structure catalyst prepared using this ligand is shown in Fig. 11 and suggests that the high molecular weights can be attributed to the bulky substituent blocking at least one of the axial positions on the palladium center.

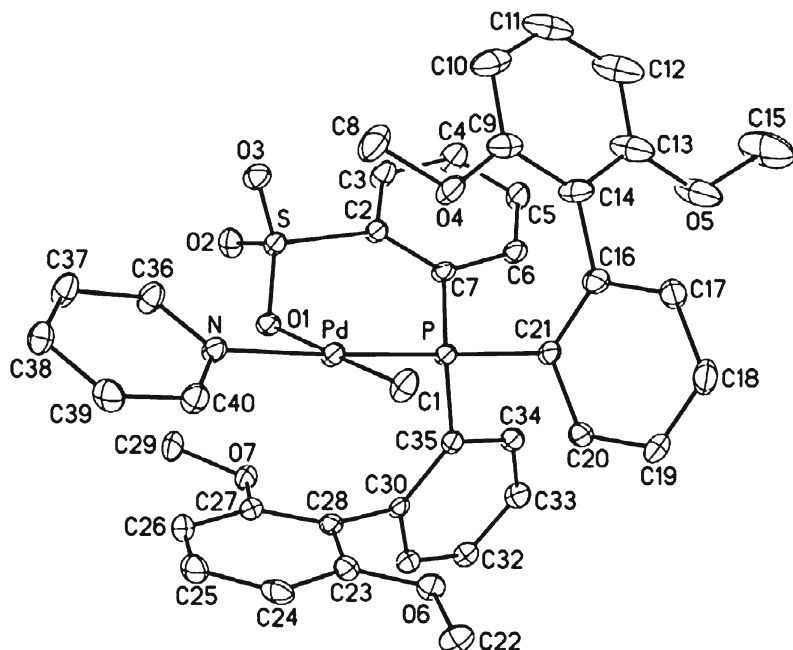
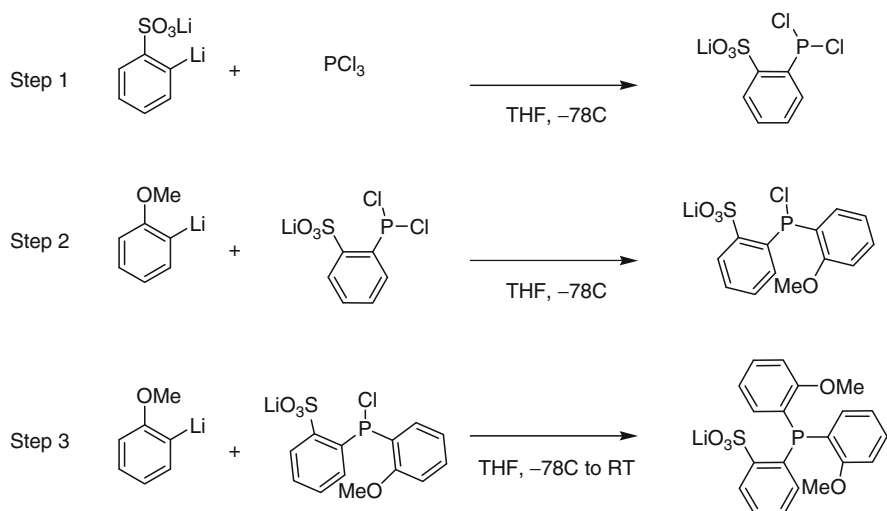


Fig. 11 X-ray crystal structure of palladium catalyst based on ligand **b** in Fig. 10



Scheme 6 Single-pot synthesis of sulfonic acid phosphine ligands

A relevant question pertains to the uniqueness of this ligand set. Why do no other ligands of this general class (Keim-type ligands, which have been extensively studied for 40 years) show the ability to give active catalysts for ethylene/acrylate copolymerization? Is the sulfonic acid function unique and if so why? And, finally, aryl sulfonates are good leaving groups, so why are they such good chelate ligands in this system? The following is speculation to a degree, but it would appear that the fact that the sulfonate function is a good leaving group is critical to the success of this system. For example, the carbonate analog (Fig. 10c) gives a totally inert catalyst that rapidly precipitates palladium as a black powder. There is evidence to suggest that the culprit is the innate ability of palladium to catalyze carbon-carbon coupling reactions (e.g., Suzuki coupling) such that the alkyl group (growing polymer chain) on the palladium couples to the anion on the ligand, resulting in loss of the chelate ligand effect and precipitation of the metal.

These catalysts represent the current state-of-the-art in ethylene copolymerization with polar olefinic monomers, being able to copolymerize a wide variety of polar monomers containing both O and N heteroatoms to generate completely linear, high molecular weight, random copolymers. There are leads to enhance the modest activity of these catalysts, and it will be interesting to watch further developments over the next few years.

In addition to the foregoing late transition metal catalyst developments, which have led to the discovery of sophisticated palladium systems capable of the catalytic (coordination) copolymerization of ethylene with acrylates, there have also been some interesting studies into systems where it eventually transpired that the mechanism was actually free radical rather than catalytic.

Early in the current decade Robert Stibrany and coworkers at Exxon-Mobil [58, 59] described the deployment of unusual (for olefin polymerization catalysis) bis(benzimidazole) copper(II) complexes (Fig. 12) in the presence of a methaluminoxane (MAO) cocatalyst. The catalysts were claimed to homopolymerize ethylene to afford high molecular weight linear (very high T_m) polyethylene. This is, in itself, a surprising observation and probably the first and only description of a copper catalyst for ethylene polymerization, and one that merits further investigation. Even more surprising, the same catalyst/cocatalyst combinations were reported to copolymerize ethylene with a variety of polar monomers such as acrylates and even methacrylates. However, further scrutiny raises some questions since the authors give numerous examples of ethylene/(meth)acrylate comonomers containing high levels (e.g., 50–80%) of the (meth)acrylate comonomers yet none with high levels of ethylene. Copolymers synthesized with *t*-butyl methacrylate comonomer exhibited the highest ethylene contents (31–63%), whereas those prepared with methyl acrylate contained only low levels of ethylene (<15%). Furthermore, copolymerizations carried out at lowered acrylate feed levels generally had increased ethylene contents but showed smaller yields, lowered molecular weights, and increased branching. This is inconsistent and counterintuitive for a coordination catalyzed copolymerization, where the high reactivity ratio of ethylene relative to (meth)acrylates dictates that ethylene is likely to be (by far) the most predominant monomer under these conditions. Furthermore, the ease with which methacrylate is

incorporated would be shocking for a late transition metal-catalyzed coordination mechanism, since acrylate monomers insert into the metal–carbon bond in a 2,1 fashion (see earlier in this chapter) placing the ester functionality on the carbon *alpha* to the metal center. In the case of methacrylates this would result in a *tertiary alpha* carbon center (bearing a methyl group, an ester function, and the growing polymer chain) *alpha* to the metal center. Insertion of another monomer *tertiary alpha* carbon–metal bond is exceedingly unlikely (unprecedented?) and would be expected to result in a dormant site, and in the best case scenario *beta*-hydride elimination and termination/chain transfer.

Indeed, the above results seem to point toward a free radical mechanism. Sen and coworkers [60] studied a model copper complex (Fig. 13) and concluded that the polymerization proceeds via a free radical mechanism (Scheme 7) and that the copper complex/MAO system is in fact a new example of a “redox” free radical generator, in which the role of MAO is to reduce copper(II) to copper(I) completing the “redox” cycle. This rationale also offers a simple explanation for the observation that very high excesses of MAO are required for the ethylene/acrylate copoly-

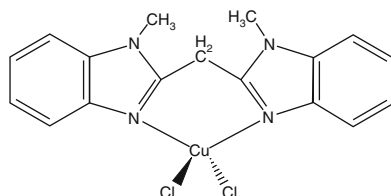


Fig. 12 Bis(benzimidazole) copper(II) complex

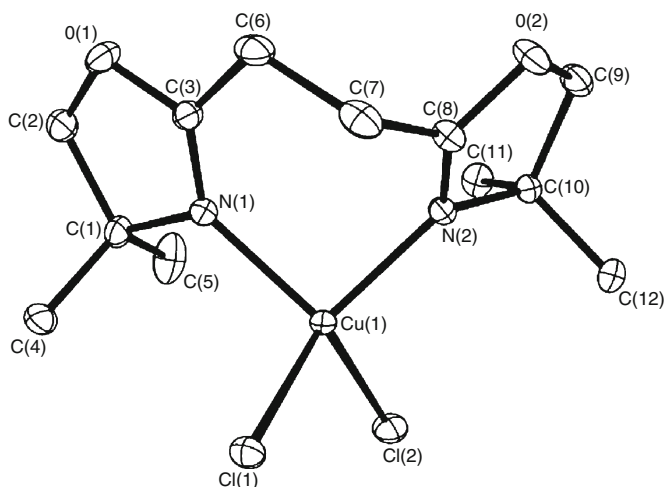
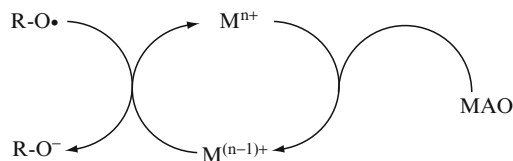


Fig. 13 Sen's model complex



R-O• = Radical Trap
 $M^{n+/(n-1)+}$ = Redox-active metal species
 MAO = Methyl aluminoxane

Scheme 7 Proposed redox-radical process

merization, whereas *much* lower levels of MAO are adequate to initiate the ethylene homopolymerization with the same catalyst (again this latter reaction is presumably a coordination catalytic polymerization).

There have also been several papers [61–63] on the importance of carefully establishing the reaction mechanism when attempting the copolymerization of olefins with polar monomers since many transition metal complexes can spawn active free radical species, especially in the presence of traces of moisture. The minimum controls that need to be carried out are to run the copolymerization in the presence of various radical traps (but this is not always sufficient) to attempt to exclude free radical pathways, and secondly to apply solvent extraction techniques to the polymer formed to determine if it is truly a copolymer or a blend of different polymers and copolymers. Indeed, even in the Drent paper [48], buried in the supplementary material, is described how the true transition metal-catalyzed random copolymer had to be freed of acrylate homopolymer (free radical-derived) by solvent extraction prior to analysis.

4 Conclusion

After five decades of catalyst research there is slowly emerging a family of discrete late transition metal catalysts that are capable of generating high molecular weight, linear, random copolymers of ethylene and polar comonomers such as acrylates. Further advances in the efficiency of these catalysts will likely give rise to new families of commercial polyolefins with a wealth of new performance properties imparted by the polar groups attached to the polymer backbone.

References

1. Padwa AR (1989) *Prog Polym Sci* 14:811
2. Patil AO, Schulz DN, Novak BM (eds) (1998) *Functional polymers: modern synthetic methods and novel structures*. ACS Symposium Series, vol 704. American Chemical Society, Washington, DC

3. Killian CM (2001) Single site success Chem Eng News 79(43):35–36
4. Boffa LS, Novak BM (2000) Chem Rev 100:1479–1495
5. Ittel SD, Johnson LK, Brookhart M (2000) Chem Rev 100:1160–1205
6. Drent E, van Broekhoven JAM, Doyle MJ, Wong PK (1995) In: Fink G, Muhlhaupt R, Britzinger HH(eds) Ziegler catalysts. Springer, Berlin Heidelberg New York, pp 481–496
7. SRI International (2002) SRI International receives polymer patent portfolios from Shell Oil Company. SRI, Menlo Park, CA www.sri.com/news/releases/07-01-02.html. Last accessed 9 Sept 2008
8. SRI International (2006) SRI International licenses high performance polymer technology to Asahi Kasei Fibers. SRI, Menlo Park, CA <http://www.sri.com/news/releases/101106.html>. Last accessed 9 Sept 2008
9. SRI International (2002) Carilon thermoplastic polymers. SRI, Menlo Park, CA www.sri.com/rd/carilon.pdf. Last accessed 9 Sept 2008
10. McMillan FM (1979) The chain straighteners. Macmillan, London
11. SRI International (2000) Chemical economics handbook 1999. SRI, Menlo Park, CA
12. Ewen J, (1997) Scientific American, May 1997, pp 86–91
13. Hagman, J. F. Crary, J. W. (1985) In: InMark HF, Bikales NM, Overberger CG, Menges G, Kroschwitz JI (eds) In: Encyclopedia of polymer science and engineering, vol 1. Mark, H. F., Bikales, N. M., Overberger, C. G., Menges, G., Kroschwitz, J. I., Eds. Wiley-Interscience:, New York, 1985; Vol. 1, p 325
14. Boor J. (1979) Ziegler–Natta catalysts and polymerizations. Academic, New York
15. Chung TC, Rhubright D (1993) Macromolecules 26:3019
16. (a) Hamada, Y., Machida, S., Amano, J., Asahi, S. (1990) JP Patent 02308803, 21 Dec 21, 1990 to Idemitsu Kosan Co., Ltd., Japan.
17. Tanaka, M, Machida, S. (1988). EP Patent Application 283972, 28 Sept 28, 1988 to Idemitsu Kosan Co., Ltd., Japan
18. Tanaka, M., Machida, S., Uoi, M (1989). U.S. Patent 4833224, 27 June 27, 1989 to Idemitsu Kosan Co., Ltd., Japan.
19. Tanaka, M., Machida, S. (1987) JP Patent 63270709 to Idemitsu Kosan Co., Ltd., Japan, priority date 3 April 3, 1987
20. Novak BM, Hiromitsu T (1999) Polym Mater Sci Eng 80:45.
21. Marques MM, Correia SG, Ascenso JR, Ribeiro AFG, Gomes PT, Dias AR, Foster P, Rausch MD, Chien JCWJ (1999) Polym Sci Part A: Polym Chem 37:2457
22. McLain SJ, McCord EF, Arthur SD, Hauptman E, Feldman J, Nugent WA, Johnson LK, Mecking S, Brookhart M (1997) Polym Mater Sci Eng 76:246–247
23. Bansleben, D. A., Huynh-Tran, T.-C. T., Blanski, R. L., Hughes, P. A., Roberts, W. P., Grubbs, R. H., Hatfield, G. R (1998). WO Patent Application 9950331 to Cryovac, Inc., priority date 31 March 31, 1998
24. Crabtree RH (1988) The organometallic chemistry of the transition metals. Wiley-Interscience, New York, p 51
25. Johnson LK, Killian CM, Brookhart M (1995) J Am Chem Soc 117:6414–6415
26. Goodall BL et-al. (1998) Polym Prepr (Am Chem Soc Div Polym Chem) 39(1):216–217
27. Johnson LK, Mecking S, Brookhart M (1996) J Am Chem Soc 118:267–268
28. Goodall BL (2008) In: Late transition metal olefin polymerization. Wiley, New York (in press)
29. Goodall, B. L (2001)., Encyclopedia of materials:: Science. and Technology., Elsevier Science Ltd., Amsterdam, (2001) 1959–1963
30. Britovsek GJP, Gibson VC, Wass DF (1999) Angew Chem Int Ed 38:429
31. Gibson VC, Spizmesser SK (2003) Chem Rev 103:283–315
32. Haras A, Anderson GDW, Michalak A, Rieger B, Ziegler T (2006) Organometallics 25(19):4491–4497
33. Meinhard D, Wegner M, Kipiani G, Hearley A, Reuter P, Fischer S, Marti O, Rieger B (2007) J Am Chem Soc 129(29):9182–9191
34. Jia L, Yang X, Ishihara A, Marks TJ (1995) Organometallics 14(7):3135–3137

35. McLain SJ, Sweetman KJ, Johnson LK, McCord E (2002) *Polym Mater Sci Eng* 86:320–321
36. Matsumura K, Fukumoto O (1971) *J Poly Sci Part A-1* 9:471–483
37. Popeney CS, Camacho DH, Guan Z (2007) *J Am Chem Soc* 129(33):10062–10063
38. Camacho DH, Salo EV, Ziller JW, Guan Z (2004) *Angew Chem Intl Ed* 43(14):1821–1825
39. Philipp DM, Muller RP, Goddard WA, Storer J, McAdon M, Mullins M (2002) *J Am Chem Soc* 124:10198–10210
40. Michalak A, Ziegler T (2001) *J Am Chem Soc* 123:12266–12278
41. Michalak A, Ziegler T (2001) *Organometallics* 20:1521–1532
42. Younkin TR, Connor EF, Henderson JL, Friederich SK, Grubbs RH, Bansleben DA (2000) *Science* 297:460–462
43. Connor EF, Younkin TR, Henderson JI, Waltman, AW, Grubbs RH (2003) *Chem Commun* 2003:2272–2273
44. Waltman AW, Younkin TR, Grubbs RH (2004) *Organometallics* 23(22):5121–5123
45. Waltman AW, Grubbs RH (2004) *Organometallics* 23(13):3105–3107
46. Waltman AW, Ritter T, Grubbs RH (2006) *Organometallics* 25(18):4238–4239
47. Goodall BL Grubbs RH, and Waltman AW, (2005) (Rohm and Haas Company). U.S. Patent. Application. Publ. Rohm and Haas Company.,(2005), US 2005215738 A1
48. Drent E, van Dijk R, van Ginkel R, van Oort B, Pugh RI (2002) *JCS Chem Commun* 2002:744–745
49. Behr A, Keim W (1985) *Arabian J Sci Eng* 10(4):377–390
50. Allen NT, Goodall BL, and McIntosh LH, (2007) (Rohm and Haas Company). U.S. Patent. Application. Publ. (2007), Rohm and Haas Company., US 20070287627 A1
51. Allen NT, Goodall BL, and McIntosh ,LH (2007) (Rohm and Haas Company). US Patent Application U.S. Pat. Appl. Publ. (2007), Rohm and Haas Company., US 20070049712 A1
52. Luo S, Vela J, Lief JR, Jordan RF (2007) *J Am Chem Soc* 129:8946–8947
53. Weng W, Shen Z, Jordan RF (2007) *J Am Chem Soc* 129:15460–15461
54. Skupov KM, Piche L, Claverie JP (2008) *Macromolecules* 41(7):2309–2310
55. Skupov KM, Marella PR, Hobbs JL, McIntosh LH, Goodall BL, Claverie JP (2006) *Macromolecules* 39(13):4279–4281
56. Allen NT, Goodall BL, Kirk TC, and McIntosh LH, (2008) US Patent (Rohm and Haas Company),. U.S. 7,339,075 B2 (2008)
57. Skupov KM, Marella PR, Simard M, Yap GPA, Allen NT, Conner D, Goodall BL, Claverie JP (2007) *Macromol Rapid Commun* 28(20):2033–2038
58. Stibrany RT, Schulz DN, Kacker S, Patil AO, Baugh LS, Sissano JA, Kacker S, Berluche E, Stibrany RT, Schulz DN, and Rucker SP (2006), US Patent, (Exxon Research and Engineering Co.,). US 6,417,303 B1;.
59. Baugh LS, Sissano JA, Kacker S, Berluche E, Stibrany RT, Schulz DN, Rucker SP (2006) *J Polym Sci Part A: Polym Chem* 44(6):1817–1840
60. Nagel M, Paxton WF, Sen A, Zakharov L, Rheingold AL (2004) *Macromolecules* 37(25):9305–9307
61. Sen A, Borkar S (2007) *J Organometal Chem* 692(15):3291–3299
62. Nagel M, Sen A (2006) *Organometallics* 25(20):4722–4724
63. Tian G, Boone HW, Novak BM (2001) *Macromolecules* 34(22):7656–7663

Recent Progress in Late Transition Metal α -Diimine Catalysts for Olefin Polymerization

Zhibin Guan and Chris S. Popeney

Abstract This chapter reviews recent development of cationic α -diimine nickel(II) and palladium(II) complexes for olefin polymerization. The contributions of ligand structure to the catalytic polymerization properties of late metal complexes are particularly emphasized in this review. Unique among transition metal polymerization systems, these late metal complexes also catalyze the formation of branched polymers. The mechanisms of elemental reaction steps for these catalytic systems are discussed. The Pd(II) system also permits the copolymerization of ethylene and α -olefins with various polar comonomers, especially acrylates. Finally, a discussion of new research in ligand design is provided. A new class of cyclophane-based ligands has exhibited high thermal stability. The mechanism of copolymerizations is significantly altered, leading to elevated incorporations of polar monomers. An axial-donation hemilabile cyclic ligand is also discussed, the Ni(II) and Pd(II) complexes of which afford high molecular weight polyethylene despite their reduced steric bulk.

Keywords Alpha-diimine, Catalyst, Late transition metal, Nickel, Olefin, Palladium, Polymerization, Polyolefins

Contents

1	Introduction	180
2	General Features of Late Transition Metal α -Diimine Polymerization Catalysts	184
2.1	Synthesis of Complexes and Generation of Active Species	184
2.2	Characteristics of Polymerization	186
3	The Polymerization Mechanism	188
3.1	Polymer Chain Growth by Migratory Insertion	188
3.2	Chain Isomerization and Polymer Branching	190
3.3	Chain Transfer	192
3.4	Catalyst Decomposition	193

Z. Guan(✉) and C.S. Popeney
Department of Chemistry, 1102 Natural Sciences II, University of California,
Irvine, CA 92697-2025, USA
e-mail: zguan@uci.edu

4	Functional Group Tolerance and Copolymerization.....	194
4.1	Polymerization of Higher Olefins.....	194
4.2	Other Non-Polar Monomers.....	196
4.3	Catalyst Functional Group Tolerance.....	196
4.4	Polar Monomers.....	197
5	Ligand Design.....	200
5.1	Modification of Substituted α -Diimines.....	200
5.2	Catalysts of Related Nitrogen-Containing Ligands.....	203
5.3	Teraryl-Substituted α -Diimines.....	205
5.4	Catalysts Derived from Cyclic α -Diimine Ligands.....	206
5.5	Hemilabile Axial Donating α -Diimine Ligands.....	212
6	Summary.....	215
	References.....	216

Abbreviations

acac	Acetylacetonato
An	Acenaphthyl
Ar	Aryl
COD	1,5-Cyclooctadiene
<i>t</i> -Bu	<i>tert</i> -Butyl
e ⁻	Electron
Et	Ethyl
<i>i</i> -Pr	Isopropyl
K_{eq}	Equilibrium constant
k_{ins}	Monomer insertion rate constant
k_{trap}	Monomer trapping rate constant
MA	Methyl acrylate
MAO	Methyl aluminoxane
Me	Methyl
M_n	Number-averaged molecular weight
M_w	Weight-averaged molecular weight
NMR	Nuclear magnetic resonance
PDI	Polydispersity index
PE	Polyethylene
Ph	Phenyl
SHOP	Shell high olefin process

1 Introduction

Billions of pounds of polyolefins are produced annually in the world [1]. Through simple insertion reactions, inexpensive and abundant olefins are transformed into polymeric materials for a wide range of applications including plastics, fibers, and elastomers. Despite its long history, the polyolefin industry continues to grow steadily and remains technologically driven because of continuous discovery of

new catalysts, processes, and polyolefin materials with better properties [1]. One exciting direction in this field is to develop new catalytic routes that can transform simple olefin monomers into high value polymeric materials having novel architectures and high functionalities [2].

Transition metal catalysis plays a key role in the polyolefin industry. The discovery by Ziegler and Natta of the coordination polymerization of ethylene, propylene, and other non-polar α -olefins using titanium-based catalysts, revolutionized the industry. These catalysts, along with titanium- and zirconium-based metallocene systems and aluminum cocatalysts, are still the workhorse in the manufacture of commodity polyolefin materials such as polyethylene and polypropylene [3–6].

While it is unlikely that the dominance of early transition metal-based olefin polymerization catalysts will be challenged anytime soon, there are some serious limitations with these systems. Most importantly, these electropositive, strongly Lewis acidic metals are unable to facilitate the general incorporation of polar olefins, such as acrylates, vinyl acetate, vinyl halides, and acrylonitrile. The strong tendency of the early transition metals to preferentially bind to the electronegative atoms of these monomers instead of the olefin moiety prevents migratory insertion into the olefin. Copolymers of polar and non-polar olefins are attractive for their chemical and materials properties [7, 8], so alternative catalytic systems, particularly late transition metal complexes, have received increasing attention because of their better tolerance to polar functional groups.

Catalysts based on nickel that dimerize or oligomerize α -olefins have been known for many years and are commercially valuable. The Shell higher olefin process (SHOP), for example, uses Ni(II) catalysts developed by Keim and co-workers such as **1.1** and **1.2** bearing P–O chelating ligands to oligomerize ethylene into higher olefins in the manufacture of surfactants, lubricants, and fine chemicals (Fig. 1) [9–11]. Late transition metals are more suited for the polymerization of

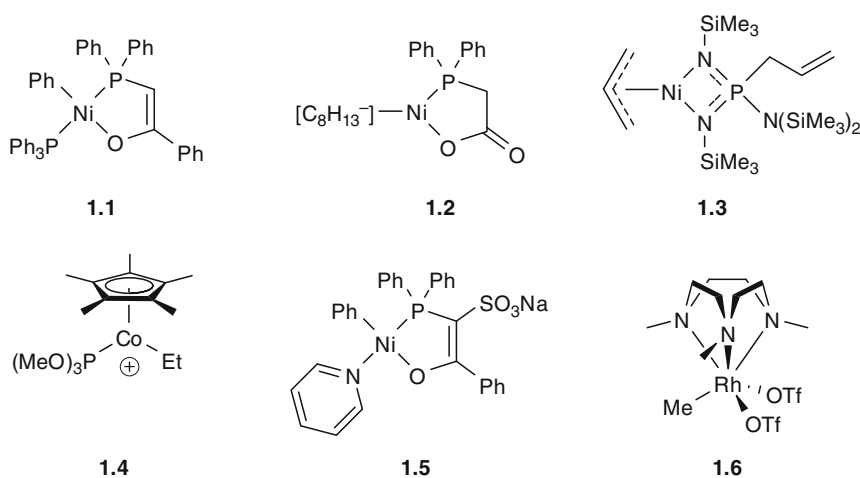


Fig. 1 Early examples of late transition metal olefin oligomerization and polymerization catalysts

polar olefins because of their reduced oxophilicity. Systems based on Pd [12, 13], Ru [14, 15], and Rh [14, 16] have been reported that successfully dimerize acrylates. In contrast to early transition metals, until recently there were few reports of late transition metal catalysts for the polymerization of olefins. This is due to the fact that late metal catalysts generally exhibit lower activities for olefin insertion relative to early metal catalysts, and more importantly, β -hydride elimination typically competes with chain growth. Late transition metals are notorious for their high tendency to undergo β -hydride elimination reactions, a property that has been exploited in synthetically useful processes such as the Pd-catalyzed Heck reaction. However, this reactive tendency of late transition metals has restricted their ability to afford high molecular weight polyolefins because the elimination process is followed by associative chain transfer of the olefin by incoming monomer [9, 10].

Although the majority of early generation late transition metal-based polymerization catalysts afforded linear oligomers or low molecular weight polymers, a few examples of branched polymer formation were noticed. The oligomers and polymers produced from Ni(II) amino-bis-(imino)phosphorane complex **1.3** [17] were found to exhibit uniquely branched microstructures [18]. In contrast, the polyolefins afforded by early transition metal catalysts are remarkably linear and short-chain branches must be introduced by the copolymerization of higher α -olefins. Fink and coworkers proposed a chain isomerization mechanism to explain the occurrence of methyl branches in polymers from their Ni(II) system [18]. A 1,2-metal-hydride shift was believed to take place, leading to migration of the metal along the polymer chain. Chain growth from an internal carbon would therefore lead to a branch in the chain. This chain isomerization process leading to branched polymers from simple monomers is another unique and potentially useful property of late transition metal-based polymerization catalysts because this can potentially provide an efficient route to form branched polymers with different architectures from simple olefins. The relatively low activity of this complex and the low polymer molecular weights of the oligomers and polymers formed, however, hampered further development of this system. This catalyst was recently reexamined by Collins [19], and discrete unsaturated Ni allyl iminophosphorane complexes generated in situ were found to oligomerize, but not polymerize, ethylene.

High molecular weight polyethylene could be produced by a few systems under certain conditions. The SHOP catalysts **1.1** and **1.2**, for example, afforded high molecular weight polymer if hexane, in which the catalyst was poorly soluble, was used as the reaction solvent instead of toluene [20]. Other examples of note include a cobalt-based catalyst **1.4** [21] and a modified SHOP-type catalyst **1.5** bearing a weakly coordinating and displaceable pyridine ligand instead of the typical phosphine ligand [22, 23]. In the latter case, Klabunde and Ittel were able to carry out copolymerizations with polar olefins as long as the polar functionality was distanced from the olefin group to prevent adverse interactions with the metal. Despite these accomplishments, these systems were not particularly active and were unable

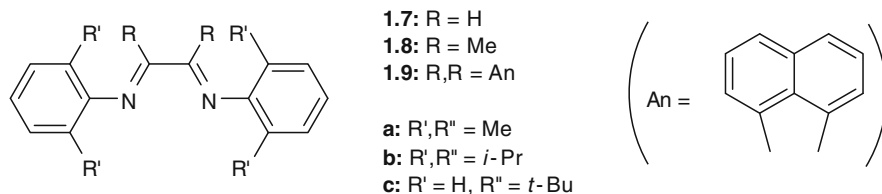


Fig. 2 α -Diimine ligands used in Brookhart's Ni(II) and Pd(II) catalysts

to polymerize higher olefins or effectively copolymerize ethylene with polar olefins under general conditions. However, the catalysts exhibited far higher tolerances to polar additives than early transition metal systems. In a particularly striking example, a rhodium catalyst **1.6** was able to oligomerize ethylene in aqueous suspension, albeit at extremely low activity [24].

In 1995, Brookhart and coworkers discovered that complexes of Ni(II) and Pd(II) bearing chelating nitrogen-based α -diimine ligands (Fig. 2) afforded high molecular weight polymer in high catalytic activity [25, 26]. The Ni(II) catalysts are highly active, rivaling many early metal systems. The Pd(II) catalysts, although of far less activity, afforded highly branched polymers and could both tolerate and incorporate polar olefins [27]. In contrast to the earlier late transition metal systems, which utilized anionic chelating ligands, the diimine ligands were neutral and thus afforded active catalytic species that were cationic in nature. Furthermore, a key insight from Brookhart and coworkers is that the incorporation of sterically bulky axial substituents in the α -diimine ligand is essential in the generation of high molecular weight polymer because the bulky axial substituents dramatically retard the rates of chain transfer [25, 28]. In addition, the high activities of the catalysts were attributed to destabilization of the reactive ground state species by steric interactions with the ligand.

Since Brookhart's seminal discovery, there has been renewed interest in late transition metal-based catalysts, both for the industrial-scale preparation of commodity linear α -olefins and polyolefins, and the development of polymers with more specialized structures and applications [26]. While exciting progress has been made recently in the development of new neutral Ni(II) and Pd(II) catalysts bearing anionic ligands [29–35], this review will concentrate on the research and development of cationic Ni(II) and Pd(II) α -diimine-based polymerization catalysts. Similarly, the Fe(II) and Co(II) complexes with bis(imino)pyridine tridentate ligands [36–38] will not be included in this review, nor will reports of the copolymerization of olefins and carbon monoxide with Pd(II) catalysts, although extensive reviews and other publications on these systems are available, along with more general references [39–41]. Instead, this review will focus on recent investigations on mechanistic details, the reaction scope, and the design of new ligands for the polymerization of olefins using cationic Ni(II) and Pd(II) α -diimine-based complexes.

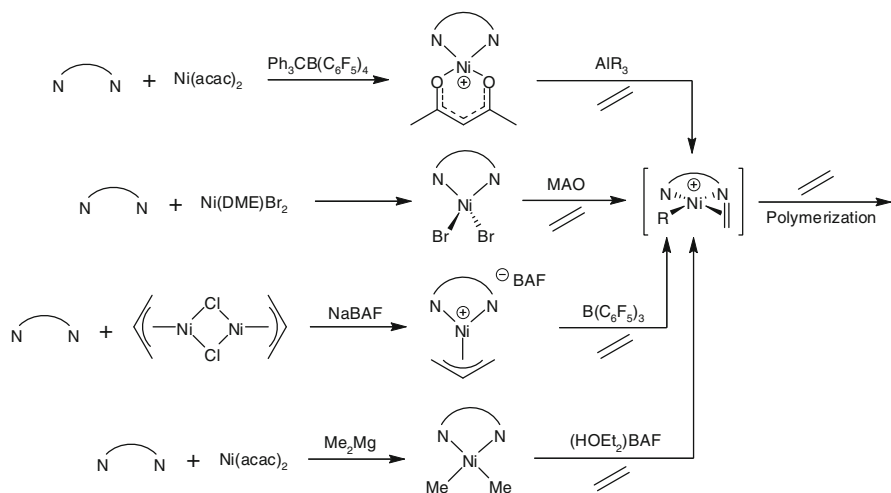
2 General Features of Late Transition Metal α -Diimine Polymerization Catalysts

2.1 *Synthesis of Complexes and Generation of Active Species*

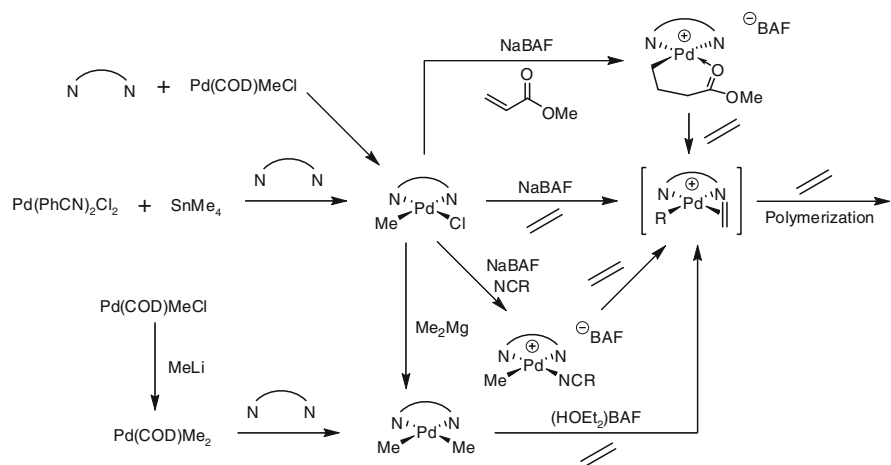
The α -diimine ligands are a versatile class of bidentate ligands used in a variety of transition metal-catalyzed processes. They are chemically stable, good σ -donors and π -acceptors, and exhibit a variety of possible coordination modes [42]. Their effectiveness in organometallic chemistry has also been suggested to result from their rigidity, which increases chelation strength and forces a *cis* ligand geometry [43–45]. Furthermore, their straightforward synthesis by acid-catalyzed condensation of amines with dicarbonyls allows for the preparation of ligands bearing a large variety of functionalities and substitution patterns [46, 47].

The corresponding Ni(II) complexes, most commonly the neutral dibromo adducts (diimine)NiBr₂, are prepared by ligand displacement from Ni(DME)Br₂ (DME = 1,2-dimethoxyethane). The cationic species responsible for polymerization are often generated *in situ* by activation of these neutral, stable, and more readily available precursors. In the case of Ni catalysts, this is frequently performed by treatment of the dibromo complexes with organoaluminum reagents [25], particularly methylaluminumoxane (MAO) [48]. This process is analogous to similar methods used in the activation of early transition metal systems. Presumably, transmetallation occurs with aluminum, doubly alkylating the polymerizing metal which is followed by mono-dealkylation from the metal center to afford a vacant coordination site so that ethylene can bind [5]. Alternatively, the salts of the diamagnetic complex [(diimine)Ni(acac)]⁺(acac = acetylacetonato) are useful precursors that afford active catalysts upon treatment with trialkylaluminum reagents [49]. Similarly, cationic π -allyl complexes also serve as useful catalysts after activation with borane. Cationic precursors, prepared by anionic ligand abstraction by sodium or trityl cation, are advantageous if sterically encumbered α -diimines are to be used. The sodium salt of the anion tetrakis(3,5-bis(trifluoromethyl)phenyl)borate (BAF⁻) is a commonly used halide abstracting reagent for use in the preparation of active catalysts [50, 51]. Bulky, weakly coordinating tetraarylborate counterions such as BAF⁻ and B(C₆F₅)₄⁻ are necessary to achieve high polymerization rates. Although convenient for polymerization procedures, *in situ* catalyst generation involves complex mixtures that are not easily studied. Instead, well-defined active species, for small-scale or mechanistic work, can be prepared by protonolysis of dialkylnickel complexes with one equivalent of Brønsted acid [25]. A summary of activation procedures is given in Scheme 1. In any case, active monoalkyl [(diimine)NiR(olefin)]⁺ complexes are presumed to be the active species for polymerization.

In contrast to Ni, alkylpalladium precursors can be easily prepared and isolated owing to their greater stability (Scheme 2). The monomethyl chloride adducts of formula (diimine)PdMeCl can be conveniently synthesized via diimine displacement of other weakly coordinating ligands, such as COD from Pd(COD)MeCl (COD = 1,5-cyclooctadiene) [44], or by *in situ* alkylation-complexation with tetramethyltin [52]. The chloride ligand can then be cleanly abstracted by metathesis with NaBAF



Scheme 1 General routes to the preparation and activation of Ni(II) polymerization catalysts



Scheme 2 General routes to the preparation and activation of Pd(II) polymerization catalysts

or silver(I) salts to permit the *in situ* activation for polymerization. Preactivated complexes for preparatory-scale Pd(II)-catalyzed polymerization synthesis include the acetonitrile adduct $[(\text{diimine})\text{PdMe}(\text{NCMe})]^+$, which can also be prepared in one pot by reaction of diimine, Pd(COD)MeCl, and NaBAF [53]. Formed by the addition of methyl acrylate, the ester chelate $[(\text{diimine})\text{PdMe}((\text{CH}_2)_3\text{C}(\text{O})\text{OCH}_3)]^+$ is stable enough for long term storage [27]. Both of these cationic complexes only require addition of olefin to initiate polymerization. For mechanistic studies, the dimethyl complexes can be employed, which are available by several preparative routes [53]. As with the nickel analogs, these are activated by the addition of acid.

2.2 Characteristics of Polymerization

The branched polymers produced by the Ni(II) and Pd(II) α -diimine catalysts shown in Fig. 3 set them apart from the common early transition metal systems. The Pd catalysts, for example, are able to afford hyperbranched polymer from a feedstock of pure ethylene, a monomer which, on its own, offers no predisposition toward branch formation. Polymer branches result from metal migration along the chain due to the facile nature of late metals to perform β -hydride elimination and reinsertion reactions. This process is similar to the early mechanism proposed by Fink briefly mentioned above [18], and is discussed in more detail below. The chain walking mechanism obviously has dramatic effects on the microstructure, or topology, of the polymer. Since β -hydride elimination is less favored in the Ni(II) catalysts compared to the Pd(II) catalysts, the former system affords polymer with a low to moderate density of short-chain branches, mostly methyl groups.

The structure of the α -diimine ligand has an enormous effect on the nature of the polymerization. Indeed, both the high activity of α -diimine catalysts and the high molecular weight polymers they produce compared to other late transition metal systems is attributed to the bulky nature of the ligands. This has been shown by theoretical studies to destabilize the catalytic ground state and accelerate the monomer insertion process, leading to high catalytic activity [54, 55]. Furthermore, the ligands restrict monomer access to the axial coordination sites of the metal, greatly retarding the rate of chain transfer and allowing for high molecular weight polymer [25].

The identity of the *ortho*-alkyl substituents on the diimine aryl rings has a significant effect on polymer properties. In the Ni(II) system, a large increase in polymer molecular weight occurs as the *ortho*-alkyl substituent increases in size (Table 1). Catalysts **1.10b**, **1.11b**, and **1.12b**, bearing isopropyl groups in this position all afford higher molecular weight polymer than the corresponding methyl-substituted catalysts **1.10a**, **1.11a**, and **1.12a**. A dramatic increase in polymerization activity can also be discerned. The analogous trends are also exhibited in the Pd(II) catalysts (Table 2), with catalysts bearing isopropyl substitution (**b**) again giving higher molecular weight polymer than the corresponding methyl-substituted catalysts (**a**). The bulkiness of α -diimine ligands has been quantified using a Rh(I) oxidative addition system, where the *ortho*-alkyl substituents have a predictable influence on reactivity [56].

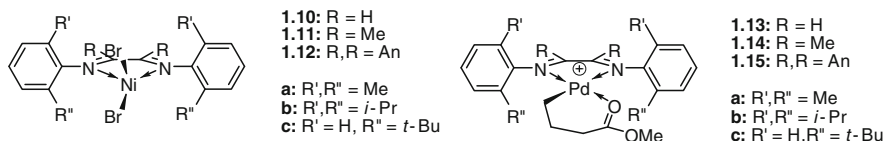


Fig. 3 Ni(II) and Pd(II) complexes used for ethylene polymerization

Table 1 Polymerization results for the Ni(II) complexes/MAO^a

Entry	Complex	<i>T</i> (°C)	C ₂ H ₄ pressure	TOF ^b (× 10 ⁻³ h ⁻¹)	<i>M</i> _n ^c (kg mol ⁻¹)	<i>M</i> _w / <i>M</i> _n ^c	<i>B</i> ^d	<i>T</i> _m ^e (°C)	Reference
1	1.10a	0	1 atm	14.3	43	2.5	1.2	132	[17]
2	1.10b	0	1 atm	218	110	2.7	7.0	129	[17]
3	1.11a	0	1 atm	64.2	170	2.6	20	115	[17]
4	1.11b	0	1 atm	107	520	1.6	48	109	[17]
5	1.12a	35	200 psi	1620	59.2	2.5	13	128	[20]
6	1.12a	60	200 psi	900	22.8	2.3	25	114	[20]
7	1.12a	85	200 psi	150	12.9	2.9	44	90, 114	[20]
8	1.12b	0	1 atm	29.4	170	2.3	74	97	[17]
9	1.12b	35	1 atm	56	125	1.8	106	-17	[20]
10	1.12b	35	200 psi	2400	337	1.8	24	110	[20]
11	1.12b	60	200 psi	1380	155	1.8	58	68	[20]
12	1.12b	85	200 psi	420	62.7	1.9	83	24	[20]

^aPolymerization conditions: 1000 equivalents MAO per Ni

^bTurnover frequency (moles of ethylene polymerized per mole of Ni per hour)

^cDetermined by size exclusion chromatography with polystyrene standard in 1,2,4-trichlorobenzene

^dBranching density per 1000 carbons determined by ¹H NMR

^eMelting temperature of crystalline domains determined by differential scanning calorimetry

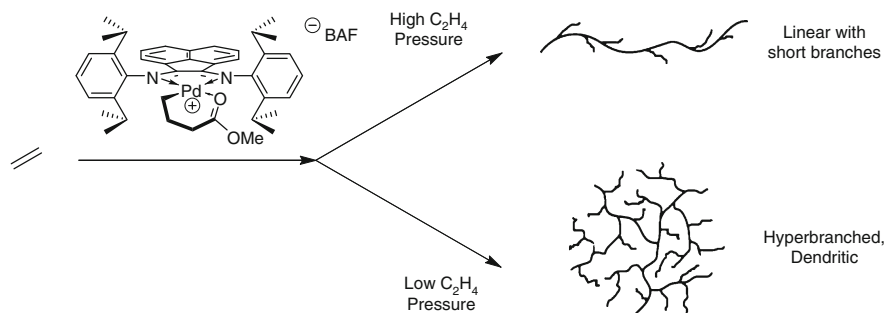
Table 2 Polymerization results for the Pd(II) complexes^a

Entry	Complex	C ₂ H ₄ pressure (atm)	TOF (h ⁻¹)	<i>M</i> _n ^b (kg mol)	<i>M</i> _w / <i>M</i> _n ^b	<i>B</i>	Reference
1	1.13b	1	144	0.6	3.0	116	[17]
2	1.14a	11	720	445, 28	bi. ^c	106	[47]
3	1.14b	2	1630	297	3.5	102	[19]
4	1.14b	11	2630	490	2.7	100	[47]

^aPolymerization conditions: 25 °C

^bDetermined by size exclusion chromatography with polystyrene standard in 1,2,4-trichlorobenzene^c-Bimodal distribution

A noticeable trend in molecular weight and polymerization activity is also observed upon changing the groups on the diimine backbone. The respective Ni(II) and Pd(II) catalysts bearing the methyl-substituted diimine ligand, **1.11** and **1.14**, afford polymer of higher molecular weight in higher activity than the catalysts bearing the cyclic acenaphthyl diimine backbone, **1.12** and **1.15**. From X-ray diffraction measurements of the Pd(II) complexes [53], steric repulsion of the methyl groups on the backbone forces the aryl rings into a concave shape, narrowing the N–Pd–N bite angle, and increasing the steric crowding of the metal coordination plane. In contrast, the cyclic acenaphthyl backbone in the latter case holds the aryl rings away from the metal, reducing steric interactions [47]. The Ni(II) catalysts **1.10** and Pd(II) catalysts **1.13** exhibiting the unsubstituted backbone produce polymer of the lowest molecular weight.



Scheme 3 Control of polymer topology by modification of ethylene pressure in polymerizations with Pd(II) catalyst

The Pd(II) system undergoes extensive chain walking that results in heavily branched or even hyperbranched polymers with long chain branch-on-branch structures. We have shown that the conditions of polymerization have a strong effect on the overall structure of the polymer [2, 57–59]. While the branching density remains relatively independent of ethylene pressure (concentration), the length and placement of the branches changes drastically. At low ethylene pressure, chain walking is not interrupted by trapping by ethylene, allowing the metal to migrate large distances between insertions. Hyperbranched or even dendritic polymers are produced. Under conditions of high ethylene pressure, however, rapid trapping by ethylene leads to less chain walking, and a polymer that is linear with relatively short branches results. This phenomenon is represented in Scheme 3.

3 The Polymerization Mechanism

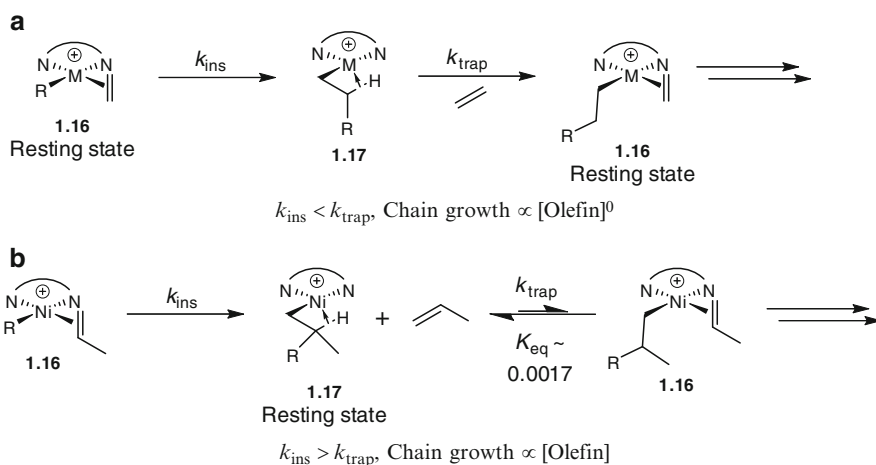
The Brookhart laboratory has contributed much of the knowledge of the polymerization mechanism for the late transition metal α -diimine catalysts. The review by Ittel provides a concise summary of the mechanistic understanding as of the year 2000 [26]. Some of the early findings will be reviewed here and additional insights reported afterward will be presented. In addition to the experimental work, many theoretical and computational studies worthy of discussion have also been carried out. These efforts have been most important in providing insight into the mechanistic details of the highly reactive nickel system, which is often difficult to study experimentally.

3.1 Polymer Chain Growth by Migratory Insertion

Polymerization occurs by repeated migratory insertion of olefin into the *cis*-oriented metal–carbon bond by the generally accepted Cossee mechanism [5, 60]. This mechanism is believed to be shared by all transition metal coordination polymerization

catalysts (apart from the ring-closing metathesis systems), including the early metal systems for which it was first proposed. Two different species make up the catalytic cycle: an alkyl olefin complex **1.16** and an alkyl agostic complex **1.17**. Insertion of olefin into the M–C bond of **1.16** results in a coordinatively unsaturated $14e^-$ complex **1.17** bearing a new alkyl group with a main chain length that is two carbon atoms longer than before. As was recently proposed computationally for early metals [61], this unsaturated intermediate **1.17** has been shown by low temperature NMR investigations to exist as a β -agostic complex in late metal systems [53, 62, 63]. In the presence of free monomer, the Pd(II) catalyst exists almost entirely as the alkyl olefin complex **1.16**, which serves as the catalyst resting state (Scheme 4a) [25, 62]. The Ni(II) system was found to be somewhat more complicated since the nature of the lowest energy intermediate depended on the size of the olefin. The alkyl ethylene Ni(II) complex was observed as a resting state, although only agostic species could be identified in reactions involving propylene and larger α -olefins (Scheme 4b) [62]. For systems in which the alkyl olefin complex is most stable, the insertion step is rate-limiting and the polymerization growth rate is largely independent of olefin concentration. Low ethylene polymerization activity of the Ni(II) catalyst at low pressure is attributed to mass transport limitations [28]. The Ni(II)-catalyzed polymerization of α -olefins, however, is first order in olefin concentration and is thus far slower than the corresponding ethylene polymerization, reflecting the rate-limiting trapping step.

Ethylene polymerization by Ni(II) α -diimine catalysts is over 1000 times more active than that of the analogous Pd(II) catalysts [25]. The respective barriers for migratory insertion have been determined by ^1H NMR analysis at low temperature and reflect the polymerization rate difference. While the barrier to ethylene insertion

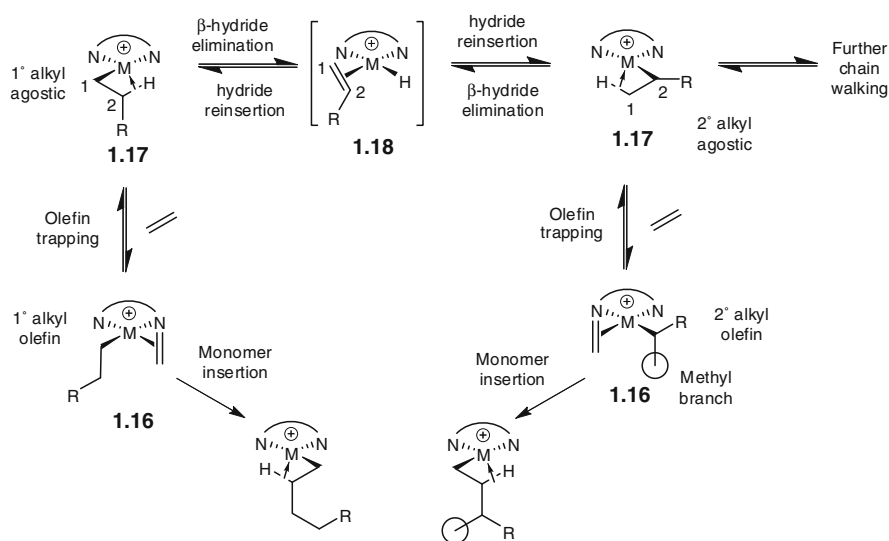


Scheme 4 Mechanism of chain growth for **a** all Pd(II) polymerizations and ethylene polymerizations with Ni(II), and **b** α -olefin polymerizations with Ni(II). Specific kinetic data shown for Ni catalyst **1.15b** [63]

for the Pd(II) catalyst derived from **1.15b** was 16.9 kcal mol⁻¹, the barrier to insertion for the analogous Ni(II) catalyst derived from **1.12b** was 13.5 kcal mol⁻¹ [62]. Continuing the trend, platinum, as the heaviest group 10 metal, is inactive toward insertion under normal conditions. For both Ni and Pd, insertion rates increase as ligand steric bulk increases. Computational work by Ziegler and Morokuma have shown that the decrease in insertion barrier for more bulkier ligands is due to destabilization of the alkyl olefin ground state [54, 64, 65]. Going from *ortho*-methyl to *ortho*-isopropyl substitution results in a 0.6 kcal mol⁻¹ decrease in the migratory insertion barrier in the case of Pd(II) [53], while the Ni(II) system is similarly perturbed with a 0.5 kcal mol⁻¹ decrease [66]. The insertion of ethylene into secondary alkyls is faster than it is into primary alkyl groups for Pd, but the situation is opposite for Ni.

3.2 Chain Isomerization and Polymer Branching

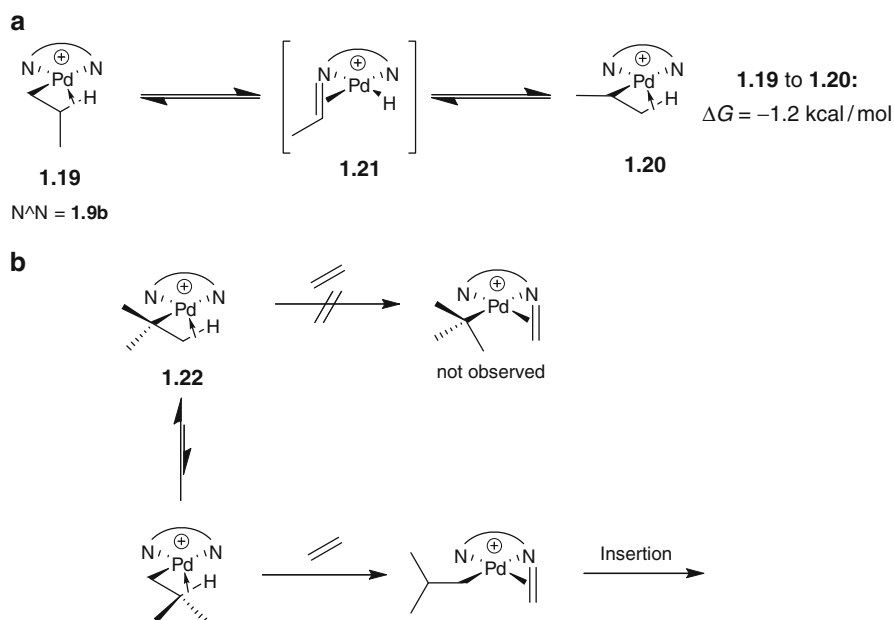
One of the most defining characteristics of the late metal α -diimine polymerization systems is the uniquely branched polyolefins that they afford. This arises from facile β -hydride elimination that late transition metal alkyl complexes undergo. The characteristics of the isomerization process have been the subject of much investigation, particularly with the more easily studied Pd(II) α -diimine system. The process is initiated by β -hydride elimination from the unsaturated alkyl agostic complex **1.17**, followed by hydride reinsertion into olefin hydride intermediate **1.18** in a non-regioselective manner (Scheme 5). In doing so, the metal center may migrate



Scheme 5 The chain walking process. The formation of a methyl branch is shown

one carbon along the chain. The process may repeat many times over before the agostic intermediate is trapped by olefin and insertion resumes again.

The Pd(II) catalysts afford more heavily branched polymer with longer branch lengths and more branch-on-branch occurrences than the Ni(II) catalysts because of more competitive rates of the chain walking process as compared to migratory insertion [57]. The strong tendency of Pd to undergo rapid and reversible β -hydride elimination and reinsertion leads to the extensive chain walking observed. Fine mechanistic studies of Pd(II) propyl agostic species have determined that isomerization from the *n*-propyl complex **1.19** to the isopropyl agostic species **1.20** via propylene hydride intermediate **1.21** (Scheme 6a) is accompanied by a barrier of only 10.7 kcal mol⁻¹, far smaller than the barrier to migratory insertion [53]. Experimental [67] and theoretical studies [55] suggest that the β -hydride elimination step is extremely rapid, with a calculated barrier of just over 8 kcal mol⁻¹, less than the overall isomerization barrier. In fact, metal–carbon bond rotation in the agostic species is believed to proceed more slowly than elimination and reinsertion [63]. Furthermore, the elimination/reinsertion cycle has been proposed to proceed in a nearly concerted manner. Although often depicted as a true intermediate, the mediating olefin hydride complex **1.18** can undergo hydride reinsertion with energy barriers less than 1 kcal mol⁻¹ [55], meaning its existence is extremely short-lived and transition state-like.



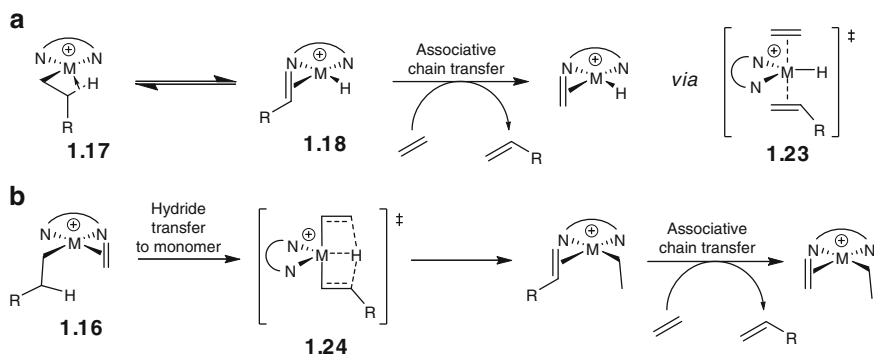
Scheme 6 a Isomerization of β -agostic propyl complexes **1.19** and **1.20**. b Isomerization and trapping by ethylene of *tert*-butyl complex **1.22**, showing unfavorability of ethylene complexation to 3° agostic complexes

Further studies of Pd(II) alkyl agostic complexes have provided more insight into the details of polymer chain walking. In propyl and larger alkyl agostic complexes, isomers with Pd bound to an internal carbon were more stable, most likely due to stabilization of the partial double bond-character between the α and β carbons by alkyl substituents [53]. As a result, there exists a thermodynamic tendency for the metal to walk away from chain ends and to the middle of branches. In addition, a *tert*-butyl agostic complex **1.21** was observed but failed to undergo ethylene insertion, indicating that the metal may walk through a tertiary carbon but not insert into one (Scheme 6b) [63]. This agrees with polymer microstructure analysis, which confirmed the absence of quaternary carbons by ^{13}C NMR. Lastly, migratory insertion of ethylene into 2° metal alkyl bonds was faster than into primary metal alkyls [63]. Therefore, the tendency for insertion to occur in the middle of branches or the main chain, resulting in further branching, also exists. The extensive branching of polymers prepared by the Pd(II) α -diimine catalysts, as well as their branch-on-branch nature, can thus be explained mechanistically.

The isomerization process for the Ni(II) catalysts has been modeled theoretically and determined experimentally. As with the palladium system, computational investigations have suggested that isomerization in the Ni(II) system is also concerted and occurs without formation of a discrete olefin hydride intermediate **1.18** [54, 55]. The barrier to hydride elimination was also calculated to be significantly higher for Ni than Pd (14 kcal mol $^{-1}$ instead of \sim 5 kcal mol $^{-1}$) [65], which is in good agreement with experimental results (16 kcal mol $^{-1}$) [66]. Furthermore, although the addition of steric bulk had little effect on the branching densities of polymers from Pd catalysts, a clear trend of increased polymer branching in Ni catalysts with bulkier substituents was observed [28]. The Ni(II) system was also far more sensitive to monomer concentration in this respect. Polymer branching density was substantially reduced at high ethylene concentrations due to fast trapping of the alkyl agostic complexes [66].

3.3 Chain Transfer

The presence of steric bulk on the α -diimine ligand clearly promotes the formation of high molecular weight polymer by suppression of chain transfer processes. Chain transfer is normally believed to proceed via associative ligand substitution of the olefin-terminated polymer by ethylene from the olefin hydride complex **1.18**. As previously mentioned, however, the olefin hydride intermediate has been determined theoretically to be a transient species, or even a transition state, in the chain isomerization process [54]. In response, a concerted chain transfer mechanism was proposed to occur via hydrogen transfer between the alkyl olefin resting state **1.16** and incoming monomer. Both processes are expected to proceed through similar, 5-coordinate transition states **1.23** and **1.24** that should be disrupted substantially

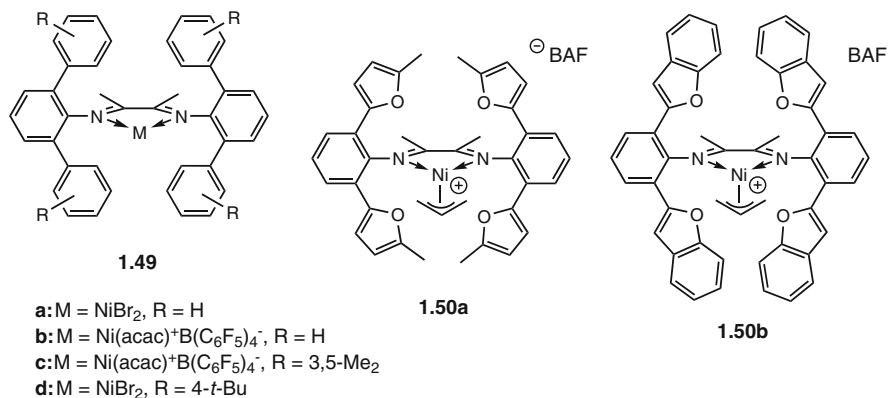


Scheme 7 **a** Chain transfer through associative olefin displacement via hydride complex **1.18**. **b** Chain transfer by concerted hydride transfer from alkyl to monomer via transition state **1.24**. Note the similarity in the structures of **1.23** and **1.24**

by the presence of ligand axial steric bulk (Scheme 7) [64, 65]. Therefore, experimental results to date have not conclusively favored one mechanism over the other [63], although associative exchange from the olefin hydride complex has been proposed to be dominant in the Pd system [55].

3.4 Catalyst Decomposition

Unlike many early transition metal polymerization catalysts, the late transition metal α -diimine systems are prone to deactivation under comparatively mild conditions via pathways that are still not well understood. The better characterized Pd(II) system has yielded some insight into potential modes of deactivation. Studies by Brookhart indicate that these catalysts undergo C–H activation with alkyl groups on the diimine ligand to form palladacyclic intermediates, which have been observed by NMR [53]. A free coordination site on the metal, normally introduced by the loss of a weakly coordinating ligand, is required for this process. Accessibility of the ligand alkyl groups to the metal coordination plane is also necessary. Catalysts bearing *ortho*-dimethyl groups, for example, are catalytically active for days at room temperature while catalysts bearing larger diisopropyl groups are less stable. Increasing the steric bulk on the diimine backbone was also shown to reduce the rate of decomposition, presumably by inhibiting rotation of the aryl moieties into the metal coordination plane. For *ortho-tert*-butyl-substituted complexes: for example, complex **1.26c**, bearing the acenaphthyl backbone undergoes faster C–H activation than complex **1.25c**, bearing the dimethyl-substituted backbone (Scheme 8). The facility of ligand C–H activation plays an important role in the stability of the Pd(II) catalysts. The palladacycles can insert ethylene, so additional unknown processes must occur after C–H activation to result in complete deactivation. The observation



Scheme 8 Ligand C–H activation at the *ortho-tert*-butyl substituents to afford palladacycles **1.27c** and **1.28c** [53]

of palladium black in the polymerizing mixture is a general occurrence with catalyst decomposition, so reduction of the metal takes place by some means.

There has been little insight into potential decomposition pathways for the Ni(II) system due to sparse experimental evidence. Polymerization results with catalysts bearing different alkyl and fluorinated substituents have suggested that a C–H activation process analogous to that occurring with the Pd(II) catalysts is unlikely with Ni(II) [28]. Instead, side reactions between Ni and the aluminum coactivator, present as it is in such large excess, have been implicated. The formation of nickel dialkyl species and their subsequent reductive elimination to Ni(0) is one possible deactivation mechanism [68].

4 Functional Group Tolerance and Copolymerization

4.1 Polymerization of Higher Olefins

The α -diimine Ni(II) and Pd(II) catalysts were the first late metal systems to homopolymerize α -olefins, although activities are lower overall than ethylene polymerization. For the polymerization of propylene by the Pd(II) system, chain propagation is limited by reduced migratory insertion rates compared to ethylene [25, 69]. In contrast, the slower trapping rate of propylene leads to its lower polymerization rate as compared to ethylene in the Ni(II) system [62]. As mentioned above, the alkyl agostic intermediate **1.17** is the resting state for Ni-catalyzed α -olefin polymerizations, making chain growth process overall first order in olefin concentration.

In addition to the unique insertion kinetics, the polymerization of α -olefins by the Ni(II) catalysts affords polymers of narrow molecular weight distributions at low temperature. At -10 °C, chain transfer becomes reduced to the extent that polymerizations are living with polydispersities below 1.10 (Table 3) [70]. This was

verified by a linear increase of molecular weight with polymerization time and through the assembly of block copolymers of various higher olefins. Similarly, the Pd(II) catalysts afford living polymerization of ethylene below 5 °C [71], and can also afford block copolymers with α -olefins [72].

Unlike ethylene, α -olefins insert slowly into secondary Ni or Pd alkyl bonds, meaning the metal must walk to the end of the branch before the next insertion [25, 70]. As a result, insertion of these monomers only occurs at the end of branches to give rise to polymers of significantly reduced branching densities than would be predicted in the absence of chain walking. In the polymerization of propylene, for example, branching densities are significantly below the expected value of 333 per 1000 carbon atoms without chain walking. The regiochemistry of α -olefin insertion also affects the branching density and the polymer topology. In a 1,2-insertion into propylene, for example, affording a primary metal alkyl, a methyl branch will be placed on the polymer backbone (Scheme 9). Because a sizeable fraction of olefin

Table 3 Polymerization of α -olefins by Ni(II) catalysts **1.12b** and **c** from [48]^a

Entry	Complex	Olefin ^b	<i>T</i> (°C)	TOF (h ⁻¹)	<i>M_n</i> ^c (kg mol ⁻¹)	<i>M_w</i> / <i>M_n</i> ^c	<i>B</i>
1	1.12b	P	23	3000	190	1.44	272
2	1.12b	P	-10	2500	160	1.13	297
3	1.12b	H	-10	530	44	1.09	135
4	1.12b	O	0	180	45	1.09	50
5	1.12c	P	23	1300	60	1.59	159
6	1.12c	P	-10	660	36	1.27	214
7	1.12c	H	-10	260	26	1.15	118
8	1.12c	O ^d	-10	25	19	1.14	39 ^e

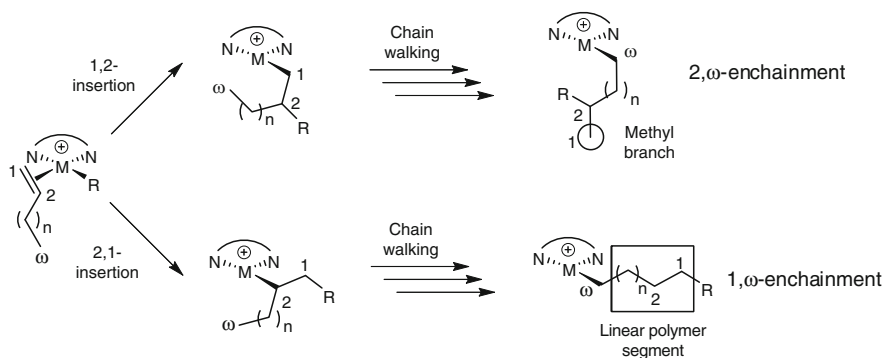
^aPolymerization conditions: 100 equivalents of MAO or MMAO per Ni; time 60 min; solvent toluene, 50 mL total volume

^bP propylene at 1 atm, H 1-hexene at 0.8 M, O 1-octadecene at 0.3 M

^cDetermined by size exclusion chromatography with polystyrene standard

^dPolymerization time 120 min

^eMelting temperature of 60 °C observed



Scheme 9 Modes of catalyst enchainment in polymerizations of α -olefins as a result of 1,2- or 2,1-insertion

is inserted in a 2,1 fashion, the metal will walk to the chain end before the next insertion without forming a branch in the polymer. This “chain straightening” process can lead to highly linear polymer, especially from long chain α -olefins [70]. In the copolymerization of α -olefins with ethylene, many of the restrictions of α -olefin insertion may be overcome by the insertion of ethylene instead. Branching densities in copolymers are higher than in the α -olefin homopolymers.

4.2 Other Non-Polar Monomers

With few exceptions, dienes and styrenes do not undergo polymerization because of the stable allyl or benzyl complexes that result after insertion. A similar process also involving the formation of π -allyl complexes was shown to prevent the polymerization of alkynes by Pd(II) α -diimine catalysts [73]. Polymerization can be carried out if a suitable distance or blocking group lies between the two unsaturated groups so the metal is not able or unlikely to interact with both [26]. Osakada and coworkers, for example, reported the successful Pd(II)-catalyzed homopolymerization [74] and copolymerization [75] of cyclic diallylmalonates possessing a 1,6-heptadienyl moiety and a blocking quaternary carbon in the 4-position. The two olefins insert consecutively to afford a polymer with *trans*-1,2-substituted five-membered rings in the main chain in controllable stereoregularity. The effectiveness of polymerization of internal acyclic olefins, while possible, is isomer-dependent. The Pd(II) catalyst polymerizes *trans*-2-butene at a higher rate than the *cis* isomer, albeit at overall low activities [76]. This reactivity preference is exaggerated greatly in the Ni(II) system, which is quite active in the polymerization of *trans*-2-butene but inert toward the *cis* isomer, mostly because of its low binding affinity [77].

4.3 Catalyst Functional Group Tolerance

The cationic nickel catalysts are sensitive to water and especially to oxygen, and thus require the exclusion of air for effective polymerization. The Ni(II) α -diimine system is also intolerant to polar monomers in general. Exceptions to this include monomers in which the polar functionality is well removed from the olefin, as discussed below. The aluminum coactivator, usually present in large excess, can act as a scavenger of species that might otherwise react detrimentally with the metal, such as residual water. In contrast, the neutral nickel catalysts exhibit far higher tolerance to polar environments, with polymerizations in water and CO₂ possible [78, 79].

The cationic palladium α -diimine catalysts exhibit superior functional group tolerance compared to their nickel counterparts. The catalyst is not significantly inhibited by the presence of weakly Lewis-basic functionalities like esters and ethers. As a particularly striking example of the tolerance of the Pd(II) catalyst, Mecking and coworkers have carried out the emulsion polymerization of ethylene in water [80, 81]. The catalyst is protected within the polymer emulsion from water attack and exhibits

only a slight activity decrease compared to polymerizations in organic solvent. In a homogeneous water–acetone solution, however, the catalyst decomposes upon addition of ethylene [82], presumably by protonolysis of the palladium alkyl bond [83] or, more likely, a Wacker-type process [84]. Nitrogen-containing functional groups are less tolerated and inhibit polymerization by competitive binding.

4.4 Polar Monomers

In order to incorporate polar-functionalized olefins, the catalyst system must exhibit tolerance to the functionality as described above. Therefore, polar monomer incorporation by the Ni(II) catalysts is generally not observed. Traces of methyl acrylate can be incorporated by the Ni(II) catalyst only under low loadings of that monomer [85]. Acrylamide has been incorporated after prior treatment with triisobutylaluminum to block the amide donor sites, although polymerization activities are still relatively low [86]. A similar “protection” of Lewis-basic functionalities by the coactivator has been cited to explain the copolymerization of certain monomers by early transition metal systems as well [40].

The cationic Pd(II) catalysts exhibit effective copolymerizations of ethylene and other α -olefins with polar-functionalized comonomers, with the majority of insertions occurring at the ends of branches. Among the best tolerated monomers are those bearing fluorine or oxygen-containing functionalities, such as esters, ketones, and ethers. The copolymerization of ethylene and acrylates, attractive because the monomers are inexpensive and the copolymers exhibit unique physical properties, has been well-studied mechanistically [27, 69]. Examples of copolymerizations of ethylene and α -olefins with methyl acrylate are shown in Table 4. In general, the amount of comonomer incorporation varies linearly with its reaction concentration and

Table 4 Copolymerizations of ethylene and α -olefins with methyl acrylate (MA) by Pd(II) α -diimine catalysts^a

Entry	Complex	Olefin (conc) ^b	MA conc. (M)	TON		MA (mol%)	M_n^c (kgmol ⁻¹)	M_w/M_n^c	Reference
				E, P, H	MA				
1	1.13b	E (6 atm)	5.8	355	19	5.0	0.3	n/a	[19]
2	1.14a	E (6 atm)	5.8	542	90	14.2	7	2.1	[47]
3 ^d	1.14a	H (1.7 M)	1.1	343	87	20.3	26	1.5	[47]
4	1.14b	E (2 atm)	0.6	7710	78	1.0	88	1.8	[19]
5	1.14b	E (2 atm)	5.8	455	63	12.1	11	1.6	[19]
6	1.14b	E (6 atm)	5.8	3560	148	4.0	42	1.8	[19]
7	1.14b	P (6 atm)	0.6	1179	13	1.1	37	1.8	[19]
8 ^d	1.14b	H (1.6 M)	1.2	187	22	10.3	24	1.6	[47]
9	1.15b	E (6 atm)	5.8	364	18	4.7	10	1.8	[19]

^a Polymerization conditions: temperature 35 °C; time 18.5 h; solvent CH₂Cl₂, 100 mL total volume

^b TON turnover number, E ethylene, P propylene, H 1-hexene

^c Determined by size exclusion chromatography with polystyrene standard

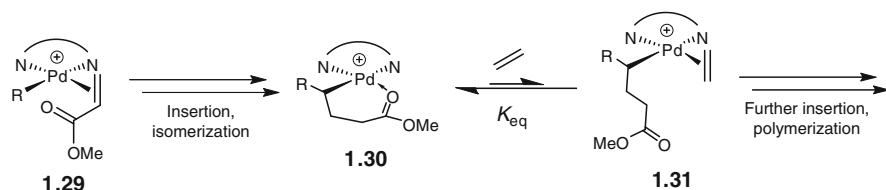
^d Temperature 25 °C

inversely to the ethylene pressure (compare entries 4, 5, and 6) [69]. Typical methyl acrylate incorporations achieved in copolymerizations with ethylene can be as high as 10%. The presence of sterically bulkier groups on the ligand suppresses the binding of olefins larger than ethylene (entries 3 and 4). Measurement of ethylene and acrylate insertion rates as well as the olefin complexation equilibria has been performed by low temperature NMR mechanistic analysis [69]. Because the monomer–metal complexes equilibrate rapidly relative to the insertion rates, the incorporation follows Curtin–Hammett kinetics. The percentage of electron-deficient acrylates in copolymers tends to be low, despite their faster insertion rates compared to ethylene, because of their relatively low binding strength. Higher acrylate incorporations can be achieved in copolymerizations with bulkier α -olefins because acrylate complexation can then be competitive (compare entries 4 and 8).

Unfortunately, catalyst activity is markedly suppressed by the incorporation of some comonomers such as acrylates. Following insertion of methyl acrylate, the catalyst has been shown to isomerize to form a stable six-membered ring chelate **1.30** (Scheme 10), the unfavorable opening of which is required for further chain growth [69]. The weakly binding acrylates are unable to reinitiate polymerization by chelate opening, preventing acrylate homopolymerization. Furthermore, opening of the chelate by α -olefins is less favorable than by ethylene, so activities for α -olefin-acrylate copolymerizations are even lower. In accordance with deactivation by chelate formation, polymerization of a fluorinated acrylate proceeds with far more productivity due to the reduced Lewis basicity of the carbonyl group [27].

A range of comonomers bearing interesting and potentially useful functionalities have been copolymerized with ethylene by the Pd(II) catalysts with varying efficiencies. The system also retains its ability to afford polymer of variable topology in the copolymerization with ethers, esters, epoxides, and siloxy groups [87]. As in the copolymerization of acrylates, a loss of activity may be observed, depending on the ability of the polar functionality to interact with the metal after insertion. Free hydroxyl groups deactivate the catalyst. Small ether groups can competitively bind to the metal or be eliminated to induce catalyst deactivation. The bulky *tert*-butyldiphenylsilyl group can effectively mask hydroxyl moieties so that they exhibit no inhibitory behavior on polymerizations.

The β -alkoxy elimination pathway is important during the incorporation of oxygen-containing monomers. Therefore, it is often necessary to provide distance between the olefin and the polar group, or to prevent chain walking close to the group that can be eliminated by the placement of a quaternary carbon spacer [87]. The incorporation of acrolein dimethyl acetal is accompanied by reduced activity and full catalyst

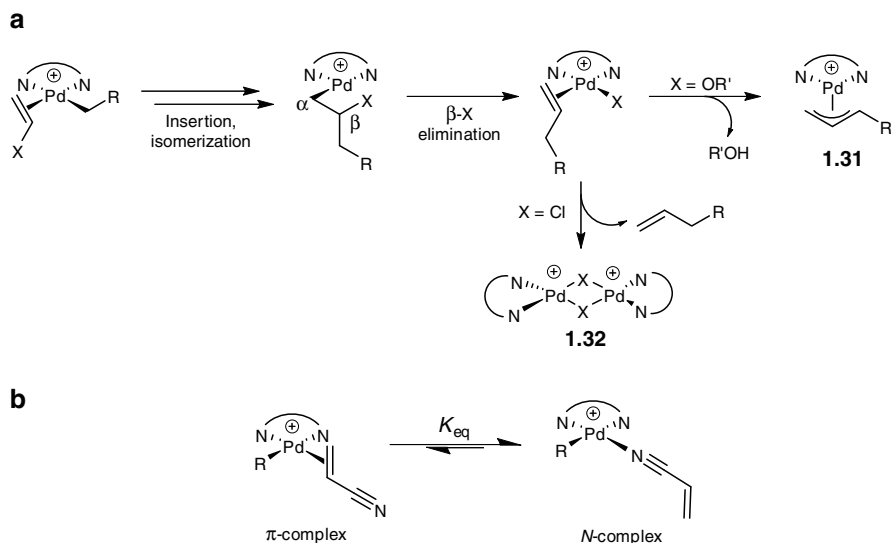


Scheme 10 Activity reduction in ethylene-methyl acrylate copolymerizations due to the formation of stable chelate **1.30**

deactivation after 20 h [88]. This was believed to occur by methoxy elimination to afford a stable allyl complex **1.31**; however, the rate of elimination could be slowed by the addition of methanol. Alkyl vinyl ethers typically undergo cationic polymerization initiated by the cationic Pd(II) center. Silyl vinyl ethers, however, can be copolymerized with 1-hexene by a true coordination mechanism [89]. Again, deactivation by siloxy elimination to afford Pd(II) allyl complexes like **1.31** was observed.

Several important classes of polar monomers have so far eluded copolymerization by the Pd(II) system. Vinyl chloride insertion, for example, leads to catalyst deactivation following β -halide elimination to form inert chloride species such as **1.32**, as shown by Jordan [90]. Similarly, attempted vinyl acetate copolymerization results in deactivation by an analogous acetate elimination process, although the ester chelate intermediate that forms after insertion also effectively shuts down the reaction [90]. Therefore, β -elimination of polar groups represents a significant and unresolved problem for late transition metal polymerization systems unless access of the metal to it is restricted.

Many nitrogen-containing monomers bind strongly to the metal preferentially by *N*-complexation via the nitrogen atom as opposed to through the olefin, and are thus not incorporated. Several studies have focused on copolymerizations with acrylonitrile, in particular. Experimental [91, 92] and theoretical [93, 94] reports both suggest that olefin π -complexation is disfavored with respect to *N*-complexation in the α -diimine system, likely because the cationic nature of the complexes favor interaction with nitrogen. Allyl dimethylamine was found to undergo insertion but the resulting five-membered chelate is inactive toward ethylene [95]. On the other hand, *N*-alkeny-substituted carbazoles afford three-membered chelates that can be displaced by ethylene and show copolymerization activity. A summary of common monomer-induced deactivation mechanisms is shown in Scheme 11.



Scheme 11 Catalyst deactivation routes in copolymerizations with polar olefins: **a** β -elimination of a leaving group to afford allylic or dimeric species, **b** poisoning by *N*-complexation in the attempted copolymerization of acrylonitrile

The incorporation of these monomers remains an unsolved problem in polymerization by cationic late transition metal catalysts. Various reports have attempted to address the broad picture of polar monomer incorporation with the Pd α -diimine catalysts. The rates of monomer insertion have been shown to be dependent on the nature of the substituent on the olefin. Sen and coworkers have observed a positive linear correlation between insertion rate and the increasing electron-withdrawing ability of the olefin-bound substituent [96]. Several computational studies by Ziegler and Goddard have reached conclusions that parallel previously discussed experimental results. In all examples of polar olefin copolymerization, the complexation of the functional group to the metal is the source of the difficulties, either by preventing the binding of the comonomer olefin moiety, the binding of subsequent olefins, or by catalyst-deactivating elimination processes [94, 97–99]. In addition, the catalyst's chain walking ability often exacerbates the problem through isomerization to chelates that are especially unreactive.

Although beyond the scope of this review, these computational studies have also suggested that recent neutral Pd(II) catalyst systems bearing anionic ligands should better accommodate polar monomer incorporation (although at lower activities) [94, 98]. Indeed, these systems, particularly the Pd phosphine sulfonate catalysts, have proven to be especially promising [31–35]. For example, the first transition metal-catalyzed copolymerization of ethylene and acrylonitrile was recently performed using a phosphine sulfonate Pd(II) catalyst [32]. The neutral catalysts apparently weaken the binding of electronegative groups to the metal through reduction of electrostatic interactions.

5 Ligand Design

Numerous modifications to the bis(aryl)- α -diimine ligand motif have been reported, especially in the patent literature. The review by Ittel includes an index of diimine and related ligands in proprietary publications up to the year 2000 [26]. Instead, this discussion will focus on academic reports of Ni(II) and Pd(II) polymerization catalysts bearing α -diimine or other closely related chelating neutral nitrogen ligands.

5.1 Modification of Substituted α -Diimines

A few studies have screened ligands of different functionalities while retaining the overall bis(aryl)- α -diimine layout, in response to the effects of *ortho*-alkyl and diimine backbone substitution. A report involving halogenated α -diimines described a large enhancement of ethylene polymerization activity and an increase in polymer molecular weight in Ni(II) catalysts bearing bulky *ortho*-iodo substituents as compared to unsubstituted analogs [100]. A small rate enhancement was also observed in catalysts bearing electron-withdrawing

para-fluoro substitution on the diimine ligands. Conversely, a catalyst bearing the *para-tert*-butyldiphenylsilyl-substituted analog of **1.12b** was found to exhibit higher activity in ethylene and propylene polymerization, an effect attributed to the electron-donating silyl group [101]. In fact, the elucidation of the electronic effects on the catalytic properties has yielded conflicting results in other studies as well [28].

A systematic investigation of electronic effects on ligand binding strength and the Lewis acidity of the resulting Pd(0) or Pd(II) metal fragment was carried out by Ragaini and coworkers for a series of bis(aryl) α -diimine ligands bearing electron donating or withdrawing groups but lacking *ortho*-alkyl groups [102]. A clear linear correlation was observed between the Hammett constant [103] of the substituent parameters such as pK_a and complexation strength, as determined by complexation equilibria. A series of asymmetric ligands were prepared in which donating and withdrawing groups were placed on different aryl groups [104]. Ligand complexation strength was found to be the average expected of the substituents, although the N–Pd bond lengths were nearly constant in all cases and thus are not reflective of coordination strength. Polymerization by catalysts bearing these ligands was not attempted.

Our laboratory has examined the electronic effects of α -diimine ligands on the polymerization properties of their late metal complexes. A series of bis(aryl)- α -diimine ligands **1.42a–g** were synthesized bearing a range of electron donating and withdrawing substituents to probe the ligand electronic effects on late transition metal olefin polymerization catalysts (Fig. 4) [105]. The following general trends were observed from this study (Popeney and Guan, unpublished results): (i) more electron-donating ligands result in more stable catalysts for ethylene polymerization for the corresponding Ni(II) and Pd(II) catalysts; (ii) higher molecular weights and more linear macromolecular topology was found in polyethylenes prepared using catalysts bearing more strongly electron-donating ligands; and (iii) catalysts bearing strongly electron-donating ligands were more tolerant to polar comonomers and afforded copolymers with higher incorporation of the polar comonomer.

Inspired by the design of metallocene catalysts, there has been research into the use of C_2 -symmetric Ni α -diimine catalysts for the preparation of polyolefins with stereoregularity. Such catalysts were shown to afford higher degrees of isotacticity in polypropylenes as compared to the standard C_{2v} -symmetric catalysts, which afford mostly syndiotactic polymer [106]. Coates and coworkers have studied

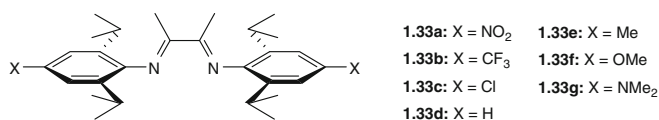


Fig. 4 Substituent electronic effects on Ni(II) and Pd(II) α -diimine catalysts

C_2 -symmetric Ni(II) catalysts bearing chiral *sec*-phenethyl moieties in the *ortho*-aryl positions of diimines such as **1.34** (Fig. 5) in order to prepare polyolefins with regio- and stereoregularity [107]. The polymerization of *trans*-2-butene by the catalyst proceeded with high regio- and stereoregularity to produce linear polymer with a methyl branch every three carbons with significantly enhanced isotacticity. The catalyst was also capable of polymerizing propylene in a living manner at low temperatures with high isotacticity and regio-regularity [108]. Polymerization at low, then ambient temperatures led to the formation of an isotactic-atactic

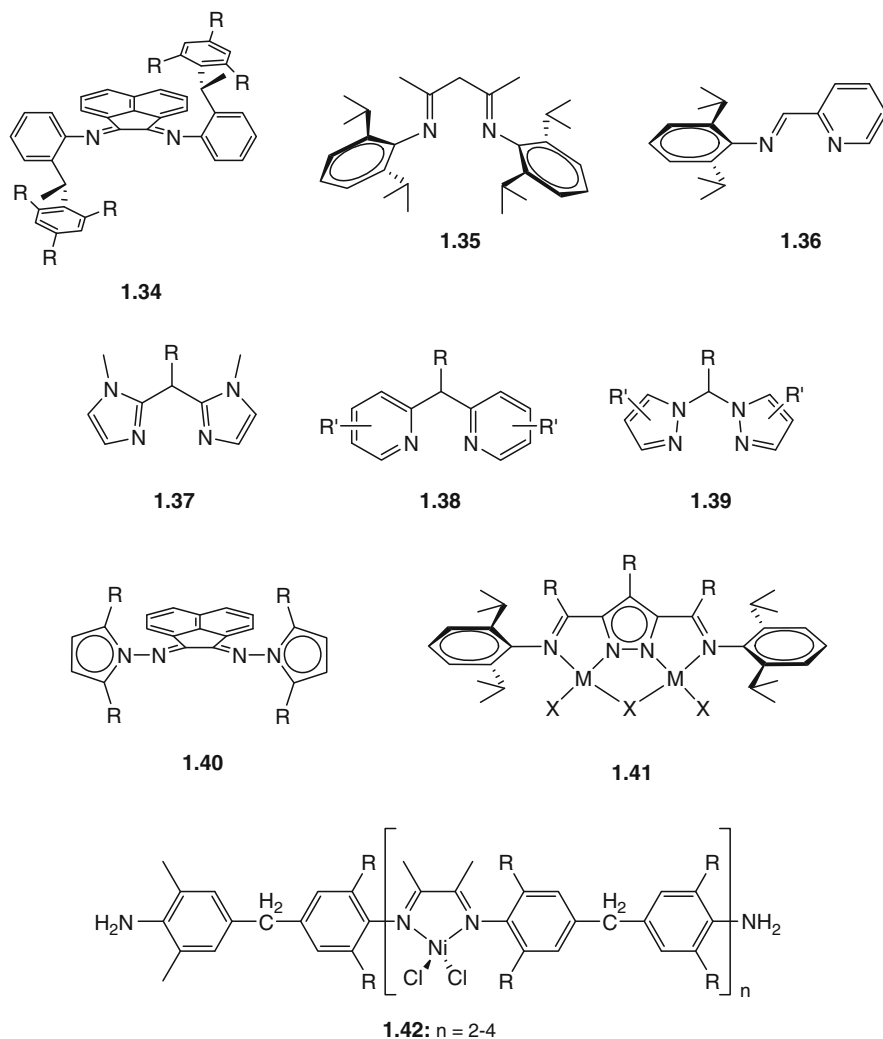


Fig. 5 α -Diimine and related neutral nitrogen ligands (and complexes) utilized in ethylene and α -olefin polymerizations

regioregular–regioirregular block-copolymer. The same catalyst permitted the precise control of branching in α -olefin polymerizations by the optimization of reaction conditions to favor or disfavor 1,2 monomer insertion [109].

Insertion of a methylene spacer between the two imine carbons to afford the corresponding β -diimine **1.35** led to Ni(II) and Pd(II) catalysts that produced polyethylene of lower molecular weight, branching density, and activity compared to the α -diimine **1.8b** [110]. The active complex, exhibiting a six-membered as opposed to five-membered metal chelate ring and a wide N–M–N bite angle, is thought to be less sterically cumbersome and unable to effectively accelerate insertion and isomerization or retard chain transfer. A Ni(II) pyridylimine catalyst bearing a ligand **1.36** in which one imine group was replaced by pyridine also resulted in lower molecular weight polyethylene [111]. Ligands possessing other N-heterocyclic moieties in place of imines have been explored. Imidazolyl- (**1.37**), pyridyl- (**1.38**), and pyrazoyl-based (**1.39**) ligands for use in Pd(II)-catalyzed ethylene polymerization have been reported [112]. The highest polymerization activity was observed with the more electron-deficient pyrazoyl-based ligands, although polymer productivity and molecular weight were still far lower than with the α -diimines due to the sterically small nature of these new ligands. Lastly, a class of bis(pyrrolyl) α -diimine Ni catalysts, such as **1.40**, afforded polymer of comparable activity and molecular weight to the standard bis(aryl) catalysts, providing the ligands were of similar steric bulkiness [113]. It appears from these reports, therefore, that the ligand steric bulk is the property that most strongly affects the catalyst's polymerization ability, and that other variations in structure exhibit less influence.

In a study involving dinuclear diimine pyrazolate Ni(II) and Pd(II) catalysts **1.41** exhibiting analogous substituents, similar trends with bulky substituents were noted as with the mononuclear α -diimine catalysts [114]. The perpendicular orientation of the aryl ring in α -diimine complexes, absent from these other systems, is an important factor in increasing the steric crowding of the metal coordination plane [112]. Another di- and multinuclear Ni-based catalyst (**1.42**) was capable of producing polyethylene in higher activity than the standard mononuclear analog exhibiting the same *ortho*-alkyl substitution [115]. The authors attribute this advantageous behavior to the additional steric bulk provided by the linker in *para*-position.

5.2 Catalysts of Related Nitrogen-Containing Ligands

Although distinct from the α -diimine catalysts, some interesting observations have been made in polymerizations with Ni(II) catalysts bearing N-heterocyclic carbene ligands (Fig. 6) Complex **1.43** is capable of polymerizing ethylene in moderate activity and norbornene in high activity upon treatment with MAO, despite the absence of bulky groups on the ligands [116]. The authors attribute this unique catalytic behavior to the hemilabile pyridine moieties. In contrast, complex **1.44** afforded only ethylene dimerization in low activity, presumably because of excessive ligand steric bulk that prevented olefin coordination [117]. Lastly, Ni(II) complex **1.45**

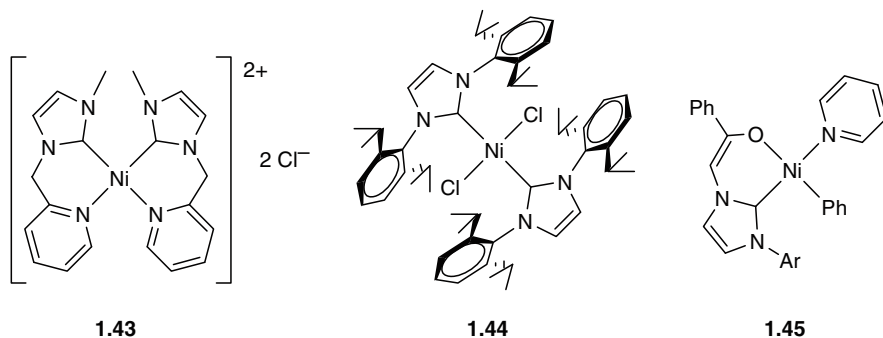


Fig. 6 *N*-Heterocyclic carbene-based Ni(II) olefin polymerization catalysts

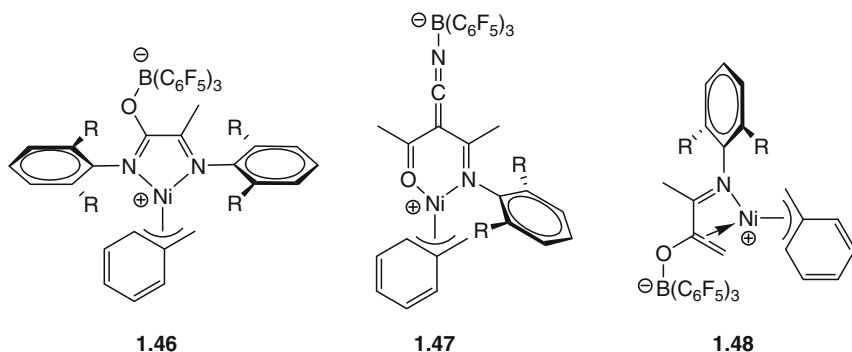


Fig. 7 Zwitterionic Ni(II) olefin polymerization catalysts

bearing an anionic carbene enolate exhibited activity comparable to the SHOP catalysts, which are phosphine-based as opposed to carbene-based [118]. Polymers were of low molecular weight but highly linear in comparison to those prepared by α -diimine or other neutral Ni(II) systems. From these results, it appears that the steric requirements for the realization of active carbene catalysts that can afford high molecular weight polymer is unlike those of the diimine catalysts, likely a result of different electronic properties.

An interesting zwitterionic series of late metal catalysts similar to the α -diimines has been studied by Bazan and coworkers. They report olefin polymerization upon the treatment of neutral α -iminocarboxamido Ni(II) complexes with boranes to afford zwitterionic complexes [119]. In the presumed active catalyst **1.46**, boron is coordinated to oxygen in the ligand backbone and nickel is coordinated via nitrogen, thus implying a cationic nature of the metal. The catalyst affords high molecular weight polyethylene with a branched structure, and gives copolymers with functionalized norbornenes [120]. A large excess of coactivator is not required, suggesting that these catalysts, the dominant resonance structures shown in Fig. 7, have properties intermediate between cationic and neutral analogs, which do not require activation.

Conjugation between the imino and acyl [121], or nitrile (in complex **1.47**) [122] moieties permitted the remote activation of nickel. Another catalyst (**1.48**) exhibiting coordination via an alkenyl moiety is noteworthy because of its sterically small size, which should prohibit the production of high molecular weight polymers [123]. This is believed to be possible because of the catalyst's unique electronic properties. As bulkier imino-aryl substituents are introduced, polymerization activity and polymer molecular weight increases, as expected [124].

5.3 Teraryl-Substituted α -Diimines

Recently, new systems have emerged based on diimine ligands bearing *ortho*-diaryl moieties to provide steric demand in place of alkyl substituents. Rieger has reported a series of catalysts bearing substituted *meta*-terphenyl-based α -diimine ligands **1.49a–d** (Fig. 8). Although, the Pd(II) complexes are inherently unstable and decompose within minutes, the Ni(II) catalysts outperform the standard *ortho*-diisopropyl-substituted catalysts, under certain conditions [125]. Substitution on the phenyl rings causes a displacement of the dihedral angle between the diimine plane and the aryl groups, leading to different axial blocking capacity and accommodation of coordination. This effect corresponds to a dramatic increase in polymer molecular weight and branching density (Table 5, entries 4–6) [126]. The unsubstituted terphenyl catalyst **1.49b** exhibits unprecedentedly high activity at ambient temperatures when activated with trimethylaluminum, affording highly linear polymer (entry 2). Furthermore, hydrogen may be used as an effective chain transfer reagent, reducing molecular weight without compromising catalyst activity and thermal stability (entries 2–3). This is not possible with the standard series of catalysts.

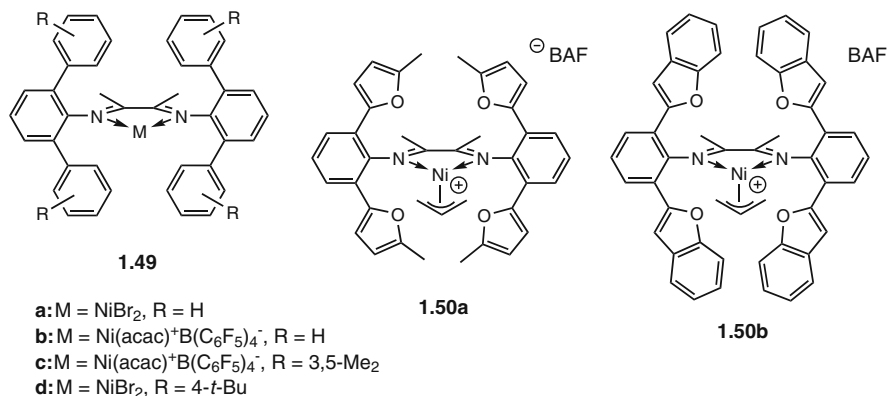


Fig. 8 Teraryl-substituted α -diimine ligand-based Ni(II) polymerization catalysts

Table 5 Ethylene polymerizations by teraryl-substituted α -diimine Ni(II) catalysts^a

Entry	Complex	T (°C)	C_2H_4 pressure	TOF(\times $10^{-3} h^{-1}$)	M_n ($kg mol^{-1}$)	M_w/M_n	B	T_m (°C)	Reference
1	1.49a ^b	25	10 bar	50	n/a	n/a	n/a	133	[78]
2	1.49b ^c	30	10 bar	17,600	56 ^d	3.9	3	134	[79]
3	1.49b ^c	60	10 bar	854	89 ^d	3.5	3	129	[79]
4	1.49 c ^c	30	10 bar	149	1210	2.5	5	128	[79]
5	1.49 c ^c	60	10 bar	140	283	1.8	21	109	[79]
6	1.49d ^b	25	10 bar	235	3460	1.3	n/a	130	[78]
7	1.50a ^e	120	600 psi	8.9	28	2.3	70	66	[80]
8	1.50b ^e	70	600 psi	159	68	36.8	14	117	[80]
9	1.50b ^e	120	600 psi	145	20	2.7	37	87	[80]

^a See references for specific polymerization conditions

^b 500 equivalents of MAO used per Ni

^c 500 equivalents of $AlMe_3$ used per Ni

^d Hydrogen added to promote chain transfer

^e 20 equivalents of $B(C_6F_5)_3$ used per Ni

Ionkin has reported a similar series of Ni(II) catalysts **1.50a** and **b** bearing *ortho*-difuryl substituents that are noteworthy for their high thermal stability [127]. The bulkier benzofuranyl-substituted catalyst **1.50b** possesses the most attractive catalytic properties (Table 5, entry 9): the ability to form high molecular weight polymers (albeit in high polydispersity) and reasonable activity even at 150 °C. Even under these harsh conditions, the polymer branching density is still relatively low.

5.4 Catalysts Derived from Cyclic α -Diimine Ligands

An explanation for the success of the α -diimine ligand design in late transition metal polymerization systems is that their relative rigidity compared to other bidentate ligands imparts conformational stability to the catalysts [45]. This is important in providing consistent steric bulk in the axial sites and increasing catalyst lifetime. Nevertheless, the axial protecting ability and, especially, the catalyst thermal stability suffer at elevated polymerization temperatures, where thermal ligand flexibility leads to dramatic polymer molecular weight reduction and catalyst deactivation. With the attempt to address these issues, studies on a series of new macrocyclic ligands have been pursued by our laboratory to address the shortcomings of the existing system. Their closed cyclic structure was designed to dramatically reduce ligand thermal motion, leaving axial blocking groups in their proper positions to prevent chain transfer and to prevent catalyst deactivation processes.

Our rationale for macrocyclic ligand design is as follows: Examination of successful homogeneous polymerization catalyst systems, ranging from metallocene to late transition metal catalysts [128–130], indicates that a good ligand generally shares the following common features:

1. It matches the coordination number and geometry of the metal ion and forms a stable complex with the metal ion
2. It provides appropriate electronic donation to the metal center
3. It often provides a sterically crowded microenvironment that protects the active catalytic center
4. Upon activation, the complex only has two *cis*-coordination sites in the front: one for monomer entry and the other for polymer growth

With these features in mind, we envisioned a new family of macrocyclic ligands for olefin polymerization catalysis (Fig. 9) [131, 132]. We utilized macrocycles as the ligand framework and installed the catalytic metal center in the core of the macrocycles. Appropriate intra-annular binding sites are introduced into cyclophane framework that not only match the coordination geometry of a chosen metal but also provide the appropriate electronic donation to metal center. The cyclophane framework would provide a microenvironment to shield the catalytic center from all angles, but leaving two *cis* coordination sites open in the front: one for monomer coordination and the other for the growing polymer chain. This could potentially protect the catalytic center and prevent it from decomposition or vulnerable side reactions.

Cyclophanes and other macrocycles have been exploited for various applications in molecular recognition, supramolecular chemistry, and biomimics [133]. Macrocycles, particularly crown ethers and porphyrins, have been used as ligands in metal-catalyzed reactions [134]. The unique macrocyclic ligands offer unique properties to their metal complexes. The metal ions are relatively inert to ligand substitution as compared to a non-macrocyclic complex. The rigidity of macrocyclic ligands imposes an additional stability to the complexes [135]. Macrocyclic–metal complexes also exhibit blocking effects due to the sterics surrounding the metal. This provides limited accessibility to open attack by incoming reagents, thus limiting the approach of the reagents to specific sites. Despite these promising properties, the use of cyclophanes as ligands for transition metal polymerization catalysis remains mostly unexplored [136, 137].

A specific goal we have in mind is to design cyclophane-based α -diimine ligands for overcoming the low thermal stability of the regular α -diimine catalyst systems.

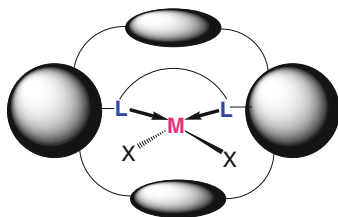


Fig. 9 Design of cyclophane-based complexes

In the acyclic complex **1.51**, the aryl groups are roughly perpendicular to the coordination plane so the isopropyl substituents on the aryls are positioned at the axial directions to block the associative chain transfer of ethylene (Fig. 10) [27, 138]. At elevated temperature, however, the aryl groups may rotate away from the perpendicular orientation, resulting in increased associative chain transfer and decreased molecular weight of the PE formed [139]. Moreover, as the aryl groups rotate toward the coordination plane, the isopropyl substituents on the aryl rings reach proximity to the metal center for C–H activation to form metallacycles, which was proposed as one potential deactivation pathway for this family of catalysts [140]. In our cyclophane-based complex **1.52**, the metal center is positioned at the core of the ligand so that the macrocycle completely blocks the axial faces of the metal, leaving only two *cis*-coordination sites for monomer entry and polymer growth [131]. The rigid framework of the ligand prohibits free rotation of the aryl–nitrogen bonds, which should allow the catalyst to make high molecular weight polymers at elevated temperature. The lack of rotational flexibility could reduce the C–H activation reaction, which could potentially eliminate a potential catalyst deactivation pathway. Our initial successes strongly support this hypothesis, which encourages us to propose further studies for investigating the cyclophane ligand system for late transition metal olefin polymerization catalysis.

Of our new cyclic ligand designs, the aromatic cyclophane-based macrocyclic ligand has seen the most success (Fig. 11) [131, 132]. The cyclophane-based ligand resembles the *meta*-terphenyl-based ligand developed by Rieger except that the ethylene bridge that forms the cycle effectively limits conformational flexibility. The X-ray structure of the Pd(II) complex **1.53b** shows that the cyclophane framework effectively protects the catalytic center from all angles while leaving two front *cis* coordination sites accessible for polymerization (Fig. 12). Ethylene polymerizations with the Ni(II) catalyst **1.53a** affords high molecular weight polymer at high temperatures, implying that the axial blocking effect of the ligand is not compromised under these harsh conditions [131]. Furthermore, appreciable deactivation

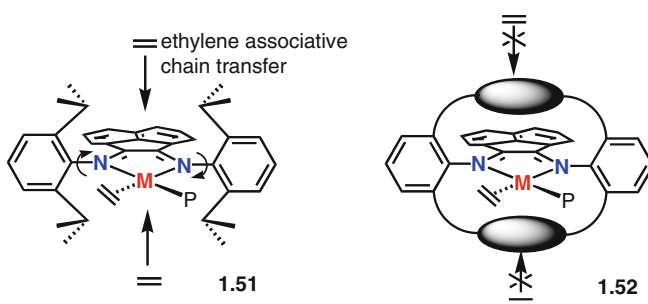


Fig. 10 Comparison of acyclic and cyclophane α -diimine complexes

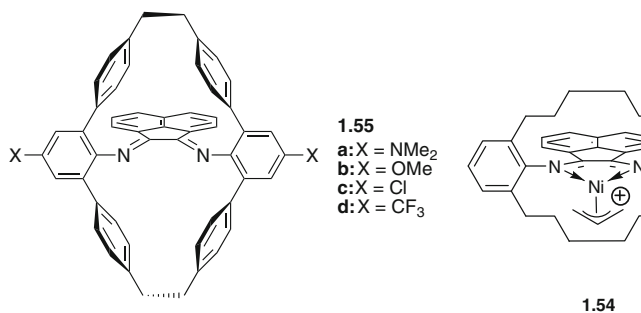


Fig. 11 Late transition metal polymerization catalysts from cyclic α -diimine ligands

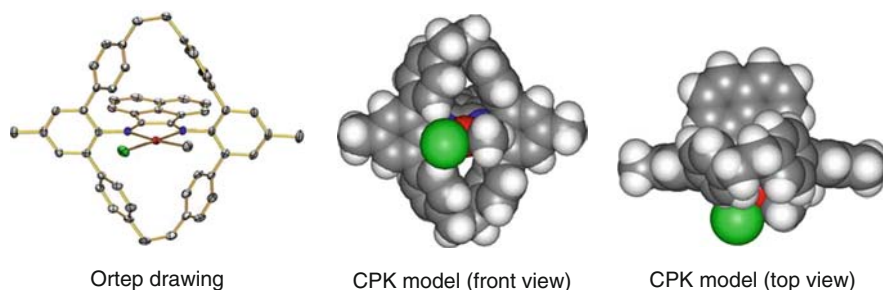


Fig. 12 X-ray crystal structure for complex **1.53b**

Table 6 Olefin polymerizations with Ni(II) cyclic α -diimine catalysts^a

Entry	Complex	T (°C)	Olefin (conc.)	TOF ($\times 10^{-3} \text{ h}^{-1}$)	M_n (kg mol ⁻¹)	M_w/M_n	B	T_m (°C)	Reference
1	1.53a	30	E (200 psi)	1436	288	1.30	73	n/a	[81]
2	1.53a	70	E (200 psi)	1307	619	1.43	89	n/a	[81]
3	1.53a	90	E (200 psi)	1007	462	1.64	96	n/a	[81]
4	1.53a	35	P (1 atm)	2205	154	1.06	104	– ^b	[83]
5	1.53a	50	P (1 atm)	2032	133	1.13	105	– ^b	[83]
6	1.53a	75	H (2.66 M)	1822	5.29	1.17	52	58	[83]

^a See references for specific polymerization conditions. 2000 equivalents of MMAO per Ni

^b Amorphous

^c 3000 equivalents of AlMe₂Cl used per Ni

does not occur below 90 °C, extending the effective operating temperature range of α -diimine catalysts considerably. Polymerization results with the cyclophane-based catalyst are shown in Table 6.

The closed structure of the cyclophane ligand also induces dramatic changes in the polymer microstructure. Polyethylene from the cyclophane catalyst **1.53a** is considerably more branched than with catalysts bearing acyclic ligands, which suggests

an accelerated rate of chain walking [131]. In the polymerization of α -olefins, this property becomes especially pronounced [141]. As discussed earlier, the chain walking process results in a pronounced chain-straightening effect in the polymerization of propylene and other higher olefins. Due to the elevated rate of chain walking, this phenomenon is exacerbated by **1.53a**. In propylene polymerizations, for example, branching densities are only slightly above 100 (compare Table 6, entries 4 and 5 with Table 3, entries 1 and 2), about half the value afforded by the acyclic catalyst [70]. Poly(1-hexene) afforded by the cyclophane catalyst is semicrystalline due to the chain straightening effect (entry 6).

The cyclophane-Ni(II) catalyst **1.53a** was also investigated for polymerization of α -olefins. Living polymerization of propylene and 1-hexene was obtained at very high temperatures ranging from 50 to 75 °C [142]. Polyolefins were prepared with controlled molecular weight and narrow molecular distribution. The number-averaged molecular weight (M_n) of polypropylene increased linearly with polymerization time over a broad molecular weight range. The polydispersities remain narrow (near 1.1) under conditions that are far harsher than those required for the acyclic catalysts. The excellent living polymerization feature at elevated temperature is attributed to the protective effects of the cyclophane ligand environment. With enhanced stability and living nature at elevated temperature, this highly active and robust catalyst system offers opportunities for practical design of various polyolefin architectures.

The Pd(II)-cyclophane catalyst **1.53b** was investigated for ethylene copolymerization with acrylate polar comonomers. The copolymerization of ethylene and methyl acrylate (MA) or *tert*-butyl acrylate (TBA) were performed with a Pd(II)-cyclophane catalyst in parallel with the acyclic analog. Significantly increased incorporation of acrylates in copolymers was observed. At relatively low concentration of acrylates, significantly higher incorporations of acrylates were seen for the cyclophane-Pd catalyst [143]. This unique behavior was due to the unique environment of the cyclophane ligand. The olefin insertion rates, as determined by low temperature NMR, for both the cyclophane and acyclic catalysts were similar, which could not account for the observed difference in incorporation behavior. Detailed mechanistic studies revealed that slow olefin exchange on the metal center contributes to the high efficiency for incorporating polar olefins [143] (Popeney and Guan, unpublished results). When olefin exchange was retarded so that it was on the order of, or slower than, the insertion rate, the catalyst would insert comonomers more on a “first come, first serve” basis. This would reduce the preference for incorporating ethylene and afford polymers with high acrylate loadings. This exciting observation encourages us to further develop new cyclophane-based late metal catalysts for copolymerization with polar olefins.

In an effort to optimize the cyclophane system, a series of *para*-substituted cyclophane ligands **1.55a–d** (Fig. 13) was prepared, with ligands bearing electron donating (OMe and NMe₂) and withdrawing (Cl and CF₃) substituents in the *para* position of the α -diimine aryl rings synthesized (Popeney and Guan, unpublished results). The substituted cyclophane ligands were prepared by routes similar to the

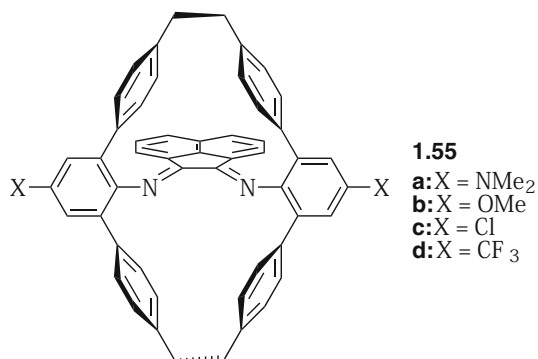
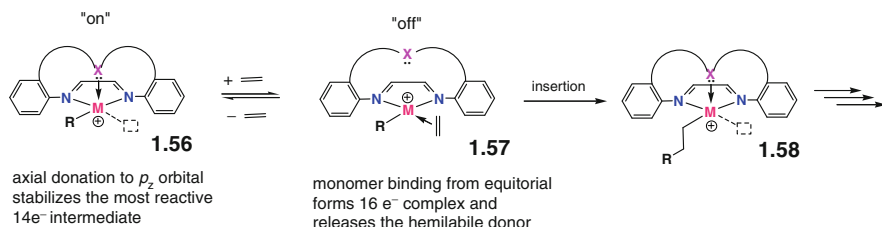


Fig. 13 Substituted cyclophane α -diimine ligands

original cyclophane ligand; however, significant modifications were required in many cases. The preparation of the key terphenyl aniline intermediate was simplified to one step by either Suzuki or Negishi cross-coupling reactions between a styrene ligand and a substituted *ortho*-dibromoaniline.

The effect of *para*-aryl ligand substitution on a family of cyclophane-based Ni(II) and Pd(II) catalysts was then examined. The Ni(II) polymerizations of ethylene at high temperature were relatively insensitive to electronic perturbation, affording polyethylene in slightly increasing activity and thermal stability in the presence of ligand electron-withdrawing groups. At the same time, molecular weights increased as metal electron density decreased. The polymers were heavily branched and of low crystallinity. Branching density was increased by the presence of electron-withdrawing ligands. Electronic effects in the Pd(II) series of cyclophane catalysts were significant. The chloro-substituted cyclophane catalyst alone exhibited exceptionally high activity and stability at temperatures as high as 60 °C. In contrast, the polymer molecular weight dependence on substituent was pronounced and easily related to the electronic properties of the substituent. More electron-deficient catalysts afforded polymer with significantly higher molecular weight. Because this trend was opposite to the acyclic catalyst family, a different mechanism for chain transfer may operate in the Pd(II)-cyclophane system. Copolymerizations with MA with these substituted catalysts was also investigated.

Another cyclic ligand bearing a six-carbon aliphatic bridge above and below the metal coordination plane was also synthesized [144]. However, the rate of polymerization from the corresponding Pd(II) and Ni(II) (**1.54**) catalysts was low, presumably because of excessive steric crowding of the metal coordination environment. Ligand steric bulkiness is thus a double-edged sword, required to block chain transfer and destabilize the catalyst resting state but also potentially disruptive of monomer coordination.



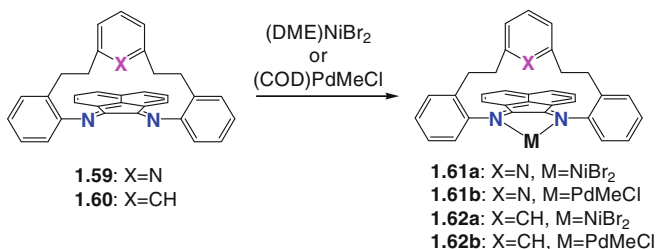
Scheme 12 Concept of hemilabile axial donor α -diimine ligand

5.5 Hemilabile Axial Donating α -Diimine Ligands

In another recent study, we demonstrated a hemilabile axial donating ligand concept for olefin polymerization catalysis. Hemilabile ligands are interesting for organometallic catalysis because a hemilabile donor can reversibly interact with the metal to provide additional control of the catalytic properties [145–147]. While the highly reactive intermediates of transition metal catalysts can be stabilized by the extra donor to suppress potential side reactions, the hemilabile ligand will be able to release from the metal and allow the desired reaction to proceed. In principle, careful introduction of hemilabile donor to ligands can potentially lead to novel catalysts that can maintain high reactivity for positive reactions while suppress undesired side reactions. There are a few reports in the literature describing hemilabile ligand effects on transition metal complexes for olefin oligomerization and polymerization [148–150].

The general concept of hemilabile axial donor ligand design is shown in Scheme 12. We propose that, during the polymerization, the most reactive electrophilic $14e^-$ intermediate **1.56** can be stabilized by the hemilabile axial donor. This could potentially suppress side reactions associated with this reactive species, such as chain transfer and catalyst deactivation. Binding of an ethylene monomer affords the $16e^-$ complex (resting state, **1.57**), which releases the axial donor and allows monomer insertion to proceed. It should be noted that the hemilabile donor is in the axial orientation to interact with the appropriate orbital of the metal, in this case the empty p_z orbital [151]. This is orthogonal to the equatorial d orbital that an incoming monomer will coordinate to. Without this geometrical constraint, an extra donor ligand will bind to the equatorial site and cause inhibition to the polymerization.

The coordination of the hemilabile donor may also influence the binding of other ligands (such as olefin) to the metal center, particularly those in the *trans* position through the so-called *trans* effect. Most of the late transition metal catalysts reported in the literature relied upon changes in steric bulk or the ligand backbone to produce effective polymerization activities. *Instead of relying upon steric bulk, here we propose the use of an axial donating ligand to modify α -diimine catalysts, resulting in more stable catalysts while suppressing chain transfer process.* The tethered donor would be flexible enough to coordinate to the metal center but labile enough to dissociate and permit reactivity. Constrained by the conformation of



Scheme 13 Hemilabile axial pyridine donor α -diimine ligand and complexes

macrocycles, the hemilabile donor is restricted to interact with the metal center *only* through axial direction. This is critical because coordination of extra donor at equatorial site often leads to inhibition and reduction in catalytic activity.

In one hemilabile ligand design, we introduced a pyridine group to reversibly interact with the catalytic center from the axial direction [152]. In Brookhart's α -diimine ligand systems, steric bulkiness at axial direction is crucial for preventing chain transfer processes for formation of high mass polymers [139, 153]. One specific hypothesis we wanted to test here is that instead of sterics, reversible binding of the pyridine donor can stabilize the active catalytic species and suppress the chain transfer process. To demonstrate this concept, we have synthesized the ligand **1.59** in three convenient steps. For close comparison, a control ligand (**1.60**) having the same sterics and geometry but without the nitrogen donor was also prepared (Scheme 13). ¹H NMR spectra indicate the flexibility of the pyridine tether linkage. The pyridine ring can swing forwards and backwards into different conformers. At relatively low temperature ($-10\text{ }^{\circ}\text{C}$), this process is slow and the diastereotopic ethylene protons can be resolved on NMR time scale. At elevated temperature, the process becomes fast and the signals coalesce. From the coalescence temperature, the activation energy for the exchange of the two conformers is estimated to be $\sim 12.5\text{ kcal mol}^{-1}$. This conformational flexibility may provide a mechanism to turn the axial donation "on" and "off".

These ligands were successfully complexed to NiBr₂ and Pd(Me)Cl (**1.61** and **1.62**). X-ray crystal structures were obtained for both the free ligand and its Pd(Me)Cl complex (Fig. 14) [152]. The polymerization activity of the NiBr₂ catalyst was first investigated. After screening for appropriate aluminum activators, it was found that AlMe₂Cl provided the highest activities. Traditional activators such as MAO, MMAO, AlMe₃, and AlMeCl₂ gave low levels of activity. In consideration of the ligand geometry and the relatively long distance between the pyridine N and the metal center [N(3)–Pd(1) 3.814 Å in complex **1.61b**], we propose that AlMe₂Cl bind to the pyridine N and deliver an axial interaction between the Cl and the metal center. Using excess AlMe₂Cl as activator the Ni(II) complex **1.61a** polymerized ethylene at 35 °C at 600,000 TOF per hour, or 16,800 kg PE mol⁻¹ Ni h⁻¹). The PE formed has $T_m > 130\text{ }^{\circ}\text{C}$, indicating the formation of highly linear, crystalline polyethylene.

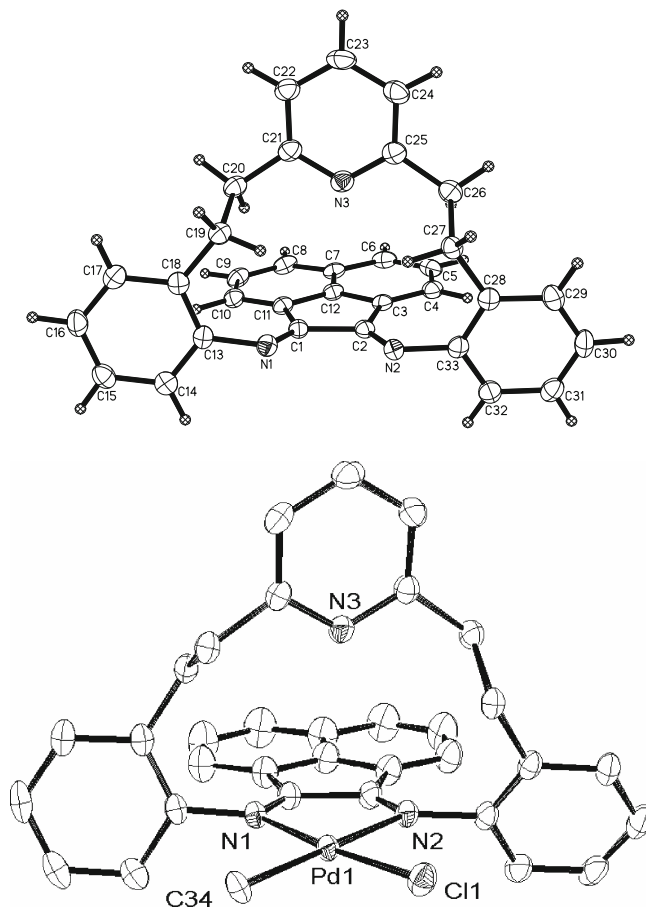


Fig. 14 Single X-ray diffraction structure of ligand **1.59** (*left*) and its Pd(Me)Cl complex (**1.61b**) (*right*)

With the bottom rim of the ligand wide open, it was surprising that the complex still afforded PE with high molecular weight (M_n 56,460 g mol⁻¹, PDI 2.2, at 200 psi ethylene and 35 °C). This is in contrast to regular α -diimine complexes for which the ligands with no or mono *ortho*-substituents on the anilines only afford very short oligomers [139]. For direct comparison, the control complex **1.62a** upon activation at identical conditions only afford PE with very low molecular weight and broad polydispersity (M_n 6900 g mol⁻¹, PDI 5.6, at 200 psi ethylene and 35 °C). The activities of the two systems are comparable. Presumably, due to the so-called *trans* effect, a reversible interaction with the catalytic center from the axial direction prevents ethylene association from the *trans* axial direction, hence suppressing the associative chain transfer process.

The Pd(II) catalyst **1.61b** showed an even more dramatic difference from the control system **1.62b** [152]. Addition of NaBAR₄ to complex **1.61b** in presence of

excess AlMe_2Cl resulted in active ethylene polymerization to afford PE with high molecular weight (M_n 880,000 g mol^{-1} , PDI 1.9, at 1 atm of ethylene and 25 °C) and high crystallinity (T_m 134 °C). In sharp contrast, the control complex **1.62b** only produced short oligomers ($M_n \sim 1000$ g mol^{-1} , PDI 1.5, at 1 atm of ethylene and 25 °C) with high branching density (104 branches per 1000°C). Again, the axial pyridine nitrogen presumably interacts with the catalytic center, which suppressed the chain walking process. It should be noted that AlMe_2Cl is not simply acting as a Lewis acid to inhibit the pyridine N. This was confirmed by comparing the polymerization results between complexes **1.61b** and **1.62b**. In another set of control experiments, addition of a typical Lewis acid, BF_3 , did not result in active polymerization catalysts.

6 Summary

Since their discovery over a decade ago, late transition metal α -diimine polymerization catalysts have offered new opportunities in the development of novel materials. The Ni(II) catalysts are highly active and attractive for industrial polyolefin production, while the Pd(II) catalysts exhibit unparalleled functional group tolerance and a propensity to form unusually branched polymers from simple monomers. Much of the success of these catalysts derives from the properties of the α -diimine ligands, whose steric bulk is necessary to accelerate the insertion process and inhibit chain transfer.

The ability of the catalysts to afford branched polymers arises from the chain walking process, which occurs by non-regioselective β -hydride elimination and reinsertion reactions. Chain walking is especially facile in the Pd(II) system and accounts for the heavily branched nature of the polymers prepared by the Pd α -diimine catalysts. At the same time, the Ni(II) catalysts promote rapid migratory insertion and high polymerization activity, making these catalysts attractive in industrial applications. The mechanistic understanding has been gathered by observations from polymerization, detailed spectroscopic studies, and theoretical calculations.

The Ni(II) and Pd(II) catalysts are effective in the polymerization of α -olefins, in addition to ethylene. The polymerizations of α -olefins exhibit living behavior under appropriate conditions. The Pd(II) system can copolymerize acrylate-based monomers and other functionalized olefins bearing oxygen-containing groups. Copolymerizations of monomers containing leaving groups are prone to deactivation by elimination, while nitrogen-containing monomers poison the catalyst by competitive binding.

Promising progress has been made in the development of new ligands for late transition metal polymerization catalysts. Other similar nitrogen-containing ligands have been prepared, although their polymerization properties are typically inferior to the original α -diimine ligands. The terphenyl-based ligands afford some interesting catalysts, which exhibit a combination of high activity and stability. Our own laboratory has shown a series of macrocyclic ligands that impart increased thermal

stability and reduced chain termination rates for late transition metal polymerization catalysts. Living polymerizations of α -olefins have been achieved for Ni(II)-cyclophane catalyst at temperatures far higher than with acyclic catalysts. The Pd(II)-cyclophane catalyst is much more efficient in incorporating acrylate comonomer in ethylene copolymerization. Finally, our laboratory recently demonstrated the introduction of hemilabile axial donor groups to α -diimine ligands as a novel concept for design of late metal polymerization catalysts.

The recent progress surveyed in this review shows the promise that late transition metal catalysts can provide in the production of new materials. We will continue our exploration of new catalyst design for the synthesis of new functional materials with unconventional topologies. Given the unique features of late transition-metal polymerization catalysts and further improvement in catalyst stability and activity for copolymerization with polar comonomers, the future of designing novel functional polymeric materials with late-transition-metal catalysts is very promising.

Acknowledgments We would like to thank the National Science Foundation (DMR-0135233, DMR-0703988, Chem-0456719, Chem-0723497), the ACS Petroleum Research Fund (36730-G7), the Dupont Company, the 3 M Company, the Simitomo Company, the Rhom and Haas Company, and the University of California at Irvine for generous financial support. ZG gratefully acknowledges a Friedrich Wilhelm Bessel Research Award granted by the Alexander von Humboldt Foundation, a National Science Foundation CAREER Award, and a Camille Dreyfus Teacher-Scholar Award. CSP acknowledges an Allergan Fellowship, a UCI dissertation fellowship, and the Joan Rowland award from UCI.

References

1. Scheirs J, Kaminsky W (eds) (2000) *Metalloocene-based polyolefins*, vol 1. Wiley, Chichester
2. Guan Z (2003) *J Polym Sci Part A: Polym Chem* 41:3680–3692
4. Kaminsky W, Külper K, Brintzinger HH, Wild FRWP (1985) *Angew Chem Int Ed* 24:507–508
5. Brintzinger HH, Fischer D, Mühlaupt R, Rieger B, Waymouth RM (1995) *Angew Chem Int Ed* 34:1143–1170
6. Coates GW, Waymouth RM (1995) *Science* 267:217–219
7. Doak KW (1986) *Encyclopedia of polymer science and engineering*, vol 6. Wiley, New York
8. Edgcombe BD, Stein JA, Frechet JMJ, Xu Z, Kramer EJ (1998) *Macromolecules* 31:1292–1304
9. Peuckert M, Keim W (1983) *Organometallics* 2:594–597
10. Keim W (1990) *Angew Chem Int Ed* 29:235–244
11. Kuhn P, Semeril D, Matt D, Chetcuti MJ, Lutz P (2007) *Dalton Trans* 2007:515–528
12. Barlow MG, Bryant MJ, Haszeldine RN, Mackie AG (1970) *J Organomet Chem* 21:215–226
13. Nugent WA, Hobbs FW Jr (1983) *J Org Chem* 48:5364–5366
14. Alderson T, Jenner EL, Lindsey RV Jr (1965) *J Am Chem Soc* 87:5638–5645
15. McKinney RJ, Colton MC (1986) *Organometallics* 5:1080–1085
16. Brookhart M, Sabo-Etienne S (1991) *J Am Chem Soc* 113:2777–2779
17. Keim W, Appel R, Storek A, Kruger C, Goddard R (1981) *Angew Chem Int Ed* 20:116–117
18. Möhring VM, Fink G (1985) *Angew Chem Int Ed* 24:1001–1003
19. Stapleton RL, Chai J, Taylor NJ, Collins S (2006) *Organometallics* 25:2514–2524

20. Keim W, Kowaldt FH, Goddard R, Krüger C (1978) *Angew Chem Int Ed* 17:466–467
21. Schmidt GF, Brookhart M (1985) *J Am Chem Soc* 107:1443–1444
22. Klabunde U, Mulhaupt R, Herskovitz T, Jankowicz AH, Calabrese J, Ittel SD (1987) *J Polym Sci Part A: Polym Chem* 25:1989–2003
23. Klabunde U, Ittel SD (1987) *J Mol Catal* 41:123–134
24. Wang L, Lu RS, Bau R, Flood TC (1993) *J Am Chem Soc* 115:6999–7000
25. Johnson LK, Killian CM, Brookhart M (1995) *J Am Chem Soc* 117:6414–6415
26. Ittel SD, Johnson LK, Brookhart M (2000) *Chem Rev* 100:1169–1203
27. Johnson LK, Mecking S, Brookhart M (1996) *J Am Chem Soc* 118:267–268
28. Gates DP, Svejda SK, Onate E, Killian CM, Johnson LK, White PS, Brookhart M (2000) *Macromolecules* 33:2320–2334
29. Younkin TR, Connor EF, Henderson JI, Friedrich SK, Grubbs RH, Bansleben DA (2000) *Science* 287:460–462
30. Hicks FA, Brookhart M (2001) *Organometallics* 20:3217–3219
31. Drent E, van Dijk R, van Ginkel R, van Oort B, Pugh RI (2002) *Chem Commun* 2002:744–745
32. Kochi T, Noda S, Yoshimura K, Nozaki K (2007) *J Am Chem Soc* 129:8948–8949
33. Luo S, Vela J, Lief GR, Jordan RF (2007) *J Am Chem Soc* 129:8946–8947
34. Szuromi E, Shen H, Goodall BL, Jordan RF (2008) *Organometallics* 27:402–409
35. Berkefeld A, Mecking S (2008) *Angew Chem Int Ed* 47:2538–2542
36. Small BL, Brookhart M, Bennett AMA (1998) *J Am Chem Soc* 120:4049–4050
37. Small BL, Brookhart M (1998) *J Am Chem Soc* 120:7143–7144
38. Britovsek GJP, Gibson VC, McTavish SJ, Solan GA, White AJP, Williams DJ, Kimberley BS, Maddox PJ (1998) *Chem Commun* 1998:849–850
39. Britovsek GJP, Gibson VC, Wass DF (1999) *Angew Chem Int Ed* 38:428–447
40. Boffa LS, Novak BM (2000) *Chem Rev* 100:1479–1493
41. Gibson VC, Spitzmesser SK (2003) *Chem Rev* 103:283–315
42. Vrieze K (1986) *J Organomet Chem* 300:307–326
43. van Asselt R, Elsevier CJ (1992) *Organometallics* 11:1999–2001
44. van Asselt R, Elsevier CJ, Smeets WJJ, Spek AL (1994) *Inorg Chem* 33:1521–1531
45. van Asselt R, Gielens EECG, Rulke RE, Vrieze K, Elsevier CJ (1994) *J Am Chem Soc* 116:977–985
46. tom Dieck H, Svoboda M, Greiser T (1981) *Naturforschung* 36B:823–832
47. van Asselt R, Elsevier CJ, Smeets WJJ, Spek AL, Benedix R (1994) *Rec Trav Chim Pays-Bas* 113:88–98
48. Kaminsky W, Miri M, Sinn H, Woldt R (1983) *Macromol Rapid Commun* 4:417
49. Moody LS, Mackenzie PB, Killian CM, Lavoie GG, Ponasik JA Jr, Barrett AG, Smith TW, Pearson JC (2002) *World patent* WO
50. Brookhart M, Grant B, Volpe AF (1992) *Organometallics* 11:3920–3922
51. Yakelis NA, Bergman RG (2005) *Organometallics* 24:3579–3581
52. Salo EV, Guan Z (2003) *Organometallics* 22:5033–5046
53. Tempel DJ, Johnson LK, Huff RL, White PS, Brookhart M (2000) *J Am Chem Soc* 122:6686–6700
54. Deng L, Woo TK, Cavallo L, Margl PM, Ziegler T (1997) *J Am Chem Soc* 119:6177–6186
55. Musaeu DG, Svensson M, Morokuma K, Stromberg S, Zetterberg K, Siegbahn PEM (1997) *Organometallics* 16:1933–1945
56. Gonsalvi L, Gaunt JA, Adams H, Castro A, Sunley GJ, Haynes A (2003) *Organometallics* 22:1047–1054
57. Guan Z, Cotts PM, McCord EF, McLain SJ (1999) *Science* 283:2059–2062
58. Cotts PM, Guan Z, McCord E, McLain S (2000) *Macromolecules* 33:6945–6952
59. Guan Z (2002) *Chem Eur J* 8:3086–3092
60. Cossee P (1964) *J Catal* 3:80–88
61. Fan L, Harrison D, Woo TK, Ziegler T (1995) *Organometallics* 14:2018–2026
62. Svejda SK, Johnson LK, Brookhart M (1999) *J Am Chem Soc* 121:10634–10635
63. Shultz LH, Tempel DJ, Brookhart M (2001) *J Am Chem Soc* 123:11539–11555

64. Deng L, Margl P, Ziegler T (1997) *J Am Chem Soc* 119:1094–1100
65. Froese RDJ, Musaev DG, Morokuma K (1998) *J Am Chem Soc* 120:1581–1587
66. Leatherman M, Svejda SA, Johnson LK, Brookhart M (2003) *J Am Chem Soc* 125:3068–3081
67. Shultz LH, Brookhart M (2001) *Organometallics* 20:3975–3982
68. Svoboda M, tom Dieck H (1980) *J Organomet Chem* 191:321–328
69. Mecking S, Johnson LK, Wang L, Brookhart M (1998) *J Am Chem Soc* 120:888–899
70. Killian CM, Tempel DJ, Johnson LK (1996) *J Am Chem Soc* 118:11664–11665
71. Gottfried AC, Brookhart M (2001) *Macromolecules* 34:1140–1142
72. Gottfried AC, Brookhart M (2003) *Macromolecules* 36:3085–3100
73. LaPointe AM, Brookhart M (1998) *Organometallics* 17:1530–1537
74. Park S, Takeuchi D, Osakada K (2006) *J Am Chem Soc* 128:3510–3511
75. Okada T, Park S, Takeuchi D, Osakada K (2007) *Angew Chem Int Ed* 46:6141–6143
76. Liu W, Brookhart M (2004) *Organometallics* 23:6099–6107
77. Leatherman M, Brookhart M (2001) *Macromolecules* 34:2748–2750
78. Gottker-Schnetmann I, Korthals B, Mecking S (2006) *J Am Chem Soc* 128:7708–7709
79. Yu S-M, Berkefeld A, Gottker-Schnetmann I, Muller G, Mecking S (2007) *Macromolecules* 40:421–428
80. Held A, Bauers FM, Mecking S (2000) *Chem Commun* 2000:301–302
81. Berkefeld A, Mecking S (2006) *Angew Chem Int Ed* 45:6044–6046
82. Held A, Mecking S (2000) *Chem Eur J* 6:4623–4629
83. Hristov IH, DeKock RL, Anderson GDW, Gottker-Schnetmann I, Mecking S, Ziegler T (2005) *Inorg Chem* 44:7806–7818
84. DeKock RL, Hristov IH, Anderson GDW, Gottker-Schnetmann I, Mecking S, Ziegler T (2005) *Organometallics* 24:2679–2687
85. Johnson LK, Wang L, McLain S, Bennett A, Dobbs K, Hauptman E, Ionkin A, Ittel S, Kunitzky K, Marshall W, McCord E, Radzewich C, Rinehart A, Sweetman KJ, Wang Y, Yin Z, Brookhart M (2003) In: Hlatky GG, Patil AO (eds) *Beyond metallocenes*. ACS symposium series, vol 857. American Chemical Society, Washington, DC, pp 131–142
86. Marques MM, Fernandes S, Correia SG, Ascenso JR, Caroco S, Gomes PT, Mano J, Pereira SG, Nunes T, Dias AR, Rausch MD, Chien JCW (2000) *Macromol Chem Phys* 201:2464–2468
87. Chen G, Ma XS, Guan Z (2003) *J Am Chem Soc* 125:6697–6704
88. Li W, Zhang X, Meetsma A, Hessen B (2004) *J Am Chem Soc* 126:12246–12247
89. Luo S, Jordan RF (2006) *J Am Chem Soc* 128:12072–12073. Foley SR, Stockland RA Jr, Shen H, Jordan RF (2003) *J Am Chem Soc* 125:4350–4361
90. Williams BS, Leatherman MD, White PS, Brookhart M (2005) *J Am Chem Soc* 127:5132–5146
91. Wu F, Foley SR, Burns CT, Jordan RF (2005) *J Am Chem Soc* 127:1841–1853
92. Stojcevic G, Prokopchuk EM, Baird MC (2005) *J Organomet Chem* 690:4349–4355
93. Deubel DV, Ziegler T (2002) *Organometallics* 21:1603–1611
94. Szabo MJ, Jordan RF, Michalak A, Piers WE, Weiss T, Yang S-Y, Ziegler T (2004) *Organometallics* 23:5565–5572
95. Li W, Zhang X, Meetsma A, Hessen B (2008) *Organometallics* 27:2052–2057
96. Kang M, Sen A, Zakharov L, Rheingold AL (2002) *J Am Chem Soc* 124:12080–12081
97. Michalak A, Ziegler T (2001) *J Am Chem Soc* 123:12266–12278
98. Michalak A, Ziegler T (2001) *Organometallics* 20:1521–1532
99. Philipp DM, Muller RP, Goddard WA III, Storer J, McAdon M, Mullins M (2002) *J Am Chem Soc* 124:10198–10210
100. Helldörfer M, Backhaus J, Alt HG (2003) *Inorg Chim Acta* 351:34–42
101. Liu H, Gomes PT, Costa SI, Duarte MT, Branquinho R, Fernandes AC, Chien JCW, Singh RP, Marques MM (2005) *J Organomet Chem* 690:1314–1323
102. Gasperini M, Ragaini F (2004) *Organometallics* 23:995–1001
103. Hansch C, Leo A, Taft RW (1991) *Chem Rev* 91:165–195

104. Gasperini M, Ragaini F, Gazzola E, Caselli A, Macchi P (2004) *Dalton Trans* 2004:3376–3382
105. Popeney C, Guan Z (2005) *Organometallics* 24:1145
106. Pappalardo D, Mazzeo M, Antinucci S, Pellicchia C (2000) *Macromolecules* 33:9483–9487
107. Cherian AE, Lobkovsky EB, Coates GW (2003) *Chem Commun* 2003:2566–2567
108. Cherian AE, Rose JW, Lobkovsky EB, Coates GW (2005) *J Am Chem Soc* 127:13770–13771
109. Rose JW, Cherian AE, Coates GW (2006) *J Am Chem Soc* 128:4186–4187
110. Feldman J, McLain SJ, Parthasarathy A, Marshall WJ, Calabrese JC, Arthur SD (1997) *Organometallics* 16:1514–1516
111. Laine TV, Lappalainen K, Liimatta J, Aitola E, Löfgren B, Leskela M (1999) *Macromol Rapid Commun* 20:487–491
112. Burns CT, Jordan RF (2007) *Organometallics* 26:6737–6749
113. Luinstra GA, Queisser J, Bildstein B, Gortz H, Amort C, Malaun M, Krajete A, Werne G, Kristen MO, Huber N, Gernert C (2003) In: Striegler S (ed) *Late transition metal polymerization catalysis*. Wiley-VCH, Weinheim, pp 59–99
114. Noël G, Röder JC, Dechert S, Pritzkow H, Bolk L, Mecking S, Meyer F (2006) *Adv Synth Catal* 348:887–897
115. Luo H-K, Schumann H (2005) *J Mol Catal A: Chem* 227:153–161
116. Wang X, Liu S, Jin G-X (2004) *Organometallics* 23:6002–6007
117. MacKinnon AL, Baird MC (2003) *J Organomet Chem* 683:114–119
118. Ketz BE, Ottenwaelder XG, Waymouth RM (2005) *Chem Commun* 2005:5693–5695
119. Lee BY, Bazan GC, Vela J, Komon ZJA, Bu X (2001) *J Am Chem Soc* 123:5352–5353
120. Diamanti SJ, Ghosh P, Shimizu F, Bazan GC (2003) *Macromolecules* 36:9731–9735
121. Chen Y, Wu G, Bazan GC (2005) *Angew Chem Int Ed* 44:1108–1112
122. Boardman BM, Valderrama JM, Munoz F, Wu G, Bazan GC, Rojas R (2008) *Organometallics* 27:1671–1674
123. Chen Y, Boardman BM, Wu G, Bazan GC (2007) *J Organomet Chem* 692:4745–4749
124. Azoulay JD, Itigaki K, Wu G, Bazan GC (2008) *Organometallics* 27:2273–2280
125. Schmid M, Eberhardt R, Klinga M, Leskela M, Rieger B (2001) *Organometallics* 20:2321–2330
126. Meinhard D, Wegner M, Kipiani G, Hearley A, Reuter P, Fischer S, Marti O, Rieger B (2007) *J Am Chem Soc* 129:9182–9191
127. Ionkin AS, Marshall WJ (2004) *Organometallics* 23:3276–3283
128. Collman JP, Hiedas L, Norton J, Finke R (1989). *Principles and applications of organometallic chemistry, part 1*. University Science Books, Mill Valley, CA
129. McKnight AL, Waymouth RM (1998) *Chem Rev* 98:2587–2598
130. Coates GW (2000) *Chem Rev* 100:1223–1252
131. Camacho DH, Salo EV, Ziller JW, Guan Z (2004) *Angew Chem Int Ed* 43:1821–1825
132. Camacho DH, Salo EV, Guan Z (2004) *Org Lett* 6:865–868
133. Vogtle F (1999) *Cyclophane chemistry*. Wiley, Chichester
134. Brothers PJ, Collman JP (1986) *Acc Chem Res* 19:209–215
135. Baker MVSBW, White AH, Williams CC (2001) *Dalton Trans* 2001:111–120
136. Uhrhammer R, Black DG, Gardner TG, Olsen JD, Jordan RF (1993) *J Am Chem Soc* 115:8493–8494
137. Small BL (1998) PhD dissertation. University of North Carolina, Chapel Hill, p 103
138. Johnson LK, Killian CM, Brookhart M (1995) *J Am Chem Soc* 117:6414–6415
139. Gates DP, Svejda SA, Onate E, Killian CM, Johnson LK, White PS, Brookhart M (2000) *Macromolecules* 33:2320–2334
140. Tempel DJ, Johnson LK, Huff RL, White PS, Brookhart M (2000) *J Am Chem Soc* 122:6686–6700
141. Camacho DH, Guan Z (2005) *Macromolecules* 38:2544–2546
142. Camacho DH, Guan Z (2005) *Macromolecules* 38:2544–2546

143. Popeney CS, Camacho DH, Guan Z (2007) *J Am Chem Soc* 129:10062–10063
144. Camacho DH, Salo EV, Guan Z, Ziller JW (2005) *Organometallics* 24:4933–4939
145. Bader A, Lindner E (1991) *Coord Chem Rev* 108:27–110
146. Braunstein P, Naud F (2001) *Angew Chem Int Ed* 40:680–699
147. Slone CS, Weinberger DA, Mirkin CA (1999) *Prog Inorg Chem* 48:233–350
148. Milione S, Bertolasi V, Cuenca T, Grassi A (2005) *Organometallics* 24:4915–4925
149. Gareau D, Sui-Seng C, Groux LF, Brisse F, Zargarian D (2005) *Organometallics* 24:4003–4013
150. Deckers PJW, Hessen B, Teuben JH (2001) *Angew Chem Int Ed* 40:2516–2519
151. Langford CH, Gray HB (1974) *Ligand substitution processes*, 2nd edn.
152. Leung DH, Ziller JW, Guan Z (2008) *J Am Chem Soc* 130:7538–7539
153. Johnson LK, Killian CM, Brookhart M (1995) *J Am Chem Soc* 117:6414–6415

Structural and Mechanistic Aspects of Copper Catalyzed Atom Transfer Radical Polymerization

Tomislav Pintauer and Krzysztof Matyjaszewski

Abstract During the past decade, atom transfer radical polymerization (ATRP) has had a tremendous impact on the synthesis of macromolecules with well-defined compositions, architectures, and functionalities. Structural features of copper(I) and copper(II) complexes with bidentate, tridentate, tetradentate, and multidentate nitrogen-based ligands commonly utilized in ATRP are reviewed and discussed. Additionally, recent advances in mechanistic understanding of copper-mediated ATRP are outlined.

Keywords Atom transfer radical polymerization, ATRP, Copper complexes, Mechanistic understanding, Structures

Contents

1	Introduction and Background	222
1.1	Principles of Atom Transfer Radical Addition (ATRA)	222
1.2	Principles of Atom Transfer Radical Polymerization	224
2	Structural Understanding of ATRP Active Copper Complexes	227
2.1	Structural Features of Copper(I) Complexes in ATRP	229
2.2	Structural Features of Copper(II) Complexes in ATRP	235
3	Mechanistic Understanding of Copper-Catalyzed ATRP	237
3.1	ATRP Equilibrium	238
3.2	Quantifying Activation and Deactivation Rate Constants	239
3.3	Correlating Redox Potential with Equilibrium Constant for Atom Transfer	242
3.4	ATRA and ATRP Catalyzed by ppm Amounts of Copper Complexes	243
4	Conclusions and Future Outlook	246
	References	247

T. Pintauer(✉)

Department of Chemistry and Biochemistry, Duquesne University, 600 Forbes Avenue,
Pittsburgh, PA 15282, USA
e-mail: pintauert@duq.edu

K. Matyjaszewski(✉)

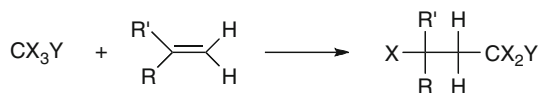
Department of Chemistry, Carnegie Mellon University, 4400 Fifth Avenue, Pittsburgh, PA 15213, USA
e-mail: km3b@andrew.cmu.edu

Abbreviations:

ATRA	Atom transfer radical addition
TMC ATRA	Transition metal-catalyzed atom transfer radical addition
ATRP	Atom transfer radical polymerization
K_{ATRP}	Equilibrium constant for atom transfer
k_a	Activation rate constant for atom transfer
k_d	Deactivation rate constant for atom transfer
bpy	2,2'-Bipyridine
dNbpy	4,4'-Di(5-nonyl)-2,2'-bipyridine
NPrPMI	<i>N</i> -propyl(2-pyridyl)methanimine
tpy	2,2':6',2''-Terpyridine
tNtpy	4,4',4''-Tris(5-nonyl)-2,2':6',2''-terpyridine
PMDETA	<i>N, N, N', N'', N''</i> -Pentamethyldiethylenetriamine
HMTETA	1,1,4,7,10,10-Hexamethyltriethylenetetramine
Me ₆ TREN	Tris[2-(dimethylaminoethyl)]amine
TPMA	Tris[(2-pyridyl)methyl]amine
Me ₄ CYCLAM	1,4,8,11-Tetraaza-1,4,8,11-tetramethylcyclotetradecane
TPEDA	<i>N, N, N', N'</i> -Tetrakis(2-pyridylmethyl)ethylenediamine
DMCBCy	Dimethylated 1,8-ethylene cross-bridged 1,4,8,11-tetraazacyclotetradecane
Sn(EH) ₂	Tin(II) 2-ethylhexanote
MA	Methyl acrylate
Sty	Styrene
<i>n</i> -BA	<i>n</i> -Butyl acrylate
EBrIB	Ethyl 2-bromoisobutyrate
PEBr	1-(Bromoethyl)benzene
PECl	1-(Chloroethyl)benzene
BzBr	Benzyl bromide
MBrP	Methyl 2-bromopropionate
MCIP	Methyl 2-chloropropionate
MClAc	Methyl chloroacetate

1 Introduction and Background**1.1 Principles of Atom Transfer Radical Addition (ATRA)**

Carbon–carbon bond formation is a fundamental reaction in organic synthesis [1, 2,3,4]. One way to form such a bond and, thus, extend a carbon chain is by the addition of a polyhalogenated alkane to an alkene to form a 1:1 adduct, as shown in Scheme 1. This reaction was first reported in the 1940s and today is known as the Kharasch addition or atom transfer radical addition (ATRA) [5,6]. Historically, Kharasch addition reactions were conducted in the presence of radical initiators or



X = halogen; Y = H, halogen, CF₃, or other electronegative group

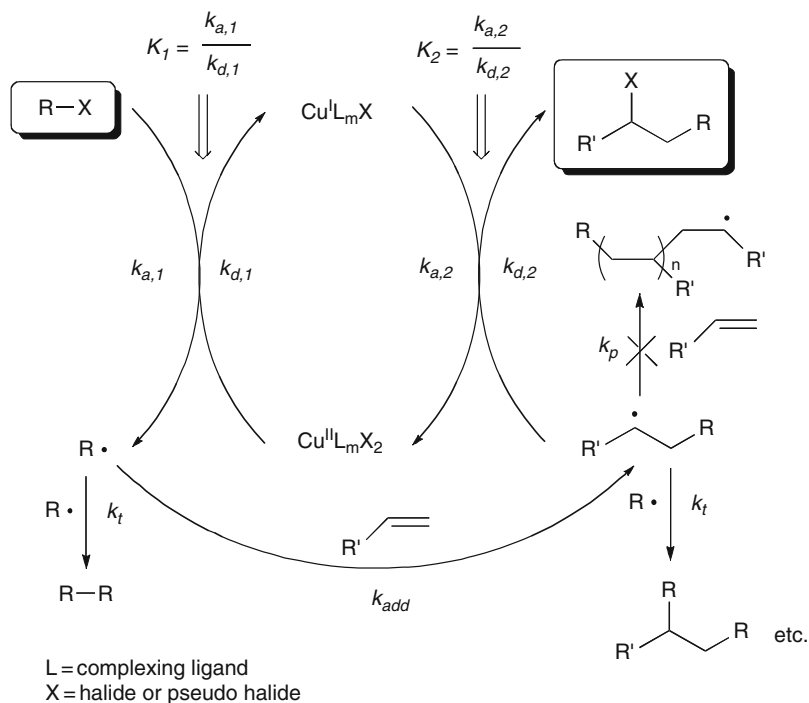
Scheme 1 Addition of polyhalogenated alkane to alkene

light. Very high yields of the monoadduct were obtained in ATRA of CCl₄ and CBr₄ to simple α -olefins (1-hexene, 1-octene, and 1-decene), but were significantly decreased for more reactive monomers such as methyl acrylate or styrene [7]. For more reactive monomers, the principle reason for decreased yield of the monoadduct was radical–radical coupling and repeating radical addition to alkene to generate oligomers. Although, radical–radical coupling reactions could be suppressed by decreasing radical concentration, telomerization reactions could not be avoided because of the low chain transfer constant. The research in this area was thus shifted to finding means to control product distribution by developing more efficient halogen transfer agents.

In the 1960s, several research groups began to investigate the use of transition metal complexes to catalyze ATRA reactions. High chemoselectivity of the monoadduct was achieved by recognizing that transition metal complexes are more effective halogen transfer agents than alkyl halides. Complexes of copper [8,9,10,11,12], iron [8,13,14,15], ruthenium [16,17,18], and nickel [19,20,21] were found to be particularly active catalysts for ATRA. Apart from controlling product distribution, great progress has also been made in utilizing a variety of halogenated compounds (alkyl and aryl halides [22,23,24], *N*-chloroamines [24], alkylsulfonyl halides [8,25,26,27,28,29], and polyhalogenated compounds [8,14,29,30]), as well as alkenes (styrene, alkyl acrylates, and acrylonitrile). Therefore, transition metal-catalyzed (TMC) ATRA became a broadly applicable synthetic tool [4,10,18,19,31].

Based on chemo-, regio-, and stereoselectivity, it is generally accepted that the mechanism of TMC ATRA involves free radical intermediates [8,24]. The proposed mechanism in the case of copper complexes is shown in Scheme 2. Homolytic cleavage of an alkyl halide bond by a copper(I) complex generates a corresponding copper(II) complex and an organic radical ($k_{a,1}$). The radical may terminate (k_t) or add to an alkene (k_{add}) in an inter- or intramolecular fashion or it can abstract the halogen atom from the copper(II) complex and return to the original dormant alkyl halide species ($k_{d,1}$). If the abstraction of the halogen atom occurs after the first addition to an alkene, the desired monoadduct will be formed ($k_{d,2}$). This step regenerates the corresponding copper(I) complex and therefore completes the catalytic cycle.

There are several guidelines that should be followed in order to increase the chemoselectivity of the monoadduct. Firstly, radical concentration must be low in order to suppress radical termination reactions (rate constant of activation [$k_{a,1}$ and $k_{a,2}$] \ll rate constant of deactivation [$k_{d,1}$ and $k_{d,2}$]). Secondly, further activation of the monoadduct should be avoided ($k_{a,1} > k_{a,2}$). Lastly, formation of oligomers should be suppressed, indicating that the rate of deactivation ($k_{d,2}$ [Cu^{II}L_mX]) should be much larger than the rate of propagation (k_p [alkene]). Alkyl halides for copper-catalyzed ATRA are typically chosen such that if addition occurs, then the newly



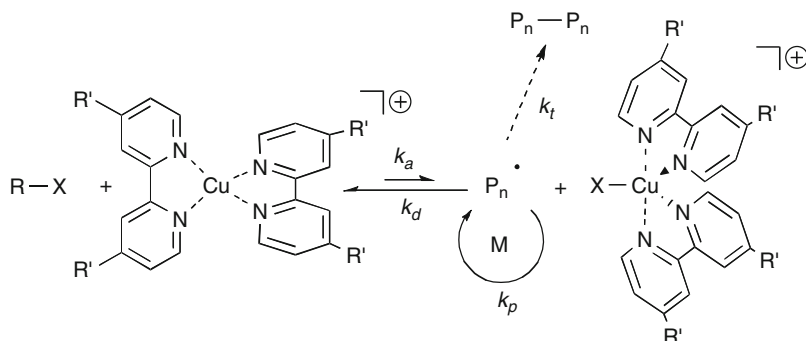
Scheme 2 Proposed mechanism for copper-catalyzed ATRA

formed radical is much less stabilized than the initial radical and will essentially irreversibly react with a copper(II) complex to form an inactive monoadduct.

TMC ATRA reactions can also be conducted intramolecularly when alkyl halide and alkene functionalities are part of the same molecule. Intramolecular TMC ATRA or atom transfer radical cyclization (ATRC) is a very attractive synthetic tool because it enables the synthesis of functionalized ring systems that can be used as starting materials for the preparation of complex organic molecules [10,11]. Furthermore, halide functionality in the resulting product can be very beneficial because it can be easily reduced, eliminated, displaced, converted to a Grignard reagent, or if desired serve as a further radical precursor. The use of copper-mediated ATRC in organic synthesis has been reviewed recently and some illustrative examples are shown in Scheme 3 [10, 11, 31, 32, 33].

1.2 Principles of Atom Transfer Radical Polymerization

In 1995, a new class of controlled/"living" radical polymerization methods was reported by the groups of Matyjaszewski [34] and Sawamoto [35]. This new process, named atom transfer radical polymerization (ATRP) [34], has had a tremendous



Scheme 4 Proposed mechanism for copper(I) 2,2'-bipyridine-catalyzed ATRP

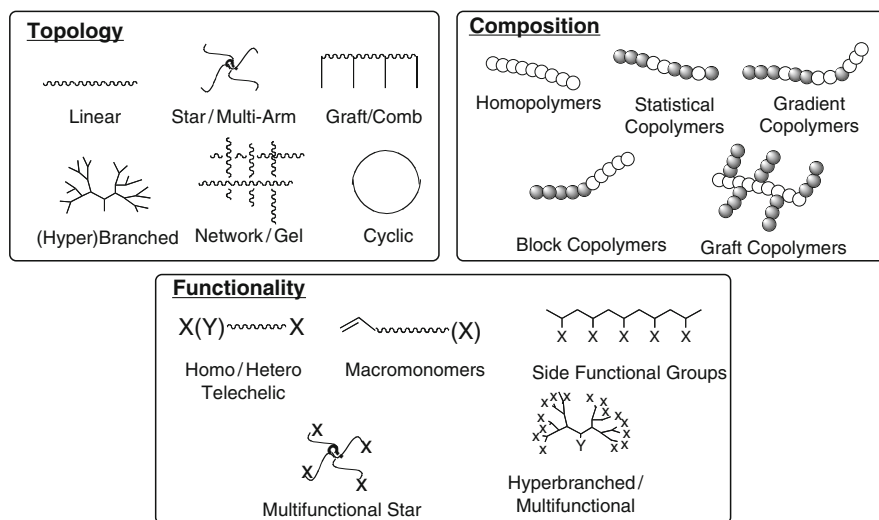
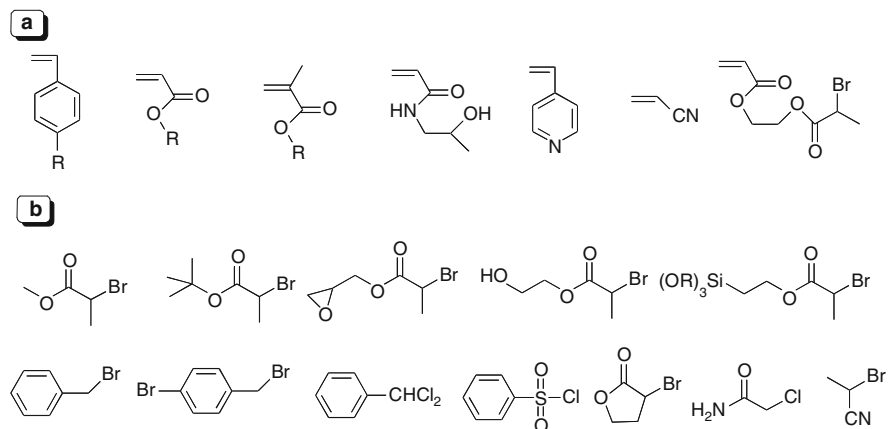


Fig. 1 Schematic representation of polymers with controlled topology, composition, and functionality synthesized using copper-catalyzed ATRP

ATRP, formation of radicals is reversible and stationary radical concentration is low because the equilibrium between the activation (k_a) and deactivation (k_d) processes, $K_{\text{ATRP}} = k_a/k_d$, is strongly shifted to the left-hand side ($k_a < k_d$). This in turn minimizes radical termination reactions and enables synthesis of polymers with predetermined molecular weights, narrow molecular weight distributions, and high functionalities [37]. Copper-catalyzed ATRP is well suited for the preparation of (co)polymers with controlled topologies, including star- and comb-like polymers, as well as branched, hyperbranched, dendritic, network, and cyclic type structures [46]. The basic strategies for producing polymeric materials by ATRP are illustrated in Fig. 1.

Copper-catalyzed ATRP is a multicomponent system, consisting of a monomer, an initiator with a transferable (pseudo)halogen, and a copper complex (composed of a copper(I) (pseudo)halide and nitrogen-based complexing ligand). For a successful



Scheme 5 Examples of vinyl monomers (a) and alkyl halide initiators (b) that are used in copper-mediated ATRP

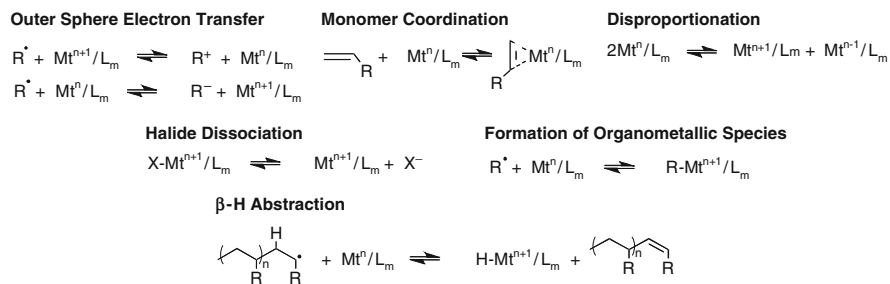
ATRP, other factors, such as solvent and temperature, must also be taken into consideration. Typical monomers and alkyl halide initiators that are used in ATRP are shown in Scheme 5 [47]. The copper complex is perhaps the most important component of this catalytic system because it regulates the dynamic equilibrium between dormant and active species. In this article, structural and mechanistic aspects of copper-catalyzed ATRP are discussed.

2 Structural Understanding of ATRP Active Copper Complexes

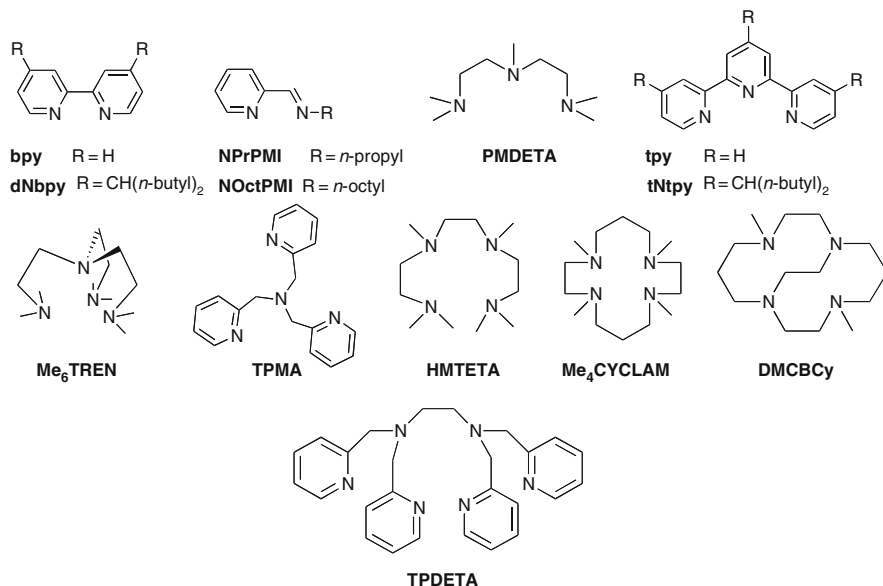
Structural characterization of transition metal complexes involved in catalysis is essential for understanding of the reaction mechanism and can provide invaluable information regarding catalyst design and performance. In ATRA and ATRP reactions, the catalyst typically consists of a transition metal accompanied by a complexing ligand and counterion, which can form a covalent or ionic bond with the metal center. An efficient catalyst should be able to expand its coordination sphere and oxidation number upon halogen atom abstraction from an alkyl halide or dormant polymer species. Additionally, the catalyst should not participate in any side reactions, as they would result in lowering of the catalytic activity. Concurrent reactions that can occur during the ATRA or ATRP process include the following (Scheme 6) [36, 49, 50, 51, 52, 71, 72]:

1. Monomer, solvent, or radical coordination to the metal center
2. Oxidation/reduction of radicals to radical cations/anions, respectively
3. β -Halogen abstraction
4. Disproportionation

In copper-catalyzed ATRA and ATRP, bidentate, tridentate, tetradentate, and multidentate nitrogen-based ligands are employed (Scheme 7). In the following sections, solid state structural features of copper(I) and copper(II) complexes with 2,2'-bipyridine (bpy) [34], 4,4'-di(5-nonyl)-2,2'-bipyridine (dNbpy) [70, 73], *N*-propyl(2-pyridyl)methanimine (NPrPMI) [74, 75, 76, 77, 78], 2,2':6',2''-terpyridine (tpy) [79], 4,4',4''-tris(5-nonyl)-2,2':6',2''-terpyridine (tNtpy) [79], *N,N,N',N'',N'''*-pentamethyldiethylenetriamine (PMDETA) [80], 1, 1, 4, 7, 10, 10-hexamethyltriethylenetetramine (HMTETA) [81, 82], tris[(2-dimethylaminoethyl)amine (Me₆TREN) [83], tris[(2-pyridyl)methyl]amine (TPMA) [80], tripodal imidazole containing ligands [84], 1, 4, 8, 11-tetraaza-1,4,8,11-tetramethylcyclotetradecane (Me₄CYCLAM) [85], *N,N,N',N'*-tetrakis(2-pyridylmethyl)ethylenediamine



Scheme 6 Possible side reactions in metal-catalyzed ATRA/ATRP



Scheme 7 Nitrogen-based ligands commonly used in copper-catalyzed ATRA and ATRP

(TPEDA) [86], and dimethylated 1,8-ethylene cross bridged 1,4,8,11-tetraazacyclotetradecane (DMCBCy) [87] in ATRA and ATRP will be outlined.

2.1 Structural Features of Copper(I) Complexes in ATRP

2.1.1 Bidentate Ligands

Bidentate nitrogen-based ligand 2,2'-bipyridine (bpy) was historically the first ligand that was successfully used in copper-catalyzed ATRP [34]. Alkyl substitutions in the 4 and 4' positions of the bipyridine ring, such as in the dNbpy ligand, further improved solubility of the complex in nonpolar medium, which resulted in higher monomer conversions with polydispersities remaining low [73]. Copper(I) complexes with bpy-based ligands are typically prepared by reacting copper(I) salts, or their complexes with CH_3CN , with two equivalents of the ligand. The general formula of the resulting complexes is $[\text{Cu}^{\text{I}}(\text{bpy})_2][\text{Y}]$ (where $\text{Y} = \text{Br}^-$, Cl^- , PF_6^- , ClO_4^- , BF_4^- , $\text{Cu}^{\text{I}}\text{Br}_2^-$, and $\text{Cu}^{\text{I}}\text{Cl}_2^-$). In the solid state, $[\text{Cu}^{\text{I}}(\text{bpy})_2]^+$ cations are distorted tetrahedral in geometry (Fig. 2) and the copper(I) center is coordinated by four nitrogen atoms from two bpy units [88, 89, 90, 91, 92, 93, 94]. The average Cu–N bond length ranges from 1.985 to 2.075 Å and is not greatly affected by either the counterion or the substituents in the 4 and 4' positions of the bpy ligand.

Furthermore, the “bite” angles are typically between 80° and 83° due to the rigid geometry of the bpy-based ligand. Perhaps, the only more pronounced difference in the structure of $[\text{Cu}^{\text{I}}(\text{bpy})_2]^+$ cation in $[\text{Cu}^{\text{I}}(\text{bpy})_2][\text{Y}]$ complexes can be seen in a wide variation of the dihedral angles between CuN_2 planes. Based on the structurally isolated complexes, the smallest dihedral angle was observed in $[\text{Cu}^{\text{I}}(\text{bpy})_2][\text{PF}_6^-]$ (44.6°) [90] complex and the largest one in $[\text{Cu}^{\text{I}}(\text{dNEObpy})_2][\text{Cu}^{\text{I}}\text{Br}_2^-]$ (89.0°) [91], which is also an effective catalyst in ATRP. The differences in dihedral angles

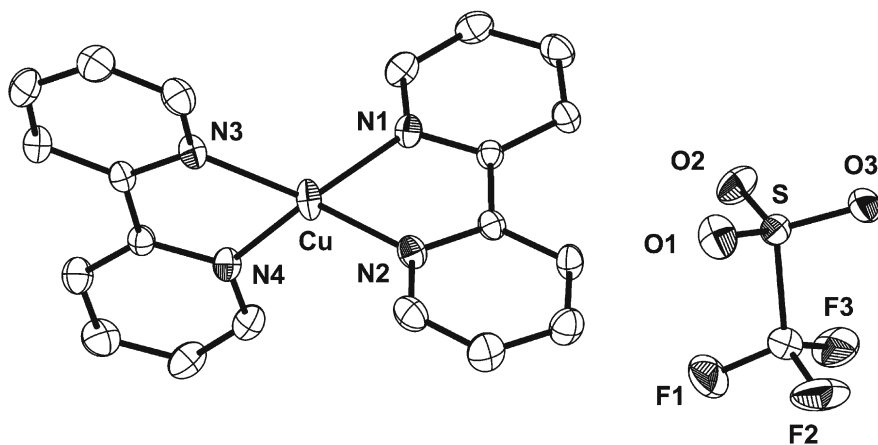


Fig. 2 Molecular structure of $[\text{Cu}^{\text{I}}(\text{bpy})_2][\text{CF}_3\text{SO}_3^-]$ [88]

can mostly be attributed to crystal packing forces, as discussed in the literature [95, 96]. It has also been observed that the dihedral angle affects the redox potential of the $[\text{Cu}^{\text{I}}(\text{bpy})_2]^+$ cation, and consequently the stability constants of $[\text{Cu}^{\text{I}}(\text{bpy})_2]^+$ and $[\text{Cu}^{\text{II}}(\text{bpy})_2]^{2+}$ cations [92, 97].

In the case of $\text{Cu}^{\text{I}}\text{X}$ ($\text{X} = \text{halide}$) complexes with bpy-based ligands, an additional mode of coordination was observed, which includes formation of a halide-bridged complex [93]. This has been demonstrated in the solid state structure of $[\text{Cu}^{\text{I}}(\text{bpy})\text{Br}]_2$ and $[\text{Cu}^{\text{I}}(\text{bpy})\text{I}]_2$ dimers. In $[\text{Cu}^{\text{I}}(\text{bpy})\text{Br}]_2$, the copper(I) center is distorted tetrahedral in geometry and is coordinated by two nitrogen atoms of a bpy ligand ($\text{Cu}^{\text{I}}\text{-N} = 2.083(6)$ and $2.099(5)$ Å) and two bromide anions ($\text{Cu}^{\text{I}}\text{-Br} = 2.428(2)$ and $2.463(1)$ Å). The structure of the $[\text{Cu}^{\text{I}}(\text{bpy})\text{I}]_2$ dimer was analogous to $[\text{Cu}^{\text{I}}(\text{bpy})\text{Br}]_2$ ($\text{Cu}^{\text{I}}\text{-N} = 2.070(8)$ and $2.080(1)$ Å, $\text{Cu}^{\text{I}}\text{-I} = 2.583(3)$ and $2.587(4)$ Å).

Bipyridine-based ligands typically coordinate to the copper(I) center with a relatively large equilibrium constant for the coordination of the first bpy ligand ($K_1 = 10^7\text{--}10^9$), followed by much weaker coordination of the second one ($K_2 = 10^3\text{--}10^4$) [98, 99, 100]. Therefore, ligand substitution reactions are likely to occur only by the substitution of one of the two bpy ligands. In the simplest case, coordination of the solvent can occur, as demonstrated in the case of the $[\text{Cu}^{\text{I}}(\text{bpy})(\text{CH}_3\text{CN})_2][\text{ClO}_4]$ complex [101]. In ATRA and ATRP processes, bpy ligand can be substituted by monomer, which is typically present in large excess relative to copper(I) complex. Monomer coordination has been demonstrated in the case of $[\text{Cu}^{\text{I}}(\text{bpy})(\pi\text{-styrene})][\text{A}]$ ($\text{A} = \text{ClO}_4^-$, PF_6^- , and CF_3SO_3^-) and $[\text{Cu}^{\text{I}}(\text{bpy})(\pi\text{-methyl acrylate})][\text{A}]$ ($\text{A} = \text{ClO}_4^-$, PF_6^- , and CF_3SO_3^-) complexes (Fig. 3) [101, 102]. Additionally, $\text{Cu}^{\text{I}}/\text{bpy}$ complexes with ethylene, propylene, and series of other olefins with the general formula $[\text{Cu}^{\text{I}}(\text{bpy})(\pi\text{-olefin})][\text{A}]$ have been reported [103, 104].

Chelating bis(imine) ligands such as *N*-alkyl(2-pyridyl)methanimine (AlkPMI) have also been successfully utilized in copper-mediated ATRP [74, 75, 76, 77, 78]. In

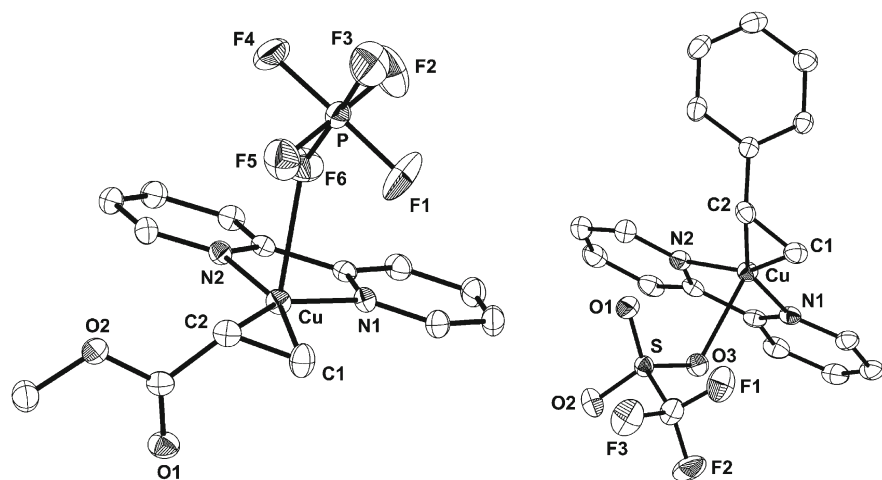


Fig. 3 Molecular structures of $[\text{Cu}^{\text{I}}(\text{bpy})(\pi\text{-methyl acrylate})][\text{PF}_6]$ and $[\text{Cu}^{\text{I}}(\text{bpy})(\pi\text{-styrene})][\text{CF}_3\text{SO}_3]$ [101, 102]

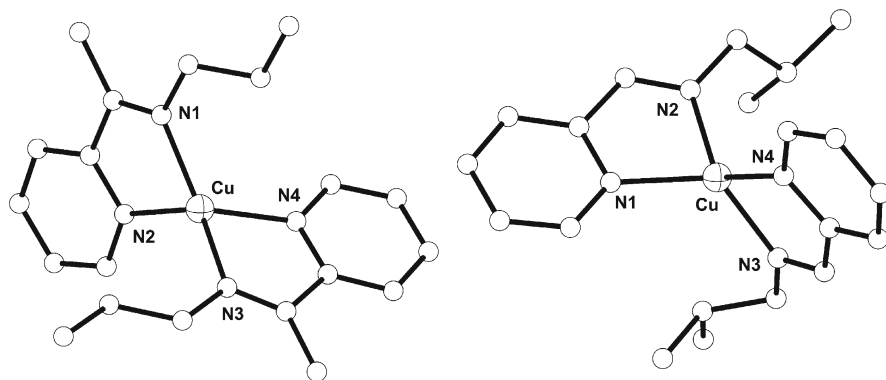


Fig. 4 Structures of $[\text{Cu}^{\text{I}}(n\text{PrPMI})_2]^+$ and $[\text{Cu}^{\text{I}}(i\text{BuPMI})_2]^+$ cations [76]

particular, complexes $[\text{Cu}^{\text{I}}(n\text{PrPMI})_2][\text{PF}_6]$, $[\text{Cu}^{\text{I}}(i\text{BuPMI})][\text{BF}_4]$, and $[\text{Cu}^{\text{I}}(\text{secBuPMI})_2][\text{BF}_4]$ have been isolated and structurally characterized so far (Fig. 4) [76]. In all three complexes, copper(I) centers were distorted tetrahedral in geometry with average $\text{Cu}^{\text{I}}\text{-N}$ bond lengths of 2.019 Å (*nPr*), 2.037 Å (*iBu*), and 2.087 Å (*secBu*) and dihedral angles of 80.75° (*nPr*), 81.09° (*iBu*), and 81.12° (*secBu*), similar to bpy derivatives. The similarity in the solid state structures of $\text{Cu}^{\text{I}}/\text{AlkPMI}$ and $\text{Cu}^{\text{I}}/\text{bpy}$ complexes is also reflected in their comparable ATRP activity. However, the two classes of complexes might undergo different side reactions in solution, such as loss of ligand followed by monomer and/or solvent coordination. Monomer coordination has been demonstrated in the case of ATRP of aminoethyl methacrylates and methoxy[poly(ethylene glycol)]methacrylates catalyzed by the $\text{Cu}^{\text{I}}\text{Br}/2n\text{PrPMI}$ complex [78].

2.1.2 Tridentate Ligands

Apart from substituted bipyridines, other linear and cyclic amines were successfully used as ligands in copper-catalyzed ATRP [80, 81, 82, 83]. Particularly, commercially available tridentate *N,N,N',N'',N'''*-pentamethyldiethylenetriamine (PMDETA) showed a high potential for the controlled polymerization of a variety of monomers. Typically, ligand to copper(I) halide ratio used in the polymerization was 1:1. Copper(I) complexes with PMDETA have been much less extensively studied than the corresponding complexes with bpy-based ligands. In all complexes isolated so far that contain noncoordinating counterions, PMDETA acts as a tridentate ligand and the fourth coordination site is typically occupied by monodentate ligands such as CO, CH_3CN , or olefin/monomer [105, 106, 107, 108, 109, 110, 111]. In the case of $\text{Cu}^{\text{I}}\text{X}$ ($\text{X} = \text{Br}^-$ and Cl^-), it is therefore reasonable to assume that neutral $\text{Cu}^{\text{I}}(\text{PMDETA})\text{X}$ complexes will be formed.

We were recently able to isolate and structurally characterize a series of $[\text{Cu}^{\text{I}}(\text{PMDETA})(\pi\text{-M})][\text{BPh}_4]$ complexes ($\text{M} = \text{styrene}$, methyl acrylate, methyl methacrylate, and 1-octene) [110, 111]. Molecular structures of $[\text{Cu}^{\text{I}}(\text{PMDETA})(\pi\text{-methyl acrylate})][\text{BPh}_4]$ and $[\text{Cu}^{\text{I}}(\text{PMDETA})(\pi\text{-styrene})][\text{BPh}_4]$ are shown in Fig. 5. In all complexes, PMDETA acted as a tridentate ligand, while the

pseudotetrahedral coordination geometry around copper(I) was completed by a π -interaction with the C=C double bond of monomer in the presence of noncoordinating counterion (BPh_4^-). No significant lengthening of the C=C vinyl bond in methyl acrylate or 1-octene upon coordination was observed, while the C=C bond length of styrene increased from 1.325(2) to 1.367(3) Å. A decrease in the C=C IR stretching frequencies of $\Delta(\text{C}=\text{C}) = -110, -80, \text{ and } -109 \text{ cm}^{-1}$ for complexes with methyl acrylate, styrene, and 1-octene, respectively, was observed upon coordination. Furthermore, the upfield shift of vinyl proton resonances indicated the presence of significant π -back bonding. In solution, the affinity of monomers for the copper(I) center was found to increase in the order methyl acrylate > 1-octene > styrene > methyl methacrylate with formation constants at room temperature equal to 760, 320, 250 and 6 M^{-1} . The lower equilibrium constant for methyl methacrylate binding was explained in terms of steric hindrance imposed by the methyl group.

Substituted terpyridine, 4,4',4''-tris(5-nonyl)-2,2':6',2''-terpyridine (tNtpy), is a planar tridentate ligand that was successfully used in homogeneous ATRP of methyl acrylate and styrene [79]. Polymerization of both monomers was controlled and the resulting polymers had relatively low polydispersities ($M_w/M_n < 1.2$). Similarly to PMDETA, the typical ligand to copper(I) halide ratio used in the polymerization was 1:1. Terpyridine and its derivatives are expected to form tetra-coordinated complexes with copper(I) in which the fourth coordination sphere is occupied by a monodentate ligand (Br^- , Cl^- , solvent, monomer, etc.). Although,

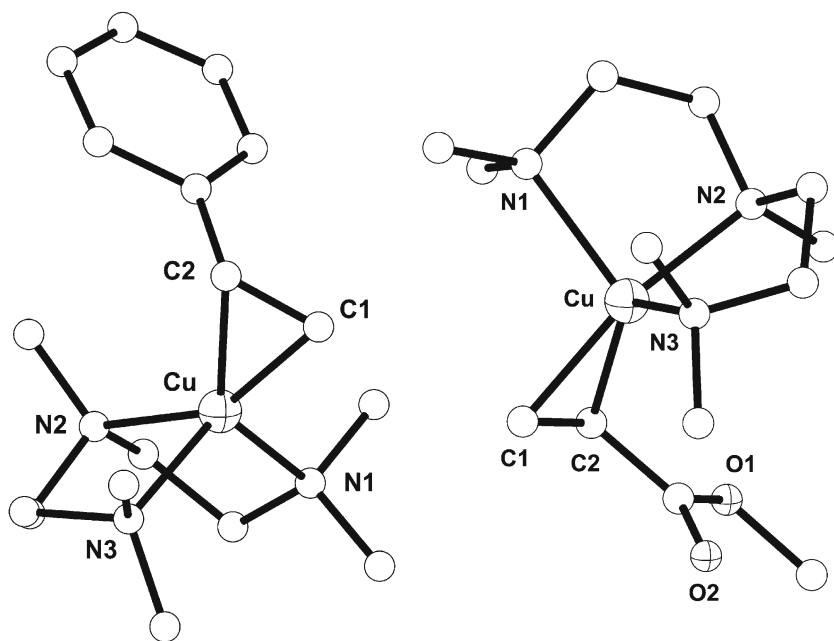


Fig. 5 Molecular structures of $[\text{Cu}^{\text{I}}(\text{PMDETA})(\pi\text{-styrene})][\text{BPh}_4]$ and $[\text{Cu}^{\text{I}}(\text{PMDETA})(\pi\text{-methyl acrylate})][\text{BPh}_4]$. The $[\text{BPh}_4]^-$ counterion has been removed for clarity [110]

$\text{Cu}^{\text{I}}\text{X}$ ($\text{X} = \text{Br}^-$ and Cl^-) complexes with tpy-based ligands have not been isolated and characterized in the solid state, structurally related complexes include $[\text{Cu}^{\text{I}}(\text{tpy})(\text{py})][\text{ClO}_4]$ ($\text{py} = \text{pyridine}$) [112, 113] and $[\text{Cu}^{\text{I}}(\text{tpy})(\text{CH}_3\text{CN})][\text{CH}_3\text{COO}]$ [114].

2.1.3 Tetradentate Ligands

Copper(I) complexes with tetradentate nitrogen-based ligands tris[2-(dimethylaminoethyl)amine (Me_6TREN), tris[(2-pyridyl)methyl]amine (TPMA), 1,4,8,11-tetraaza-1,4,8,11-tetramethylcyclotetradecane (Me_4CYCLAM), and dimethylated 1,8-ethylene cross-bridged 1,4,8,11-tetraazacyclotetradecane (DMCBCy) are among the most active catalysts in ATRP [81, 82, 83, 86, 87, 115]. Solid state structures of copper(I) complexes with these ligands are very rare. The principal problem in isolating crystals suitable for X-ray analysis is the fact that they are extremely air- and moisture-sensitive. Schindler and coworkers have succeeded in isolating crystals of $[\text{Cu}^{\text{I}}(\text{Me}_6\text{TREN})][\text{ClO}_4]$ complex for which the X-ray analysis indicated the presence of copper(I) cations coordinated by four nitrogen atoms of Me_6TREN ligand ($\text{Cu}^{\text{I}}\text{-N}(\text{equatorial}) = 2.122(7) \text{ \AA}$ and $\text{Cu}^{\text{I}}\text{-N}(\text{axial}) = 2.200(14) \text{ \AA}$) [116]. Additionally, a weak interaction between the copper(I) center and the oxygen atom from the perchlorate anion was observed ($\text{Cu}^{\text{I}}\text{-O} = 3.53(1) \text{ \AA}$).

TPMA ligand typically coordinates to the copper(I) center in a tetradentate fashion, similarly to Me_6TREN [117]. However, the role of counterion coordination (in particular Br^- and Cl^-) in these complexes still remains very unclear. Recently, we were able to isolate and structurally characterize neutral $\text{Cu}^{\text{I}}(\text{TPMA})\text{Cl}$ [118] and $\text{Cu}^{\text{I}}(\text{TPMA})\text{Br}$ [119] complexes. To our surprise, both complexes were pseudopentacoordinated (Fig. 6). In $\text{Cu}^{\text{I}}(\text{TPMA})\text{Cl}$, the copper(I) ion was coordinated by four nitrogen atoms with bond lengths of 2.0704(11), 2.0833(11), 2.0888(11) \AA for the equatorial $\text{Cu}^{\text{I}}\text{-N}$, and 2.4366(11) \AA for the axial $\text{Cu}^{\text{I}}\text{-N}$ bonds, and a chlorine atom with a bond length of 2.3976(4) \AA . The molecular structure of $\text{Cu}^{\text{I}}(\text{TPMA})\text{Br}$ was similar to the structure of $\text{Cu}^{\text{I}}(\text{TPMA})\text{Cl}$ and the complex was also found to be pseudopentacoordinated in the solid state due to the coordination of TPMA ($\text{Cu}^{\text{I}}\text{-N}_{\text{eq}}$

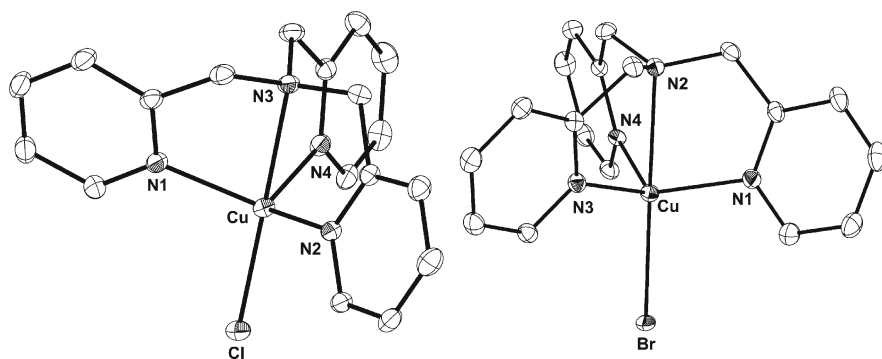


Fig. 6 Molecular structures of $\text{Cu}^{\text{I}}(\text{TPMA})\text{Cl}$ [118] and $\text{Cu}^{\text{I}}(\text{TPMA})\text{Br}$ [119] complexes

= 2.1024(15), 2.0753(15), 2.0709(15) Å, $\text{Cu}^1\text{-N}_{\text{ax}} = 2.4397(14)$ Å) and bromine atom to the copper(I) center ($\text{Cu}^1\text{-Br} = 2.5088(3)$ Å). Axial elongation of the Cu–N bond is not induced by the coordination of Br^- and Cl^- anions to $[\text{Cu}^1(\text{TPMA})]^+$ cations, because similar elongations have been observed in $[\text{Cu}^1(\text{TPMA})(\text{CH}_3\text{CN})][\text{A}]$ ($\text{A} = \text{ClO}_4^-$, PF_6^- and BPh_4^-) complexes (Eckenhoff and Pintauer, unpublished results). These results indicate that halide anions are very weakly coordinated to $[\text{Cu}^1(\text{TPMA})]^+$ cations. Therefore, from the mechanistic point of view, activation in ATRA/ATRP processes with copper complexes containing TPMA ligand proceeds with prior dissociation of halide anion from $\text{Cu}^1(\text{TPMA})\text{X}$ complex ($\text{X} = \text{Br}^-$ and Cl^-).

2.1.4 Multidentate Ligands

Multidentate nitrogen-based ligand *N,N,N',N'*-tetrakis(2-pyridylmethyl)ethylenediamine (TPEDA) has been successfully used in copper-mediated ATRA and ATRP reactions [86]. It is a highly active ligand which, in conjunction with Cu^1Br , effectively catalyzes controlled/“living” radical polymerizations of methyl acrylate, methyl methacrylate, and styrene using very low concentrations of the copper complex (6–8 ppm). The molecular structure of $\text{Cu}^1_2\text{Br}_2(\text{TPEDA})$ in the solid state indicated the formation of binuclear $\text{Cu}^1_2\text{Br}_2(\text{TPEDA})$ complex (Fig. 7). In $\text{Cu}^1_2\text{Br}_2(\text{TPEDA})$, each copper(I) center was coordinated by two nitrogen atoms from pyridyl groups ($\text{Cu}^1\text{-N} = 2.024$ and 2.057 Å), one tertiary amine nitrogen atom ($\text{Cu}^1\text{-N} = 2.336$ Å), and a bromine atom ($\text{Cu}^1\text{-Br} = 2.327$ Å), resulting in a distorted tetrahedral geometry. In solution, $\text{Cu}^1\text{Br}/\text{TPEDA}$ was found to undergo equilibrium between binuclear and mononuclear complexes.

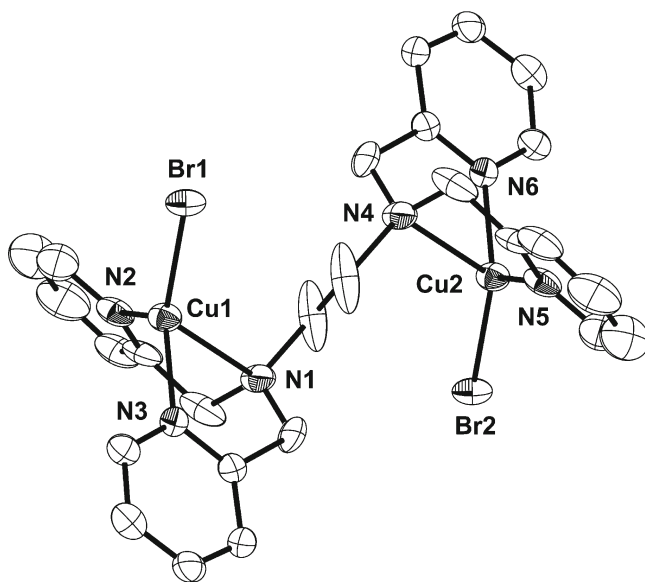


Fig. 7 Molecular structure of binuclear $\text{Cu}^1_2\text{Br}_2(\text{TPDETA})$ complex [86]

2.2 Structural Features of Copper(II) Complexes in ATRP

Copper(II) complexes that are generated during ATRA and ATRP processes are essential for the deactivation step (i.e., reversible halogen atom abstraction from a copper(II) complex by radicals to generate dormant alkyl halide species and a copper(I) complex; Schemes 2 and 4). Copper(II) complexes that were isolated from the ATRP reaction mixtures showed either a trigonal bipyramidal ($[\text{Cu}^{\text{II}}(\text{dNbpy})\text{Br}]$ $[\text{Cu}^{\text{I}}\text{Br}_2]$, $[\text{Cu}^{\text{II}}(\text{Me}_6\text{TREN})\text{Br}][\text{Br}]$ and $[\text{Cu}^{\text{II}}(\text{TPMA})\text{Br}][\text{Br}]$) or a distorted square pyramidal coordination ($\text{Cu}^{\text{II}}(\text{PMDETA})\text{Br}_2$, $\text{Cu}^{\text{II}}(\text{tNbpy})\text{Br}_2$, $[\text{Cu}^{\text{II}}(\text{Me}_4\text{CYCLAM})\text{Br}][\text{Br}]$, and $[\text{Cu}^{\text{II}}(\text{TPEDA})\text{Br}][\text{Br}]$) (Fig. 8 and Table 1) [86, 118, 119, 120]. Depending on the type of amine ligand, complexes were either neutral (triamines) or ionic (bpy and tetramines). Additionally, counterions were either bromide (Me_4CYCLAM , Me_6TREN , TPMA , and TPDETA) or linear $[\text{Cu}^{\text{I}}\text{Br}_2]^-$ (dNbpy). The simplest structural parameter that can be correlated with the kinetics of the ATRP deactivation process is the $\text{Cu}^{\text{II}}-\text{Br}$ bond length. The strength of this bond can be used as a crude estimate to evaluate the deactivation rate constant (k_d), which is responsible for the control in ATRP systems.

Table 1 Structural parameters for Cu^{II} complexes with nitrogen-based ligands

Complex	$\text{Cu}^{\text{II}}-\text{Br}$ (Å)	$\text{Cu}^{\text{II}}-\text{N}$ (Å)	τ^a	k_d ($\text{M}^{-1} \text{s}^{-1}$)
$[\text{Cu}^{\text{II}}(\text{dNbpy})\text{Br}][\text{Br}]$	2.426(3)	1.946(13)	1.0	2.1×10^7
	–	1.977(15)	–	–
	–	2.051(15)	–	–
	–	2.088(16)	–	–
$\text{Cu}^{\text{II}}(\text{tNbpy})\text{Br}_2$	2.4071(10)	1.962(5)	0.21	4.1×10^5
	2.5276(10)	2.056(5)	–	–
	–	2.062(5)	–	–
$\text{Cu}^{\text{II}}(\text{PMDETA})\text{Br}_2$	2.4462(9)	2.086(4)	0.76	6.1×10^6
	2.6442(9)	2.103(4)	–	–
	–	2.104(4)	–	–
$[\text{Cu}^{\text{II}}(\text{Me}_6\text{TREN})\text{Br}][\text{Br}]$	2.393(3)	2.143(3) _{ax}	1.0	1.4×10^7
	–	2.069(4) _{eq}	–	–
$[\text{Cu}^{\text{II}}(\text{TPMA})\text{Br}][\text{Br}]$	2.3836(6)	2.040(3) _{ax}	1.0	6.4×10^6
	–	2.073(2) _{eq}	–	–
$[\text{Cu}^{\text{II}}(\text{Me}_4\text{CYCLAM})\text{Br}][\text{Br}]$	2.8092(6)	2.071(3)	0.05	2.0×10^4
	–	2.078(3)	–	–
	–	2.098(3)	–	–
	–	2.101(3)	–	–
$[\text{Cu}^{\text{II}}(\text{TPDETA})\text{Br}][\text{Br}]$	2.686(1)	2.004(5)	0.15	5.4×10^6
	–	2.006(4)	–	–
	–	2.055(5)	–	–
	–	2.074(4)	–	–

^a τ parameter is calculated as $\tau = (\varphi_1 - \varphi_2)/60$ where φ_1 and φ_2 are the largest and second largest N– Cu^{II} –N(X) bond angles, $\tau = 1$ (regular trigonal bipyramidal geometry) and $\tau = 0$ (regular square pyramidal geometry)

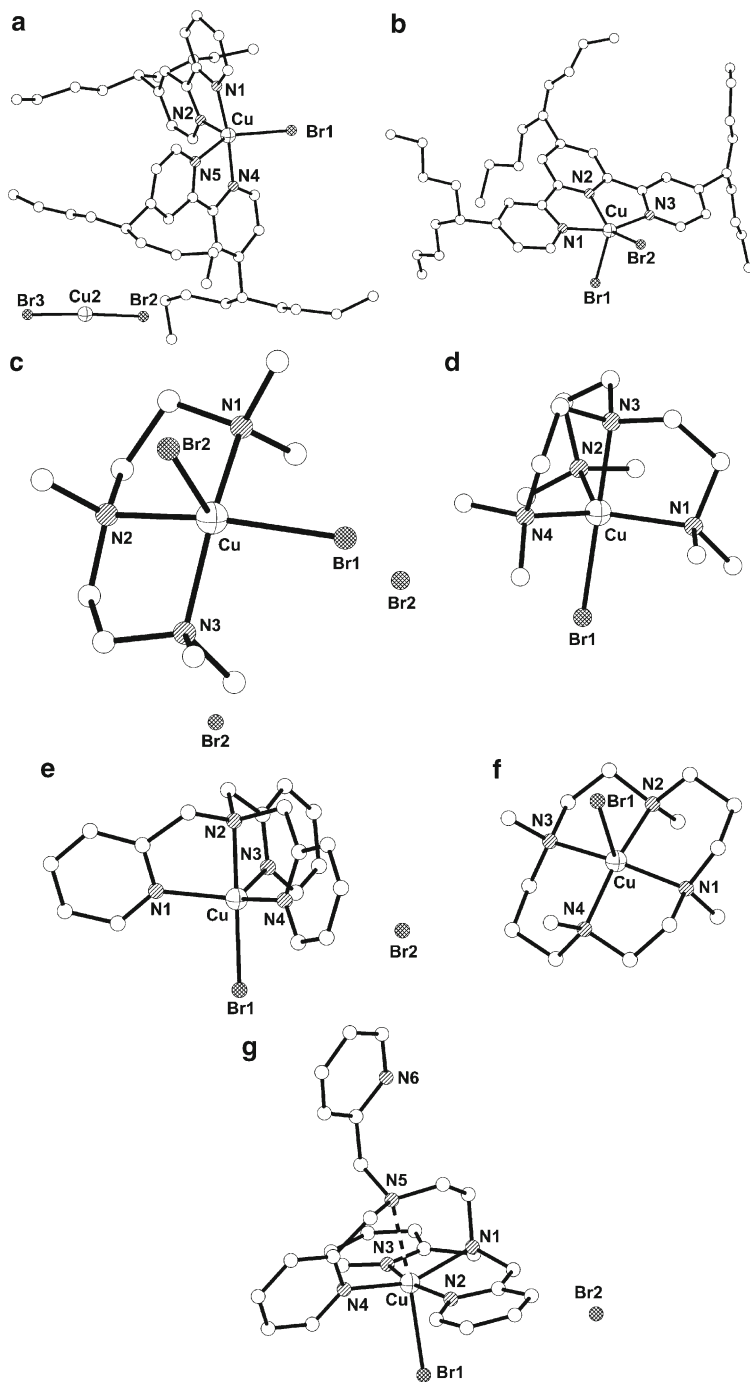


Fig. 8 Molecular structures of $[\text{Cu}^{\text{II}}(\text{dNbpy})][\text{Cu}^{\text{I}}\text{Br}_2]$ (a), $\text{Cu}^{\text{II}}(\text{tNtpy})\text{Br}_2$ (b), $\text{Cu}^{\text{II}}(\text{PMDETA})\text{Br}_2$ (c), $[\text{Cu}^{\text{II}}(\text{Me}_6\text{TREN})\text{Br}][\text{Br}]$ (d), $[\text{Cu}^{\text{II}}(\text{TPMA})\text{Br}][\text{Br}]$ (e), $[\text{Cu}^{\text{II}}(\text{Me}_4\text{CYCLAM})\text{Br}][\text{Br}]$ (f), $[\text{Cu}^{\text{II}}(\text{TPEDA})\text{Br}][\text{Br}]$ (g) [86, 118, 119, 120]

Table 1 also shows the comparison between the Cu^{II}–Br bond length and the deactivation rate constant for copper(II) complexes with the nitrogen-based ligands indicated in Fig. 8. As indicated in the table, there is no direct correlation between the length of the Cu^{II}–Br bond and the deactivation rate constant. It appears that the weaker or longer Cu^{II}–Br bond length is not the only factor that effects the deactivation ($[\text{Cu}^{\text{II}}(\text{Me}_4\text{CYCLAM})\text{Br}][\text{Br}]$ [$k_{\text{d}} = 2.0 \times 10^4 \text{ M}^{-1} \text{ s}^{-1}$ and Cu^{II}–Br = 2.8092(6) Å] vs. $[\text{Cu}^{\text{II}}(\text{Me}_6\text{TREN})\text{Br}][\text{Br}]$ [$k_{\text{d}} = 1.4 \times 10^7 \text{ M}^{-1} \text{ s}^{-1}$ and Cu^{II}–Br = 2.393(3) Å]).

The structural reorganization of copper(II) complex upon bromine atom abstraction by a corresponding radical is another important process that needs to be taken into account. For example, structural features of Cu^I(TPMA)Br (Fig. 6b) and $[\text{Cu}^{\text{II}}(\text{TPMA})\text{Br}][\text{Br}]$ (Fig. 8e) complexes, which represent the activator and deactivator, respectively, are very similar from the point of view of TPMA coordination [118,119]. In Cu^I(TPMA)Br complex, the average Cu^I–N_{eq} bond length is 0.0100 Å longer than in $[\text{Cu}^{\text{II}}(\text{TPMA})\text{Br}][\text{Br}]$. The N_{ax}–Cu–N_{eq} angles are very similar in both complexes, while the average angle in the plane N_{ax}–Cu–N_{ax} is slightly larger in $[\text{Cu}^{\text{II}}(\text{TPMA})\text{Br}][\text{Br}]$ (117.53(3)°) than in Cu^I(TPMA)Br (113.51(10)°). The only more pronounced difference in TPMA coordination to the copper center can be seen in shortening of Cu–N_{ax} bond length by approximately 0.400 Å on going from Cu^I(TPMA)Br to $[\text{Cu}^{\text{II}}(\text{TPMA})\text{Br}][\text{Br}]$. Similar observations were also made in the case of Cu^I(TPMA)Cl and $[\text{Cu}^{\text{II}}(\text{TPMA})\text{Cl}][\text{Cl}]$ complexes, in which the shortening of Cu–N_{ax} bond length on going from copper(I) to copper(II) complex was determined to be 0.389 Å. Therefore, from the structural point of view, high activity of Cu^I(TPMA)Br and $[\text{Cu}^{\text{II}}(\text{TPMA})\text{Br}][\text{Br}]$ complexes in ATRP and ATRP can be explained by minimum entropic rearrangement when Cu^I(TPMA)Br complex homolytically cleaves the R–Br bond to generate $[\text{Cu}^{\text{II}}(\text{TPMA})\text{Br}][\text{Br}]$.

3 Mechanistic Understanding of Copper-Catalyzed ATRP

Mechanistically, ATRP is a complex process based on several elementary reactions. Similarly to conventional free radical polymerization, elementary reactions in ATRP consist of initiation, propagation, and termination, which are systematically evaluated using pulse laser polymerization techniques and EPR measurements [121,122]. Perhaps the most important reaction parameters in ATRP are activation (k_{a}) and deactivation (k_{d}) rate constants and, consequently, the equilibrium constant for atom transfer ($K_{\text{ATRP}} = k_{\text{a}}/k_{\text{d}}$). These strongly depend on the structure of alkyl halide, monomer, solvent, temperature, and more importantly of the copper complex. Systematic evaluation of K_{ATRP} , k_{a} , and k_{d} is crucial in further understanding of the ATRP mechanism and can provide information about the nature and reactivity of active intermediates, and of the factors needed to design more active catalysts that can be used in smaller concentrations and also polymerize currently inactive monomers. The following paragraphs will outline strategies for mechanistic understanding of ATRA and ATRP reactions.

3.1 ATRP Equilibrium

The equilibrium constant for ATRP, $K_{\text{ATRP}} = k_a/k_d$, provides critical information about the position of dynamic equilibrium between dormant and active species during polymerization (Scheme 4). The relative magnitude of K_{ATRP} can be easily accessed from the polymerization kinetics using $\ln([M]_0/[M]_t)$ vs. t plots, which provide values for the apparent equilibrium constant $K_{\text{ATRP}}^{\text{app}} = K_{\text{ATRP}}/[Cu^{II}]$. More accurate values can be obtained from model studies using modified analytical solution of the persistent radical effect [115] originally developed by Fischer [123, 124, 125] and Fukuda [126]:

$$F(\text{Cu}^{II}\text{X}/\text{L}) = 2k_t K_{\text{ATRP}}^2 t + \frac{1}{3[\text{Cu}^I\text{X}/\text{L}]_0}$$

For the simplest case when the initial concentration of the activator $[\text{Cu}^I\text{X}/\text{L}]_0 = C_0$ is equal to the initial concentration of the alkyl halide initiator $[\text{RX}]_0 = I_0$, the function $F(\text{Cu}^{II}\text{X}/\text{L})$ can be calculated as:

$$F(\text{Cu}^{II}\text{X}/\text{L}) = \frac{C_0^2}{3(C_0 - Y)^3} - \frac{C_0}{(C_0 - Y)^2} + \frac{1}{C_0 - Y},$$

where Y is equal to the concentration of the deactivator $[\text{Cu}^{II}\text{X}/\text{L}]$. Therefore, a plot of $F(\text{Cu}^{II}\text{X}/\text{L})$ vs. time should give a straight line once the equilibrium is established and K_{ATRP} can be calculated from the slope, $K_{\text{ATRP}} = (\text{slope}/2k_t)^{1/2}$. Values of K_{ATRP} measured with various alkyl halide initiators and $\text{Cu}^I\text{X}/\text{L}$ complexes commonly used in ATRP are summarized in Table 2.

The values of K_{ATRP} reported in Table 2 illustrate the strong effect of ligand, halogen, and alkyl groups. For ethyl 2-bromoisobutyrate (EBriB), relative values of K_{ATRP} increase in the order $\text{bpy} (1) < \text{PMDETA} (20) < \text{TPMA} (2500) < \text{Me}_6\text{TREN} (40,000)$. Furthermore, the value of K_{ATRP} for $\text{Cu}^I\text{Br}/\text{TPMA}$ and EBriB (9.65×10^{-6})

Table 2 Values of K_{ATRP} for $\text{Cu}^I\text{X}/\text{L}$ complexes measured in CH_3CN at 22°C

Ligand	Cu^IX	Initiator	K_{ATRP}	Reference
bpy	Cu^IBr	EBriB	3.93×10^{-9}	[115]
PMDETA	Cu^IBr	EBriB	7.46×10^{-8}	[115]
TPEDA	Cu^IBr	EBriB	2.00×10^{-6}	[86]
TPMA	Cu^IBr	EBriB	9.65×10^{-6}	[115]
	Cu^IBr	PEBr	4.58×10^{-6}	[115]
	Cu^ICl	PECl	8.60×10^{-7}	[115]
	Cu^IBr	BzBr	6.78×10^{-7}	[115]
	Cu^IBr	MBrP	3.25×10^{-7}	[115]
	Cu^ICl	MCIP	4.28×10^{-8}	[115]
	Me_6TREN	Cu^IBr	EBriB	1.54×10^{-4}
Cu^ICl		MClAc	3.30×10^{-6}	[87]
DMCBCy	Cu^ICl	MClAc	9.90×10^{-5}	[87]

EBriB ethyl-2-bromoisobutyrate. *PEBr* 1-(bromoethyl) benzene, *PECl* 1-(chloroethyl) benzene, *BzBr* benzyl bromine, *MBrP* Methyl-2-bromopropionate, *MCIP* methyl 2-chloropropionate, *MClAc* methyl chloroacetate

is approximately 30 times larger than for MBrP (3.25×10^{-7}), indicating that tertiary alkyl halides are more reactive than secondary ones. Lastly, the values of K_{ATRP} for RBr are approximately six to ten times larger than those for Cl-based systems. These differences indicate that the C–Br bond is relatively weaker than the C–Cl bond in comparison to Cu–Br and Cu–Cl bonds.

3.2 Quantifying Activation and Deactivation Rate Constants

It is not possible to determine from K_{ATRP} alone whether the polymerization will be controlled; fast activation and more importantly fast deactivation are required to achieve good control over polymer molecular weights and molecular weight distributions. Therefore, precise measurements of the activation (k_a) and deactivation (k_d) rate constants should be used for correlation with catalyst, alkyl halide, and monomer structures.

3.2.1 Determination of Activation Rate Constant in ATRP

Activation rate constants (k_a) in ATRP/ATRA are typically determined from model studies in which copper(I) complex is reacted with alkyl halide in the presence of radical trapping agents such as TEMPO [127, 128, 129]. Rates are determined by monitoring the rate of disappearance of alkyl halide in the presence of large excess of the activator ($\text{Cu}^{\text{I}}\text{X}/\text{L}$) and TEMPO. Under such pseudo-first order conditions, the activation rate constant can be calculated $\ln([\text{RX}]_0/[\text{RX}]_t)$ vs. t plots (slope = $-k_a[\text{Cu}^{\text{I}}\text{C}/\text{L}]_0 t$). The activation rate constants are very dependent on the structures of complexing ligand, initiator, and monomer. In a recent study of a variety of copper(I) complexes with nitrogen-based ligands, values of k_a were found to span more than six orders of magnitude [130]. Representative examples are shown in Fig. 9. Generally, the activation rate constant in ATRP/ATRA will depend on the topology of the complexing ligand (cyclic ~ linear < branched), nature of the N-ligand (aryl amine < aryl imine < alkyl amine~pyridine, steric bulk around the metal center and the linking unit between the nitrogen atoms (C4 < C3 < C2) or the “bite” angle. Compounds that contain halogen atoms activated by α -carbonyl, phenyl, vinyl or cyano groups make efficient ATRP initiators (Scheme 5). The reactivity of these initiators can be correlated with bond dissociation energy (BDE) [131]. The activation rate constant in ATRP (k_a) generally depends on:

1. Degree of initiator substitution (primary < secondary < tertiary)
2. Leaving atom/group (Cl < Br < I)
3. Radical stabilizing groups (-Ph~C(O)OR << -CN)

Representative examples are given in Fig. 10. It was recently shown that the penultimate monomer unit can also have a strong effect on k_a [132]. For example, k_a for dimeric alkyl halide H-MMA-MA-Br is approximately five times higher than for

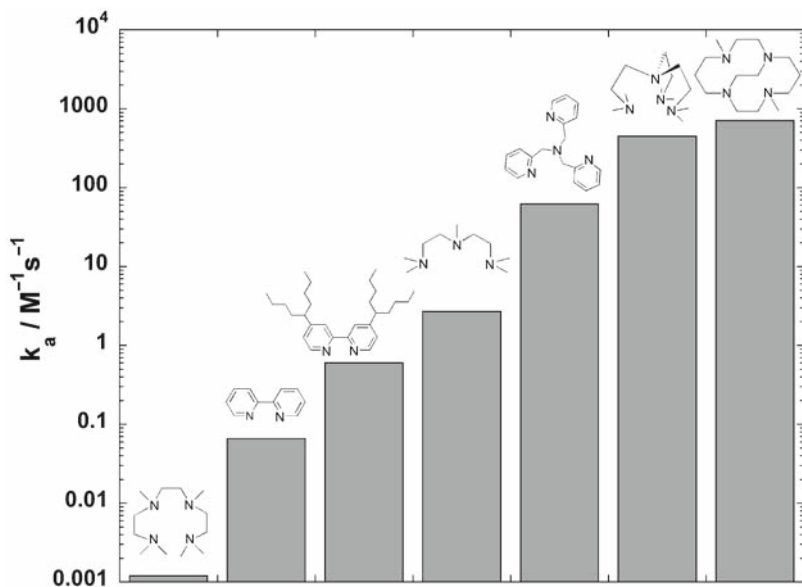


Fig. 9 Rate constant of activation (k_a in $\text{M}^{-1} \text{s}^{-1}$) for various ligands with ethyl-2-bromoisobutyrate in the presence of $\text{Cu}^{\text{I}}\text{Br}$ in CH_3CN at 35 C [130]

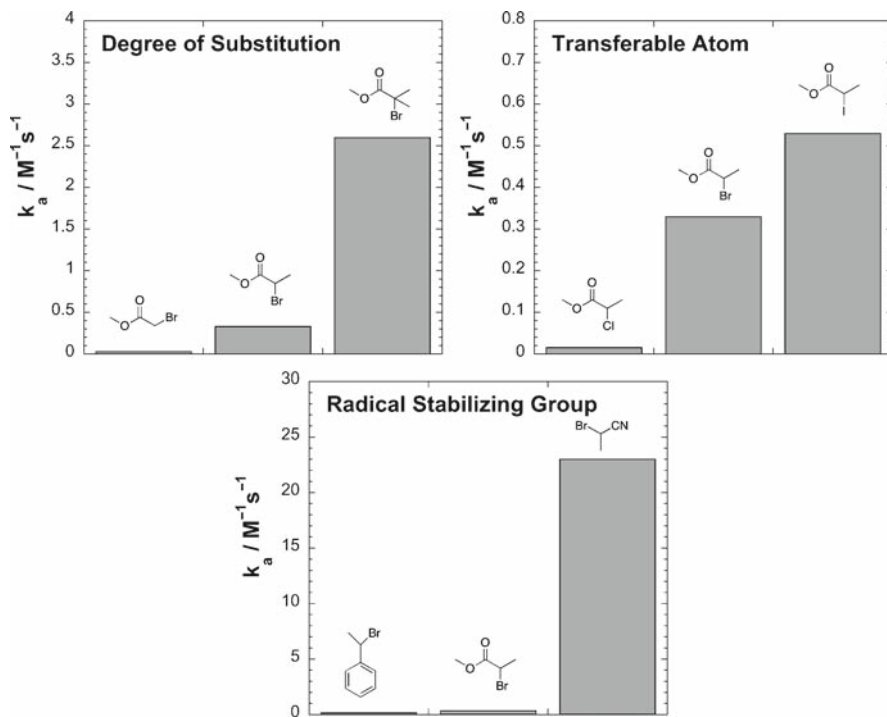


Fig. 10 Values of k_a ($\text{M}^{-1} \text{s}^{-1}$) for various initiators with $\text{Cu}^{\text{I}}\text{X}/\text{PMDETA}$ in CH_3CN at 35 C [132]

H-MA-MA-Br. This can be attributed to B-strain effect. Furthermore, the rate of activation of a dormant chain end with a MMA-Br terminal unit is approximately 20 times higher than with a MA terminal unit containing the same penultimate unit. This effect is induced by the formation of thermodynamically more stable 3° radical when compared to the less stable 2° radical. Lastly, the combined effects of B-strain and radical stability result in a ~100-fold increase of k_a for H-MMA-MMA-Br.

Other investigations include the effect of solvent, counterion, temperature, ligand/catalyst ratio, and the presence of monomer and copper(II) complexes on the activation rate constant [133, 134, 135, 136, 137, 138, 139].

3.2.2 Determination of Deactivation Rate Constant in ATRP

Deactivation rate constants (k_d) have been much less studied in ATRP. The principal reason is the lack of experimental techniques for measuring relatively fast deactivation processes. One of the methods includes the clock reaction in which the generated radicals are simultaneously trapped with TEMPO and the deactivator, $\text{Cu}^{\text{II}}\text{X}_2/\text{L}$ complex [128]. As discussed earlier (Table 1), there appears to be no direct correlation between the deactivation rate constant in ATRP and $\text{Cu}^{\text{II}}\text{-X}$ bond length for a series of bidentate, tridentate, and tetradentate nitrogen-based ligands used in ATRP. These results suggest that other parameters such as structural reorganization from $\text{Cu}^{\text{II}}\text{-X}$ to Cu^{I} complex during ATRP process might also play an important role.

In a related study, activation and deactivation rate constants in ATRP for copper complexes with a series of nitrogen based ligands commonly used in copper catalyzed ATRP were determined and correlated with redox potentials (Fig. 11) [140]. The study found that the more reducing copper catalysts formed faster activating copper(I) and slower deactivating copper(II) species. The rate of activation was dependent on the nature of the nitrogen binding site in the ligand. Generally, the activation rate constant increased for ligands with alkyl amine or pyridine complexing sites. Furthermore, the phenyl-substituted ligands formed very slow activating and fast deactivating catalysts. Slower deactivation rate constants were found for catalysts with a central pyridine unit in the ligand than for catalysts derived from ligands with a central amine unit. In general, the activity of tridentate nitrogen-based ligands decreased in the following order: alkyl amine ~ pyridine > alkyl imine >> aryl imine > aryl amine.

Additionally, deactivation rate constants (k_d) for the more active catalysts such as $\text{Cu}^{\text{I}}\text{X}/\text{Me}_4\text{CYCLAM}$ have been estimated from the initial degree of polymerization without reactivation, end functionality, and molecular weight distributions [138, 141, 142]. With recent advances in determination of the equilibrium constant for atom transfer ($K_{\text{ATRP}} = k_a/k_d$), deactivation rate constants ($k_d = k_a/K_{\text{ATRP}}$) can now be easily obtained from readily accessible activation rate constants (k_a) [115].

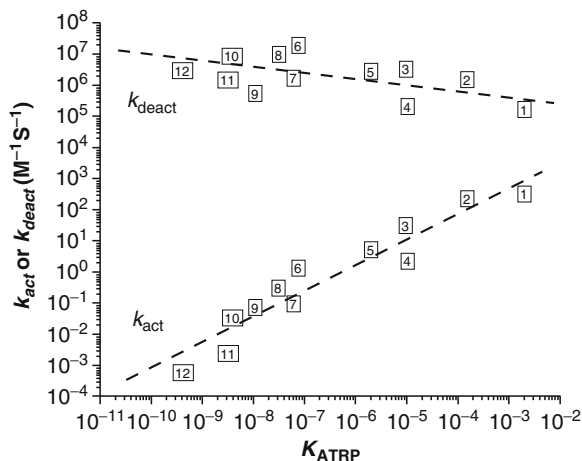


Fig. 11 Correlation of activation rate constants (k_{act}) and deactivation rate constants (k_{deact}) with equilibrium constants (K_{ATRP}) for various $\text{Cu}^{\text{I}}\text{Br}/\text{ligands}$ with EtBriB at 22° C in MeCN (the broken lines are just to guide reader's eye). The k_{act} values were extrapolated from those at 35° C. 1: Cyclam-B, 2: Me_6TREN , 3: TPMA, 4: BPED, 5: TPEDA, 6: PMDETA, 7: BPMPA, 8: dN bpy, 9: HMTETA, 10: bpy, 11: $\text{N}4[3,2,3]$, 12: $\text{N}4[2,3,2]$. Reproduced with permission from reference [140]. Copyright 2008, American Chemical Society.

3.3 Correlating Redox Potential with Equilibrium Constant for Atom Transfer

The equilibrium constant for atom transfer ($K_{ATRP} = k_a/k_d$) can be expressed in terms of four reversible reactions (Scheme 8) [49,50]:

1. Electron transfer or oxidation of metal complex (K_{ET})
2. Electron affinity or reduction of halide radical to halide anion (K_{EA})
3. Bond homolysis of alkyl halide (K_{BH})
4. "Halidophilicity" or association of halide anion to metal complex (K_X)

Generally, these equilibrium constants are very solvent dependent. In particular, the values of K_{EA} are expected to be relatively high in protic solvents because halide anions can be stabilized through solvation in such media [143]. Also, on the other hand, K_X values will be likewise affected with changes in solvent polarity [50]. Low values of K_X in polar and protic media have direct implications on the degree of polymerization control because of the decreased amounts of deactivator ($\text{Mt}^{n+1}\text{X}/\text{L}$), as a result of halide anion dissociation from the metal center.

Catalyst activity (in terms of K_{ATRP}) is also intrinsically dependent on the redox potential of the metal complex. The latter, in turn, depends on the relative stability of the higher (Mt^{n+1}/L) and lower (Mt^n/L) oxidation states. For the case of relatively stable 1:1 copper complexes, the redox potential can be calculated using the following equation [98, 144, 145, 146]:

$$\beta_k^m = \frac{[\text{Cu}^m \text{L}_k]}{[\text{Cu}^m][\text{L}]^k}; m = \text{I or II}$$

$$E \approx E^0 + \frac{RT}{F} \ln \frac{[\text{Cu}^{\text{II}}]_{\text{total}}}{[\text{Cu}^{\text{I}}]_{\text{total}}} - \frac{RT}{F} \ln \frac{\beta^{\text{II}}}{\beta^{\text{I}}}.$$

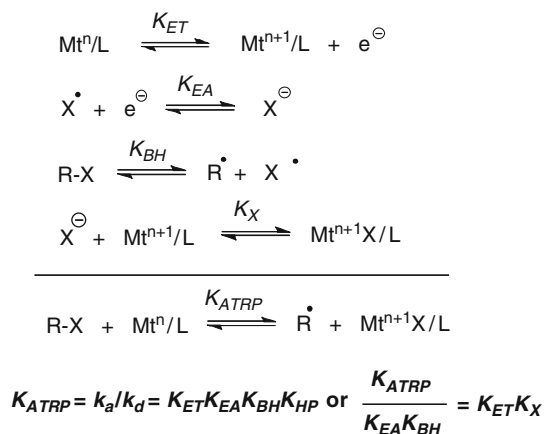
The redox potential of $\text{Cu}^{\text{II}}\text{L}/\text{Cu}^{\text{I}}\text{L}$ couple is related to the equilibrium constant for electron transfer (K_{ET}) according to the equation:

$$E = -\frac{RT}{F} \ln K_{\text{ET}}.$$

As indicated in Scheme 8, for a given alkyl halide R-X , the activity of the catalyst in ATRP does not only depend on the redox potential, but also on the “halidophilicity” of the metal complex (K_X). Both parameters are affected by the nature of transition metal and complexing ligand (including binding constants, basicity, back bonding, etc.). For complexes that have similar “halidophilicities”, the redox potential can be used as a measure of catalyst activity in ATRP. This was demonstrated in linear correlation between K_{ATRP} and $E_{1/2}$ values for a series of copper(I) complexes with nitrogen-based ligands [115,140,147] (Fig. 12).

3.4 ATRA and ATRP Catalyzed by ppm Amounts of Copper Complexes

Over the past decade, copper-mediated ATRP has had a tremendous impact on the synthesis of polymeric materials with well defined compositions, architectures, and functionalities [36, 37, 38, 39, 40, 41, 42, 43, 44, 45, 46, 47, 48, 49, 50, 51, 52]. Apart



Scheme 8 Subequilibria in K_{ATRP}

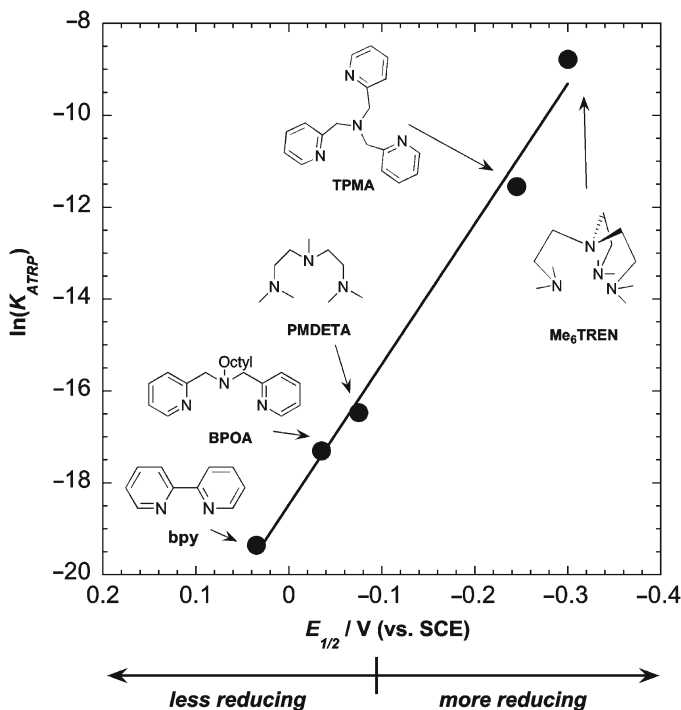


Fig. 12 Plot of $\ln(K_{ATRP})$ vs. $E_{1/2}$. K_{ATRP} values are reported for $\text{Cu}^{\text{I}}\text{Br}/\text{L}$ complexes and ethyl 2-bromoisobutyrate and $E_{1/2}$ was measured relative to SCE (solvent CH_3CN , 22 C) [115,140,147]

from the synthetic, structural, and mechanistic aspects of copper-catalyzed ATRP, considerable effort has also been devoted to development of methodologies to decrease the amount of catalyst needed in these systems [52]. Such movement towards “greening” of copper-mediated ATRP was needed in order to overcome the drawback of traditional ATRP, which required relatively large amounts of copper catalysts (typically on the order of 0.1–1 mol% relative to monomer). Various methodologies have been developed and they include:

1. Simple removal of the catalyst using ion-exchange resins, extractions with water or polymer precipitation [148, 149, 150, 151]
2. Use of biphasic systems such as fluorinated solvents [152,153]
3. Solid supported catalysts [154, 155, 156, 157, 158, 159, 160, 161]
4. Development of highly active catalysts based on ligand design [86, 87]

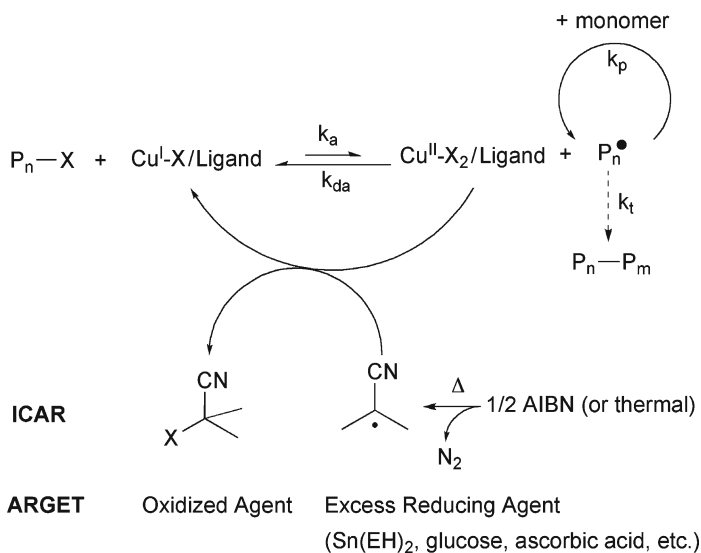
Perhaps the most significant solution to the problem of catalyst recycling and regeneration in ATRP relies on the use of reducing agents that effectively regenerate copper(I) complex during polymerization [162, 163, 164, 165, 166, 167]. The following paragraphs will briefly outline two techniques commonly used, namely activators regenerated by electron transfer (ARGET) ATRP and initiators for continuous activator regeneration (ICAR) ATRP.

3.4.1 ARGET ATRP

A copper-based ATRP catalyst that is sufficiently stable and active can be used at very low concentrations. However, it is very important to mention that a copper(I) complex is constantly being converted to the corresponding copper(II) complex as a result of unavoidable and often diffusion-controlled radical termination reactions ($k_t = 1.0\text{--}4.0 \times 10^9 \text{ M}^{-1} \text{ s}^{-1}$). Therefore, the deactivator (copper(II) complex) will accumulate as the reaction proceeds resulting in slowing down of the polymerization rate and limiting high monomer conversions.

The rate of monomer consumption in ATRP depends only on the absolute ratio of the activator (Cu^{I}) and deactivator (Cu^{II}) [47]. Therefore, the absolute amount of copper catalyst in ATRP can be decreased under normal ATRP conditions without affecting the rate of polymerization. In ARGET (activators regenerated by electron transfer) ATRP, the presence of large excess of reducing agent relative to the copper(I) complex enables polymerization to be conducted using very small amounts of copper catalysts (Scheme 9) [164, 165, 167, 168]. The reducing agents that are typically used include tin(II) 2-ethylhexanoate $\text{Sn}(\text{EH})_2$, glucose, and ascorbic acid.

ARGET ATRP has been successfully applied for polymerization of methyl methacrylate, *n*-butyl acrylate and styrene in the presence of $\text{Sn}(\text{EH})_2$ (10 mol% vs. alkyl halide initiator or 0.07 mol% vs. monomer) [164, 165]. For all monomers, polymerizations were well controlled using between 10 and 50 ppm of copper complexes with highly active TPMA and Me_6TREN ligands. ARGET ATRP has also been utilized in the synthesis of block copolymers (poly(*n*-butyl acrylate)-*b*-polystyrene and polystyrene-*b*-poly(*n*-butyl acrylate) [164, 165] and grafting



Scheme 9 Proposed mechanism for regeneration of copper(I) complexes in ARGET and ICAR ATRP

from various surfaces [168]. Furthermore, excess reducing agent in this technique for catalyst regeneration can be used to consume oxygen and other inhibitors from the reaction mixture, thus eliminating the deoxygenation step.

3.4.2 ICAR ATRP

Initiators for continuous activator regeneration (ICAR) ATRP is another technique that can be used to both scavenge oxidations and also decrease the amounts of catalyst (Scheme 9) [166]. In ICAR ATRP, free radicals are slowly and continuously generated by conventional free radical initiators (e.g., AIBN) throughout the polymerization to constantly reduce copper(II) complex that accumulates as a persistent radical. The potential of ICAR ATRP has been demonstrated in recent studies utilizing ATRP catalysts with a broad range of equilibrium constants for atom transfer (K_{ATRP}) [166]. These included $\text{Cu}^{\text{II}}\text{Cl}_2$ complexes with Me_6TREN , TPMA, PMDETA, and dNbpy ligands. Rates of the polymerization of styrene at 60 °C in the presence of AIBN (0.1 equiv. vs. initiator ethyl 2-bromoisobutyrate) and 50 ppm of $\text{Cu}^{\text{II}}\text{Cl}_2$ were found to be relatively independent of the complexing ligand. These results indicated that the polymerization rate and radical concentration in ICAR ATRP are controlled by the rate of free radical initiator decomposition. Similarly to ARGET ATRP, ICAR ATRP of styrene, methyl methacrylate, and *n*-butyl acrylate were very well controlled using between 10 and 50 ppm of copper complexes with Me_6TREN and TPMA ligands.

This technique for catalyst regeneration has recently been utilized with great success in ATRA reactions catalyzed by $[\text{Cp}^*\text{Ru}^{\text{III}}\text{Cl}_2(\text{PPh}_3)]$ [169,170] and $[\text{Cu}^{\text{II}}(\text{TPMA})\text{X}][\text{X}]$ [118,119] ($\text{X} = \text{Br}^-$ and Cl^-) complexes. The activity of $[\text{Cu}^{\text{II}}(\text{TPMA})\text{Br}][\text{Br}]$ complex in ATRA of polybrominated compounds to alkenes in the presence of AIBN, based on catalyst loading, conversion of alkene, and the yield of monoadduct, was approximately ten times higher than the activity of $[\text{Cu}^{\text{II}}(\text{TPMA})\text{Cl}][\text{Cl}]$. This complex, in conjunction with AIBN, effectively catalyzed ATRA reactions with concentrations between 5 and 100 ppm, which was by far the lowest number achieved in copper-mediated ATRA.

Development of ARGET and ICAR ATRP techniques for catalyst regeneration can have profound industrial implications in polymer and small molecule synthesis because they lower the amount of necessary copper catalyst from several thousand ppm, under normal reaction conditions, to < 10 ppm [171].

4 Conclusions and Future Outlook

Over the past decade, copper-catalyzed atom transfer radical polymerization (ATRP) has had a tremendous impact on the synthesis of macromolecules with well-defined architectures, functionalities, and compositions. Structural and mechanistic

understanding of copper-mediated ATRP has played a pivotal role in the development of this useful polymerization technique. Structural features of copper(I) and copper(II) complexes employed in ATRP were discussed and correlated with reaction parameters such as redox potential, activation (k_a) and deactivation (k_d) rate constants, as well as the overall equilibrium constant for atom transfer (K_{ATRP}). Recent progress in the area of development of highly active copper-based ATRP catalysts, and methodologies to decrease the amount of catalyst needed in this system was also reviewed.

Acknowledgement: KM acknowledges financial support from National Science Foundation (CHE 07-15494). TP acknowledges financial support from Duquesne University (start-up fund and faculty development fund) and National Science Foundation X-ray facility grant (NSF CRIF 0234872).

References

1. Trost BM, Fleming I (1991) *Comprehensive organic synthesis-selectivity, strategy and efficiency in modern organic chemistry*. Elsevier, Oxford
2. Curran DP (1988) *Synthesis* 7:489
3. Curran DP (1988) *Synthesis* 6:417
4. Curran DP (1992) *Comprehensive organic synthesis*. Pergamon, New York
5. Kharasch MS, Jensen EV, Urry WH (1945) *Science* 102:128
6. Kharasch MS, Jensen EV, Urry WH (1945) *J Am Chem Soc* 67:1626
7. Kharasch MS, Jensen EV, Urry WH (1946) *J Am Chem Soc* 68:154
8. Asscher M, Vofsi D (1961) *J Chem Soc* 1961:2261
9. Bellius D (1985) *Pure Appl Chem* 57:1827
10. Clark AJ (2002) *Chem Soc Rev* 31:1
11. Clark AJ, Battle GM, Bridge A (2001) *Tetrahedron Lett* 42:4409
12. Udding JH, Tuijip CJM, van Zanden NA, Hiemstra H, Speckamp WN (1994) *J Org Chem* 59:1993
13. Bendetti M, Forti L, Ghelfi F, Pagnoni UM, Ronzoni R (1997) *Tetrahedron* 53:14031
14. Freidlina RK, Velichko FK (1977) *Synthesis* 3:145
15. Lee GM, Weinreb SM (1990) *J Org Chem* 55:1281
16. Bland WJ, Davis R, Durrant JLA (1984) *J Organomet Chem* 260:C75
17. Matsumoto H, Nakano T, Nagai Y (1973) *Tetrahedron Lett* 51:5147
18. Severin K (2006) *Curr Org Chem* 10:217
19. Gossage RA, Van De Kuil LA, Van Koten G (1998) *Acc Chem Res* 31:423
20. Grove DM, van Koten G, Verschuuren AHM (1988) *J Mol Catal* 45:169
21. Sasson Y, Rempel GL (1975) *Synthesis* 1975:448
22. Baban JA, Roberts BP (1981) *J Chem Soc Perkin Trans* 1:161
23. Caronna T, Citterio A, Ghirardini M, Minisci F (1977) *Tetrahedron* 33:793
24. Minisci F (1975) *Acc Chem Res* 8:165
25. Sinnreich J, Asscher M (1972) *J Chem Soc Perkin Trans* 1:1543
26. Kamigata N, Sawada H, Kobayashi M (1983) *J Org Chem* 48:3793
27. Block E, Aslam M, Eswarakrishnan V, Gebreyes K, Hutchinson J, Iyer RS, Laffitte JA (1986) *J Am Chem Soc* 108:4568
28. Amiel Y (1974) *J Org Chem* 39:3867
29. Truce WE, Wolf GC (1971) *J Org Chem* 36:1727
30. Julia M, Sasussine L, Thuillier GI (1979) *J Organomet Chem* 174:359

31. De Campo F, Lastecoueres D, Verlhac J-B (2000) *J Chem Soc Perkin Trans 1*:575
32. Nagashima H, Seki K, Ozaki N, Wakamatsu H, Itoh K, Tomo Y, Tsuyi J (1990) *J Org Chem* 55:985
33. Yang D, Yan Y-L, Zheng B-F, Gao Q, Zhu N-Y (2006) *Org Lett* 8:5757
34. Wang J-S, Matyjaszewski K (1995) *J Am Chem Soc* 117:5614
35. Kato M, Kamigaito M, Sawamoto M, Higashimura T (1995) *Macromolecules* 28:1721
36. Braunecker WA, Matyjaszewski K (2007) *Prog Polym Sci* 32:93
37. Coessens V, Pintauer T, Matyjaszewski K (2001) *Prog Polym Sci* 26:337
38. Kamigaito M, Ando T, Sawamoto M (2001) *Chem Rev* 101:3689
39. Matyjaszewski K, Gaynor S, Greszta D, Mardare D, Shigemoto T (1995) *J Phys Org Chem* 8:306
40. Oh JK, Drumright R, Siegwart DJ, Matyjaszewski K (2008) *Prog Polym Sci* 33:448
41. Sheiko SS, Sumerlin BS, Matyjaszewski K (2008) *Prog Polym Sci* 33:759
42. Matyjaszewski K (2003) *Macromol Symp* 195:25
43. Matyjaszewski K (2005) *Prog Polym Sci* 30:858
44. Matyjaszewski K (ed) (2006) *Controlled radical polymerization. from synthesis to materials*. ACS Symposium Series, vol 944. American Chemical Society, Washington, DC
45. Matyjaszewski K, Davis TP (2002) *Handbook of radical polymerization*. Wiley, Hoboken
46. Matyjaszewski K, Gnanou Y, Leibler L (2007) *Macromolecular engineering-precise synthesis, materials properties, applications*. Wiley-VCH, Weinheim
47. Matyjaszewski K, Xia J (2001) *Chem Rev* 101:2921
48. Patten TE, Matyjaszewski K (1999) *Acc Chem Res* 32:895
49. Pintauer T, Matyjaszewski K (2005) *Coord Chem Rev* 249:1155
50. Pintauer T, McKenzie B, Matyjaszewski K (2003) *ACS Symp Ser* 854:130
51. Tsarevsky NV, Braunecker WA, Vacca A, Gans P, Matyjaszewski K (2007) *Macromol Symp* 248:60
52. Tsarevsky NV, Matyjaszewski K (2007) *Chem Rev* 107:2270
53. Kabachii YA, Kochev SY, Bronstein LM, Blagodatskih IB, Valetsky PM (2003) *Polym Bull* 50:271
54. Le Grogne E, Claverie J, Poli R (2001) *J Am Chem Soc* 123:9513
55. Brandts JAM, van de Geijn P, van Faassen EE, Boersma J, van Koten G (1999) *J Organomet Chem* 584:246
56. Maria S, Stoffelbach F, Matta J, Darran J-C, Richard P, Poli R (2005) *J Am Chem Soc* 127:5946
57. Kotani Y, Kamigaito M, Sawamoto M (1999) *Macromolecules* 32:2420
58. Matyjaszewski K, Wei M, Xia J, McDermott NE (1997) *Macromolecules* 30:8161
59. Ando T, Kamigaito M, Sawamoto M (1997) *Macromolecules* 30:4507
60. O'Reilly RK, Gibson VC, White AJP, Williams DJ (2004) *Polyhedron* 23:2921
61. Teodorescu M, Gaynor S, Matyjaszewski K (2000) *Macromolecules* 33:2335
62. Simal F, Demonceau A, Noels AF (1999) *Angew Chem Int Ed Eng* 38:538
63. Braunecker WA, Itami Y, Matyjaszewski K (2005) *Macromolecules* 38:9402
64. Braunecker WA, Brown WC, Morelli BC, Tang W, Poli R, Matyjaszewski K (2007) *Macromolecules* 40:8576
65. Percec V, Barboiu B, Neumann A, Ronda JC, Zhao M (1996) *Macromolecules* 29:3665
66. Wang B, Zhuang Y, Luo X, Xu S, Zhou X (2003) *Macromolecules* 36:9684
67. Granel C, Dubois P, Jerome R, Teyssie P (1996) *Macromolecules* 29:8576
69. Lecomte P, Drapier I, Dubois P, Teyssie P, Jerome R (1997) *Macromolecules* 30:7631
70. Patten TE (1996) *Science* 272:866
71. Matyjaszewski K (1998) *Macromolecules* 31:4710
72. Tsarevsky NV, Braunecker WA, Matyjaszewski K (2007) *J Organomet Chem* 692:3212
73. Matyjaszewski K, Patten TE, Xia J (1997) *J Am Chem Soc* 119:674
74. Clark AJ, Battle GM, Heming AM, Haddleton DM, Bridge A (2001) *Tetrahedron Lett* 42:2003
75. Haddleton DM, Crossman MC, Hunt KH (1997) *Macromolecules* 30:3992

76. Haddleton DM, Duncalf DJ, Kukulj D, Crossman MC, Jackson SG, Bon SAF, Clark AJ, Shooter AJ (1998) *Eur J Inorg Chem* 1998:1799
77. Haddleton DM, Jasieczek CB, Hannon MJ, Shooter AJ (1997) *Macromolecules* 30:2190
78. Lad J, Harrison S, Mantovani G, Haddleton DM (2003) *Dalton Trans* 2003:4175
79. Kickelbick G, Matyjaszewski K (1999) *Macromol Rapid Commun* 20:341
80. Xia J, Zhang X, Matyjaszewski K (2000) *ACS Symposium Series* 760:207
81. Xia J, Matyjaszewski K (1997) *Macromolecules* 30:7697
82. Xia J, Matyjaszewski K (1999) *Macromolecules* 32:2434
83. Xia J, Gaynor SG, Matyjaszewski K (1998) *Macromolecules* 31:5958
84. Yamamura Y, Matyjaszewski K (2008) *J Polym Sci Part A: Polym Chem* 46:2015
85. Konak C, Ganchev B, Teodorescu M, Matyjaszewski K, Kopeckova P, Kopecek J (2002) *Polymer* 43:3735
86. Tang H, Arulsamy N, Radosz M, Shen Y, Tsarevsky NV, Braunecker WA, Tang W, Matyjaszewski K (2006) *J Am Chem Soc* 128:16277
87. Tsarevsky NV, Braunecker WA, Tang W, Brook SJ, Matyjaszewski K, Weismann GR (2006) *J Mol Catal A: Chem* 257:132
88. Pintauer T (2006) *Acta Cryst Sec E* E62:m620
89. Burke PJ, McMillin DR, Robinson WR (1980) *Inorg Chem* 19:1211
90. Foley J, Tyagi S, Hathaway BJ (1984) *J Chem Soc Dalton Trans* 1984:1
91. Levy AT, Olmstead MM, Patten TE (2000) *Inorg Chem* 39:1628
92. Munakata M, Kitagawa S, Asahara A, Masuda H (1987) *Bull Chem Soc Jpn* 60:1927
93. Skelton BW, Waters AF, White AH (1991) *Aust J Chem* 44:1207
94. Willett RD, Pon G, Nagy C (2001) *Inorg Chem* 40:4342
95. Dobson JF, Green BE, Healy PC, Kennard CHL, Pukawatchai C, White AH (1984) *Inorg Chem* 23:649
96. Goodwin KV, McMillin DR, Robinson WR (1986) *Inorg Chem* 25:2033
97. James BR, Williams RJP (1961) *J Chem Soc* 1961:2007
98. Rossotti FJC, Rossotti H (1961) *The determination of stability constants*. McGraw Hill, New York
99. Beck MT (1970) *Chemistry of complex equilibria*. Van Nostrand Reinhold, London
100. Martell AE, Motekaitis RJ (1988) *The determination and use of stability constants*. VCH, New York
101. Munakata M, Kitagawa S, Kosome S, Asahara A (1986) *Inorg Chem* 25:2622
102. Pintauer T (2006) *J Organomet Chem* 691:3948
103. Masuda H, Machida K, Munakata M, Kitagawa S, Shimono H (1988) *J Chem Soc Dalton Trans* 1988:1907
104. Stamp L, Dieck T (1987) *Inorg Chim Acta* 129:107
105. Pasquali M, Marchetti F, Floriani C (1978) *Inorg Chem* 17:1684
106. Bruce MI (1972) *J Organomet Chem* 44:209
107. Kimura E, Koike T, Kodama M, Meyerstein D (1989) *Inorg Chem* 28:2998
108. Ogura T (1976) *Inorg Chem* 15:2301
109. Pasquali M, Floriani C, Gaetani-Manfredotti A, Chiesi-Villa A (1979) *Inorg Chem* 18:3535
110. Braunecker WA, Pintauer T, Tsarevsky NV, Kickelbick G, Matyjaszewski K (2005) *J Organomet Chem* 690:916
111. Braunecker WA, Tsarevsky NV, Pintauer T, Gil RR, Matyjaszewski K (2005) *Macromolecules* 38:4081
112. Costas M, Llobet A (1999) *J Mol Catal A* 142:113
113. Gagne RR, Allison JL, Koval CA, Mialki WS, Smith TJ, Walton RA (1980) *J Am Chem Soc* 102:1095
114. Munakata M, Shigeru N, Hiromasa S (1980) *J Chem Soc Chem Commun* 1980(5):219
115. Tang W, Tsarevsky NV, Matyjaszewski K (2006) *J Am Chem Soc* 128:1598
116. Becker M, Heinemann FW, Schindler S (1999) *Chem Eur J* 5:3124
117. Karlin KD, Zubieta J (1983) *Copper coordination chemistry: biochemical and inorganic perspectives*. Adenine, New York

118. Eckenhoff WT, Pintauer T (2007) *Inorg Chem* 46:5844
119. Eckenhoff WT, Garrity ST, Pintauer T (2008) *Eur J Inorg Chem* 2007:563
120. Kickelbick G, Pintauer T, Matyjaszewski K (2002) *New J Chem* 26:462
121. Beuermann S, Buback M (2002) *Prog Polym Sci* 27:191
122. Fischer H, Radom L (2001) *Angew Chem Int Ed Eng* 40:1340
123. Fischer H (1986) *J Am Chem Soc* 108:3925
124. Fischer H (1999) *J Polym Sci Part A: Polym Chem* 37:1885
125. Fischer H (2001) *Chem Rev* 101:3581
126. Goto A, Fukuda T (2004) *Prog Polym Sci* 29:329
127. Goto A, Fukuda T (1999) *Macromol Rapid Commun* 20:633
128. Matyjaszewski K, Paik H-j, Zhou P, Diamanti SJ (2001) *Macromolecules* 34:5125
129. Ohno K, Goto A, Fukuda T, Xia J, Matyjaszewski K (1998) *Macromolecules* 31:2699
130. Tang W, Matyjaszewski K (2006) *Macromolecules* 39:4953
131. Gillies MB, Matyjaszewski K, Norrby P-O, Pintauer T, Poli R, Richard PA (2003) *Macromolecules* 36:8551
132. Nanda AK, Matyjaszewski K (2003) *Macromolecules* 36:8222
133. Tang W, Nanda AK, Matyjaszewski K (2005) *Macromol Chem Phys* 206:1171
134. Nanda AK, Matyjaszewski K (2003) *Macromolecules* 36:1487
135. Nanda AK, Matyjaszewski K (2003) *Macromolecules* 36:599
136. Matyjaszewski K, Nanda AK, Tang W (2005) *Macromolecules* 38:2015
137. Chambard G, Klumperman B, German AL (2000) *Macromolecules* 33:4417
138. Chambard G, Klumperman B, German AL (2002) *Macromolecules* 35:3420
139. Tang W, Matyjaszewski K (2007) *Macromolecules* 40:1858
140. Tang W, Kwak Y, Braunecker W, Tsarevsky NV, Coote ML, Matyjaszewski K (2008) *J Am Chem Soc* 130:10702.
141. Gromada J, Matyjaszewski K (2002) *Macromolecules* 35:6167
142. Groszta D, Matyjaszewski K (1996) *Macromolecules* 29:7661
143. Asrshadi M, Yamdagni R, Kebarle P (1970) *J Phys Chem* 74:1475
144. Lingane JJ (1941) *Chem Rev* 29:1
145. Vlcek AA (1963) *Prog Inorg Chem* 5:211
146. Buckingham DA, Sargeson AM (1964) In: Dwyer FP, Mellor DP (eds) *Chelating agents and metal chelates*. Academic, New York
147. Qiu J, Matyjaszewski K, Thounin L, Amatore C (2000) *Macromol Chem Phys* 201:1625
148. Matyjaszewski K, Pintauer T, Gaynor S (2000) *Macromolecules* 33:1476
149. Honigfort ME, Brittain WJ (2003) *Macromolecules* 36:3111
150. Sarbu T, Pintauer T, McKenzie B, Matyjaszewski K (2002) *J Polym Sci Part A: Polym Chem* 40:3153
151. Kasko AM, Heintz AM, Pugh C (1998) *Macromolecules* 31:256
152. De Campo F, Lastecoueres D, Vincent J-M, Verlhac J-B (1999) *J Org Chem* 64:4969
153. Haddleton DM, Jackson SG, Bon SAF (2000) *J Am Chem Soc* 122:1542
154. Kickelbick G, Paik H-J, Matyjaszewski K (1999) *Macromolecules* 32:2941
155. Haddleton DM, Duncalf DJ, Kukulj D, Radigue AP (1999) *Macromolecules* 32:4769
156. Shen Y, Zhu S, Zeng F, Pelton RH (2000) *Macromolecules* 33:5427
157. Shen Y, Zhu S, Pelton RH (2000) *Macromol Rapid Commun* 21:956
158. Shen Y, Zhu S, Zeng F, Pelton RH (2001) *J Polym Sci Part A: Polym Chem* 39:1051
159. Hong SC, Matyjaszewski K (2002) *Macromolecules* 35:7592
160. Duquesne E, Degee P, Habimana J, Dubois P (2004) *Chem Commun* 2004:640
161. Min K, Gao H, Matyjaszewski K (2006) *J Am Chem Soc* 128:10521
162. Jakubowski W, Matyjaszewski K (2005) *Macromolecules* 38:4139
163. Jakubowski W, Matyjaszewski K (2006) *Angew Chem* 118:4594
164. Jakubowski W, Matyjaszewski K (2006) *Angew Chem Int Ed* 45:4482
165. Jakubowski W, Min K, Matyjaszewski K (2006) *Macromolecules* 39:39
166. Matyjaszewski K, Jakubowski W, Min K, Tang W, Huang J, Braunecker WA, Tsarevsky NV (2006) *Proc Natl Acad Sci U S A* 103:15309

167. Min K, Gao H, Matyjaszewski K (2007) *Macromolecules* 40:1789
168. Matyjaszewski K, Dong H, Jakubowski W, Pietrasik J, Kusumo A (2007) *Langmuir* 23:4528
169. Quebatte L, Thommes K, Severin K (2006) *J Am Chem Soc* 128:7440
170. Thommes K, Icli B, Scopelliti R, Severin K (2007) *Chem Eur J* 13:6899
171. Pintauer T, Matyjaszewski K (2008) *Chem Soc Rev* 37:1087–1097

Index

A

- Acrylate comonomers, 159
- Activation rate constants, 239
- Activators regenerated by electron transfer (ARGET) ATRP, 244
- Alkylaluminoxanes, 54
- Alpha-diimine, 179
- ARGET, 244
- Atom transfer radical addition (ATRA), 222, 224
 - copper-catalyzed, 224
- Atom transfer radical cyclization (ATRC), 224
- Atom transfer radical polymerization (ATRP), 221
 - activators regenerated by electron transfer (ARGET), 245
 - active copper complexes, 227
 - copper-catalyzed, mechanistic understanding, 237
 - deactivation rate constants, 241
 - equilibrium, 238
 - initiators for continuous activator regeneration (ICAR ATRP), 244, 246
- Aufbau reaction, 161

B

- 2,2'-Bipyridine (bpy), 229
- 2,6-Bis(arylimino)pyridine, 107, 110
- Bis(benzimidazole) copper(II) complex, 175
- Bis(dibenzylideneacetone) palladium(0), 168
- 2,6-Bis(imino)pyridine iron halide/MAO, 110, 120
- Bis(phenoxy-imine), 6, 10, 18
- Bishydrazone, 124
- Block copolymer, 3
- Borane, 56

- Borate, 56
 - activation, 47
- Brookhart catalyst, 109, 163, 183, 193

C

- Carbosilane dendrimers, 139
- Catalyst design concept, 7
- Catalyst functional group tolerance, 196
- Catalyzed chain growth (CCG), 70
- Catalyzed olefin polymerization, 65
- Chain shuttling, continuous reactor, 89
 - deuterium labeling, 86
- Chain shuttling agent (CSA), 65, 69
 - selection, 81
- Chain shuttling catalysis, 65
- Chain shuttling catalyst systems, 74
- Chain transfer, 65
- Chain transfer agents (CTAs), 29, 41, 70, 80
- Chain transfer pathways, 128
- Chain transfer polymerization, coordinative, 69
- Cobalt catalysts, 107, 143
- Cobalt halide/MAO catalysts, 110, 120
- Cocatalysts, 54
 - MgCl₂-based, 18
- Comonomers, linear, random copolymers
 - of ethylene, 168
- Coordinative chain transfer polymerization (CCTP), 70
- Copolymers, ultra-high molecular weight, 22
- Copper complexes, ATRP, 221
 - Cu(I), 229
 - Cu(II), 235
- Cossee-type propagation, 128
- Cyclodextrins, 142
- Cyclophane diimine palladium(II) catalysts, 165
- Cyclophane-palladium complex, 166

D

- Deactivation rate constants, 239
- α -Diimine ligands, cyclic, catalysts, 206
 - hemilabile axial donating, 212
- α -Diimines, substituted, modification, 200
 - teraryl-substituted, 205
- Diblock OBCs, CCTP, 98
- Diisopropylphenyl catalysts, 128
- Dual-catalyst systems, reversible chain transfer, 71
- Dual-side catalysts, 51

E

- Ethyl-2-bromoisobutyrate, 240
- Ethylene, 159
- Ethylene polymerizations, highly active molecular catalysts, 9
 - i*-Bu₃Al/Ph₃CB(C₆F₅)₄ cocatalyst, 17
 - living, 28
 - MgCl₂-based cocatalyst, 18
 - Zr-/Ti-FI catalysts, 14
- Ethylene/methyl acrylate copolymerization, 169
- Ethylene/ α -olefin amorphous copolymers, 4
- Ethylene/polar comonomers, copolymerization, 161
- Ethylene/propylene/diene elastomers (EPDMs), 4
- Ethylene-LAO, 68

F

- FI catalysts, 3, 11, 19
 - ethylene polymerization activity, 10
 - high activity, 13
 - structure, 11
- Flexible polyvinylchloride (f-PVC), 69
- Functional group tolerance, 194

G

- Grubbs nickel, 168

H

- Hafnium amidinate, 71
- Hafnocene catalysts, 47
 - activities, 57
 - characterization, 49
 - molecular weights, 57
 - stereoselectivity, 57
- HDPE, 67, 69, 109

I

- i*-Bu₃Al/Ph₃CB(C₆F₅)₄ cocatalyst, ethylene polymerizations, 17
- Initiators for continuous activator regeneration (ICAR) ATRP, 244, 246
- Iron catalysts, 107, 143

L

- LAO, 67
- Late transition metal, 162, 179
- LDPE, 67, 69, 161
- Ligand design, 200
- Ligand preparation, 110
- Linear α olefin (LAO), 67
- Living olefin polymerization, 3, 27
 - origin, 32
- Living polymers, catalytic production, 41
- LLDPE, 67, 69, 143

M

- Metallocenes, 4, 49, 54, 67, 162
- Methylaluminoxane (MAO), 9, 17, 47, 54, 107, 125
 - “active species”, 125
- Methyl acrylate (MA), 164, 169, 174, 185, 197, 210
 - homogeneous ATRP, 232
- Methyl methacrylate (MMA), 125, 231, 245
- Monomers, polar/nonpolar, 196, 197

N

- Ni(II) amino-bis-(imino)phosphorane, 182
- Nickel, 179
- Nickel effect, 161
- Nitrogen-containing ligands, catalysts, 203
- Nucleophilic heterocyclic carbene (NHC) ligands, 167

O

- Olefin block copolymers (OBCs), 65, 69
 - CCTP, 97
 - chain shuttling catalysis, 91
 - diblock, continuous process, 97
 - continuous reactor, 89
- Olefin polymerization, 3, 47, 107
 - chain transfer to metal, 69
- Olefins, block copolymers, 69
 - higher, polymerization, 194

P

- Palladium catalysts, 159, 163, 168, 179, 192
- Palladium(II) acetate, 168
- Palladium α -diimine catalysts, 196
- PE-*b*-sPP, 39
- PE-*b*-poly(ethylene-*co*-propylene), 39
- PE-*b*-poly(ethylene-*co*-propylene)-*b*-PE, 39
- PE-*b*-poly(ethylene-*co*-propylene)-*b*-sPP, 39
- Phenoxy-imine, 3, 11
- Phosphine ligands, 171
- Polar groups, 159
- Polyacrylates, 125
- Polyethylenes (PEs), 4, 19, 107
 - LDPE, 67, 69, 161
 - multimodal, 22
 - ULDPE, 143
 - vinyl-/Al-terminated, 19
- Polymer architectures, continuous CCTP, 100
- Polymer back-biting, 164
- Polymerization catalysis, 159
- Polyolefinic block copolymers, well-defined, 39
- Polyolefins, ultrahigh M_w , 44
- Polypropylenes (PPs), 4, 71
 - atactic, 71
 - isotactic, 25, 71
 - syndiotactic, 24
 - sPP-*b*-poly(ethylene-*co*-propylene), 39
 - stereoregularity, 54
- Polyurethanes, thermoplastic (TPUs), 69
- Polyvinylchloride, flexible (f-PVC), 69
- Poly(1-hexene)s, 26
- Poly(4-methyl-1-pentene)s, 26
- Poly(1-octene)s, 26
- Propagation pathways, 128
- Propylene polymerization, stereospecific living, 36

R

- Random copolymers, 159
- Redox potential/equilibrium constant, atom transfer, 242

S

- Single catalyst batch reactions, mathematical simulation, 74
- Styrene, homogeneous ATRP, 232
- Sulfonic acid phosphine ligands, 173
- Supported catalysts, 135

T

- Tandem catalysis, 143
- Tetraethylaluminum, 131
- Tetrakis(2-pyridylmethyl)ethylenediamine (TPEDA), 234
- Thermoplastic elastomers, 65
- Thermoplastic polyurethanes (TPUs), 69
- Thermoplastic vulcanates (TPVs), 69
- TIBA/borate, 47
- Ti-FI catalysts, fluorinated, 16, 41
- Titanocene, 51
- Triisobutylaluminum (TIBA), 57
- Tris(dibenzylideneacetone) dipalladium(0), 168
- Tris[(2-pyridyl)methyl]amine (TPMA), 233
- Tris[2-(dimethylaminoethyl)amine (Me₆ TREN), 228, 233, 246

U

- ULDPE, 143

V

- Vulcanates, thermoplastic (TPVs), 69

Z

- Zirconocenes, 44
- Zr-FI catalysts, ethylene polymerization, 15
- Zr-FI catalysts, structure, 17, 21